Coastal and seasonal hydrodynamics and morphodynamics of the Mekong Delta

Phan, Hung

DOI
10.4233/uuid:2bcb33bf-5b73-4873-9168-08b1e7a2836f

Publication date
2020

Document Version
Final published version

Citation (APA)
Phan, H. (2020). *Coastal and seasonal hydrodynamics and morphodynamics of the Mekong Delta*. [Dissertation (TU Delft), Delft University of Technology]. https://doi.org/10.4233/uuid:2bcb33bf-5b73-4873-9168-08b1e7a2836f

COASTAL AND SEASONAL HYDRODYNAMICS AND MORPHODYNAMICS OF THE MEKONG DELTA

COASTAL AND SEASONAL HYDRODYNAMICS AND MORPHODYNAMICS OF THE MEKONG DELTA

Dissertation

for the purpose of obtaining the degree of doctor
at Delft University of Technology
by the authority of the Rector Magnificus prof.dr.ir. T.H.J.J. van der Hagen
chair of the Board for Doctorates,
to be defended publicly on
Monday 23rd March 2020 at 12:30 o'clock

by

Hung Manh PHAN

Master of Science in Water Science and Engineering
IHE- Delft Institute for Water Education, Delft, Netherlands
born in Nha Trang, Vietnam.

This dissertation has been approved by the promotors

Composition of the doctoral committee:

Rector Magnificus,	chairperson
Prof. dr. ir. M. J. F. Stive,	Delft University of Technology, promotor
Prof. dr. ir. A. J. H. M. Reniers,	Delft University of Technology, promotor
Dr. Q. Ye	Deltares, copromotor

Independent members:

Prof. dr. ir. T. V. Nguyen	Thuy Loi University, Vietnam
Dr. C. A. Katsman	Delft University of Technology
Prof. dr. ir. S. G. J. Aarninkhof	Delft University of Technology
Prof. dr. ir. Z. B. Wang	Delft University of Technology

Keywords: Mekong Delta, hydrodynamics, morphodynamics, monsoon climate

Printed by: Hung M. Phan

ISBN 978-94-028-1991-5

An electronic version of this dissertation is available at
http://repository.tudelft.nl/.

Dedicated to my family and people living in the Mekong Delta.

Contents

Summary

Coastal retreat problems occur in many deltas over the world. Coastal features are not constant over time and are affected by sea level rise, river runoff, sediment supply, wave and tidal energy, underlying geology and climate. In addition, human activities profoundly influence the coastal processes as a result of changing natural patterns of runoff, littoral sediment supply and construction and reconstruction of engineering works.

The Mekong Delta, the largest delta in South East Asia, and especially the Mekong deltaic coast, is suffering under intense pressures from the above-mentioned factors. Shoreline observation is the indispensable base to provide an overview and to understand the process of coastline evolution. This study employs integrated methods for remote sensing, geographic information and statistics to inspect the coastline evolution over the period of 1973 to 2015 using Multispectral (MSS), Thematic Mapper (TM), Enhanced Thematic Mapper Plus (ETM+) and Operational Land Imager (OLI) of Landsat images. The results show a varying pattern of accretion and erosion. The eastern coast has undergone both significant sedimentation and erosion, with a particularly high sedimentation near and in the Mekong river mouths and an annual large erosion of up to 40 meter in eastern Camau Province. Meanwhile the shoreline retreat of western coast is less severe than the eastern coast, with an especially high accretion rising to 90 m/yr at the Datmui Commune of western Camau Province. This study indicates there is a variation in the coastline change rate among the periods of 1973-1990, 1990-2005 and 2005-present. The results illustrate, using a statistical approach, that the rate of shoreline change is largely related to the sediment flux of the Mekong River, in particular the decrease of sediment flow as a result of dam construction and sand mining in the Mekong River during the past 15 years. Of crucial importance in sustaining a healthy coastal ecosystem are the mangroves that offer a natural habitat to numerous species and especially contribute to a stable coastline. Nevertheless, the mangroves along the Mekong deltaic coast have faced threats from both natural and anthropogenic causes. Because the evolution of mangroves as well as other land covers in the coastal Mekong Delta is not well known, this study aims to contribute through quantitative research to the evolution of the mangrove area during 43 years, i.e. between 1973 and 2015. Satellite Landsat images have been employed for mapping land cover categories comprising mangroves, aquaculture, soils, plants and water along the coastal districts of the Mekong Delta, applying a classification method encompassing Iso Cluster and Maximum Likelihood algorithms. The findings reveal that the total mangrove area diminished and that the total mangrove loss was attributable to the expansion of aquaculture, as well as to coastal erosion. A minor increase in mangrove area resulted from projects to protect from coastal erosion and to restore mangroves.

It is essential to gain an understanding of the tidal wave characteristics, one of the main forcings for manipulating morphodynamics of Mekong Delta, on the Mekong deltaic shelf from the South China Sea (a.k.a. East Sea) and the Gulf of Thailand (a.k.a. West Sea). The study employed a two-dimensional, barotropic numerical model to look into the dynamics of tidal wave propagation. The study indicates that tidal waves spread from the Pacific Ocean into the South China Sea, mostly crossing the Luzon Strait (LS), where, as a result of a quarter wavelength, the K_1 diurnal tide controls the resonance in this basin. For the tidal wave propagation over the Mekong deltaic shelf the incoming tidal wave from the Celebes open boundary is dominant over the tidal wave from the Andaman and Flores open boundaries. By means of Green's law, the formula of Clarke and Battisti and the theory of standing waves, the study illuminated that the considerably enlarged M_2 semidiurnal amplitude, leading to a dominant mixed semidiurnal tide, is triggered by both shoaling influence, the continental shelf oscillation resonance phenomenon and the location of the anti-node line of the standing wave. Moreover, the existence of radial tidal currents along the southern Mekong estuarine coast has not been revealed in earlier studies. Based on numerical, geometrically schematised investigations, it is proposed that the relationship between the greatly intensified amplitude near the coastline and the surrounding adjacent low amplitude system is the cause of the radial tidal currents system over the Mekong deltaic shelf. The study showed that the wind monsoon climate can trigger diminished or magnified tidal amplitudes over the Mekong deltaic coast by atmospheric pressure, the tangential stress of wind over the water surface and wind boosted bottom friction. The study indicated that the tidal generating forces should be taken into account to attain precise simulation results depending on the geographical region of interest.

The action of waves approaching the Mekong deltaic coast at an angle produces the wave incident angle for the potential longshore sediment transport. The study evaluated the representative wave climate and the accompanying longshore wave-driven sediment transport capability along the Mekong deltaic coast. The wave climate is obtained using the state-of-the-art spectral wave model SWAN (Simulating WAves Nearshore). The results demonstrate that the wave field growth on the Mekong deltaic shelf is dominated by the monsoon climate system. While considerable breaking wave dissipation occurs in the estuarine zones in the winter monsoon climate, large breaking wave dissipation takes place along the western Camau Cape during the summer monsoon climate. Whereas the wind fields in the winter monsoon climate only affect wave fields along the eastern coast, the wind system considerably impacts on the wave processes in both the eastern and the western coasts during the summer monsoon climate. Furthermore, larger wave heights are realized in the northeastern area of the Mekong deltaic shelf, while they diminish in the southwest and western coast of the Mekong Delta during the winter monsoon. In contrast, significant wave heights on the western shelf are larger compared to the eastern coast during the summer monsoon climate. The CERC formula is utilized to construct a Longshore Sediment Transport (LST) capacity to calculate the response of coastline variations of the Mekong Delta from wave environments under the monsoon climate system. The study exposed that the highest potential LST rate in the whole Mekong deltaic coast occurs in the outer areas of the Mekong river estuaries; the winter dominated potential LST gradients control a pattern of erosion and accretion among the adjacent coastal areas of the eastern estuarine regions.

This study utilised the process based model of Delft3D to understand the mechanism of the sediment transport as well as the alongshore sediment budget along the Mekong deltaic coast under the monsoon climate system with wind, wave and tide forcings. As a result of the large magnitude difference of the sediment transport between summer and winter monsoon climate, the mechanism of annual residual transport, the sediment transport and the corresponding morphodynamics along Mekong deltaic coast are controlled by the winter monsoon. The study illustrated that the morphodynamical process in the eastern Mekong deltaic coast is more complicated than in the western deltaic coast. The study found that the wind and tide forcings increase the residual sediment transport rate along the eastern coast of Camau and this results in critical erosion. Moreover, the study hypothesized that the connected channel systems and overwash areas connecting the East and West deltaic coast supported transport of sediment from the eastern Camau coast to the western Camau coast. The inadequate sediment supply from the Mekong River, relative sea level rise and mangrove squeeze trigger the shoreline to retreat critically. This study intends to contribute to the knowledge and future planning and management of exposed coastlines in general, and the Mekong River deltaic coastline in particular.

Samenvatting

In delta's over de gehele wereld treedt erosie op door het terugtrekken van de kust landinwaarts. Kustformaties worden beinvloed door zeespiegelstijging, door rivier afvoer en sediment toevoer, de energie van getijde- en golfbewegingen, de geologische en klimatologische situatie, en zijn dynamisch en altijd in verandering. Daarnaast hebben menselijke activiteiten een verregaande invloed op de kustdynamiek ten gevolge van de voortdurende constructie en reconstructie van infrastructuur, veranderende afvoerpatronen en sedimenttoevoer in het kustgebied.

De Mekong Delta, de grootste delta van Zuidoost-Azië, en in het bijzonder de kust van de Mekong Delta is onderhevig aan de druk van bovengenoemde factoren. Observatie en studie van de kustlijn is in dit geval een onmisbare basis om een inzicht te krijgen in de evolutie van de kustlijn. Deze studie maakt gebruik van de geïntegreerde methoden van 'Remote Sensing', geografische informatie en statistiek om de evolutie van de kustlijn over de periode van 1973 tot 2015 te onderzoeken aan de hand van multispectrale Landsat-beelden (MSS), 'Thematic Mapper' (TM), een verbeterde versie van 'Thematic Mapper Plus' (ETM +) en 'Operational Land Imager' (OLI). De resultaten laten een algemeen patroon van accretie en erosie zien. De oostelijke kust ondergaat zowel aanzienlijke sedimentatie en erosie, met een uitzonderlijk hoge sedimentatie in de omgeving van en in de Mekong riviermonding, en jaarlijkse hoge erosie van maximaal 40 meter in de *oostelijke* Camau provincie. Ondertussen is de westkust redelijk stabiel met een bijzonder hoge aanwas van land van jaarlijks 90 m bij de commune van Datmui in de westelijke Camau provincie. Deze studie observeert een variatie in de veranderingen van de kustlijn tussen de perioden van 1973-1990, 1990-2005 en 2005-heden. De resultaten illustreren, met behulp van een statistische benadering, dat de mate van kustlijnveranderingen grotendeels verband houdt met de sediment stroom uit de Mekong Rivier, in het bijzonder de afname van sediment als gevolg van de bouw van dammen en zandwinning in de Mekong Rivier gedurende de afgelopen 15 jaar. Voor het behoud van een gezond ecosysteem en kustgebied zijn mangroves van cruciaal belang; mangroves vormen een natuurlijke habitat voor talrijke soorten en dragen bij aan een stabiele kustlijn. Niettemin wordt het bestaan van de mangroven aan de kust van de Mekong Delta bedreigd door zowel natuurlijke gebeurtenissen als door menselijk ingrijpen. Deze studie wil een bijdrage leveren aan het kwantitatieve onderzoek naar de evolutie van het mangrove gebied tijdens 43 jaar, d.w.z. tussen 1973 en 2015, met als doel de evolutie van mangroven en ander landgebruik in de Mekong Delta te documenteren. Landsat-satelliet afbeeldingen zijn gebruikt voor het in kaart brengen van landcategorieën, bestaande uit mangroves, aquacultuur, grondsoorten, en planten en water langs en in de kustgebieden van de Mekong Delta; een classificatie methode is toegepast die 'Iso Cluster' en 'maximale waarschijnlijkheid' algoritmes omvat.

De bevindingen onthullen dat het totale mangrove gebied is geslonken en dat het totale mangrove verlies het gevolg is van zowel de uitbreiding van aquacultuur als van erosie van de kust. Een minimale toename van het mangrove gebied is het gevolg van de natuurbeschermingsprojecten voor het herstel van mangroven en tegen erosie van de kustlijn.

Het is van essentieel belang om een goed inzicht te krijgen in de specifieke kenmerken van de getijdebewegingen voor het manipuleren van de morfodynamica in de Mekong Delta, op de plaat van de Mekong Delta in de Zuid Chinese Zee (South China Sea, a.k.a. East Sea) en de Golf van Thailand (a.k.a. West Sea). De studie gebruikt een tweedimensionaal, barotropisch numeriek model om de dynamiek van de getijdebeweging te bestuderen. De studie geeft aan dat de getijdebeweging zich uitstrekt van de Stille Oceaan tot de Zuid-Chinese Zee, de Straat van Luzon (LS) kruisend, waar, als gevolg van een kwartale golflengte, het dagelijkse K_1 getijde onder controle van de resonantie in dit bekken valt. In het geval van het getij over de shelf van de Mekong Delta is het getij vanuit Celebes dominant over het getij vanuit het gebied van Andaman en Flores. Met behulp van Green's Law, de formule van Clarke en Battisti, en de theorie van de staande golven, werpt de studie een nieuw licht op de aanzienlijk vergrote M_2 semi-dagelijkse amplitude, wat leidt tot een dominante en gemengd semi-dagelijkse vloed, welke o.a. wordt veroorzaakt door de invloed van zandbanken, het fenomeen van oscillatie resonantie van de continentale plaat en de locatie van de anti-node lijn van de staande golf. Bovendien is het bestaan van radiale getijde stromingen langs de zuidelijke kust van de monding van de Mekong niet eerder gepubliceerd in voorgaande studies. Op basis van numeriek en geometrisch geschematiseerd onderzoek wordt voorgesteld dat de relatie tussen de versterkte amplitude bij de kustlijn en het omringende aangrenzende lage amplitude systeem de oorzaak zijn van het radiale getijdenstroomsysteem over de plaat van de Mekong Delta. De studie toont aan dat het moesson klimaat kan leiden tot verminderde óf vergrote amplitudes langs de kust van de Mekong Delta ten gevolge van atmosferische druk, de schuifspanning van de wind over het wateroppervlak en de door de wind versterkte bodemwrijving. De studie geeft aan dat de getijde genererende krachten in acht genomen moeten worden om tot precieze simulatieresultaten te komen, afhankelijk van de geografische regio.

De actie van golven die de kust van de Mekong Delta onder een hoek benaderen veroorzaakt de invallende stromingshoek voor het potentiële kustlangse sedimenttransport. De studie evalueert het specifieke golf klimaat en het bijbehorende paralelle golfgedreven sedimenttransport langs de kust van de Mekong Delta. Het golf klimaat wordt verkregen met behulp van de 'state-of-the-art' spectrale golf model SWAN (Simulating WAves Nearshore). De resultaten tonen aan dat de toename van golfenergie op de shelf van de Mekong Delta door het systeem van het moesson klimaat beheerst wordt. Hoewel in het mondingsgebied een aanzienlijke dissipatie van de branding plaatsvindt tijdens de winter moesson, vindt een aanzienlijke dissipatie van branding langs de westelijke kaap van Camau plaats tijdens de zomer moesson. Terwijl de windvelden in de winter moesson alleen invloed hebben op de golfvelden langs de oostkust, heeft het windsysteem tijdens de zomer moesson een grote invloed op de golven aan zowel de oostelijke als de westelijke kust. Verder zijn de golven hoger in het noordoostelijke gebied van de plaat van de Mekong Delta, terwijl ze afnemen aan de zuidwestelijke en westelijke kust van de Mekong Delta tijdens de winter moesson. Significante golfhoogtes op de westelijke plaat zijn daarentegen groter in vergelijking met de oostelijke kust tijdens

de zomer moesson. De CERC-formule wordt gebruikt om de capaciteit van kustlangs sediment transport (LST) te construeren om de reactie te berekenen van de diverse kustvariaties van de Mekong Delta op het golfklimaat onder invloed van de moessons. De studie toont aan dat de hoogste potentiële LST van de gehele Mekong Delta kust zich voordoet in de buitengebieden van de mondingen van de Mekong Rivier; in de winter worden de potentiële LST gradiënten gedomineerd door een patroon van erosie en accretie tussen de aangrenzende kustgebieden van de oostelijke riviermondingen.

Deze studie gebruikt het model van Delft3D om het mechanisme van het sedimenttransport en het kustlangse sediment budget langs de kust van de Mekong Delta tijdens de moesson met wind-, golf- en getijden velden te begrijpen. Als gevolg van het grote verschil in sedimenttransport tussen de zomer en winter moesson wordt het mechanisme van het jaarlijkse residuele transport, het sedimenttransport en de bijbehorende morfodynamica langs de kust van de Mekong Delta beheerst door de winter moesson. De studie illustreert dat het morfodynamische proces aan de oostelijke kust van de Mekong Delta ingewikkelder is dan aan de kust van de westelijke delta. Uit de studie blijkt dat wind en getij een impact hebben op de mate en de toename van het resterend sedimenttransport langs de oostelijke kust van Camau en dat het resulteert in kritieke erosie. Bovendien heeft de studie de hypothese gesteld dat de aangesloten kanaalsystemen en overstromingsgebieden de kust van de oostelijke en westelijke delta hebben bijgedragen aan het transport van sediment van de oostelijke kust van Camau naar de westelijke kust van Camau. Onvoldoende sediment toevoer van de Mekong Rivier, een relatieve zeespiegelstijging en de ‘mangrove squeeze’ zijn de oorzaken van een zeer kritiek terugtrekken van de kustlijn. Deze studie beoogt een bijdrage te leveren aan de kennis, de toekomstige planning en het beheer van kwetsbare kusten in het algemeen en de kustlijn van de Mekong Rivier in het bijzonder.

1

Introduction

1

1.1 General problem definition

A delta is described as the partly subaerial place of sediment deposition where a river flows into a body of water (Galloway, 1975). Deltaic research, from a geological perspective, began in the late 1880s and focused on the facies architecture, sedimentary processes and stratigraphic evolution of deltaic sedimentary successions (Le Blanc, 1975). Deltas can be categorized in some groups including (1) the dominant process (Galloway, 1975); (2) grain size (Orton et al, 1993); (3) delta morphology (Weise, 1980); (4) sort of feeder; (5) water depth; and (6) mouth-bar category (Postma, 1990).

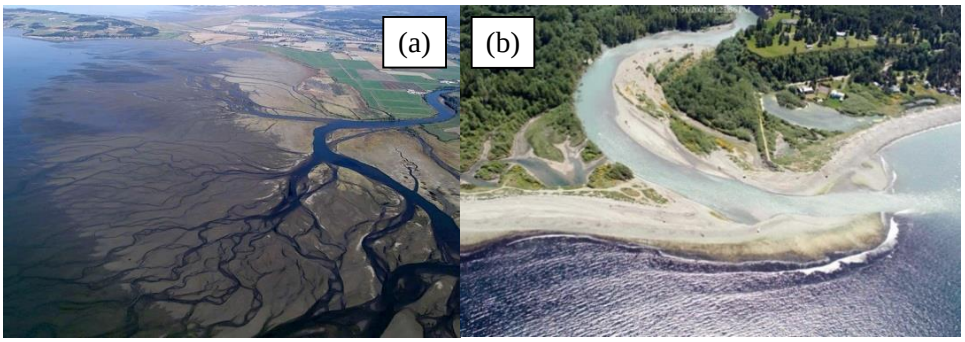

Figure 1.1: River dominated delta (a) Wave dominated delta (b)
(Source: http://www.pugetsoundnearshore.org/landforms.html)

River deltas throughout the world result from the interaction of fluvial and marine forces. Since commonly changes in the dominant processes occur, the evolution of a deltaic system is a non-steady process. Based on the fact that physical conditions along the coast are always changing at least on longer time scales, one may as well conclude that there is no such thing as a "long-term equilibrium" state for any coastal form. Consequently, shorefaces continue to change over time in response to varying wave and meteorological conditions. In addition, all over the world people continue to profoundly influence the coastal environment, changing natural patterns of runoff and littoral sediment supply and by constantly building and modifying engineering works. Deltas worldwide undergo spatial and temporal variations in erosion and sedimentation that affect the deltaic coasts. In the present case of the Mekong Delta this impact is particularly strong. Moreover, the Mekong deltaic coast is strongly dominated by a seasonal monsoon climate through trade winds (Hordoir et al., 2006). Winds are coming mostly from north-eastern directions during the winter monsoon season (from November to April), while south-western winds prevail during the summer monsoon (from May to October). The processes controlling the sediment transport as well as the morphodynamics along the Mekong deltaic coast are inadequately understood. According to the delta classification of Galloway, the Mekong Delta is a tide dominated delta. However, the influence of the tide on the transport of sediment is not completely identified. Also, under the monsoon climate pattern, the role of winds and waves in the sediment transport as well as in the morphodynamics has not been adequately explained to date. Therefore, understanding the mechanism of seasonal sediment dynamics along the Mekong deltaic coast is necessary.

1.2 The Mekong Deltaic Coast

The Mekong River System is the world's second richest river basin in terms of biodiversity (WWF, 2004) with a total length of 4,800 km and an area of 795,000-800,000 km^2; there is a mean annual water discharge of 470 km^3 (Lu and Siew, 2006). The Mekong River discharge is collected from many sources in six countries: China, Myanmar, Lao, Thailand, Cambodia and Vietnam. More than 60 million people from more than 95 distinct ethnic groups live along the main river and its tributaries (WWF, 2004).

The Mekong River Basin covers a vast range of geographic and climatic zones; as a result, it is endowed with diverse and abundant natural resources. Among the world's river basins, only the Amazon has a more diversity of plants and animals. On average, a surprising 15,000 m^3/s of water flows into the Mekong mainstream from the surrounding basin area. Large areas of forest and wetlands which supply constructing materials, food and homes for thousands of species are irrigated.

The Mekong deltaic plain which begins at Phnom Penh covers an area of 62,520 km2. The delta plain can be split into two zones : the inner delta plain situated upstream and controlled by fluvial (river) processes, and the outer delta plain situated nearer the sea which is affected by marine processes such as the impact of tides, waves and ocean currents (Nguyen et al. 2000; Ta et al. 2002). The outer delta is of a moderately higher elevation than the inner delta owing to the development of sand dunes near the coast. The Mekong Delta covers a massive flood plain with an elevation of 0-4 m above mean sea level. It is shaped by eroded sediments in the upper basin which are accumulated in the lower basin (Fedra, 1991).

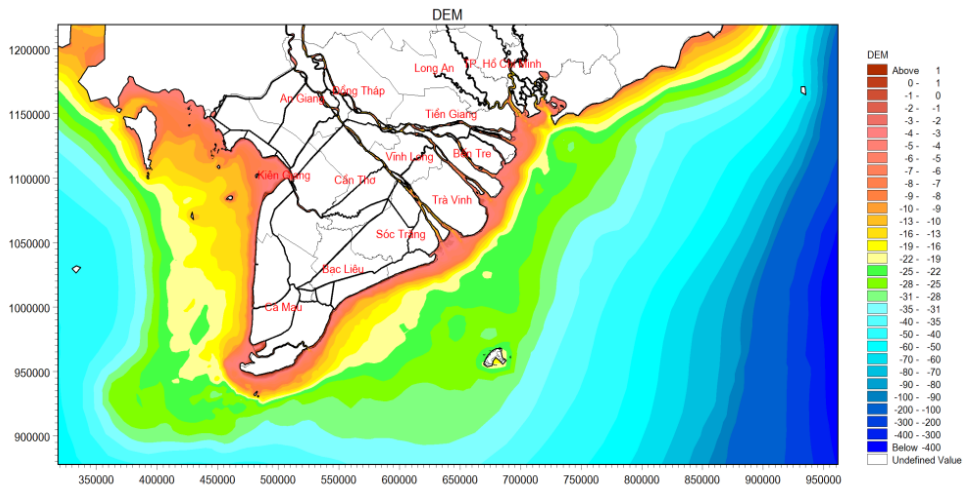

Figure 1.2: Bathymetry (m) of the Mekong deltaic shelf

The river network of the Mekong as it reaches the delta is rather complicated with 9 estuaries laterally connected through a dense canal network. Tonle Sap River joins the Mekong River just west of Phnom Penh. The Mekong then flows across the border into Vietnam, where it soon splits into the Tien (or Mekong) and Hau (or Bassac) Rivers. From

1

the confluence of the Mekong and the Tonle Sap River in Cambodia to the East Sea of Vietnam, the delta is mostly covered with water during the flood season. The Tien River divides into six branches and also the Hau River into three branches and together they form, what is knowned in the Vietnamese language, the "Cuu Long". The Mekong River discharge at Tan Chau is 3 to 5 times larger than that of Chau Doc (Nguyen, 2006). The Vam Nao, the connecting river 20 km downstream of Tan Chau and Chau Doc, conveys/transports water from the Tien River to the Hau River, considerably augmenting the flow downstream of this point.

The Mekong river brings large amounts of sediment to the coast and has developed an extensive delta plain with a range of $5.0 \times 10^4 km^2$ (Hori, 2000). The delta has grown approximately the past 8000 years (Nguyen et al., 2000; Ta et al., 2005; Tamura et al., 2007, 2009), and its top is placed just north of Phnom Penh, Cambodia, over 200 km from the estuaries. From its top, the delta spreads out to the southeast and, along with the Camau Peninsula, splits the South China Sea from the Gulf of Thailand. Almost all earlier studies focus on the Mekong deltaic plain; there exist only few studies on the coastal zone of the Mekong Delta (Unverricht et al, 2013, 2014; Hein et al, 2013, Xue et al, 2012). The highly dynamic coastline of the Lower Mekong Delta is influenced by waves, tidal currents, and by changing sediment loads from the Mekong River.

The whole shoreline is categorized by a dynamic process of sedimentation and erosion. The loss of land of up to 30 m per year by reason of erosion has been recorded in some areas, while in other areas land formed due to accretion can reach up to 60 m per year (Pham et al., 2009; Joffre, 2010; Pham et al., 2011). With such a dynamic shoreline, a belt of narrow mangrove forest is insufficient to keep the coast as well as the sea dykes from erosion. In such a setting, mangrove management cannot be executed effectively through a sectoral approach; it must be part of an Integrated Coastal Area Management (ICAM) approach, including climate change adaptation measures. ICAM needs risk management of the coastal area as a whole, not only of erosion locations. Different options need to be considered depending on site-specific conditions and risk spreading strategies need to be put in place over space and time to address uncertainties, such as dealing with predicted negative impacts of climate change.

The progression of erosion and/or sedimentation along the coastal Mekong Delta is still an issue of debate. In 2005, the Southern Institute of Water Resources Research of Vietnam (SIWRR) executed a study of its coastlines in 1965, 1989 and 2002. The shorelines thus obtained from satellite images were only the result of on-screen digitization using a manual technique by means of visual analysis. This manual process depends mainly on the subjective interpretation of the SIWRR researchers and results in considerable inaccuracy for shoreline outcomes. Besides, the change of coastal land cover, especially of mangrove systems, is impacted by the shoreline evolution, but not yet well assessed.

The coastline of the Mekong Delta stretches for approximately 700 km along the Vietnamese East Sea (South China Sea) and the West Sea (Gulf of Thailand). The larger part of the delta is affected by tides, e.g. through saline intrusion into the river tributaries. Based on the categorization of Davis & Hayes (1984) the coasts of the delta are a mixed-energy (tide-dominated) conditions affected by the flow regime of the Mekong River and its sediment discharge, the tidal regime of the Vietnamese East Sea and the Gulf of Thailand, as well as by the coastal long-shore currents driven by prevailing monsoon winds and the corresponding wave conditions (Delta Alliance, 2011). The East coast, north of Ben

Tre Province to Cape Ca Mau, is influenced by the irregular semi-diurnal tide of the East Sea with a tidal amplitude of 3.0 - 3.5 m. From Cape Ca Mau to Kien Giang along the west coast, the tides are irregularly diurnal with a tidal range of approximately 0.8 - 1.2 m (Delta Alliance, 2011). While several studies investigated the tidal propagation in the South China Sea, tidal wave characteristics on the shallower southern Vietnam shelf, comprising the Mekong deltaic coast, are rarely taken into account. Since the Mekong deltaic shelf is an intermediary region connecting the deep sea of the South China Sea to the shallow sea of the Gulf of Thailand, the characteristics of the tidal wave propagation along the Mekong deltaic coast are distinctive and complex. As it is expected that tidal currents are important for the coastal morphologic processes of the Mekong Delta, it is essential to gain insight in the tidal wave propagation on the Mekong deltaic shelf. At the Mekong river mouths, the maximum and mean tidal fluctuations are 3.8 m and 2.5 m, respectively (Saito, 2015). The mean tide range falls in the upstream direction (Gagliano & McIntire, 1968). All studies conclude that diurnal tides mainly dominate in the entire South China Sea, even comprising the Sunda Shelf and the Gulf of Thailand while in contrast semi-diurnal tides mostly control the region of Vung Tau and Ca Mau Cape.

The monsoons trigger apparent differences in river flow and coastal wave conditions between summer and winter (i.e., rainy and dry seasons). The rainy season starts in late May and ends during October to November. At the Kratie monitoring station on the Mekong River, the maximum daily discharge in summer is about ten times the average daily discharge in winter. There is a reversal of the direction of the propagation of ocean waves at the change of season. Waves generated by the summer south-west monsoon are mostly from the south- to south- west, whereas the winter north-east monsoon generates relatively strong waves from the north- to northeast (Gagliano and McIntire, 1968). The bimodal distributions of wave direction in spring and autumn show these to be transitional periods between the dry and wet seasons. The northeaster waves are generally higher and, thus, stronger than the southwester waves. Complicated coastal processes occurring on various temporal and spatial scales lead to shoreline changes (Stive et al, 2002). The incoming waves towards the coast at an angle cause breaking wave incident angles for the potential longshore sediment transport. Xue et al. (2012) utilizes ROMS (Regional Ocean Modeling System) for the coastal ocean movement and SWAN (Simulating WAves Nearshore) for the wave fields in the eastern Mekong deltaic coast to analyse the transport and dispersion of Mekong derived sediment during August and December in 2005. However, Xue et al. has not assessed the process of the wave evolution from the lower shoreface zone to the upper shoreface zone in adequate detail. Tas (2016) applied SWAN to convert the offshore boundary conditions into nearshore conditions and used the non-hydrostatic, wave-phase resolving model of SWASH conditions (Zijlema et al, 2011) as input to compute the wave transformation up to the western coastline of the Mekong Delta. In both studies wave measurements data to validate the wave models are absent. Moreover, the significance of the seasonal monsoon climate for the wave characteristics on the Mekong deltaic shelf was not considered in these studies.

Ocean currents show similar seasonal trends in direction as the direction of the waves (Gagliano and McIntire, 1968). Dominantly southwestward sediment transport is indicated by the asymmetric geometry of beach ridges and by the formation of the southwestern edge of the delta of the Camau Peninsula, which is composed of finer sediments than those near the river mouths (Nguyen et al., 2000; Ta et al., 2005). Earlier geology studies specify that Mekong-derived sediment has a limited cross-shelf dispersal directly seaward of the

distributary-channel mouths, in contrast to a widespread along-shelf, distal deposit extending to the Ca Mau Peninsula (Xue et al., 2010, Xue et al., 2012, Unverricht et al., 2013, Unverricht et al., 2014). Using numerical modelling with the Princeton Ocean Model, Hordoir et al. (2006) illustrated that the Mekong river plume relates to a seasonal cycle and that the reversal expanse of the Mekong river plume is produced by the monsoon climate; i.e., northeastward in winter and south-westward in summer. Meanwhile, Xue et al., 2012 indicates that a great amount of fluvial sediments was brought and dropped near the Mekong River mouths in summer. Subsequently, strong ocean mixing and coastal currents trigger resuspension and southwestward dispersion of a small fraction of earlier dropped sediments in the succeeding winter. Hein et al. (2013) indicated that the development of the sub-aquatic delta is still continuing near the river mouths. Nevertheless, these studies focus mostly on the estuarine areas; sediment dynamics in the south-eastern and western coasts of the Mekong Delta have not been considered yet. Hence, as a result of the complicated and different morphology along the entire Mekong deltaic coast, the general sediment dynamics are still inadequately identified.

1.3 Objectives and study approach

1.3.1 Objectives

The main objective of this thesis is to achieve a better understanding on the tide-induced and the wave-induced hydrodynamics, sediment dynamics and seasonal morphodynamics in the coastal zone of the Lower Mekong Delta, especially in the context of its shoreline and land cover changes.

Specific objectives:

- ✓ To define the land cover and morphology changes along the Mekong deltaic coast over the recent 43 years.
- ✓ To study the tidal wave characteristics on the Mekong deltaic shelf.
- ✓ To construct the seasonal nearshore wave climate and the subsequent wave induced alongshore sediment transport along the Mekong deltaic coast.
- ✓ To clarify the seasonal mid-term coastal morphodynamics under the forcing of tides, wind and waves in the Mekong Delta.

1.3.2 Study approach

The above reseach objectives require the use of a series of methodologies. They vary from the analysis of shoreline changes extracted by Remote Sensing and GIS techniques to theoretical analysis and numerical modelling in order to understand the mechanism of seasonal, monsoon-related morphodynamics.

Our study examines the changes of the shorelines of the Mekong deltaic coast that occurred over 43 years from 1973 to 2015. Shorelines were determined using Landsat images for 1973, 1979, 1990, 1995, 2000, 2005, 2010, 2015 through Remote Sensing and GIS techniques. The Tasseled Cap and Normalized Difference Water Index bands input was used to create a 10 class land cover data set. Then, the land cover data set was reduced from 10 to 2 classes of land and water and finally shorelines were created from 2 classes by using contour and smooth line commands. The shorelines change rates were calculated

using the Digital Shoreline Analysis System (DSAS) version 4.3, an ArcGIS extension for calculating shoreline change developed by the USGS. Besides, the transformation of coastal land cover was also analysed over 43 years in the period of 1973-2015 by using Multispectral, Thematic Mapper, Enhanced Thematic Mapper Plus, and Operational Land Imager of Landsat images. Satellite Landsat images, along with a classification method comprising the unsupervised classification methodology of Iso Cluster and the supervised classification of Maximum Likelihood algorithms, have been used for mapping land cover types including aquaculture, soils, plants and water surfaces along the coastal districts of the Mekong Delta, in particular for the mangrove forests, which latter have strongly effected shoreline changes. Finally, an analysis of post-classification change was performed.

The depth-averaged tidal dynamics model for the whole South China Sea (a.k.a. East Sea) has been constructed using Delft3D-FLOW, which includes the shallow water equations, the continuity equations and the transport equations for conservative constituents. A total of 8 primary tidal constituents (O1, K1, P1, Q1, M2, S2, K2, N2) derived from 15 years of Topex-Poseidon and Jason-1 satellite altimetry have been applied for tidal simulations. A derivation of the co-tidal patterns, tidal current ellipses of the main tidal components, the residual currents and the geographical distribution of tidal types as well as a sensitivity analysis of the open boundaries were conducted. Effects of several factors, such as wind climate monsoon and tidal generating forces were examined using numerical experiments of the tidal wave propagation.

In order to derive the seasonal nearshore wave climate and the wave induced alongshore sediment transport along the Mekong deltaic coast, the state-of-the-art spectral wave model SWAN (Simulating WAves Nearshore) was utilised. This model was executed in the third generation, nonstationary mode with spherical coordinates to accurately predict wave height fields, wave spectra and wave dissipation in the coastal region. To quantify the response of shoreline changes of the Mekong Delta to wave conditions under the monsoon climate system, the CERC formula was employed to produce a Longshore Sediment Transport capacity variation. This helped to explain in a qualitative and less accurate quantitative sense the spatially varying sedimentation and erosion along the Mekong deltaic coast.

We applied the process based numerical model of Delft3D in this study to simulate the transport and dispersal of Mekong-derived sediment. Due to the shallow water depth, wind fields play an important role for waves along the Mekong deltaic coast, especially under wind monsoon climate system. Different scenarios are established to investigate the relative effect of tide, wave and wind on the residual flow and residual sediment transport patterns under the seasonal and annual monsoon climate. Based on the results of the spatially varying sediment transport, an alongshore sediment budget is developed to analyse and explain the seasonal morphodynamics processes for the Mekong deltaic coast.

1.4 Outline

As a starting point, it is necessary to have an overview of the coastline as well as the land cover evolution along the Mekong deltaic coast in order to understand the dynamics of the present-day flat basin system. In **Chapter 2**, Remote Sensing, GIS and statistical analyses are utilized to monitor coastline and land cover changes of the coastal area of the Mekong Delta over the period of 1973 to 2015 from Landsat images. Being one of the key factors in controlling morphological processes of the Mekong deltaic coast, it is

essential to achieve a good understanding of the principal mechanisms of tidal wave propagation on the Mekong deltaic shelf from the South China Sea to the Gulf of Thailand. In **Chapter 3**, a two-dimensional, barotropic numerical model was employed to investigate the dynamics of tidal wave propagation in the South China Sea with a particular interest for its characteristics along the Mekong deltaic coast. Wave action is one of the important factors influencing the sediment transport along the Mekong deltaic coast. Knowledge of the representative wave climate and the associated longshore wave-driven sediment transport capacity is analysed in **Chapter 4**. Finally, the study employed the process-based model of Delft3D to clearly quantify the role of each factor, including tide, wind and waves influencing the residual current as well as the sediment transport along the Mekong deltaic coast under the seasonal monsoon climate system in **Chapter 5**. **Chapter 6** summarizes the results and findings in relation to the research objectives from this study and provides recommendations for further research.

References

Davis Jr., R.A., Hayes, M.O.,1984.What is a wave-dominated coast. Marine Geology 60: 313-329.

Delta Alliance, 2011. Mekong Delta Water Resources Assessment Studies – Vietnam-Netherlands Mekong Delta Masterplan Project. http://wptest.partnersvoorwater.nl/wp-content/uploads/2011/08/WATERRESOURCESfinaldraft.pdf, accessed 17.04.2013.

Fedra, K., Winkelbauer, L. and Pantulu. V.R., 1991. *An Application in the Lower Mekong Basin.* RR-91-19. International Institute for Applied Systems Analysis. A-236l Laxenburg, Austria 169p.

Gagliano, S.M., McIntire, W.G., 1968. Reports on the Mekong Delta. Coastal Studies Institute, Louisiana State University Technical Report 57, 144 p.

Galloway, W.E., 1975. Process framework for describing the morphologic and stratigraphic evolution of deltaic depositional systems. In: Broussard, M.L. (Ed.), Deltas, Models for Exploration. Houston Geol. Soc., Mem. 13, pp. 87–98.

Le Blanc, R.J., 1975. Significant studies of modern and ancient deltaic sediments. In: Broussard, M.L. (Ed.), Deltas, Models for Exploration. Houston Geol. Soc., pp. 13–85.

Lu, X.X., Siew, R.Y., 2006. Water discharge and sediment flux changes over the past decades in the Lower Mekong River: possible impacts of the Chinese dams. Hydrology and Earth System Sciences 10, 181-195.

Hein, H., Hein, B., Pohlmann, T., 2013. Recent sediment dynamics in the region of Mekong water influence. Global and Planetary Change 110, 183-194.

Hordoir, R., Polcher, J., Brun-Cottan, J.-C., Madec, G., 2006. Towards a parametrization of river discharges into ocean general circulation models: a closure through energy conservation. Climate Dynamics 31 (7–8), 891–908.

Hori, H., 2000. The Mekong: Environment and Development. United Nations University Press, Tokyo. 398 pp.

Joffre, O. (2010) Mangrove Dynamics in Soc Trang Province 1889- 1965. Deutsche Gesellschaft fur Internationale Zusammenarbeit (GIZ) GmbH Management of Natural Resources in the Coastal Zone of Soc Trang Province, Vietnam. 35 pp.

Nguyen, A. D. and Savenije, H. H. G., 2006. Salt intrusion in multi-channel estuaries: a case study in the Mekong Delta, Vietnam. Hydrol. Earth Syst. Sci., 10: 743-754.

Nguyen, L.V., Ta, T.K.O., Tateishi, M., 2000. Late Holocene depositional environments and coastal evolution of the Mekong river delta, Southern Vietnam. Journal of Asian Earth Sciences 18 (4), 427–439.

Orton, G.J., Reading, H.G., 1993. Variability of deltaic processes in terms of sediment supply, with particular emphasis on grain size. Sedimentology 40, 475–512.

Pham, T.T., Hoang, T., Tran, H.M., Le Trong , H., Schmitt, K. (2009) Tool Box for Mangrove Rehabilitation and Management. Deutsche Gesellschaft fur Technische Zusammenarbeit (GTZ) GmbH, Management of Natural Resources in the Coastal Zone of Soc Trang Province, Vietnam.

Pham, T.T., Meinardi, D., Schmitt, K. (2011) Monitoring of Mangrove Forests. Deutsche Gesellschaft fur Internationale Zusammenarbeit (GIZ) GmbH, Management of Natural Resources in the Coastal Zone of Soc Trang Province, Vietnam.

Postma, G., 1990. Depositional architecture and facies of river and fan deltas: a synthesis. In: Colella, A., Prior, D.B. (Eds.), Coarse-Grained Deltas. IAS Spec. Publ., vol. 10, pp. 13–27.

Saito, Y., Nguyen, V. L., Ta, T. K. O., Tamura, T., Kanai, Y., Nakashima, R., 2015. Tide and river influences on distributary channels of the Mekong River delta. American Geophysical Union, Fall Meeting 2015, abstract #GC41F-1148.

Stive, M.J.F., Aarninkhof, S.G.J, Hamm, L., Hanson, H., Larson, M.,Wijnberg, K.L., Nicholls, R.J., Capobianco M., 2002. Variability of shore and shoreline evolution. Coast Eng 47(2): 211–235.

Ta, T.K.O., Nguyen, V.L., Tateishi, M., Kobayashi, I., Saito, Y., Nakamura, T., 2002. Sediment facies and Late Holocene progradation of the Mekong River Delta in Bentre Province, southern Vietnam: an example of evolution from a tide- dominated to a tide- and wave-dominated delta. Sedimentary Geology 152 (3–4), 313–325.

Ta, T.K.O., Nguyen, V.L., Tateishi, M., Kobayashi, I., Tanabe, S., Saito, Y., 2002a. Holocene delta evolution and sediment discharge of the Mekong River, southern Vietnam. Quaternary Science Reviews 21 (16–17), 1807–1819.

Tamura, T., Saito, Y., Sieng, S., Ben, B., Kong, M., Choup, S., Tsukawaki, S., 2007. Depositional facies and radiocarbon ages of a drill core fromtheMekong River lowland near Phnom Penh, Cambodia: evidence for tidal sedimentation at the time of Holocenemaximum flooding. J. Asian Earth Sci. 29, 585–592.

Tamura, T., Saito, Y., Sieng, S., Ben, B., Kong, M., Sim, I., Choup, S., Akiba, F., 2009. Initiation of the Mekong River delta at 8 ka: evidence from the sedimentary succession in the Cambodian lowland. Quatern. Sci. Rev. 28, 327–344.

Unverricht, D.,Szczucinski, W., Stattegger, K., Jagodzinski, R., Le, X.T., Kwong, L.L.W., 2013. Modern sedimentation and morphology of the subaqueous Mekong Delta, Southern Vietnam. Global and Planetary Change 110, 223-235.

Unverricht, D., Nguyen, T.C., Heinrich, C., Szczucinski, W., Lahajnar, N., Stattegger, K., 2014. Suspended sediment dynamics during the inter-monsoon season in the subaqueous Mekong Delta and adjacent shelf, southern Vietnam. Journal of Asian Earth Sciences 79, 509-519.

Weise, B.R., 1980. Wave-dominated deltaic systems of the Upper Cretaceous San Miguel Formation, Maverick Basin, South Texas. Report of Investigations107, Texas Bureau of Economic Geology, Austin, Texas, 39 pp.

World Wide Fund for Nature [WWF] (2004) Seven from Mountain to Sea: Asia Pacific River Basin Big Wins. WWF International, Switzerland.

Xue, Z., He, R., Liu, J. P., Warner, J. C., 2012. Modelling transport and deposition of the Mekong river sediment. Continental Shelf research 37, 66-78.

Xue, Z., Liu, J. P., Ge, Q., 2010. Changes in hydrology and sediment delivery of the Mekong River in the last 50 years: connection to damming, monsoon, and ENSO. Earth Surf. Proccess. Landforms 36, 296-308.

Zijlema, M., Stelling, G. and Smit, P., 2011. SWASH: An operational public domain code for simulating wave fields and rapidly varied flows in coastal waters. Coast. Eng., 58, 992-1012.

2

Shorelines, mangroves and coastal land cover along the Mekong Delta

The coastal zone of the Mekong Delta is suffering under intense pressures from climate change as well as human intervention. Coastline monitoring is essential to understand and manage a coastal zone. In order to monitor coastline changes over the period of 1973 to 2015 from Landsat images of the coastal area of the Mekong Delta this study utilizes several integrated techniques of remote sensing, geographic information systems and statistics. The Tasseled Cap and Normalized Difference Water Index algorithms were applied to separate the land-water interface for extracting shorelines. A digital shoreline assessment system tool was applied to analyze the rate of shoreline changes using statistical parameters, as Shoreline Change Envelope, End Point Rate and Linear Regression. Uncertainty assessment for this methodology is based on topographic surveys and Google Earth images. This research investigated the relationship between the accretion and erosion of land and the sediment load deposits of the Mekong River, revealing a particular pattern of erosion and accretion. The eastern coast is fragmented by 9 estuaries and both significant accretion and erosion is observed, especially an annual erosion rate of around 40 meter at Bo De estuary is observed. Meanwhile, the western coast is rather stable in general, especially an annual accretion rate of up to 90-95 meter at Datmui commune of Camau Province is

This chapter is based on an under review paper of the *Journal of Coastal and Ocean Management* and a conference paper published in the *6th ICEC 2018*

observed. This study indicates that there exist differences in coastline change rates among the periods of 1973-1990, 1990-2005 and 2005- present.
Besides, in the Mekong Delta, coastal mangrove forests play an important role in sustaining a healthy and stable coastal environment, providing a natural habitat to the rich variety of plant and animal species as well as stabilizing the shorelines. However, the mangroves forests along the tidal coast of the Mekong Delta in southern Vietnam increasingly face the impact from both natural and anthropogenic drivers. Since the extent of the mangrove areas in the coastal Mekong Delta is not well surveyed, this study aims to quantitatively document the evolution of the mangroves and other land cover areas over the past 43 years, i.e. from 1973 to 2015. Satellite Landsat images, along with a classification method comprising Iso Cluster and Maximum Likelihood algorithms, have been used for mapping land cover types which include the mangroves, aquaculture uses, soils, plants and water surfaces along the coastal districts of the Mekong Delta. The study shows that remote sensing and GIS techniques can be applied to achieve mapping of the land cover, as well as to detect and analyse spatial and temporal changes caused by e.g. coastal erosion or aquaculture expansion. The findings reveal that the total mangrove area of an estimated 185,800 ha in 1973 decreased significantly to 95,960 ha in 2015. Approximately 2170 ha/yr of a total mangrove loss over 1973-2015 was due to incursion of mangrove areas by aquaculture, while roughly 430 ha/yr was lost due to coastal erosion. A slight increase in mangrove area occurred since 2010 as a result of the implementation of a series of projects to protect against coastal erosion and restoration of mangroves by the Vietnamese government and by international non-governmental and governmental organizations. The success rate of mangrove restoration are relatively low. The failure of survival of mangrove forests in the Mekong Delta is related to the main pressure drivers: pollution, land use conversion, insufficient sediment sources, coastal erosion and coastal mangrove squeeze. To succeed and to achieve a beneficial balance between both aquaculture and the ecosystem of mangrove forests, an integrated sustainable mangrove- and shrimp farming model is one of the most appropriate approaches.

2.1 Introduction

The coastal zone encompasses that area of land, which is significantly influenced by the sea and, vice versa, where the land notably influences the sea. Seventy-five per cent of the world's mega-cities are located in coastal zones and 90 per cent of the global fishery activity occurs in coastal waters. The coastal zones of the earth are extremely diverse and tremendously important, not only for human beings but for all living species. Coastlines are shaped by natural forces and often transform in response to changing environmental conditions and anthropogenic disturbances (Manoj et al., 2015). The shape of a coast is influenced by factors as: (1) relative sea level rise i.e. the sum of eustatic sea level rise, natural and human induced subsidence, (2) wave action and, most important in this study, (3) sediments (Syvitski & Saito, 2007). Sediments are primarily transported by wind-induced waves and flow currents – either tidal currents or currents in rivers that flow into the sea. Depending on the level of currents, sediments are either eroded, redistributed or deposited (accumulation), thus changing the shape of the coast over time.

In recent years, the coastal Mekong Delta is facing a severe erosion process, which is affecting the living conditions of local people. The evolution of erosion and accretion of the coastal Mekong Delta is yet a not fully understood process. Analysis of shoreline changes is instructive in determining coastal danger zones and detecting short-, medium- and long-term changes in coastal areas (Ford, 2013). The Southern Institute of Water Resources Research of Vietnam implemented the analyses of shorelines for the years 1965, 1989 and 2002 (SIWRR, 2005). The method used to extract shorelines from images is simply the on-screen digitization as a manual method using visual interpretation. This method depends largely on the subjective interpretation of implementer and it leads to high manual errors for shorelines result. Besides, none of these studies has fully assessed the accuracy of the derived shorelines through comparison with simultaneous and independent in situ observations.

Mangroves are an extremely prolific ecosystem providing numerous goods and services both to the coastal environment and its residents (Kathiresan., 2012). Mangrove forests are home to a rich variety of fish, crab, shrimp and mollusc species (Lee et al., 2014). The dense root systems of mangroves trap sediments, aiding in stabilizing the coastline and preventing erosion from waves and damaging storms (Marshall, 1994; Suzuki et al., 2011). Mangrove forests in the Mekong Delta covered more than an estimated area of 410,000 ha in 1943 (Sam et al., 2005). The dominant mangrove species in the coastal Mekong Delta include Avicennia sp., Rhizophora sp., Bruguier asp. and Sonneratia sp. (Duke et al., 2010). War, forest fires, collection of wood for fuel and timber, coastal erosion, as well as other human activities have resulted in the reduction of the mangrove forest coverage in the Mekong Delta. The use of herbicides by the USA in the Vietnam War between 1962 and 1971 devastated approximately 105,000 ha, comprising 36% of the total extent of mangroves in South Vietnam (NAS, 1974). With the end of the war, in the 1980s a change took place from a centralized economy to a household-based economy. Agriculture developed remarkably fast, converting the poverty-stricken country into a rice exporting country, nevertheless leading to mangrove degradation as a result of rice farming practices and aquaculture expansion. Especially since the end of the 1990's many areas of mangrove forests have been cleared for shrimp farming (Hao, 1999). Aquaculture area in the lower Mekong Delta of Vietnam increased 4.3%/yr from 546.800 ha to 769.000 ha in the period

of 2001-2010 (http://xttm.agroviet.gov.vn/Site/vi-vn/76/tapchi/69/108/7832/Default.aspx, MARD). Population pressure and economic development have led to an increasing need for land for agricultural and aquaculture production in recent years being one of the main drivers for the changes in mangroves area. A few studies on mangroves change were only implemented in some local areas (Veettil et al., 2019; Bullock et al., 2017), but accurate and timely information on the spatial – temporal dynamics of these changes in the whole coastal region of Mekong delta have not been investigated.

Understanding the situation of coastlines and mangrove forests by monitoring and assessing mangrove dynamics is important to allow for a better management of coastlines, mangroves and other land cover systems (Wang et al., 2004). Aerial photography and ground survey techniques are conventionally used for coastline and land cover monitoring. Observation of the temporal changes of the shoreline and the land cover areas is a challenge when based on ground surveys. Classical ground surveying produces high precision results, but are demanding, time-consuming and high-cost procedures (Alesheikh et al., 2007; Appeaning Addo et al., 2008; Van and Binh, 2009). Aerial photogrammetry can also provide high-precision information; however, for large areas this is a high-cost method and the extraction of photogrammetric data and the production of maps are highly time consuming (Alesheikh et al., 2007). In addition, these techniques are inherently limited in temporal coverage, typically being either too short to identify long term trends, or too widely spaced in time to distinguish short term, seasonal changes. A more efficient method for the mapping of coastal habitats and shoreline in recent years is Remote Sensing (Kirui et al., 2012). Remote Sensing is a powerful tool for monitoring the spatial and temporal transformations of the coastline, mangrove forests and other land covers; it is cost-effective, time-efficient and able to access remote and unreachable regions (Kuenzer et al., 2011). Furthermore, Remote Sensing and Geographic Information System (GIS) assist in the continuous detecting and monitoring of changes that can then be integrated into existing databases. The results are valuable for the planning of a sustainable management of coastal areas (Koedam et al., 2007).

Images of IKONOS, QuickBird, SPOT, WorldView, Kompsat have been widely applied for the mapping of the extent of land cover and shoreline as a result of the availability of higher resolutions of up to 0.25 meter (Wang et al., 2004, Gandhi and Sarkar, 2016; Wu et al., 2016; Wilson et al., 2019). However, the cost to realize commercial satellite images to continuously monitor long term coastline and land cover change on a large spatial scale is high. In recent years, free downloadable MODerate Imaging Spectroradiometer (MODIS) data are widely used in diverse fields of study, including land cover extent detection (Ogilvie et al., 2015; Rahimi et al., 2015), but the low spatial resolution ranging from 250 to 500 meter is a disadvantage compared to the free downloadable satellite images as Landsat. As a product provided by the U.S. Geological Survey (USGS) and NASA, Landsat stands for the longest uninterrupted collection of spatial moderate-resolution (ranging 15-30m) remote sensing data in the world. Landsat images collected over four decades are a helpful resource for global studies in agriculture, geology, forestry, land cover, the management of erosion, emergency reaction and disaster assistance (http://landsat.usgs.gov). In our study, the data from multispectral satellite sensors as Landsat MSS, TM, ETM+ or OLI, allow for/enable an effective refinement between mangrove and nearby non-mangrove regions (Haito et al., 2003, Nguyen et al., 2013, Hu et al., 2018). Although the remote sensing technique has been broadly applied for assessing

coastline change as well as the health of different types of ecosystems, detailed environmental assessments of wetlands in the coastal area of South Vietnam are still scarce.

In the lower Mekong River Delta, a few studies have applied Remote Sensing and GIS to detect changes of the coastline and mangrove cover (Binh et al., 2005; Koedam et al., 2007; Nguyen et al., 2013), but these concern local studies covering the last 10 to 20 years. An overview of shoreline, mangroves and other land-use areas in the entire coastal region of the Mekong Delta, using consistent data sources and methodologies, is not available. Moreover, the influence of two main drivers, aquaculture and agriculture, on coastal erosion has not yet been identified as a cause of a reduction in the mangrove extent in previous studies. Therefore, the objectives of this study are twofold. Firstly, it is necessary to quantify the shoreline change in the Mekong deltaic coast over the past 43 years (between 1973 and 2015). Secondly, it will present an overview of the dynamics of the mangrove forest and land cover ecosystem in the Mekong Delta on a spatial and temporal scale from 1973 to 2015, in order to contribute to a better understanding of mangrove loss associated with diverse drivers. The causes of mangrove reduction may vary from region to region as land use changes. The results are necessary to assist in setting clear goals for local conservation, economic development and coastal protection management in particular, and the development of regional action plans in general.

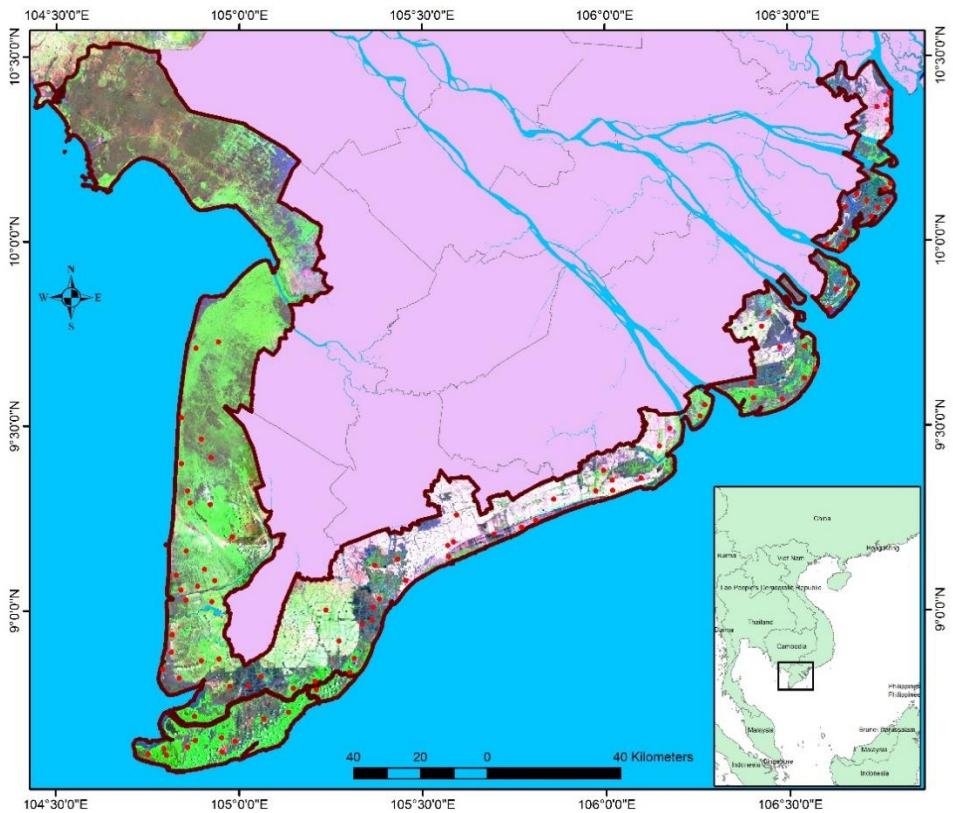

Figure 2.1: Study area and collected sites for accuracy assessment in red color along the coastal Mekong delta

2.2 Shoreline evolution along the Mekong deltaic coast

To investigate the evolution of shorelines along the Mekong deltaic coast in the recent decades, Remote Sensing and GIS techniques were employed to estimate the trends in the coastline change during 43 years. This study aims to give the overview of shoreline processes for the Mekong deltaic coast on the spatial and temporal scales.

2.2.1 Data and method

a) Data

Multitemporal remote sensing data of the Landsat Multispectral Scanner (MSS), Landsat Thematic Mapper (TM), Landsat Enhanced Thematic Mapper (ETM+) and Landsat Operational Land Imager (OLI) from 1973, 1979, 1990, 1995, 2000, 2005, 2010, 2015 are archived on U.S. Geological Survey (http://earthexplorer.usgs.gov). Due to a coastline length of 600km, five adjacent Landsat paths/rows (path 124, 125, 126 and row 53, 54) are needed to cover the entire Mekong deltaic coast.

In this study, satellite images were used to quantify the changes along the coastline of the lower Mekong Delta including the images in 1973 and 1979 are collected from the Landsat 1, 3 MSS, the images in 1990, 1995 and 2000 from Landsat 5 TM, the images in 2005 and 2010 are taken from Landsat 7 ETM+ and the image in 2015 is obtained from Landsat 8 OLI. Most of the images used in this study were taken in the dry season so that the coastline could be easily identified with a cloud cover less than 20%.

b) Method

The methods used to extract shorelines from satellite images can be divided into two groups: on-screen digitization as a manual method using visual interpretation, and semi-automatic/automatic shoreline extraction (Kusimi and Dika, 2012). Onscreen digitizing techniques have been used in various studies for spatial change mapping (Darvishzadeh, 2000; Harvey and Hill, 2001; El-Asmar and Hereher, 2011), for instance employed to TM satellite images for mapping spatial changes of sand dune positions in the Western Desert of Egypt from 1987 to 2000 (Hereher, 2010). In the growing literature on the semi-automatic/automatic extraction of shorelines using satellite images, most studies use Landsat images (Guariglia et al., 2006; Ouma and Tateishi, 2006) as they are freely available online.

NASA's satellites in the Landsat series have a critical role in monitoring, understanding and managing the resources needed for the sustainabilty of human life, such as food, water and forests. As our population exceeds seven billion people, the impact of human activities on the earth will increase, and Landsat observes those impacts as well as environmental changes. With the longest continuous data stream of the earth's surface as seen from space, NASA's earth-observing Landsat fleet has provided the world with unprecedented information on land cover changes and their residual effects since 1972. The knowledge gained from 40 years of continuous data contributes to research on climate, carbon cycles, ecosystems, water cycles, biogeochemistry and changes to earth's surface, as well as our understanding of the visible human effects on land surfaces. Landsat covers large geographical areas per scene, it has several bands containing values within a range of the

electromagnetic spectrum suitable to assess shoreline changes and it offers fast and free internet access to archived data.

This study examined the changes of the shorelines of the Mekong deltaic coast that occurred over 43 years, from 1973 to 2015. Shorelines were determined using Landsat data for 1973, 1979, 1990, 1995, 2000, 2005, 2010 and 2015. Shoreline changes of the case study were determined for these periods and the effects of shoreline changes on the lagoons were analyzed. ArcGIS 10.2 software (Esri, Redlands, CA) was used for the satellite images processing, shoreline extraction and Digital Shoreline Analysis System (DSAS) tool was used to analyse shoreline change by several statistical parameters. The methodology of the study is presented in Table 2.1. The technical properties are shown below, including atmospheric, extraction of shorelines, shoreline change detection, and accuracy assessment.

Table 2.1: Methodology in process steps for shorelines change detection.

Process Step	Process Name	Description
1	Download and Extract Images	USGS EROS DATA CENTER
2	Atmospheric correction	Sun + radiometric correction
3	Normalized Difference Water Index (NDWI)	Green and Near Infrared Bands
4	Tasseled Cap (Brightness, Greenness, Wetness)	Some bands depending on types of Landsat images
5	Developing approach for Land and Sea creation by combining NDWI and Tasseled Cap (10 classes)	Unsupervised classify by maximum algorithm to create 10 classes
6	Classify Land and Sea (2 classes)	10 classes to 2 classes
7	Create Shore Boundary	Majority filtering, contour and smooth line commands
8	Tidal Correction	Mean Sea Level
9	Shorelines Change Detection	DSAS Tool

- *Atmospheric correction*

To remove the influence of the sun angle on the remotely sensed data, radiometric corrections were carried out. The information of sun azimuth and sun elevation obtained from the image's header file were used for radiometric correction. The digital numbers from the Landsat MSS, TM and OLI images were changed to the top of atmosphere (TOA)

reflectance values. This normalization process is essential for utilizing images from various sensors and producing multi-temporal and/or spatial image mosaics. This process substantially removes variations between the images from sensor differences, the Earth-sun distance and the solar zenith angle (Bruce and Hilbert, 2006; Chander et al., 2009). All images were converted to top-of atmosphere reflectance values as per the suggestion of Chander and Markham (2003) so that a standardized measure could be obtained for comparison between images.

The images were corrected for atmospheric intervention triggered by haze, dust, smoke, etc. using the dark-object subtraction technique (Chavez, 1996). The Dark Object Subtraction (DOS) (Chavez, 1996) model was applied to data that were converted to the reflectance values at earth surface. The DOS model is widely applied and is considered as one of the appropriate methods for radiometric correction in studies of change detection (Song et al., 2001; Mancino et al., 2014). Dark Object Subtraction is a simple empirical atmospheric correction method for satellite imagery, which assumes that reflectance from dark objects includes a substantial component of atmospheric scattering. Dark object subtraction technique looks for each band for the darkest pixel value. The scattering is eliminated through subtracting this value from every pixel in the band. The DOS scheme is an image-based procedure and does not need field measurements as well as that it is simple and easy to utilize (Chavez, 1996). In order to be advantage in atmospheric correction, a toolbox is developed by using Dos model in ArcGIS software.

- *Extraction of shorelines*

The normalized difference water index NDWI was created by integrating the green band with near-infrared band to extract waterline (McFeeters et al., 1996). The green band (0.52–0.6 lm) is sensitive to water turbidity differences as well as sediment and pollution plumes because it covers the green reflectance peak from leaf surfaces. It can be effective for distinguishing wide classes of vegetation. The near-infrared band (0.7–1.1 lm) shows a considerable contrast between land and water features owing to the high degree of absorption by water and the significant reflectance by vegetation and natural features in this range. Thus, the NDWI algorithm, which is a combination of green and near-infrared bands, is ideal for discriminating between land and water at their interface.

NDWI was estimated as (Green - NIR)/(Green + NIR), where Green and NIR are the reflection in the green and near-infrared bands of the MSS, TM, ETM, OLI images, respectively. The NDWI algorithm was applied over the TM, ETM, OLI images of 1973, 1979, 1990, 1995, 2000, 2005, 2010 and 2015. This formulation of NDWI generates an image that the positive data values are characteristically open water areas; while the negative values are normally non-water features (i.e. terrestrial vegetation and bare soil dominated cover types). NDWI has a native ranging of -1 to +1.

This index is created to (1) maximize reflectance of water by employing green wavelengths; (2) minimize the low reflectance of NIR band by water body; and (3) take advantage of the high reflectance of NIR band by vegetation and soil characteristics . As a result, water features have positive values and thus are enhanced, while vegetation and soil usually have zero or negative values and therefore are suppressed (McFeeters et al., 1996).

However, the application of the NDWI dealt with calm water environment as lakes, rivers and lagoons. In water regions with a chaotic nature of wave environment in the near shore surf zone resulted in a high variability in the reflectance values in the green and IR

bands do not achieve their goal as expected. Consequently, the NDWI ratio alone was unable to adequately separate the dry beach from the surf zone.

The Tasseled Cap algorithm has been shown to be a suitable candidate for shoreline extraction (Scott et al., 2003) by using principal components analysis function for converting the original bands of an image into a new set of bands as brightness, greenness and wetness. Tasseled Cap did a good job in differentiating between waves and beach, especially when the classifier option to leave 0.5% of the pixels unclassified was chosen. However, in images with stratus clouds the differentiation between land and sea was often lost resulting in wet soil and beach being grouped into the same category as clouds. To solve this matter the NDWI band was added to band combination with the Tasseled Cap bands. Tasseled Cap and NDWI bands input was taken to create a 10 class land cover data set. Then, land cover data set was reduced from 10 to 2 classes of land and water and finally shorelines were created from 2 classes by using contour and smooth line commands.

The shorelines converted to vector type were edited by visual interpretation and were transmitted to the database after implementing the necessary corrections. Raster data were converted to vector form and then the vector data were generalized as shown in Figure 2.2. To simplify the process of shorelines creation from Landsat data, several models were developed using ESRI's Model Builder. These models helped rapidly to perform many of repetitive tasks when working with the Landsat MSS, TM, ETM+ and OLI datasets.

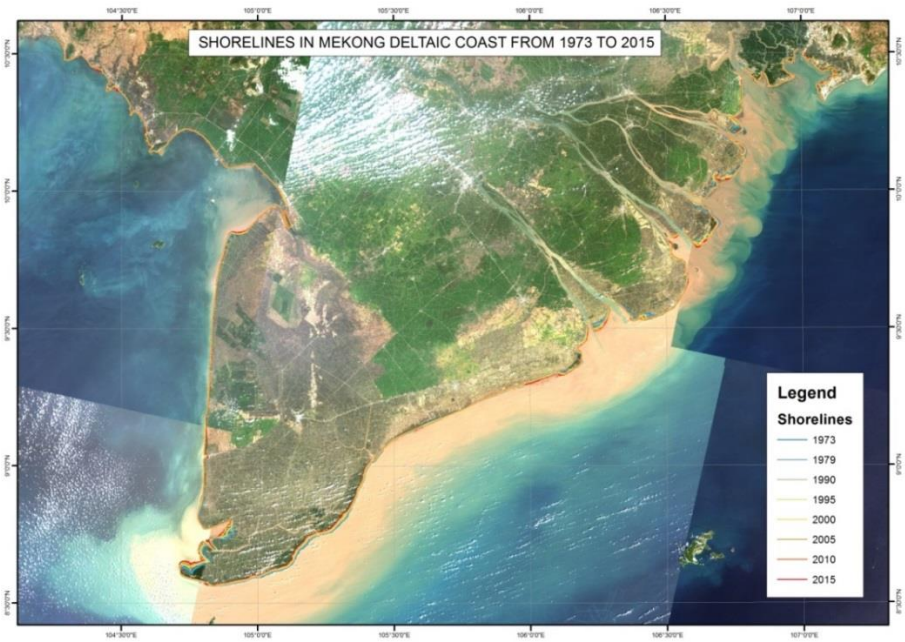

Figure 2.2: Final shorelines extracted from Landsat images from 1973 to 2015

- *Shoreline change detection*

The shorelines change rates were calculated using the Digital Shoreline Analysis System (DSAS) version 4.3, an ArcGIS extension for calculating shoreline change developed by the USGS (Thieler et al., 2009).

A roughly 600 km-long baseline was created approximately 5 km off the coast and parallel to the shorelines on the ocean side to determine the shoreline changes. A total of more than 6000 transects were formed along the baseline at 100 m intervals as shown in Figure 2.3. The 100 m interval is small enough for this study and transect intervals lower than the data resolution would not provide more advanced estimates for detection shoreline change. The changes that occurred in the measurement periods were detected using the NSM, EPR and SCE methods in GIS according to the transects. A polygon overlap investigation was also applied to determine the shoreline changes in the delta, and the areal changes were stablished . The NSM method calculates the distance between the oldest and most-recent shorelines in each transect (Manca et al., 2013).The space between the closest and farthest shorelines is calculated through the SCE method. In this method, unlike the NSM, the most significant changes are calculated independently of the date (Manca et al., 2013). Both NSM and SCE inform a distance, not a rate (Thieler et al., 2009).

The EPR method is different from the NSM and SCE methods and calculates the annual rate of change. EPR value is achieved by dividing the entire coastal change distance by the time difference.

$$\text{EPR} = \frac{\text{NSM}}{\text{Time between oldest and most recent shoreline}}$$

To consider a more detailed shoreline change rate among periods, the periods of 1973-1979, 1979-1990, 1990-1995, 1995-2000, 2000-2005, 2005-2010, 2010-2015 were chosen for the statistical evaluation in this study.

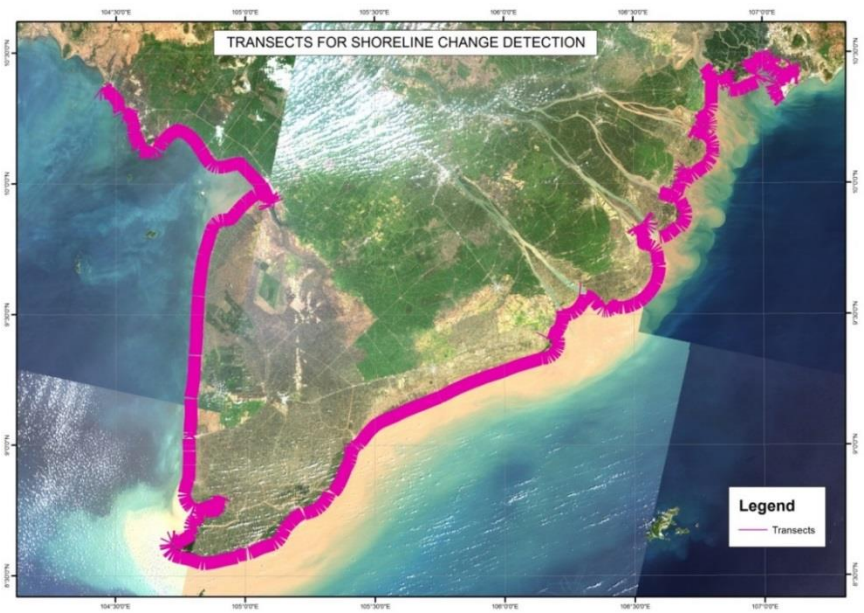

Figure 2.3: Transects generated by DSAS tool for shoreline change detection

- *Accuracy assessment*

The high spatial resolution images provided by Google Earth™ were used as reference for the image from 2000 to 2015. The dates of the reference data and the evaluated images were closely matched to minimize bias in the surface water lines that could arise due to large differences in time. For the validation of extracted shorelines the ‘‘true’’ boundaries between land and water were digitized manually on-screen from all the reference data. Subsequently, total areas were analyzed for each generated reference data and compared with classified Landsat images. To assess the accuracy of the land/water classification for all classified maps, RMSE was used.

The RMSE between the shoreline change by Google Earth and the results of extraction from satellite images was calculated to show the difference of the obtained shorelines.

$$\text{RMSE}= \sqrt{\frac{\sum_{i=1}^{n}(z_i^m - z_i^c)^2}{n}} \sim 10\text{m}$$

In which z_i^m and z_i^c are the shoreline change rates of profile i as estimated by topographic measurement and calculation from satellite images, respectively. The n is the number of profiles along the Mekong deltaic coast taken into account.

2.2.2 Results

Our results showed a variation in the shoreline change rates during the different periods, with a generally decreasing trend as shown in Figure 2.4. The coastal area extended s teadily averaging 21 km^2 in a 5-year period before 1990. However, since 1990 the accretion area started to decrease to only 0.5 km^2 in the 5-year period between 2000-2005, and in the recent years the annual rate of accretion along the Mekong deltaic coast was approximately 1-2 km^2. Although there is a rather complicated change of shoreline over 43 years, in general, sedimentation along the Mekong deltaic coast is still dominant with an annual average accretion of 1.2 km^2. The maximum average accretion rate in over 43 years, from 1973 to 2015, is 105 m/year at western Datmui Commune of Camau Province, meanwhile the maximum average erosion rate is 55 m/yr at Tamgiangdong Commune of eastern Camau Province.

According to the characteristic of morphodynamics the Mekong deltaic coast is divided into 3 areas as indicated in Figure 2.5 and 2.6: 1) the estuarine area from Vungtau to Soctrang, 2) the eastern coast from Soctrang to Camau and 3) the western coast from Camau to Kiengiang.

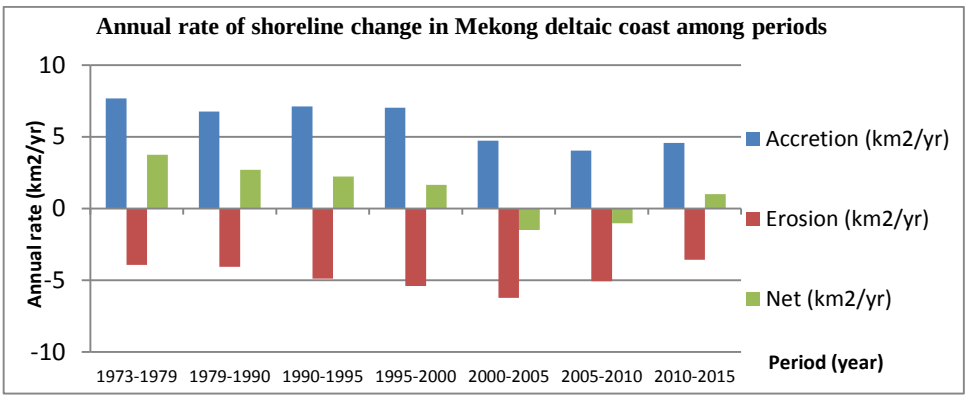

Figure 2.4: Annual rate of shoreline change in Mekong deltaic coast in between periods

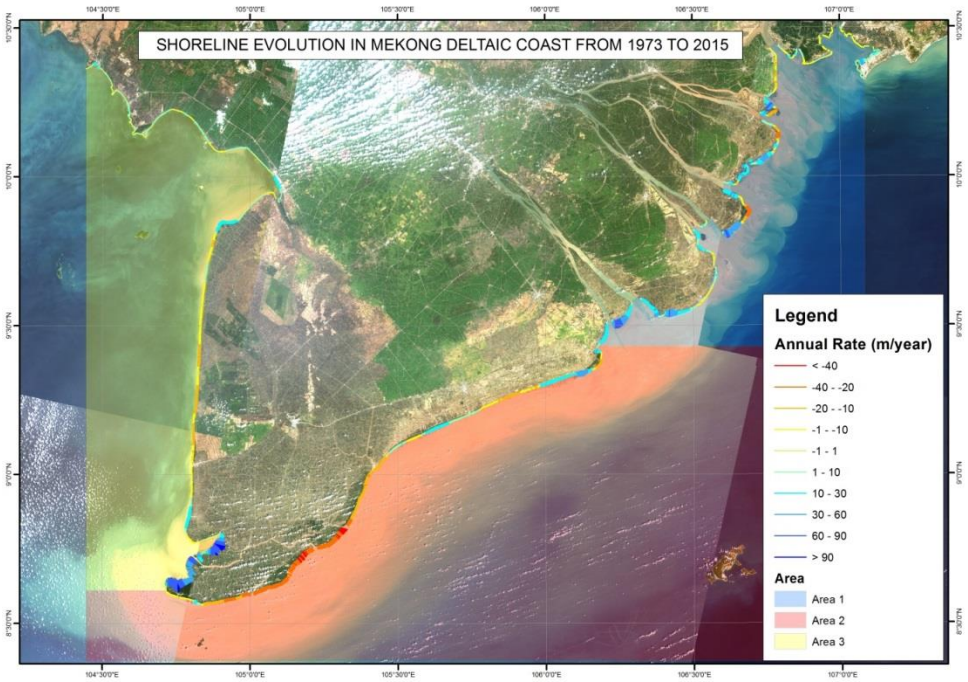

Figure 2.5: Shoreline evolution in Mekong deltaic coast from 1973 to 2015

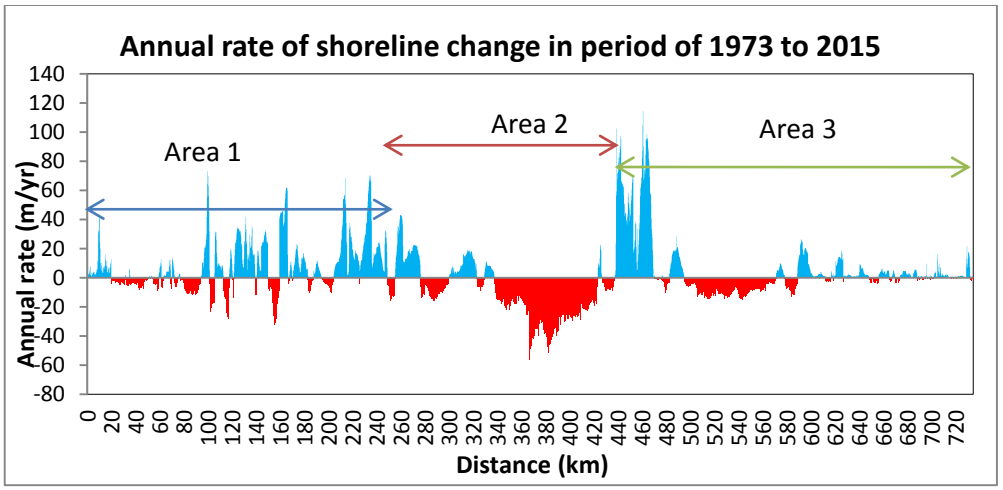

Figure 2.6: Annual rate of shoreline change in the period of 1973 to 2015

a) Area 1: estuaries from Vung Tau-Soc Trang

The distributary river mouths, where the Mekong River flows into the sea, discharge a large amount of sediment, therefore accretion prevails in this area. Accretion mostly occurs on the left-side of estuaries and erosion takes place on the right-side of estuaries; a trend that can be explained by the monsoon climate with a north-eastward affect dominating sediment transport. Figure 2.8 shows several locations where the accretion is greater than 30 m/yr: An Thanh Nam Commune, Soc Trang Province, Dong Hai Commune, Tra Vinh Province, Thanh Phong Commune, Ben Tre Province and Phu Tan Commune, Tien Giang Province. Meanwhile severe erosion occurs with more than 20 m/yr at two locations, namely at Thanh Hai commune and Thua Duc Commune, Ben Tre Province.

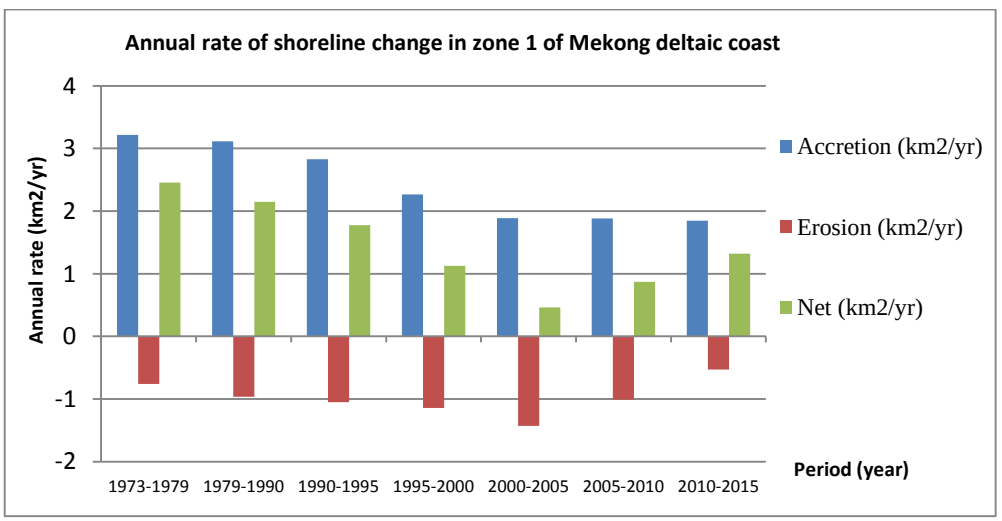

Figure 2.7: Annual rate of shoreline change in zone 1 of Mekong deltaic coast

Figure 2.7 reveals the change of accretion areas from 3.2 km^2/yr in the period 1973-1979 to approximately 1.9 km^2/yr in 2000-2015. Satellite images showed the rate of erosion in the Vungtau-SocTrang area of 0.7 km^2/yr between 1973-1979 doubling to 1.4 km^2/yr between 2000-2005. However, erosion started to decrease to 0.5 km^2/yr between 2010-2015. Consequently, in the period of 1973 to 2015 in area 1 showed a net land gain by on average 1.3 km^2/yr with the lowest value of net gain in land between 2000-2005 at nearly 0.5 km^2/yr. One of the reasons behind this phenomenon is the construction of bank protections during 2004 and 2005, such as revetments in the districts of Go Cong (Tien Giang Province) and Duyen Hai (Tra Vinh Province) and the installation of a system of seadikes along the Mekong deltaic coast (Figure 2.20a).

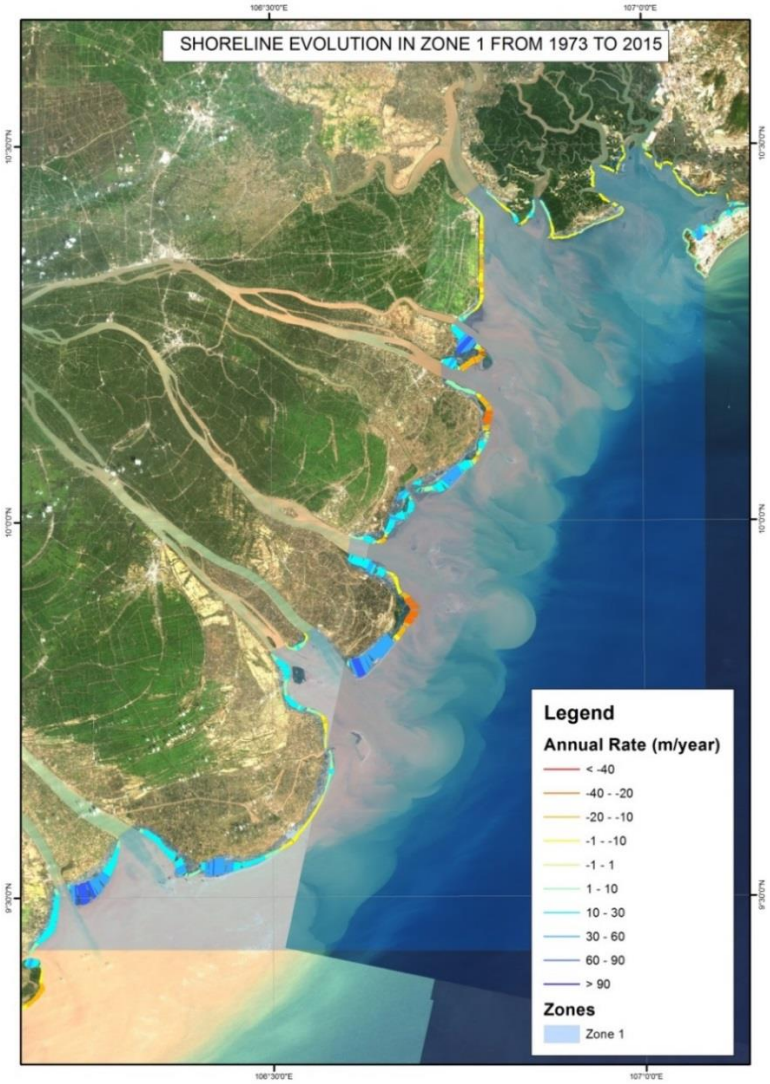

Figure 2.8: Shoreline evolution in area 1 from 1973 to 2015

b) Area 2: the Eastern coast from Soc Trang – Ca Mau

The sedimentation in this region was on average 1.23 km^2/yr from 1973-2000, however in the following 15 years it decreased to 0.81 km^2/yr with the lowest accretion occurring in 2000-2005 as shown in Figure 2.9. The highest accretion took place in Vinh Hai Commune, Soc Trang Province, with more than 30 m/yr. Meanwhile from 1973 to 2015 erosion ranges between 2.3 and 3.1 km^2/yr and in between 1990-2005 the erosion rate was even larger than 3 km^2/yr Compared with the other two areas, 1 and 3, the erosion dominated this area with an average net land loss rate of 1.6 km^2/yr, especially in the communes of Tam Giang Tay and Tam Giang Dong, Ca Mau Province, with an erosion rate higher than 40 m/yr illustrated in Figure 2.10.

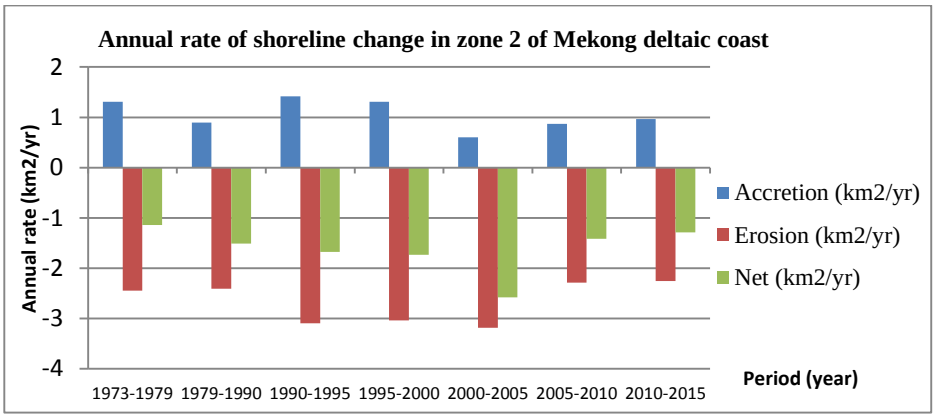

Figure 2.9: Annual rate of shoreline change in area 2 of Mekong deltaic coast

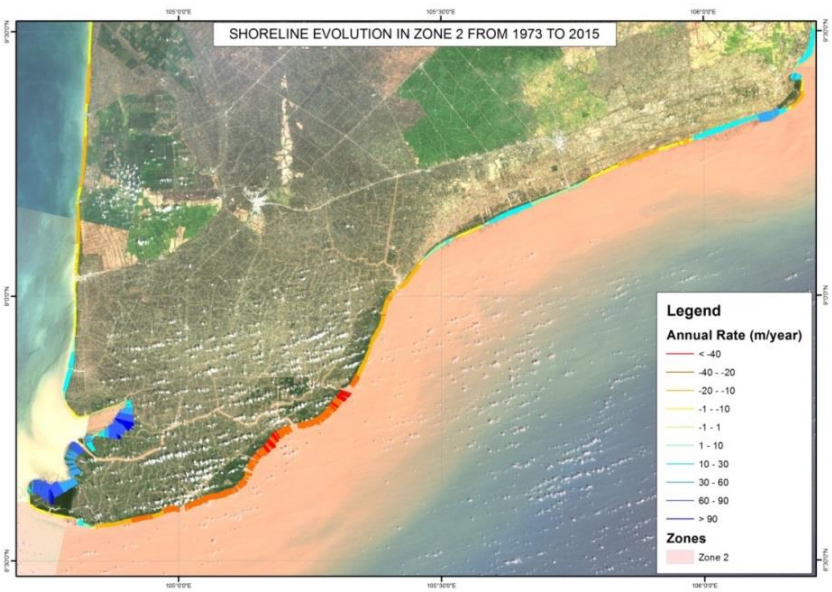

Figure 2.10: Shoreline evolution in zone 2 from 1973 to 2015

c) Area 3: The western coast from Ca Mau-Kien Giang

Compared with area 1 and 2, the coastline in area 3 is more stable with high accretion and low erosion in the period between 1973-2000 with a net land gain rate of almost 2.3 km^2/yr, shown in Figure 2.11. With the distinctive place as interaction between an irregular semi- diurnal tide ranging between 4 m on the eastern coast to an irregular diurnal tide ranging 1 m on the western coast leading the low flow currents, a large amount of sediment, including mainly fine silt and clay, is deposited in the western part with an accretion of up to 110 m/yr at Dat Mui and Lam Hai Communes, Camau Province (Figure 2.12). However, in the next periods complications occurred, when the accretion area rate suddenly decreased from nearly 3.7 km^2/yr between 1995-2000 to 1.2 km^2/yr in 2005-2010, and erosion area rate rapidly increased up to 2.8 km^2/yr in 2005-2010. A net land loss rate in area 3 of 0.4 km^2 only took place in period of 2005-2010 and the net land gain rate increased again when several groynes shown in Figure 2.20a were built in this period.

Based on the results of shorelines change along the Mekong detltaic coast, there are different characteristics among areas. While the accretion is dominated in the area 1, the severe erosion phenomenon is taking place mostly in the coastal area 2. Besides, the process of the shoreline change in the area 3 is not too large, except high sedimentation in the western coast of Camau Cape.

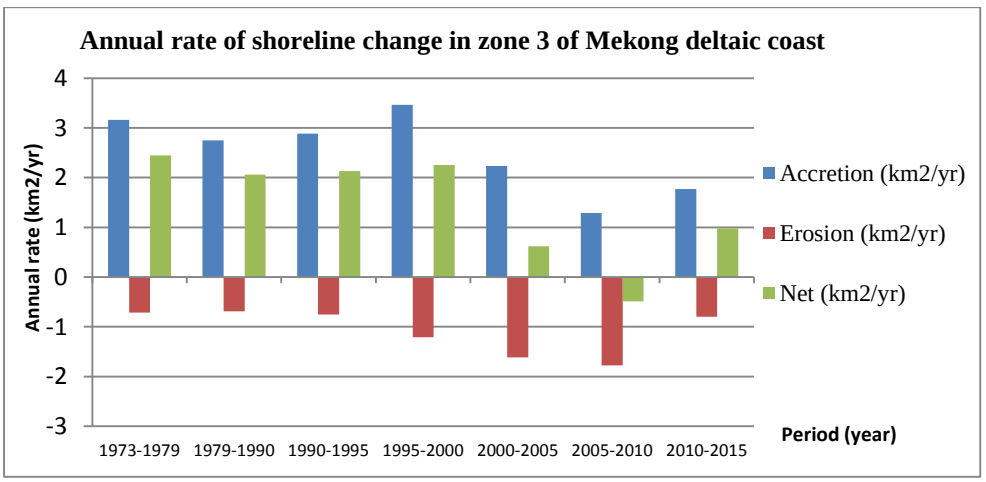

Figure 2.11: Annual rate of shoreline change in area 3 of Mekong deltaic coast

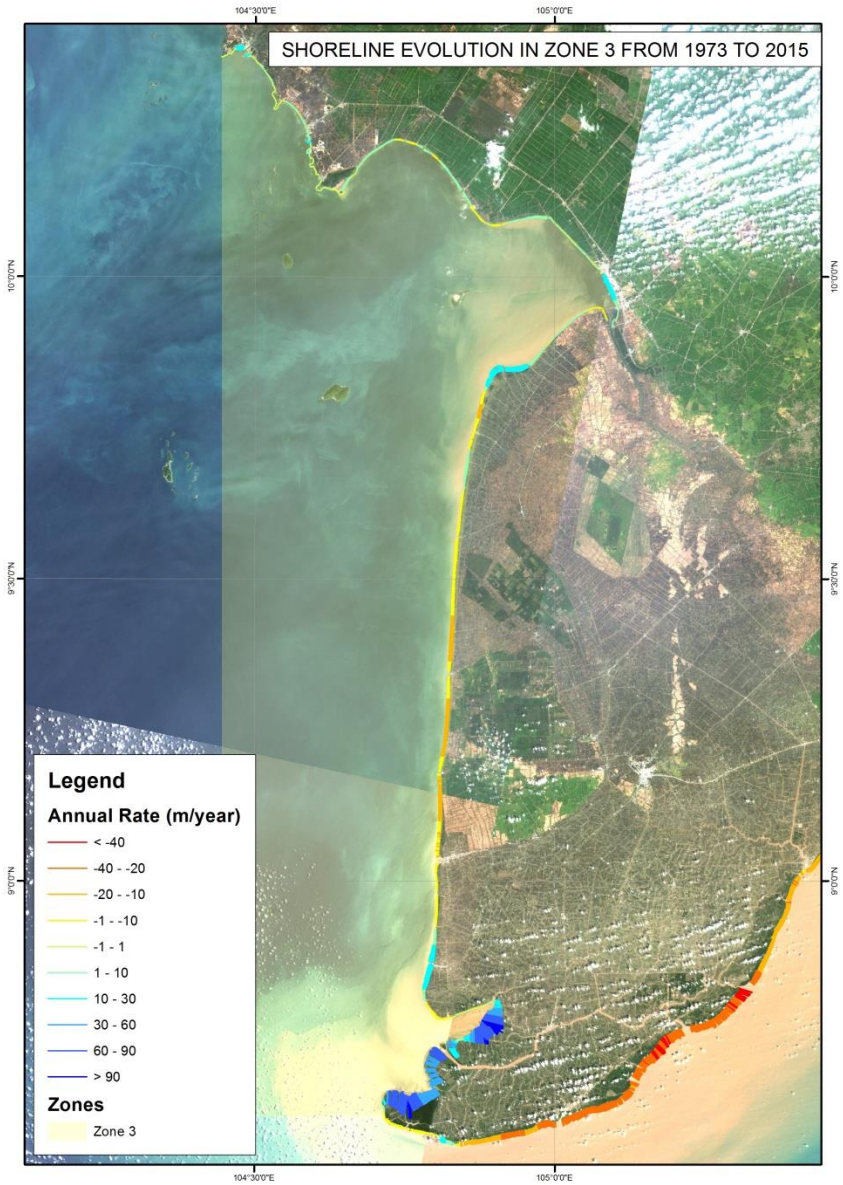

Figure 2.12: Shoreline evolution in area 3 from 1973 to 2015

2.3 Mangrove and coastal land cover in the Mekong Delta

Mangroves play an important role in not only sustaining a healthy coastal environment, providing a natural habitat to various species, forestry products but also keeping a stable shoreline. The dense root systems of mangroves trap sediments, which help stabilizing the coastline and prevent erosion from waves and storms. Any change in the

coastal land cover is likely to affect the shoreline evolution. This study aims to quantitatively document the evolution of the coastal land cover in the Mekong delta over the past 43 years, i.e. between 1973 and 2015. Satellite Landsat images, along with a classification method comprising Iso Cluster and Maximum Likelihood algorithms, have been used for mapping land cover types including mangroves, aquaculture, soils, plants and water surfaces along the coastal districts of the Mekong delta.

2.3.1 Data and methods

a) Data

The study area is the Mekong deltaic coast, which has a total length of about 600 km. It is located between 8º32'-10º22' N latitude and 104º26'-106º47' E longitude. The study focuses on those districts along the Mekong deltaic coast in Vietnam (Figure 2.1), which are facing significant threats to the mangrove forest due to the effects of rapid conversion into human land use, coastline treatment, coastal squeeze, saline intrusion and pollution.

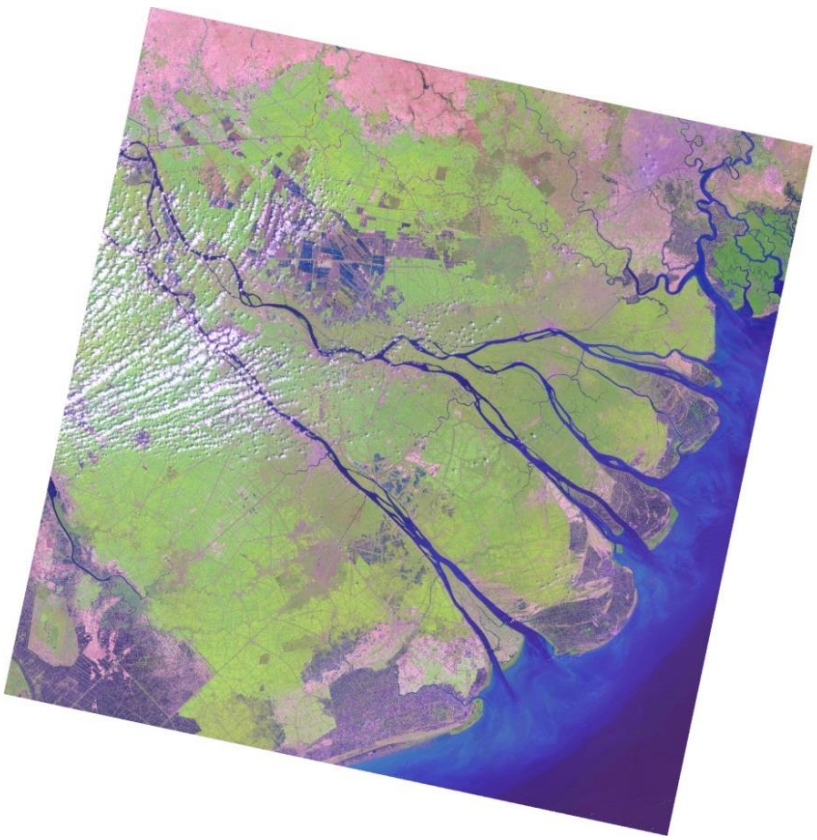

Figure 2.13. Typical Landsat image in study area

Various types of remote sensing satellite data have been used for the mapping and monitoring of mangroves at local, regional and global scales. Freely available Landsat scale (30 m) satellite data are found to be suitable for a large-scale area as the Mekong Delta. Multi-temporal remote sensing data of the Landsat Multispectral Scanner (MSS), Landsat Thematic Mapper (TM), Landsat Enhanced Thematic Mapper (ETM+) and Landsat Operational Land Imager (OLI) from 1973, 1979, 1990, 1995, 2000, 2005, 2010 and 2015 are archived by the U.S. Geological Survey (http://earthexplorer.usgs.gov). Due to a coastline length of 600 km, five adjacent Landsat paths/rows (path 124, 125, 126 and row 53, 54) are needed to cover the entire Mekong deltaic coast.

b) Method

- *Pre-processing*

The use of multi-temporal satellite data at a regional scale faces a number of challenges: geometric correction errors, noise arising from atmospheric effects and changing solar zenith angles (Homer et al., 2004). Such errors are likely to introduce noise into land use classification and change detection analyses. Hence pre-processing is necessary to remove or minimize such errors. Pre-processing steps for this study included Top Of Atmosphere (TOA) reflectance conversion and atmospheric correction. Each image was normalized for solar irradiance through changing digital number values to the TOA reflectance. The conversion algorithm of TOA is "physically based, automated, and does not introduce significant errors to the data" (Huang and Townshend, 2003). This process removes substantial variations among the images including sensor differences, the earth-sun distance and the solar zenith angle (U.S. Geological Survey, 2013). All images were converted to TOA reflectance values, as proposed by Chander and Markham (2003), so that a standardized measure could be obtained for a comparison among images. Moreover, the images were rectified for atmospheric interference using the Dark-Object Subtraction method (Chavez, 1996).

- *Image classification*

Satellite data were geo-referenced to coordinate the system of UTM WGS 84 with a Root Mean Square Error (RMSE) of less than half a pixel (<15 m). This study applied the combined unsupervised and supervised classification approach which has employed in many fields including the remote sensing (Thomas et al ., 2003; Lo and Choi, 2004; Mohammady et al., 2015; Bernabe and Plaza 2010). Five land cover classes consisting of mangrove, aquaculture, soil, plant and water were mapped in the study area. Post-classification editing was performed to remove obvious errors. Finally, a post-classification change analysis was performed.

The purpose of remote sensing for monitoring land cover is established as a response to the reflection of land cover categories to radiation in the visible and reflected infrared radiation of the electromagnetic spectrum. The reflectance of most land cover types from visible radiation is moderately low, however near-infrared radiation is reflected from almost all land cover types except water. The Normalized Difference Vegetation Index (NDVI) method was used to estimate the density cover of vegetation as well to differentiate the vegetation and non-vegetation parts. The NDVI is correlated with vegetation's biophysical properties, including fractional cover, green biomass and green leaf area. The NDVI data layer was estimated as (Red - NIR)/(Red + NIR), where Red and NIR are the reflection in

the green and near-infrared bands of the MSS, TM, ETM, OLI images, respectively. Where NIR represents the spectral reflectance in the Near-Infrared band, and R represents the Red band. The NDVI real values, by definition, would be between -1 and +1, where increasing positive values indicate increasing green vegetation, and negative values indicate non-vegetation surface features such as water, barren land or clouds. The function of NIR and Red wavelengths can also be effectively used to monitor the vegetation status and condition of a mangrove ecosystem (Gillies et al., 1997). Besides, the ratio of a short-wave infrared band and green band (Normalized Canopy Index - NCI) is often used to get information on different vegetation types more clearly, especially between forests and croplands (Vescovo and Gianelle, 2008). Therefore, this study combines the NDVI band and the NCI band to create 30 classes used by the Iso cluster unsupervised classification methodology, which uses a modified iterative optimization clustering procedure. The methodology creates a signature file containing the multivariate statistics for a subset of the cells for the identified clusters. The resultant calculations identify which cell location belongs to which cluster, the mean value for the cluster and the variance-co-variance matrix. This information is essential in the clustering and classification of the remaining un-sampled cells.

Consecutively, supervised classification by a maximum likelihood algorithm is used to reclassify the types into the 5 classes: aquaculture, mangroves, plants (rice crop, fruit trees, shrub, forest, etc.), soils (bare soil, urban, vegetable field with very low canopy cover, salt field, etc.) and water. Supervised classification is a pixel-based process, where pixels of known classes are used for classifying unknown classes. The field data supported the selection of a representative training data set for a maximum likelihood algorithm and an accuracy assessment of the classification. Maximum likelihood classification is known as one of the most effective methods in categorizing land use cover using moderate spatial resolution satellite remote sensing data (Green et al., 1998; Held et al., 2003). This method allocates each pixel to one of the different classes based on the highest probability according to the means and variances of the class signatures.

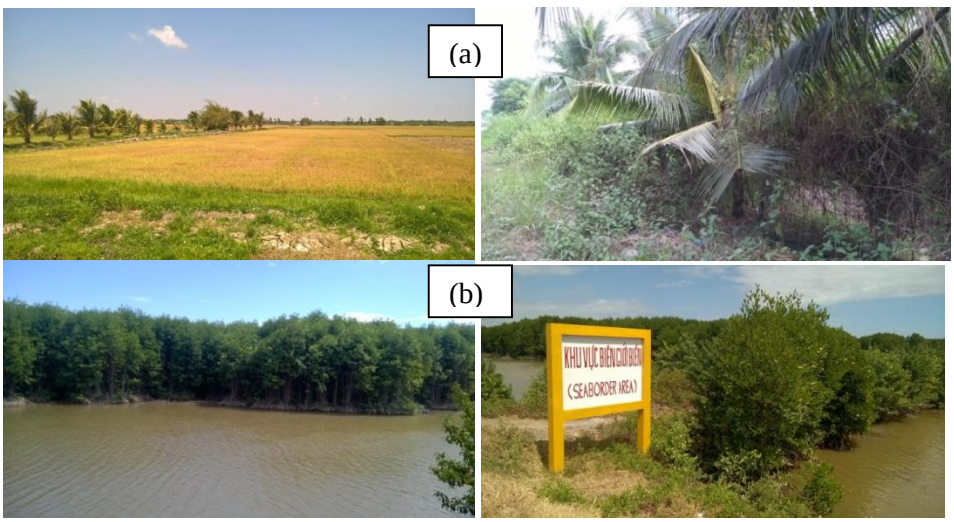

Figure 2.14: Ground survey of (a) plant types, (b) mangrove types, (c) aquaculture types and (d) soil types in 2015.

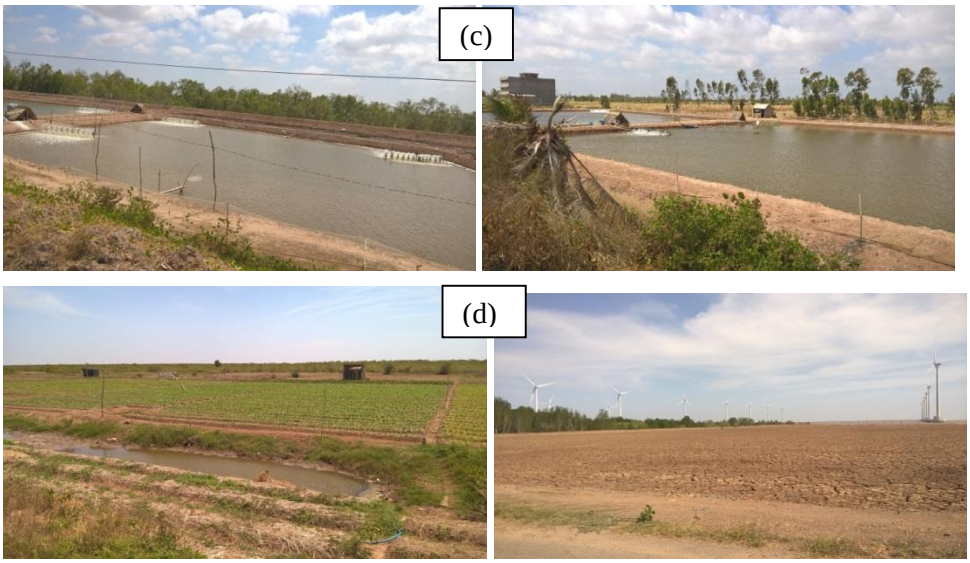

Figure 2.14, continued.

- *Accuracy assessment of classification and detection change analysis*

The accuracy assessment was implemented to determine how effective the classification process is, based on field data and other relevant information, including historical aerial photos, ortho-photos, Google Earth imagery and regional technical papers. A precision assessment was implemented using the Kappa coefficient approach to evaluate the accuracy of the classification results. The Kappa coefficient is calculated from the error matrix which compares the value achieved by the classification process of the remote sensing technique and the actual value from mentioned thermal layers (Congalton,1991). The Kappa function indicated how well the classification process is executed as compared to randomly allocated values. A random sampling with 100 pixels produced for the study area in each image, was applied to assess classification accuracy. Comparing these two values from field data and classified maps completed the error matrix table. The overall classification accuracy as well as user and producer accuracies for individual classes based on the reference data was achieved.

By the application of the change detection technique, land cover can be observed at different times. For change detection, satellite images should be attained by the same sensor and with the same resolution (Lillesand et al., 2004). Satellite devices offer cyclical images of surface coverage and help to obtain multi-temporal data sets for different use. Several measures for land cover change detection, including algebra based change detection approach (Ke et al. 2018, Ferraris et al. 2018), transform based change detection (Sadeghi et al. 2016, Massarelli 2018), classification based change detection (Radhika and Varadarajan 2018, Alonso et al., 2016), neural network and fuzzy based approach (Su et al., 2017, Zhang et al., 2017, Tian and Gong 2018) can be implemented.

In this study, a change detection technique for each land cover class was used as post-classification comparison. This approach identifies changes in land cover type comparing the classified images pixel by pixel. Assigning any value to each class can produce a

complete matrix of changes. Finally, the cross-tabulation technique by a simple mathematical function for images of t_1 and t_2 is implemented to visualise the changes in each land cover class. Further, the accuracy of this approach depends on the accuracy of the initial classifications.

Table 2.2: Steps for classification and change detection analysis of land cover types

Process Step	Process Name	Description
1	Download and Extract Images	USGS EROS DATA CENTER
2	Atmospheric correction	Sun and radiometric correction
3	Normalized Difference Vegetation Index (NDVI)	Red and Near Infrared Bands
4	Normalized Canopy Index (NCI)	Green band and Short wave infrared band
5	Developing approach for land cover creation by combining NDVI and NCI	Unsupervised classification by iso cluster algorithm to create 30 classes
6	Classify 5 classes: aquaculture, mangrove, plant, bare soil, water.	Supervised classification from 30 classes to 5 classes by maximum likelihood algorithm
7	Change detection analysis	Characteristic difference of pixel change between images from two dates

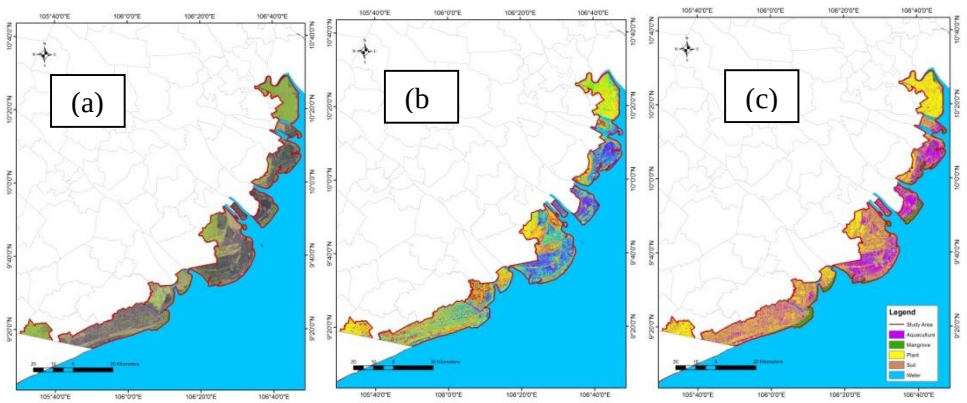

Figure 2.15. Satellite image (a), image of 30 classes (b) and final image of 5 classes (c), respectively.

2.3.2 Results

Firstly, this section presents the overview of mangroves and land cover mapping along the coastal Mekong delta. Secondly, the distribution of mangrove and aquaculture

extent in detailed at coastal province level is analysed. Finally, the change detection analysis of mangrove and aquaculture extents is implemented to determine and understand the reasons causing these changes, especially mangroves.

a) Mangroves and land cover mapping.

The mangroves and land cover mapping rule sets developed in this study were successfully implemented on the entire collection of Landsat images of MSS, TM, ETM+, OLI imagery, producing consistent image maps. Combined unsupervised and supervised classifications on Landsat MSS, TM, ETM+ and OLI 2011 indicated 5 land cover classes in agreement with the ground-truth observations. There are 5 land cover classes including aquaculture, mangroves, plants (rice crop, fruit trees, shrub, forest, etc.), soils (bare soil, urban, vegetable field, salt field, etc.) and water. The efficacy of satellite images in providing informative data from the mangrove area during the 43-year period is an advantage, as it monitors a vast area over a relative short time interval. Spatial and spectral information given by the satellite images enable classification of land use cover using pixel-by-pixel changes in every image with more than 80% of accuracy. The image classification for mangroves in 2015 indicated an accuracy assessment of 87% with Kappa statistics of 0.84 (Table 2.3). Therefore, it is assumed that classifications have been adequately performed for the purposes of assessing temporal change in mangrove extent and other land cover types.

Table 2.3: The accuracy assessment for classification of land cover mapping in 2015

Species	Mangrove	Aquaculture	Plant	Soil	Water	Total	User Accuracy
Mangrove	16	1	0	1	0	18	0.89
Aquaculture	1	23	1	0	1	26	0.88
Plant	0	2	20	1	0	23	0.87
Soil	0	1	1	15	1	18	0.83
Water	1	0	1	0	13	15	0.87
Total	18	27	23	17	15	100	
Producer accuracy	0.89	0.85	0.87	0.88	0.87		
Overall accuracy	0.87						
Kappa coefficient	0.84						

Distribution of mangroves from the classification from 1973 to 2015 is depicted in Figure 2.16. Mangroves have especially grown in coastal areas where sedimentation has occurred, such as Ben Tre, Tra Vinh, Soc Trang, Ca Mau. The total mangrove area in 1973, estimated at 185,800 ha, decreased significantly from 113,440 ha in 1990 to 92,560 ha in 2000. In the following periods, the extent of the mangroves is quite stable, slightly decreasing to 89,650 ha in 2010 and increasing again to 95,960 ha in 2015.

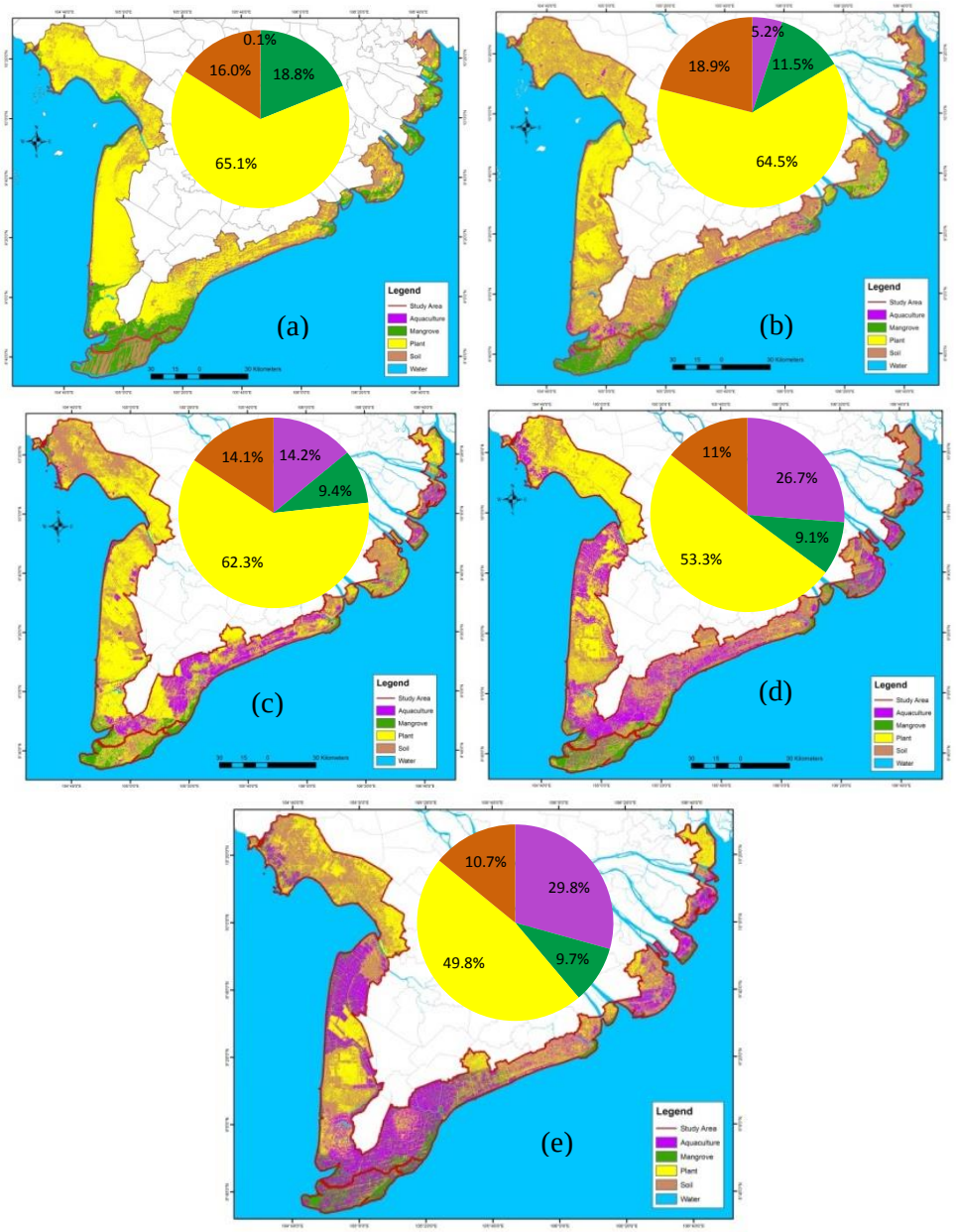

Figure 2.16: Classification results of land cover categories in the coastal Mekong Delta in (a) 1973, (b) 1990, (c) 2000, (d) 2010, and (e) 2015.

Fisheries have been very successful in the Mekong Delta, which has resulted in a significant contribution to the development of Vietnam's economic development in recent years. Aquaculture, the farming of fish, crustaceans, molluscs, aquatic plants, algae and

other organisms, covered a minor area of about 700 ha in 1973. A growth in the aquaculture extent took place, increasing to 51,370 ha in 1990 and to 264,010 ha in 2010 with an average annual increase of over 10,000 ha between 1990 and 2010. The annual increase of the aquaculture area in the period from 2010 – 2015 is half compared to the period between 2000 and 2010 resulting in an area of nearly 300,000 ha in 2015. More than half of the Camau Province is occupied by aquaculture.

Both plant and soil areas showed a steady decline for the period 1973 to 2015 in the study area. In four land cover categories, plants were the dominant cover in the study area. However, it diminished steadily during the entire study period, similar to mangrove and soil categories. Table 3 shows that plant fields started to drop gradually from 643,940 ha in 1973 to 493,160 ha in 2015. Compared with other periods, in the period between 2000 and 2010 the result indicates a quite significant decrease of plant area of nearly 9,000 ha/yr (Table 2.5). Meanwhile, there was an increase of soil area from 1973 to 1990 by 1,660 ha/yr, however the soil area also began to decline from 186,570 ha in 1990 to 106,140 ha in 2015.

Table 2.4: The four different land cover categories in the coastal Mekong Delta between 1973 and 2015

TYPE	1973		1990		2000		2010		2015	
	ha	%	ha	%	ha	%	ha	%	ha	%
Aquaculture	700	0.1	51370	5.2	141060	14.2	264010	26.7	295320	29.8
Mangrove	185800	18.8	113440	11.5	92560	9.4	89650	9.1	95960	9.7
Plant	643940	65.1	638320	64.5	617220	62.3	527900	53.3	493160	49.8
Soil	158400	16.0	186570	18.9	139100	14.1	108670	11.0	106140	10.7

Table 2.4 shows the percentage of each land cover type in the period of 1973 to 2015. The plant, mangrove and soil areas, indicating a decreasing trend between 1973 and 2015, correspond to the expansion of the aquaculture area. There was only an extremely small aquaculture area in 1973, which then gradually increased to nearly 30% of the total land cover area in 2015. The plant area occupied more or less 65% in 1973, however this area dropped to only 50% in the entire study area. The soil area remained quite steady in size; there is only a slight decline of occupied area rate from 16% to 14% for the total coastal study area in the whole period from 1973 to 2015. Similarly, the extent of mangroves in 1973 of nearly 19% of the total land cover area decreased to 9% in 2010, however it started to increase to 10% for the whole study area in 2015. The result shows that while the aquaculture area expanded rapidly from almost nil in 1973 to 300,000 hectares, the mangroves area decreased by 2 times within 43 years from 1973 to 2015 along the Mekong deltaic coast.. Besides, there is slightly drop of the plant and soil areas by 1.3-1.5 times in that period.

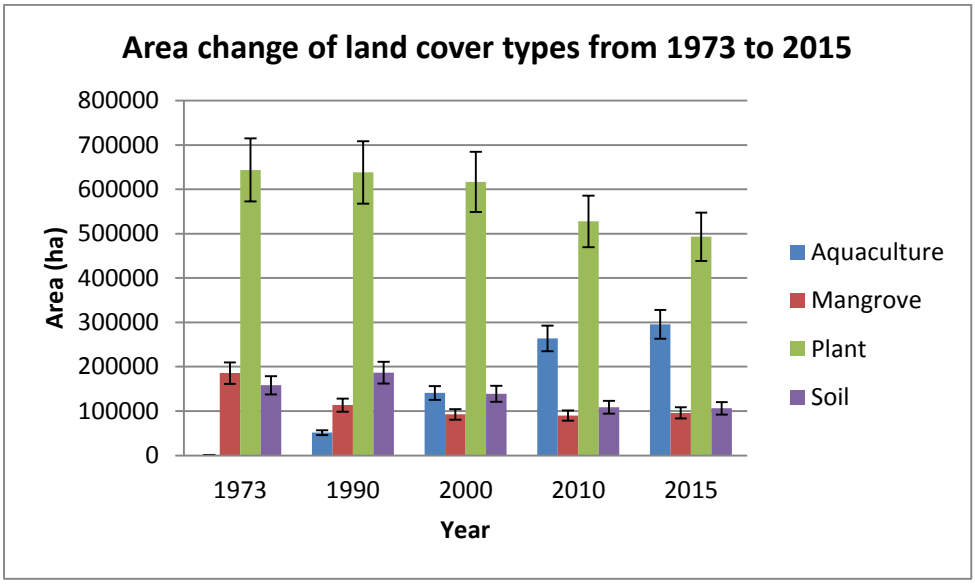

Figure 2.17: Area change of land cover types between 1973 and 2015

Table 2.5: Annual change of land cover types in periods

TYPE	ANNUAL CHANGE OF LAND COVER AREAS in PERIODS (ha/yr)			
	1990-1973	**2000-1990**	**2010-2000**	**2015-2010**
Aquaculture	2980	8970	12300	6260
Mangrove	-4260	-2090	-290	1260
Plant	-330	-2110	-8930	-6950
Soil	1660	-4750	-3040	-510

b) Distribution of mangrove and aquaculture extent at coastal province level

Land cover area data clearly showed that the extent of mangroves has decreased inversely proportional to the rise of aquaculture area taking place in most coastal districts between 1973 and 2015, except in the coastal area of Bac Lieu Province (Figure 2.16 and Table 2.6). The aquaculture area in the entire study area, particularly the aquaculture area in the three coastal provinces of Ca Mau, Kien Giang and Bac Lieu, increased remarkably compared to other provinces. Especially, the coastal Camau Province with an aquaculture area occupying 141,550 ha covers nearly 48% of the total aquaculture extent. The percentage of mangrove area among the districts of the coastal provinces is quite stable during 43 years, indicating that the decrease rate of the extent of mangroves appears widely over the whole coastal provinces of Mekong Delta. Not only the largest aquaculture extent in the total study area, the coastal area of Ca Mau Province is likewise the place where the mangrove extent has occupied most territory with roughly 64% of the total mangrove extent. Inversely, there are three coastal provinces, Kien Giang, Bac Lieu, Tien Giang,

where the percentage proportional to the total mangrove area is lower than only 5%. This result indicated the opposite evolution of mangrove and aquaculture areas at coastal province level along the Mekong deltaic coast in 43 years from 1973 to 2015.

Table 2.6: Aquaculture and mangrove extent at coastal provincial level between 1973 and 2015

PROVINCE	TYPE	1973		1990		2000		2010		2015	
		ha	%	ha	%	ha	%	ha	%	ha	%
Kien Giang	**Aquaculture**	30	4.3	6060	11.8	11580	8.2	39630	15.0	44610	15.1
	Mangrove	11000	5.9	8310	7.3	5490	5.9	4650	5.2	4770	5.0
Ca Mau	**Aquaculture**	230	32.9	15070	29.3	53270	37.8	119040	45.1	141550	47.9
	Mangrove	129660	69.8	67570	59.6	56020	60.5	54460	60.7	61330	63.9
Bac Lieu	**Aquaculture**	100	14.3	2820	5.5	33850	24.0	40080	15.2	40110	13.6
	Mangrove	1700	0.9	2470	2.2	2840	3.1	2890	3.2	3390	3.5
Soc Trang	**Aquaculture**	70	10.0	5910	11.5	11800	8.4	15270	5.8	16970	5.7
	Mangrove	8750	4.7	8810	7.8	5690	6.1	6550	7.3	6780	7.1
Tra Vinh	**Aquaculture**	60	8.6	6820	13.3	13250	9.4	26270	10.0	27330	9.3
	Mangrove	15250	8.2	12970	11.4	10750	11.6	9810	10.9	9930	10.3
Ben Tre	**Aquaculture**	100	14.3	8700	16.9	13070	9.3	17780	6.7	19000	6.4
	Mangrove	12170	6.6	9020	8.0	8410	9.1	8360	9.3	7600	7.9
Tien Giang	**Aquaculture**	110	15.7	5990	11.7	4240	3.0	5940	2.2	5750	1.9
	Mangrove	7270	3.9	4290	3.8	3360	3.6	2930	3.3	2160	2.3
Total	**Aquaculture**	700	100	51370	100	141060	100	264010	100	295320	100
	Mangrove	185800	100	113440	100	92560	100	89650	100	95960	100

c) Change detection analysis of mangrove and aquaculture extents

Mapping changes of land cover categories is necessary to determine and understand the reasons causing these changes, especially the ecosystem that includes mangroves. The results from the change detection maps (Figure 2.18 and Figure 2.19) indicate that almost mangrove changes that occurred along the coastal area are caused by the expansion of shrimp farming, in addition to agricultural activities and coastal erosion.

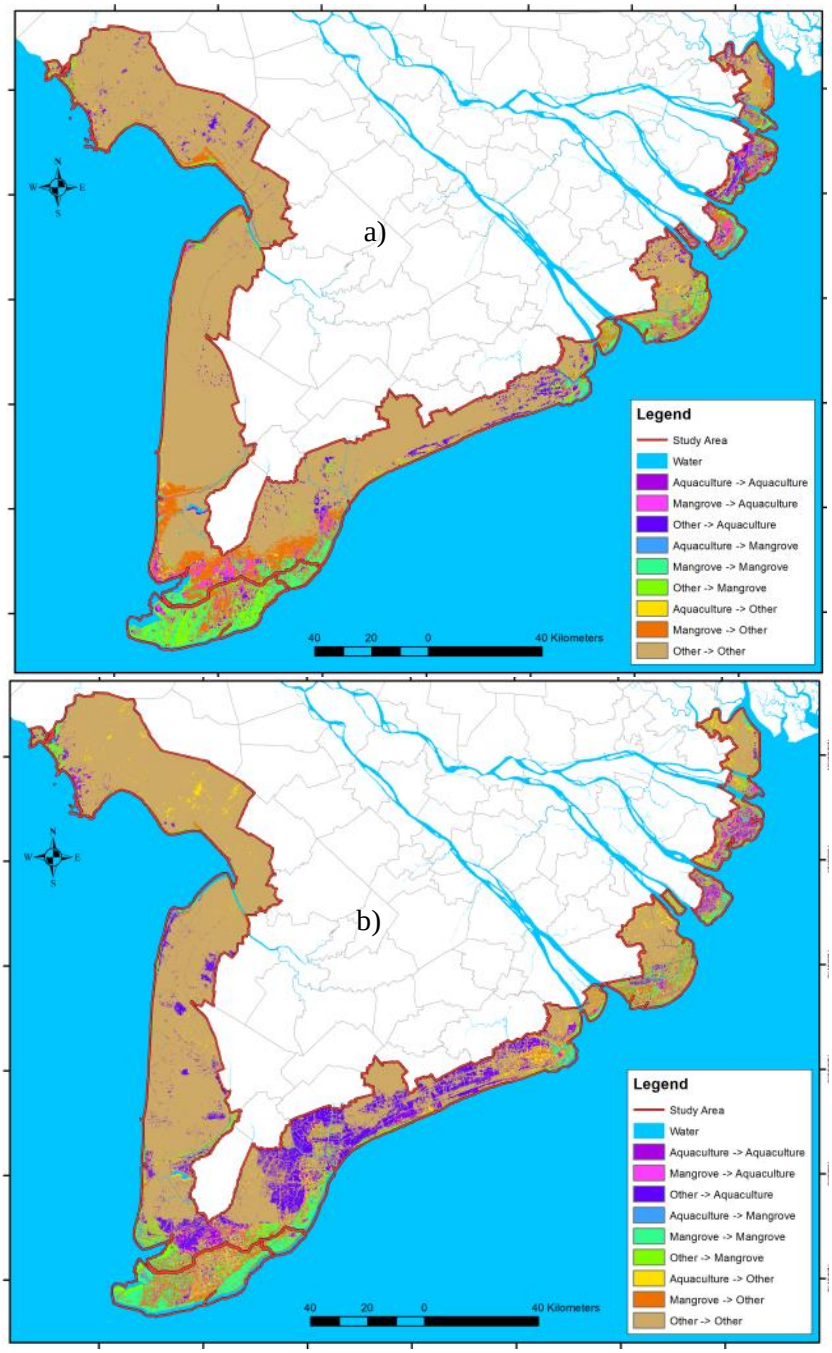

Figure 2.18: Conversion dynamics of mangrove and aquaculture in period of 1973 to 1990 (a), period of 1990 to 2000 (b), period of 2000 to 2010 (c), period of 2010 to 2015 (d) and period of 1973 to 2015 (e). 'Other' means land cover of non-determined plants and soils types.

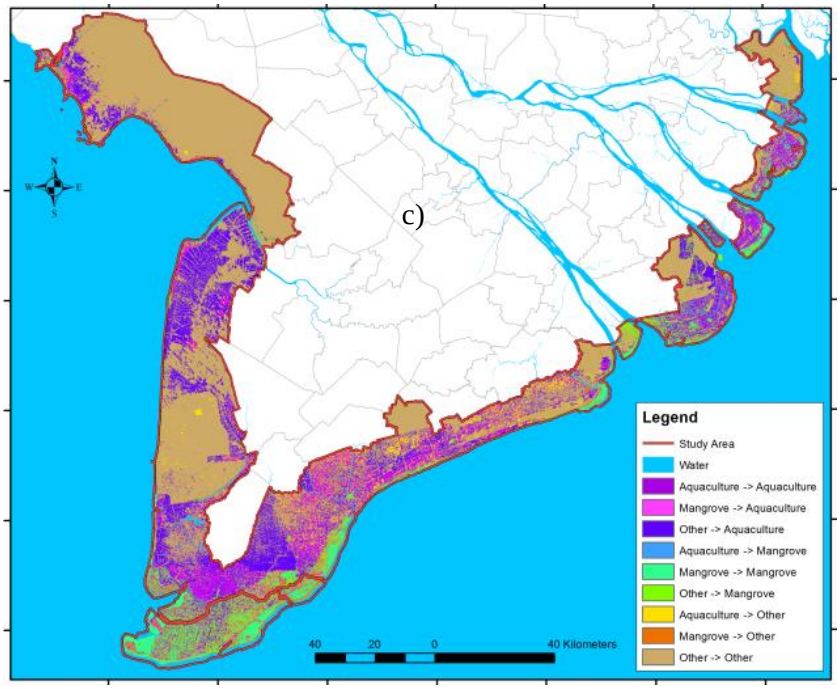

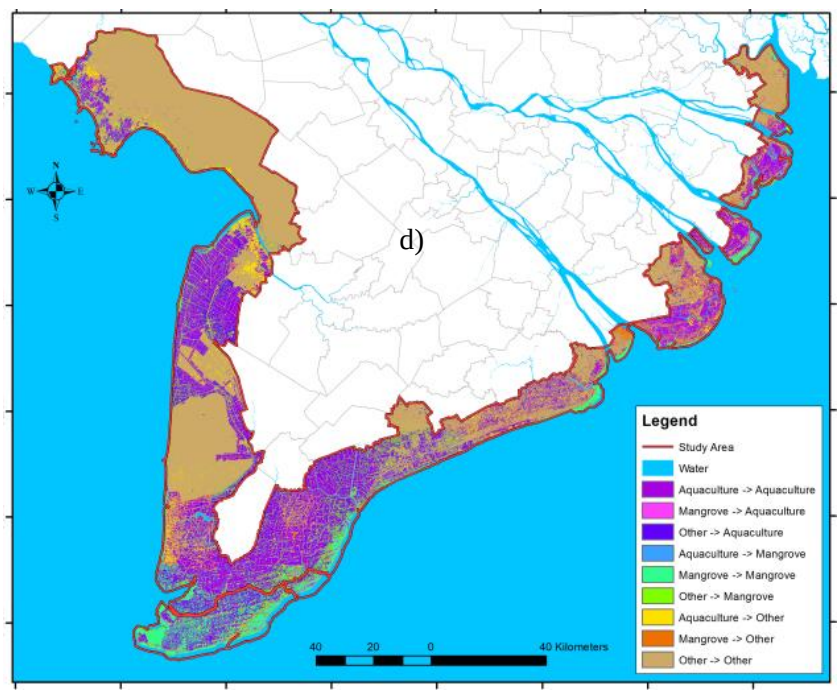

Figure 2.18, continued.

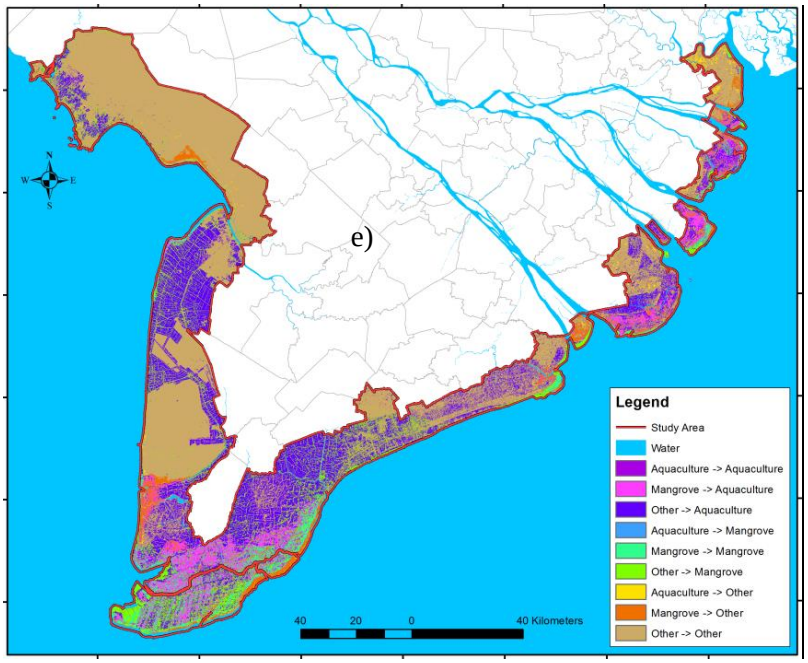

Figure 2.18, continued.

The unchanged aquaculture extent (Figure 2.19) increased dramatically from 30 ha/yr in the period of 1973-1990 to 46,740 ha/yr in the period of 2010-2015. This information clearly shows that shrimp famers not only continue to use the current aquaculture area, but also considerably expand to absorb other land categories. The Vietnamese government has encouraged shrimp farming for export since the early 1980s and it became a wide-spread economic activity. From 1980 until the late 1990s, there was rapid expansion in shrimp aquaculture throughout most of the coastal Mekong Delta, driven by opening up its economy, high profits and government promotion (Hong and San, 1993; Hashimoto, 2001). In addition, shrimp farming was promoted by international organizations, such as the World Bank and the Asian Development Bank, as a means to reduce poverty and create employment and income (Binh et al., 2005). The extent of land cover including plant and soil types changed to aquaculture from 550 ha/yr in the period of 1973 and 1990 to 10,820 ha/yr in the period of 2010 and 2015, especially at a peak rate of 16,220 ha/yr in the short period of 2000-2010. Figure 9 demonstrates that in the beginning of the 1990s, a remarkable change to aquaculture area in the coastal land cover first occurred in the three provinces of Camau, Baclieu and Soctrang. Then, the aquaculture expansion spread rapidly to the coastal zones of Travinh, Bentre and the southern part of Kien Giang Province. Meanwhile, the change of aquaculture to other land cover types is largely within the range of 4000 ha/yr to 6000 ha/yr The reason for the change is the result of several causes. A failing wastewater management from shrimp farming led to a relatively frequent loss of aquaculture areas after the success of aquaculture in some previous years (Le and Munekage, 2004; Shimizu et al., 2013). A part of this land became bare; farmers change to shrimp-rice or shrimp-forest field farming or just let the land turn bare.

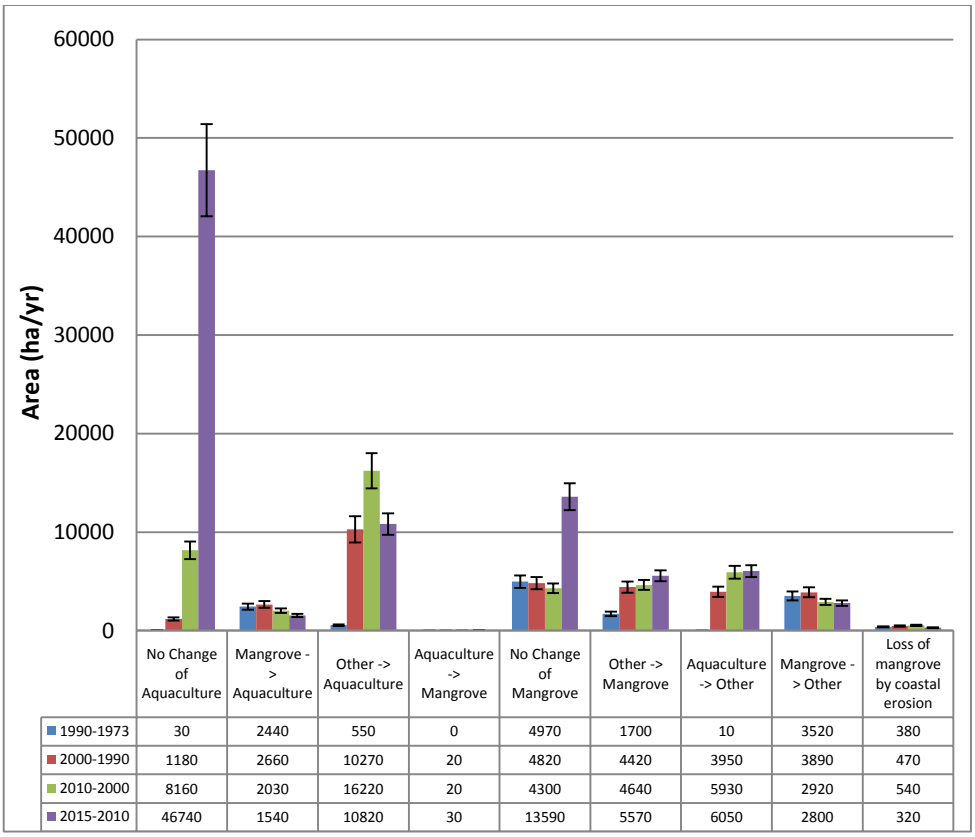

	No Change of Aquaculture	Mangrove -> Aquaculture	Other -> Aquaculture	Aquaculture -> Mangrove	No Change of Mangrove	Other -> Mangrove	Aquaculture -> Other	Mangrove -> Other	Loss of mangrove by coastal erosion
1990-1973	30	2440	550	0	4970	1700	10	3520	380
2000-1990	1180	2660	10270	20	4820	4420	3950	3890	470
2010-2000	8160	2030	16220	20	4300	4640	5930	2920	540
2015-2010	46740	1540	10820	30	13590	5570	6050	2800	320

Figure 2.19: Annual mangrove and aquaculture dynamics in the coastal Mekong Delta.

Major causes of mangrove forest loss include conversion to agriculture, aquaculture/ shrimp ponds and urban development. Similar to several other countries, in Vietnam a conflict exists between the conservation of mangroves and the development of shrimp farming (Dahdouh-Guebas et al., 2002). The loss of mangroves in the study area by the expansion of aquaculture ranges between 1500 ha/yr and 2700 ha/yr. There is a slight decreasing trend of mangrove conversion to aquaculture from 2440 ha/yr in the period of 1990-1973 to 1540 ha/yr in the period of 2010-2015; the result of a law introduced in 1991 by the Vietnamese government to protect forests (Hong, 2000). The reduction of mangrove area is/was not only due to the expansion of aquaculture, the analysis of satellite images shows that the other reasons were due to conversion to other plant cover, soil extent/agricultural practices and coastal erosion. The yearly loss of mangroves by coastal erosion and conversion to other land covers varied from 3120 ha/yr to 4360 ha/yr. In the 1990s the Vietnamese government considerably enhanced irrigation systems to develop rice fields in the Mekong Delta (Kotera et al., 2013; Tuong et al., 2003; Veettil and Quang; 2018). The irrigation structures, supported and implemented by the government, brought about the de-acidification and de-salination of brackish and salt water to be converted into fresh water to develop rice fields and fruit tree areas.

Nowadays, Vietnam is one of the biggest rice exporters in the world and nearly 90% of the Vietnamese exported rice is from the Mekong Delta (Ricepedia; Toang, 2017). The result from the high conversion from mangrove to agriculture is shown in Figure 8 during 1973 and 2015. Coastal erosion occurred early in Camau and then spread to other coastal provinces, including Tra Vinh and Ben Tre. However, despite the conversion of mangroves to other types of land cover, other types of land cover changed to mangrove type. Figure 10 indicates an obvious gradual changing growth of other types of land cover to mangroves from 1700 ha/yr in the period of 1973-1990 to 5570 ha/yr in the period of 2010-2015. Mangrove areas have expanded from original mudflats by sedimentation, which occurred in Ca Mau, Soc Trang, Tra Vinh and Ben Tre provinces. The further rise of mangrove area in recent years relates to reforestation related decisions, including instant actions for the protection and improvement of forest areas (Decision 286/QD-TTG) following a plan to create 5 million ha of forests throughout the country (Decision 661/ QD-TTG) (Binh et al., 2005). International organizations, as GIZ (Deutsche Gesellschaft für Internationale Zusammenarbeit), Australian Aid, etc., have implemented projects to boost the mangrove extent in several coastal provinces, such as Soc Trang, Bac Lieu and Kien Giang. These projects have resulted in a first-time higher accretion of mangrove area than the loss of mangrove area in the period 2010-2015. During the total study period of 1973 to 2015, the average yearly loss of mangrove by changing to other land cover types, including plants, soils, aquaculture and erosion, is 5880 ha/yr. While the change from other land cover types to mangrove was approximately 3600 ha/yr before 2010 (less than the loss of mangrove more or less 6280 ha/yr in the same time), this phenomenon is reversed in the period of 2010-2015 with 5600 ha/yr in terms of other land cover types changing into mangroves, compared with 4660 ha/yr due to mangroves to the remaining land cover types.

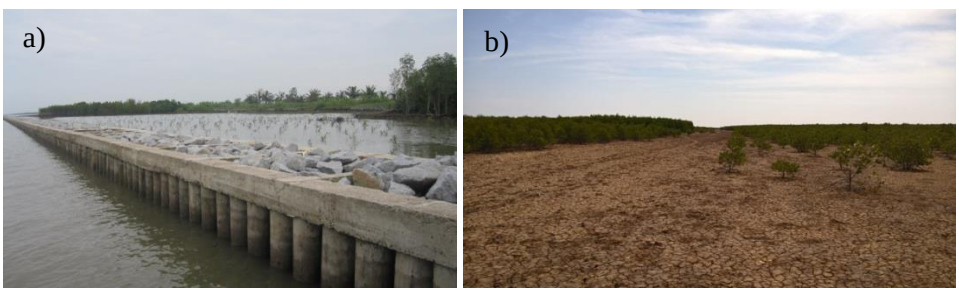

Figure 2.20: (a) Groynes Systems in Camau, (b) Mangrove Restoration Project in Baclieu, (c) Existing Coastal Protection Structures.

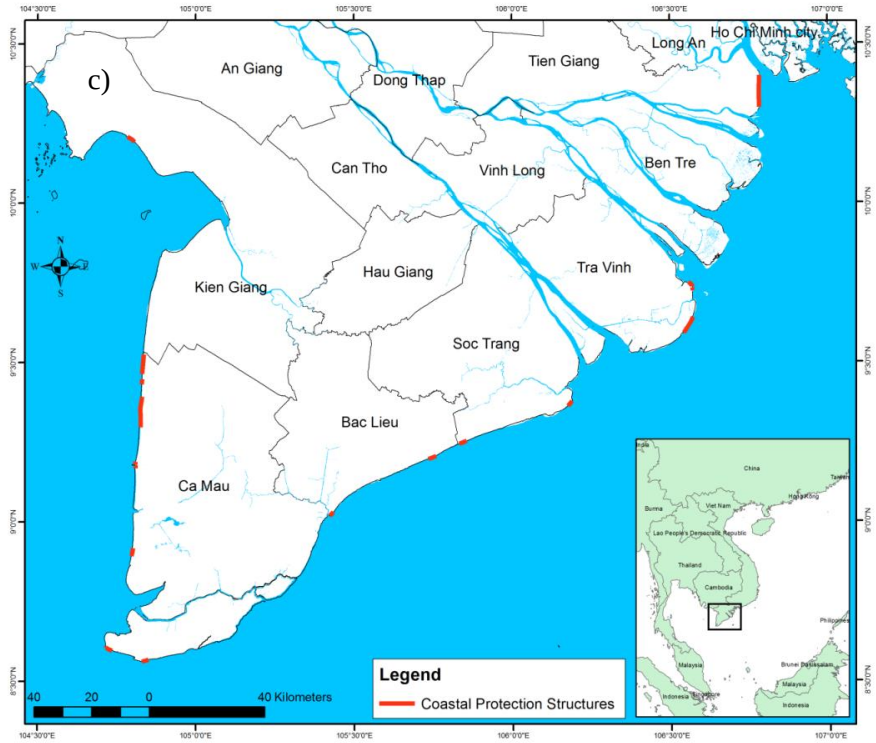

Figure 2.20, continued.

2.4 Discussion

The results showed that the shoreline evolution along the Mekong deltaic coast is taking place complicatedly and the mangroves areas that protect partly the stable coastline are reducing significantly as well. This section discusses the reasons causing the change of coastline as well as the main pressures to the survival of mangroves. Then, the solution for sustainable coastal land cover along the Mekong deltaic coast is discussed.

2.4.1 Sources and sinks towards shoreline evolution

a) Sediment sources

The Mekong River Basin has become one of the most active regions in the world for hydropower development with a large number of large hydropower projects planned. There are 26 existing medium and large dams on tributaries in the Mekong River and 13 under construction or recently completed. There are currently no dams on the Mekong mainstream downstream of the P.R. of China, but the first of 11 planned mainstream dams, the Xayaburi Dam to be located in Laos is currently in the late stages of planning and under review by the Lower Mekong Basincountries as part of the Mekong River Commission's Prior Consultation Process.

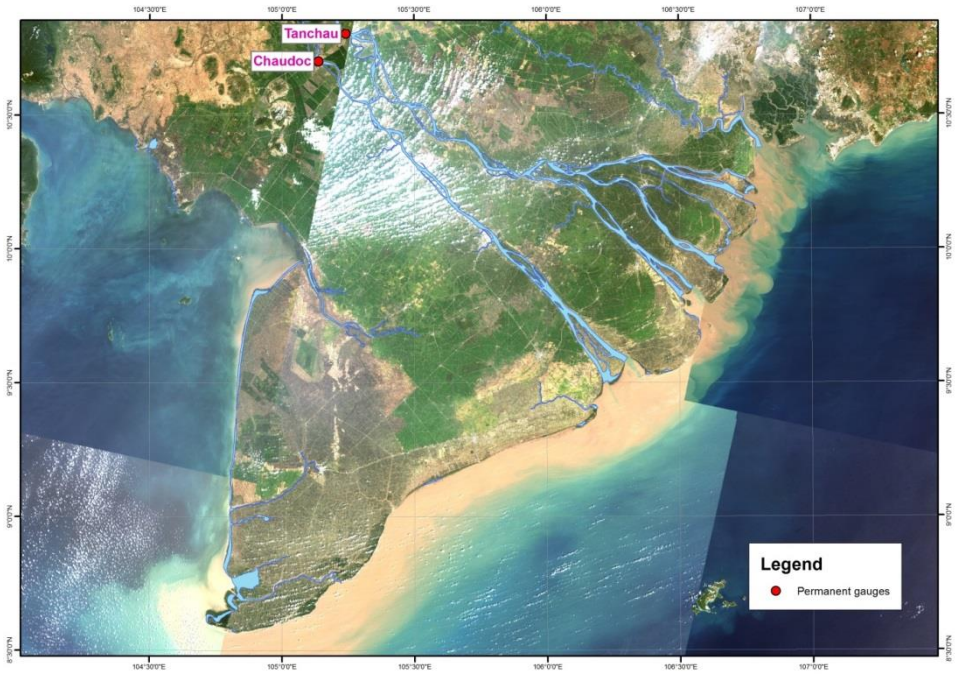

Figure 2.21: Location of two permanent gauges of Tanchau and Chaudoc

Measurements of suspended sediment concentration data at the permanent stations of Tanchau (Figure 2.21) showed that there is a marked difference among periods of 1988-1995, 1996-2000 and of 2001-2012. Although between 1988 and 2012, there is a slight growth of suspended sediment concentration starting in 2000, the suspended sediment concentration declined significantly to on average 115 mg/l in the period of 2005 - 2012 from an average 124 mg/l in the period of 1988-1995. On the other hand, the flow discharge decreased slightly in the period of 1996- 2012 as well. The results are consistent with the study of Fu and He (2008), which reported that roughly 60 % of the total sediment load was trapped between 1993 and 2003 below the Manwan reservoir in China, leading to considerable effects on sediment change in the downstream.

Furthermore, since in 1995 the U.S. economic embargo against Vietnam was lifted, the economy showed a general expansion in particular in the construction sector with an increased sand demand. Bravard (2013) reported that total sand mining approximately amounts to dozens of tons per year in the 7 provinces of the lower Mekong Delta of Vietnam, i.e. Dong Thap, An Giang, Ben Tre, Tien Giang, Tra Vinh, Vinh Long and Can Tho provinces. The sand mining also aggravated the decrease of sediment load into the coastal zone.

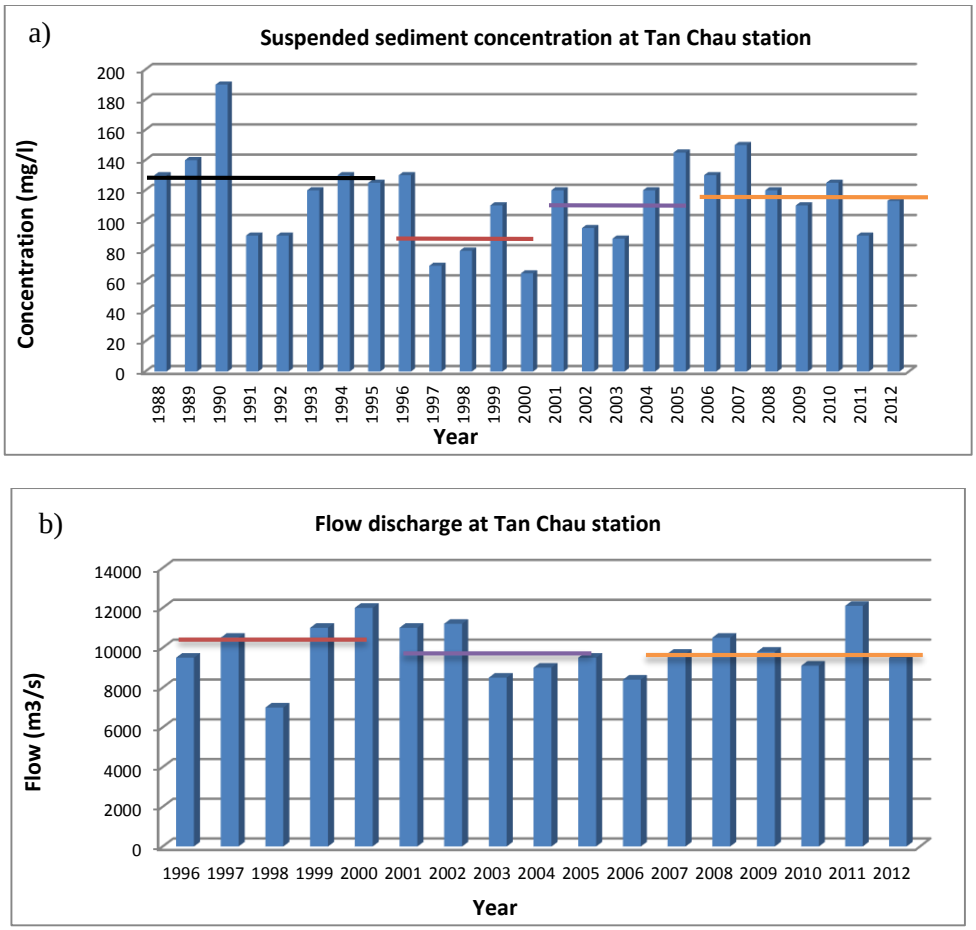

Figure 2.22: Suspended sediment concentration from 1988 to 2012 (a) and flow discharge from 1996 to 2012 (b) at Tan Chau.

b) Relative sea level rise

The data collected between 1979 – 2007 at the Vung Tau gauge station (Figure 2.23), showed that the highest water level at this station has risen by 13 cm, e.g. nearly 4.0 mm/year. In addition to sea level rise, the Mekong Delta experiences subsidence, caused by natural reasons, such as compaction of fresh deltaic deposits and as a result of human impact and groundwater extraction. It is rather severe, with an average of 1.6 cm/yr (Figure 2.24), and for the few locations where InSAR is used, compaction estimated rates are <1.0 cm yr−1 in the upper Mekong Delta and the its coastal zone (Erban et al., 2014). Therefore, the changed sediment load in the Mekong River as well as the relative sea level rise are a possible cause for coastal erosion.

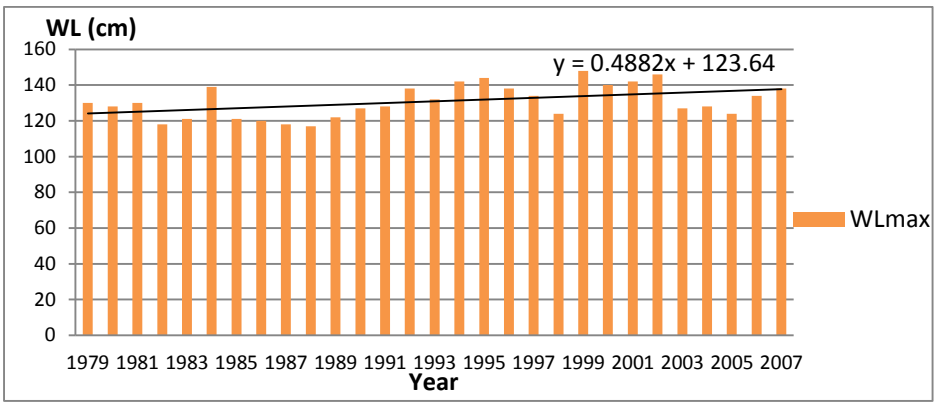

Figure 2.23: Trend of highest water level in the period 1979 to 2007 at Vung Tau station.

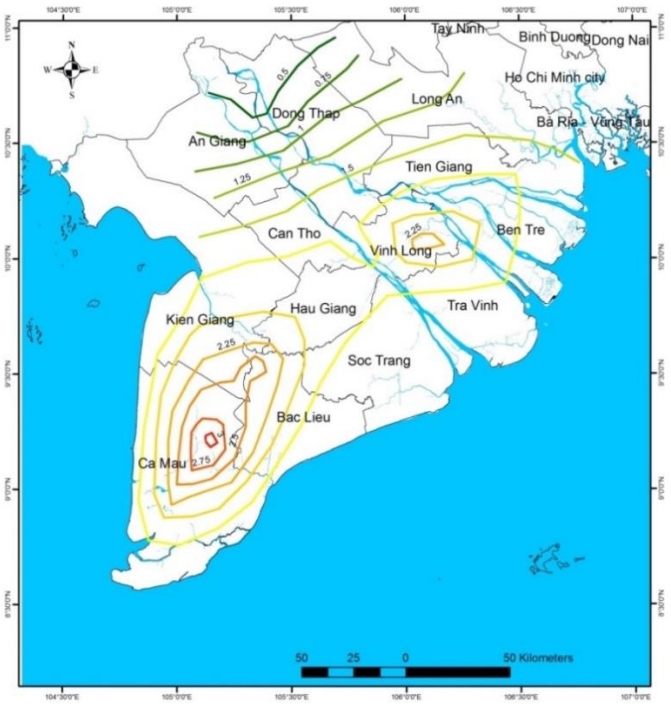

Figure 2.24: Compaction-based subsidence rates, interpolated from calculations at well locations (modified from Erban, et al., 2014)

2.4.2 Main pressures to the survival of mangroves

Mangroves, which are usually scattered along the intertidal zone of low energy tropical coastlines are highly productive ecosystems (Kathiresan and Bingham, 2001). Mangroves play an important role in the coastal ecosystem, especially in terms of

ecological, environmental, biological, medical and economical values. However, mangroves in the Mekong Delta still face survival threats by land use conversion, pollution, insufficient nutrient sediment, coastal erosion, coastal mangrove squeeze.

a) Conversion to aquaculture and other land cover types

In the mangrove regions of Asian countries, such as Thailand, Indonesia, the Philippines and Vietnam, a significant change from salt to brackish water due to aquaculture is taking place (van der Giesen et al., 2006). Approximately 50%-65% of mangroves have been lost to shrimp farm conversion since 1975 in Thailand (Barbier, 2003) and in the Philippines about half of the 279,000 ha of mangroves was lost in the years from 1951 to 1988 due to the introduction of aquaculture (Primavera, 2000). With the encouragement and support of the Vietnamese government and international organizations, such as the World Bank and the Asia Development Bank, shrimp farming areas spread along the coastal zone of the Mekong Delta. The Vietnamese Prime Minister issued the National Decree 773-TTg in 1994, stipulating that open coastal areas and water bodies could be used for aquaculture (Nguyen et al., 2013). However, it led to problems of rapid deforestation, as local authorities were incapable to control the expanding aquaculture. Although the government had indicated a priority for the use of bare soil from low productivity rice paddies or fruit tree areas to shrimp farming, local people still destroyed the mangroves for aquaculture to gain income. In this study, the loss of approximately 2170 ha/yr of mangroves through 1973-2015 was largely due to the conversion to aquaculture. The present study is consistent with numerous studies on the severe impact on the mangrove vegetation by the conversion to aquaculture (Wolanski et al., 2000; Valiela et al., 2001). The widespread aquaculture system will alter the system dynamics, interrupting the continuity of natural events as local dispersion and the migration of flora and fauna species, modifying the local hydrology and eventually leading to a weakening of mangrove health. The present study showed that mangroves were primarily changed by the conversion to other land covers, as a result of built-up land, salt fields, agriculture extent and bare soil by deforestation for firewood, with an annual rate of 3710 ha/yr, which is higher compared with the area conversion of mangroves to aquaculture.

Figure 2.25: Aquaculture expansion in adjacent mangrove forest.

b) Pollution

- *Herbicides from chemical warfare*

The forests under study experienced significant damage during the American-Vietnam War from the application of herbicides and defoliants by the U.S. Air Force. As part of the war strategy (1962-1972) large tracts of forest, including mangrove forests in the southern provinces of Vietnam, were defoliated by the use of herbicides in order to disclose military shelters and food sources (Stellman et al., 2003). NAS (1974) estimated that 104,939 ha or 36% of the area of mangrove in southern Vietnam was subjected to one or more chemical attacks. Serious defoliation not only destroyed the vegetation, but also affected heterotrophs changing the entire ecosystem (Hong and San, 1993). The profound impact of the attacks in the Mui Ca Mau is visible by the increase in bare wasteland in 1975 compared to 1953, following the pattern of the flight paths of the spray missions (NAS, 1974; Stellman et al., 2003). A large difference of mangrove growth between the affected and non-effected mangrove forest by chemical warfare was noticeable (T.T. Van, 2015). However, this factor only affected the mangrove expansion in the first study phase of 1973-1990, with almost no impact on the development of mangroves in the Mekong Delta in later years.

- *The waste of aquaculture*

Consistent with the developments in many other southeast Asian countries (Huitric et al., 2002), mangrove deforestation in Vietnam has become a serious issue, with at least 220,000 ha of mangrove forest eliminated over the last 50 years (Tuan et al., 2003). Whereas agriculture, saltpan development and the wartime use of chemicals were previously the most important threats to mangroves, for the last decades the greatest threat has been the shrimp aquaculture. Disease outbreaks and acidification of soils have led to crop failure rates as high as 70–80% in some areas of Vietnam, and have subsequently led to the abandonment of existing ponds and the expansion of shrimp cultivation to new coastal areas (Lebel et al., 2002). To reduce the risk of crop failure, Vietnamese farmers use a relatively large amount of food, pesticides and antibiotics in shrimp farming (Lan et al., 2013). A number of concerns have been raised about the usage of toxic compounds, including their persistence in aquatic ecosystems , the probability of residues in non-cultured seafood, the toxicity to non-target (off farm) species, the possible effects on sediment bio-geo-chemistry and, finally, the probable effects on the health of farmers. As other studies have noted (Mang et al., 2008), shrimp farming in Vietnam may also lead to serious water pollution with wastewaters containing high Biological Oxygen Demand (BOD), and high Nitrogen (N) and Phosphorus (P) concentrations from food residues, often released directly into canals and rivers, causing oxygen depletion and eutrophication. Several studies have also indicated that intensive shrimp farming in particular has the largest share in the overall environmental impact of all shrimp production systems (Tzachi et al., 2004). The water pollution per hectare and per crop of shrimp farming from the farming process are 1373 kg BOD, 4077 kg COD, 6201 kg TSS, 159 kg of total nitrogen and 20 kg of total phosphorus, 26 kg of Ammonia-Nitrogen (N-NH3), respectively (Pham et al., 2010). Hence, with a size of aquaculture areas in the coastal study area of nearly 300,000 ha, discharge channels release enormous amounts of harmful substances into the coastal zone. The above numbers do not include solid waste from aquaculture, which is discharged directly into the river or

discharge canal. Therefore, the estimated pollution loads into the water body could even be higher.

c) Change of sediment-nutrient source

Changes in sediment regimes in the coastal regions can have harmful effects on adjacent estuaries and coastal habitats; especially mangroves are sensitive to changes in the environment due to natural and anthropogenic impact (Gilman et al., 2008, Terrados et al., 1997). Decreased availability of sediment may lead to degradation of an ecosystem by starving it of the indispensable elements necessary for its existence, since a variety of minerals, nutrients and organic matter are attached to the sediments. A substantial fraction of the fine particle material and nutrients originate from land and are responsible for the continuous accretion of sediment, allowing the growth of the mangroves (Duarte et al., 1998). The change of sediment load is a consequence of the construction and operation of the Chinese cascade dams in the upper part of the Mekong main stream, called the Lancang River (Fu and He, 2008). Analyses of flow discharge and sediment flux at a number of gauging stations on the Lower Mekong River have indicated a trouble in water discharge, water fluctuations and sediment transport downstream of the first earliest dam (namely the Manwan Dam), since 1992 when the reservoir was taken into operation. Measurements of suspended sediment concentration data at Tanchau permanent stations showed that there is a marked difference among the periods 1988-1996, 1997-2007 and 2008-2012 (Phan et al, 2017). Suspended sediment concentrations declined significantly from 126 mg/l in the period of 1988-1996 to an average 98 mg/l in the period of 1997-2007. Although there is a slight rise of suspended sediment concentrations to 104 mg/l in the next period of 2008-2012, the declining trend of suspended sediment concentration is obvious in the lower Mekong River Delta (Phan et al., 2017).

Several studies clearly document that the growth of Rhizophora apiculata seedlings, living at the edge of progressing mangrove forests, is directly correlated with the nutrient and silt contents within the sediments of mangrove sites (Duarte, C.,et al, 1998; Tanner et al., 1998, Feller et al., 1995). Seedlings growing in nutrient-poor, coarse sediments had very low growth rates to the point that their canopy only gained a couple of new leaves per year, while the greatly branched canopy of seedlings rising over nutrient-rich, silty sediments got a new leaf every other day. Experiments with fertilization suggest that the growth of mangrove trees is constrained by insufficient nutrient supplies (Onuf et al. 1977, Boto & Wellington 1983). The mangroves sheltered muddy hydro environments facilitate the deposition of fine sediments which are supplemented with nutrients, and minerals. The concentration rate of nutrients in the mangrove sediments is significantly affected by the microbial activities. For seedlings growing in the outermost fringes of mangroves, however, variable exposure may markedly change the balance between export and import of silt and nutrients, resulting in highly variable nutrient and silt contents in the sediment (Asp et al., 2018). It is, therefore, not surprising that the growth of newly established seedlings in the mangrove progression zone is variable and strongly controlled by local differences in the nutrient content of sediment. Hence, the sediment load from a large river plays a crucial role in the development of a mangrove area.

d) Coastal erosion

Erosion was also observed as a factor contributing to the loss of mangroves at specific locations. Most of the mangrove species are influenced by hydrodynamics, including waves

and currents, and its survival is endangered under extreme weather conditions. In spite of the role of mangroves to shield coastlines against hazards as wave action and coastal erosion (Tomlinson, 1994, Cuc et al., 2013), mangroves are exposed to erosion caused by natural as well as anthropogenic intervention including waves, wind, longshore currents, insufficient sediment supply and relative sea level rise (Prasetya, 2006; Spalding M., 2014).

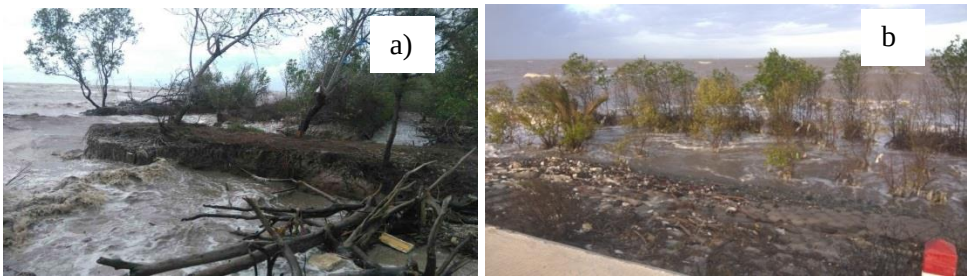

Figure 2.26: Coastal erosion to mangrove forest in Camau (a) and Tiengiang (b)

At present, the Mekong deltaic coast is facing coastal erosion of nearly 340 km of the approximately 630 km total coastline as shown in Figure 13 (Phan et al., 2017). Similar to other regions, the coastal erosion in the Mekong Delta is caused by sediment transport gradients based on wave and tidal currents, deficiency of river sediments and relative sea level rise (Marchesiello et al., 2019). A remarkable new finding of the present study is that the effect of coastal erosion on the loss of mangrove is quantified for each period. There is a gradual increase of annual loss of mangrove area by coastal erosion from 380 ha/yr to 540 ha/yr during 1973-2010, especially in the coastal province of Ca Mau. Nevertheless, the rate of mangrove loss started to decline to 320 ha/yr as a result of a series measures taken by the Vietnamese government and by several international organisations to control coastal erosion in the coastal provinces of Soc Trang, Bac Lieu, Ca Mau and Kien Giang. In addition to hard structures introduced to fix the coastline (e.g. in Tien Giang, Tra Vinh, Bac Lieu and Ca Mau provinces), in recent years local people have planted mangroves as soft structures to stabilise the shoreline. However, because of the absence of sediment supply, the planting of mangrove seedlings as well as the stabilization of the shoreline in several local regions is only moderately successful (Besset et al., 2019). Natural nourishment by trapping sediment or artificially supplying sediment from other sedimentation regions is considered as a one of the appropriate measures to resolve such problems. The close relationship between the land loss and the loss of the mangrove area along the coastal Mekong Delta, caused by coastal erosion during 43 years from 1973 to 2015, indicates a correlation value up to 99% (Figure 2.27).

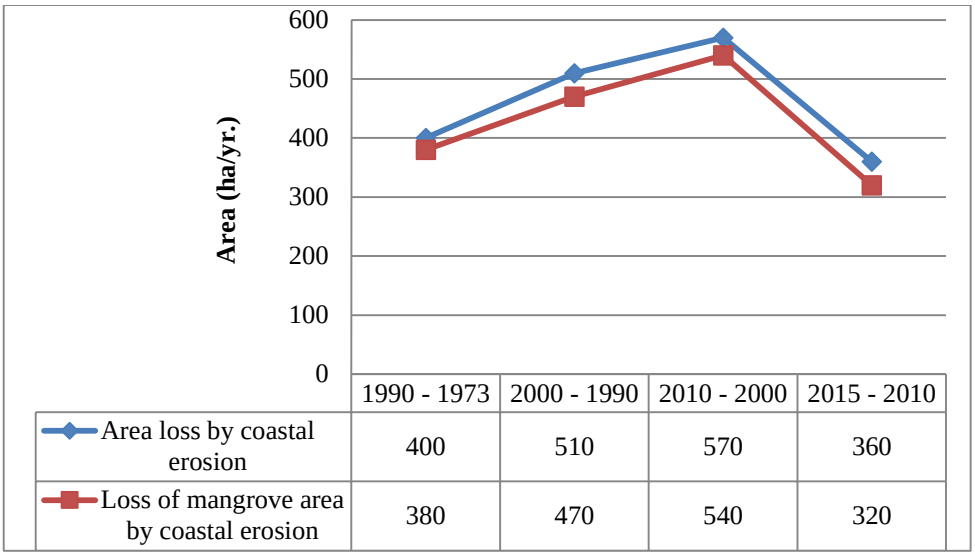

	1990 - 1973	2000 - 1990	2010 - 2000	2015 - 2010
Area loss by coastal erosion	400	510	570	360
Loss of mangrove area by coastal erosion	380	470	540	320

Figure 2.27: annual area loss of coastal erosion and mangroves due to by coastal erosion in Mekong deltaic coast in the period of 1973 to 2015.

e) Coastal Mangrove Squeeze

Marine life is endangered as well due to loss of habitat, coastal land claim, erosion and sea level rise. Coastal land claims often involves building to protect the land from erosion and/or flooding and conversion of mangrove to other land cover categories. Coastal erosion and sea level rise push mangroves landward, meaning that the mangrove habitat is squeezed into a narrowing zone when it faces the coastal land claim and, as a consequence, "coastal mangrove squeeze" takes place (Doody., 2004; Doody., 2013). Torio (2013) developed a so called Coastal Squeeze Index to evaluate the potential of a coastal marshes squeeze and to classify the threatening pressures of various wetlands in the United States and Canada. At present, the coastal Mekong Delta is facing coastal mangrove squeeze by infra-gravity waves and a sea dikes system with a critical width of 140m to maintain a healthy mangrove forest (Phan et al., 2015). Therefore, the policy makers from local and central governments need to consider the coastal mangrove squeeze with this critical width to maintain the mangrove health as well as stabilize shoreline in the Mekong delta.

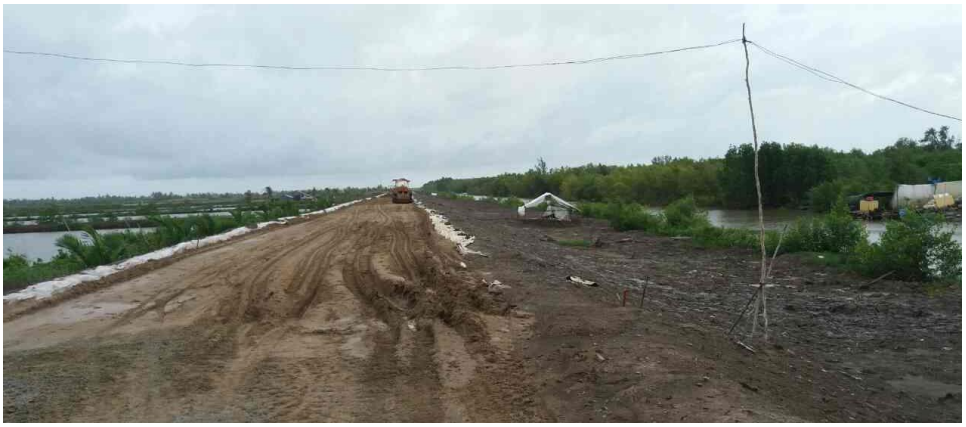

Figure 2.28: Sea dyke, shrimp farm and mangrove system in coastal area of Ca Mau province

2.4.3 Sustainable coastal land cover development

The economic development and protecting the environment are always a problematic matter to implement. The solution for sustainable coastal land cover development in the Mekong dela is necessary to carry out including improving the technique of planting mangroves as well as reconciliation of coastal protection and aquaculture.

a) Improving the technique of planting mangroves

Vietnam has implemented an effort of mangrove restoration in the beginning of the 1990s. Although there was a rise in the mangrove extent in the coastal Mekong Delta from 2010, the success rate of mangrove restoration is quite low, similar to the cases of other countries. In Bangladesh, 120,000 ha of mangroves have been planted since 1966 (Saenger & Siddiqi, 1993), however this work failed completely (Lewis, 2005). More than 44,000 ha of mangroves have been planted in Philippines and the survival rate is likewise low at 10-20% (Primavera & Esteban 2008). In Vietnam, there have been several attempts to restore mangroves in erosion-prone areas, but the success rate of mangrove planting in depositional areas was less than 50% (Duke et al., 2010; Hong, 1994; Chu., 2015).

Figure 2.29: The failure of mangrove restoration in Bac Lieu Province.

Primavera & Esteban (2008) attribute the poor survival of mangrove stands mainly to two factors: inappropriate species and sites. With respect to the experiences in the Philippines, the favoured, but unsuitable, Rhizophora species was planted in sandy substrates of exposed coastlines instead of the natural colonizers, Avicennia and Sonneratia. More significantly, planting sites are generally in the lower intertidal to subtidal zones where mangroves do not thrive, rather than in the optimal middle to upper intertidal levels. Mangrove planting on lower intertidal mudflats is to be discouraged or, at least, to be reconsidered (Samson & Rollon 2008). The most important factor in designing a successful mangrove restoration project is defining the typical hydrology (depth, duration and frequency of tidal flooding) of surviving natural mangrove plant communities in the area where restoration is executed (Lewis, 2005).

A thorough planning is an essential key to reduce the risk of failures in mangrove restoration. Analysing the reason of mangrove loss as well as infertile natural rehabilitation needs to be considered a priority before implementing mangrove restoration with the correct seedlings. Too little attention has been paid to the coastal dynamics of wave action and sediment transport, as well as implementing consistent species; the weak points in the mangrove restoration of Vietnam (IUCN, 2012). Besides, the dense oysters clinging to the seedlings and the rudimentary methods to catch crab, goby, clams, etc. by local people also affect mangrove growth. Therefore, the need to seriously study the characteristic of mangrove types, soil as well as hydrodynamics in the coastal area in the Mekong Delta is an obvious and urgent matter.

b) Reconciliation of coastal protection and aquaculture

Mangroves act as a natural wall against storms, sea level rise and erosion, and have a high potential to accumulate carbon. In addition, the mangrove ecosystems produce a natural habitat for many aquatic and terrene species, as well as providing a livelihood for coastal communities. For that reason, it is beneficial to include mangroves in the coastal protection policy. Nevertheless, along the coastal Mekong Delta, mangrove forests have been disappearing at alarming rates from 185,800 ha in 1973 to only 95,960 ha in 2015, as detailed in the analyses of the previous section. One of the reasons is that the development of the aquaculture sector generates high values on the world market. Fisheries have been very successful in the Mekong Delta, which has resulted in a significant contribution to not only a higher income for local people, but also to Vietnam's overall economic development in recent years. Along coastal districts, aquaculture covered only a few hectares in 1973, however it has exploded to roughly 300,000 hectares in 2015, adding to the aquaculture invaded mangroves area of over 2000 ha/yr within 43 years. Therefore, in recent years an approach to benefit both aquaculture and mangroves without destroying each other has received attention. Based on an evaluation framework of the costs and benefits, Tas (2016) indicated that the best coastal protection strategy is a combination with alternative use of the foreshore in the reconciliation of extensive aquaculture and mangroves. A recent success in the coastal Mekong Delta is the integrated coastal management program for mangrove restoration based on sustainable mangrove-shrimp farming and simultaneous reducing emission of SNV (Netherlands Development Organization) and the International Union for Conservation of Nature and Natural Resources. The advantage of this integrated mangrove-shrimp farming is that mangroves create a biodiversity of plankton, improve water quality as well as reduce the risk for diseases of aquatic species. Thus, not only shrimp productivity is improved, but also the risk of high fluctuation of shrimp profits can be

reduced due to benefit diversification into other aquatic yields. Integrated shrimp-mangrove farming systems along the coastal Mekong Delta provide a reasonable basis for organic production creating bio-diversity and social sustainability.

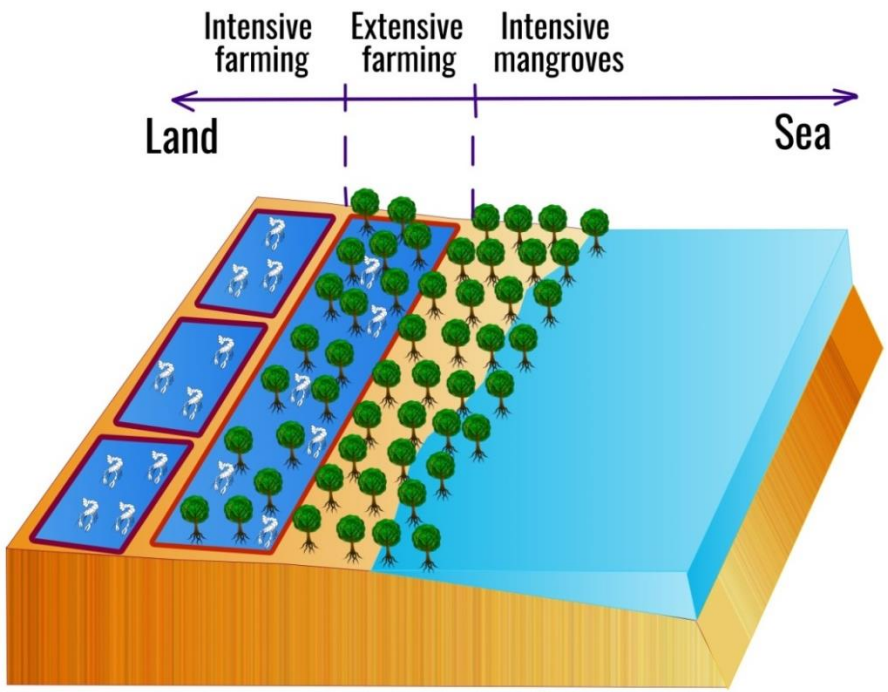

Figure 2.30: An example of extensive farming in the coastal Mekong Delta (above) and the transitional reconciliation model of mangroves and aquaculture in the coastal Mekong Delta (below).

2.5 Conclusions

Our work presents a detailed analysis of the spatio-temporal dynamics of the shoreline change of three distinctive areas in the Mekong deltaic coast from 1973 to 2015, namely the sedimentary area 1, the erosive area 2 and the relative stable area 3. However, sedimentation is still dominant in the Mekong deltaic coast with an annual average accretion of 1.2 km^2. There is a difference of coastline change rates among the periods of 1973-1990, 1990-2005 and 2005- present, where the most serious erosion took place in the period of 1990-2005. This study comprehensively contributes to the knowledge related to the evolution of the entire Mekong deltaic coast between 1973 and 2015. This study also indicates the change of sources and sinks in the Mekong Delta capable to impact the shoreline evolution in recent years.

This work provides a detailed picture of the long-term dynamics of mangroves and other land cover types in the coastal area of the Mekong Delta in Vietnam. The results reveal that there is a significant decline amounting to half the mangrove extent over the past 43 years, from 185,800 hectares in 1973 to 95,960 hectares in 2015. However, the mangrove extent, dropping to a minimum during 43 years at 89,650 ha in 2010, started to give an optimistic signal of an increase in the period of 2010-2015 after the implementation of coastal erosion limitation and mangrove restoration projects. Meanwhile, an explosive increase of aquaculture area took place, initially with only a few hectares in 1973, rising to 295,320 ha in 2015 due to the economic benefits of this farming type. It is one of the main reasons leading to the serious decline of the mangrove area in the Mekong Delta, specifically aquaculture invading mangroves approximately at a rate of 2170 ha/yr in the recent 43 years. For the first time, this study quantifies the loss of mangrove areas in the Mekong Delta due to coastal erosion, viz. an average loss of over 400 ha/yr.

The study highlights the main threatening drivers to the survival of the mangroves in the Mekong Delta, including pollution, land use conversion, insufficient nutrient-enriched sediment, coastal erosion and coastal mangrove squeeze. In order to cope with the recent historic drivers causing vast and extensive mangrove degradation, an Integrated Coastal Management Programme is an appropriate approach for the various challenges occurring in the Mekong Delta. Proper mangrove restoration techniques as well as the reconciliation of coastal protection and aquaculture need to be considered in efforts to achieve a balance between the economy of aquaculture and the environment of mangroves.

The results from these findings demonstrate that Landsat images are capable to evaluate the dynamics of shorelines, mangroves and other land cover categories on spatial and temporal scales. The study stresses the advantage and importance of the application of satellite imagery to analyse the extent of anthropogenic activities in the Mekong Delta and their impact on the shoreline and on land cover over a period of several decades. Combining aerial photography with high-resolution imagery from other satellites (e.g. Quickbird, Ikonos, Spot) could further improve the accuracy of shoreline change as well as of land cover results.

References

Addo, K.A., Quashigah, J.P.N., Kufogbe, K.S., 2011. Quantitative analysis of shoreline change using medium resolution satellite imagery in Keta, Ghana. Mar. Sci. 1 (1), 1-9.

Alesheikh, A.A., Ghorbanali, A., Nouri, N., 2007. Coastline change detection using remote sensing. Int. J. Environ. Sci. Technol. 4 (1), 61-66.

Alonso M. J., Martínez D. M., Sagrado J., Águila I. M., Batlles F.J., 2016. The application of Bayesian network classifiers to cloud classification in satellite images. Renew Energy 97:155–161. https://doi.org/10.1016/j.renene.2016.05.066.

Asp, N.E., Gomes V.J.C., Schettini C.A.F., Souza-Filho P.W.M., Siegle E., Ogston A.S., Nittrouer C.A., Queiroz M.C., 2018. Sediment dynamics of a tropical tide-dominated estuary: Turbidity maximum, mangroves and the role of the Amazon River sediment load Estuarine, Coastal and Shelf Science, 214 , pp. 10-24.

Barbier, E.B., 2003. Habitat-fishery linkages and mangrove loss in Thailand. Contemp. Econ. Policy 21 (1), 59-77.

Besset, M., Gratiot, N., Anthony, E.J., Bouchette, F., Goichot, M., Marchesiello, P. Mangroves and shoreline erosion in the Mekong River delta, Viet Nam(2019). Estuarine, Coastal and Shelf Science, 226, art. no. 106263.

Binh, T.N.K.D., Vromant, N., Hung, N.T., Hens, L., Boon, E.K., 2005. Land cover changes between 1968 and 2003 in Cai Nuoc, Ca Mau peninsula, Vietnam. Environ. Dev. Sustain. 7, 519-536.

Boto, K. and J. Wellington. 1983. Phosphorus and nitrogen nutritional status of a Northern Australian mangrove forest. Mar. Ecol. Prog. Ser. 11:63–69.

Bravard, J. P., Goichot, M., Gaillot, S., 2013. Geography of Sand and Gravel Mining in the Lower Mekong River. First Survey and Impact Assessment. 26 | 2013 : octobre 2013/décembre 2013.

Bruce, C.M., Hilbert, D.W., 2006. Pre-processing Methodology for Application to Landsat TM/ETMþ Imagery of the Wet Tropics. Research Report, Cooperative Research Centre for Tropical Rainforest Ecology and Management. James Cook University, Australia, p. 38.

Bullock, E.L., Fagherazzi, S., Nardin, W., Vo-Luong, P., Nguyen, P., Woodcock, C.E. Temporal patterns in species zonation in a mangrove forest in the Mekong Delta, Vietnam, using a time series of Landsat imagery.

Chander, G., Markham, B., 2003. Revised Landsat 5 TM Radiometric Calibration Procedures and Postcalibration Dynamic Ranges. IIEE Transactions on geoscience and remote sensing, vol. 41, No. 11.

Chander, G., Markham, B.L., Helder, D.L., 2009. Summary of current radiometric calibration coefficients for Landsat MSS, TM, ETMþ, and EO-1 ALI sensors. Remote Sens. Environ. 113, 893-903.

Chavez, P. S., 1996 Image-based atmospheric correction—revised and improved. Photogramm Eng Remote Sens 62:1025–1036.

Chu, V.C., Brown, S., Huynh, H.T., Hockings, M., 2015. Using Melaleuca fences as soft coastal engineering for mangrove restoration in Kien Giang, Vietnam. Ecological Engineering (81). p 256-265.

Congalton, R.G., 1991. A review of assessing the accuracy of classifications of remotely sensed data, Rentote Sensing of Environment, 37:35-46.

Cuc, N.T.K., Suzuki, T., Steveninck, E.D.R., Hai, H., 2013. Modelling the impacts of mangrove vegetation structure on wave dissipation in ben Tre province, Vietnam, under different climate change scenarios. J. Coast. Res., 31, pp. 340-347, 10.2112/JCOASTRES-D-12-00271.1.

Torio, D. D. and Chmura, G. L. (2014) Assessing Coastal Squeeze of Tidal Wetlands. Journal of Coastal Research: Volume 29, Issue 5: pp. 1049 – 1061.

Dahdouh-Guebas, F., 2002. The use of remote sensing and GIS in the sustainable management of tropical coastal ecosystems. Environ. Dev. Sustain. 4, 93-112.

Darvishzadeh, R. 2000. Change detection for urban spatial databases using remote sensing and GIS. In: Proceedings of ISPRS 2000–320.

Doody, J.P., 2004. Coastal squeeze e an historical perspective. Journal of Coastal Conservation 10, 129-138.

Doody, J.P., 2013. Coastal squeeze and managed realignment in southeast England, does it tell us anything about the future? Ocean and Coastal Management 79, 34-41.

Duarte, C., Geertz-Hansen, O., Thampanya, U., Terrados, J., Fortes, M., Kamp-Nielsen, L., Boromthanarath, S.,1998. Relationship between sediment conditions and mangrove Rhizophora apiculata seedling growth and nutrient status. Marine Ecology Progress Series, 175, 277-283. Retrieved January 15, 2020, from www.jstor.org/stable/24831860.

Cuc, N.T.K., Suzuki, T., Steveninck, E.D.R., Hai, H., 2013. Modelling the impacts of mangrove vegetation structure on wave dissipation in ben Tre province, Vietnam, under different climate change scenarios. J. Coast. Res., 31, pp. 340-347, 10.2112/JCOASTRES-D-12-00271.1.

Duke, N.C., Wilson, N., Mackenzie, J., Hai Hoa, N., 2010. Report on Assessing Mangrove Forests, Shorelines Conditions and Feasibility of REDD for Kien Giang Province, Vietnam, 137 pp.

El-Asmar, H.M., Hereher, M.E., 2011. Change detection of the coastal zone east of the Nile Delta using remote sensing. Environ. Earth Sci. 62 (4), 769–777.

Erban, L. E., Gorelick, S. M., Zebker, H.A., 2014. Groundwater extraction, land subsidence and sea level rise in the Mekong Delta, Vietnam. Environmental Research Letters. 9 (2014) 084010 (6pp).

Feller, I.C. 1995. Effects of nutrient enrichment on growth and herbivory of dwarf red mangrove (Rhizophora mangle). Ecol. Monogr. 65:477–505.

Ferraris V., Dobigeon N., Wei Q., Chabert M., 2018. Detecting changes between optical images of different spatial and spectral resolutions: a fusion-based approach. IEEE Trans Geosci Remote Sens 56:1566–1578

Ford, F., 2013. Shoreline changes interpreted from multi-temporal aerial photographs and high resolution satellite images: Wotje Atoll, Marshall Islands. Remote Sens. Environ. 135, 130-140.

Fu K. D and D. M. He (2008). Sedimentation in the Manwan reservoir in the Upper Mekong and its downstream impacts. Quaternary International, 186(1): 91–99. https://doi.org/10.1016/j. quaint.2007.09.041.

Gandhi, S. M., Sarkar, B. C., 2016. Essentials of Mineral Exploration and Evaluation. Elsevier. ISBN: 9780128053324.

Gilman, E.L., J. Ellison, N.C. Duke, C. Field., 2008. Threats to mangroves from climate change and adaptation options: a review. Aquat. Bot., 89, pp. 237–250.

Giesen, W., Wulffraat, S., Zieren, M., Scholten, L., 2006. Mangrove Guidebook for Southeast Asia. FAO Regional Office for Asia and the Pacific, Bangkok, Thailand, p. 769.

Gillies, R. R., Carlson, T. N., Cui, J., Kustas, W. P., & Humes, K. S. (1997). A verification of the triangle method for obtaining surface soil water content and energy fluxes from remote measurements of the Normalized Difference Vegetation Index (NDVI) and surface radiant temperature. International Journal of Remote Sensing, 18, 3145–3166.

Green, E.R., Mumby, P.J., Edwards, A.J., Clark, C.D., Ellis, A.C., 1998. The assessment of mangrove areas using high-resolution multispeciral airborne imagery. Journal of Coastal Research 14, 433-443.

Guariglia, A., Buonamassa, A., Losurdo, A., Saladino, R., 2006. A multisource approach for coastline mapping and identification of shoreline changes. Ann. Geophys. Italy 4 (1), 295-304.

Haito, H., Bellan, M.F., Al-Habshi, A., Aizpuru, M., Blasco, F., 2003. Mangrove research and coastal ecosystem studies with SPOT-4 HRVIR and TERRA ASTER in the Arabian Gulf. Int. J. Remote Sens. 24, 4073-4092.

Hao, N.V., 1999. Shrimp Health Research in Vietnam, Including Current and Planned Activities. In: Proceedings of the workshop on Towards Sustainable Shrimp Culture in Thailand and the Region, Hat Yai, Songkhla, Thailand, 28 Oct-1 Nov 1996, pp. 94-97.

Harvey, K.R., Hill, G.J.E., 2001. Vegetation mapping of a tropical freshwater swamp in the Northern Territory, Australia: a comparison of aerial photography, Landsat TM and SPOT satellite imagery. Int. J. Remote Sens. 22 (15), 2911–2925.

Hashimoto, T.R., 2001. Environmental Issues and Recent Infrastructure Development in the Mekong Delta: Review, Analysis and Recommendations with Particular Reference to Large-scale Water Control Projects and the Development of Coastal Areas. University of Sydney, Australia, p. 70.Working Paper No. 4.

Held, A., Tichehurst, C., Lymburner, L., Williams, N., 2003. High resolution mapping of tropical mangrove ecosystems using hyper-spectral and radar remote sensing. International Journal of Remote Sensing 24, 2739-2759.

Hereher, M.E., 2010. Sand movement patterns in the Western Desert of Egypt: an environmental concern. Environ. Earth Sci. 59 (5), 1119–1127.

Hong, P.N., 2000. Effects of mangrove restoration and conservation on the biodiversity and environment in Can Gio district. In: Mangrove Management and Conservation Workshop, Okinawa, Japan, 2004, pp. 111-137.

Hong, P.N., San, H.T., 1993. Mangrove of Vietnam. IUCN, Bangkok, Thailand. 173p.

Homer, C., Huang, C., Yang, L., Wylie, B., Coan, M., 2004. Development of a 2001 National Land Cover Database for the United States. Photogrammetric Engineering and Remote Sensing 70, 829-840.

Hu, L., Li, Wenyu., Xu, B., 2018. Monitoring mangrove forest change in China from 1990 to 2015 using Landsat-derived spectral-temporal variability metrics. International Journal of Applied Earth Observation and Geoinformation, volume 73, pages 88-98.

Huang, C., Townshend, J., 2003. Astepwise regression tree for nonlinear approximation: applications to estimating subpixel land cover. Int J Remote Sens 24, 75-90.

Huitric, M., Folke, C., Kautsky, N., 2002. Analysing development and government policies of the shrimp farming industry in Thailand in relation to mangrove ecosystems. Ecological Economic 40, 441–445.

IUCN (International Union for Conservation of Nature), 2012. Viet Nam national Strategy and Action Plan (2011-2013). Mangroves for the Future, Gland, Switzerland, p. 32.

Kathiresan, K., Bingham, B.L., 2001. Biology of mangroves and mangrove ecosystems. Adv. Mar. Biol. 40, 81-251.

Kathiresan, K., 2012. Importance of mangrove system. Int. J. Mar. Sci. 2 (10), 70-89.

Ke L., Lin Y., Zeng Z., Zhang L., Meng L., 2018. Adaptive change detection with significance test. IEEE Access 6:27442–27450. https://doi.org/10.1109/ACCESS.2018.2807380.

Kirui, K.B., Kairo, J.G., Bosire, J., Viergever, K.M., Rudra, S., Huxham, M., Briers, R.A., 2012. Mapping of Mangrove forest land cover change along the Kenya coastline using Landsat imagery. Ocean and Coastal Management.

Koedam, N., Dahdouh-Guebas, F., Monbaliu, D., Merken, R., Ruyck, J. De, Minh, V.Q., 2007. Improvement of Shrimp Production Sustainability and Shrimp Safety in Vietnam. Vrije Universiteit Brussel, Brussels, Belgium, p. 88. BelSPO Project Report.

Kotera,A.,Nguyen,K.D.,Sakamoto,T.,Lizumi,T.,Yakozawa,M.,2013.Amodelingapproachforassessingricecroppingcycleaffectedbyflooding,salinityintrusion,andmonsoonrainsintheMekongDelta.Vietnam.PaddyWaterEnviron12,343–354.https://doi.org/10.1007/s10333-013-0386-y.

Kuenzer, C., Bluemel, A., Gebhardt, S., Quoc, T.V., Dech, S., 2011. Remote sensing of mangrove ecosystem: a review. Remote Sens. 3, 878-928.

Kusimi, J.M., Dika, J.L., 2012. Sea erosion at Ada Foah: assessment of impacts and proposed mitigation measures. Nat. Hazards 64, 983-997.

Lan, NT. Social and ecological challenges of market-oriented shrimp farming in Vietnam. Springerplus. 2013;2:675. Published 2013 Dec 17. doi:10.1186/2193-1801-2-675.

Le, T.X., Munekage, Y., 2004. Residues of selected antibiotics in water and mud from shrimp ponds in mangrove areas in Viet Nam. Mar. Pollut. Bull., 49 (2004), pp. 922-929, 10.1016/j.marpolbul.2004.06.016.

Lee, S.Y., Primavera, J.H., Dahdouh-Guebas, F., McKee, K., Bosire, J.O., Cannicci, S., Diele, K., Fromard, F., Koedam, N., Marchand, C., Mendelssohn, I., Mukherjee, N., Record, S., 2014. Ecological role and services of tropical mangrove ecosystems: a reassessment. Glob. Ecol. Biogeogr. 23 (7), 726-743.

Lebel, L., Tri, N.H., Saengnoree, A., Pasong, S., Buatama, U., Thoa, L.K., 2002. Industrial transformation and shrimp aquaculture in Thailand and Vietnam: pathways to ecological. social, and economic sustainability. AMBIO: A Journal of the Human Environment 31, 311–323.

Lewis, R.R., Hodgson, A.B., Mauseth, G.S., 2005. Project facilitates the natural reseeding of mangrove forests (Florida). Ecol. Restor. 23, 276–277.

Lillesand, T. M., Keifer, R. W. and Chipman, J. W. 2004 Remote Sensing and Image Interpretation. 5th ed. (New York: Wiley).

Lo, C. P. and Choi, J. 2004. A hybrid approach to urban land use/cover mapping using Landsat 7 Enhanced Thematic Mapper Plus (ETM+) images.. International Journal of Remote Sensing, 25: 2687–2700.

Mang, T.L., Tran, L.T.H., Dan, N.P., 2008. Water quality assessment and propose sollutions for improvement of industrial shrimp pond in Kien Luong, Kien Giang province, Vietnam. In: Workshop on ‘‘Technical and Management Approaches to Control Wastes from Aquaculture and Seafood Processing Industries’’, An Giang province, Vietnam.

Manca, E., Pascucci, V., Deluca, M., Cossu, A., Andreucci, S., 2013. Shoreline evolution related to coastal development of a managed beach in Alghero, Sardinia, Italy. Ocean. Coast. Manag. 85, 65-76.

Mancino, G., Nol_e, A., Ripullone, F., Ferrara, A., 2014. Landsat TM imagery and NDVI differencing to detect vegetation change: assessing natural forest expansion in Basilicata, southern Italy. iForest 7 (2), 75-84.

Manoj, K.G., Lalit, K., Chandan, R., 2015. Monitoring the coastline change of Hatiya Isaland in Bangladesh using remote sensing techniques. Journal of Photogrammetry and Remote Sensing 101 (2015) 137-144.

Marchesiello, P., Nguyen, N.M., Gratiot, N., Loisel, H., Anthony, E.J., Dinh, C.S., Nguyen, T., Almar, R., Kestenare, E. Erosion of the coastal Mekong delta: Assessing natural against man induced processes(2019) Continental Shelf Research, 181, pp. 72-89.

Marshall, N., 1994. Mangrove conservation in relation to overall environmental consideration. Hydrobiologia 285, 303-309.

Massarelli C., 2018. Fast detection of significantly transformed areas due to illegal waste burial with a procedure applicable to landsat images. Int J Remote Sens 39:754–769. https://doi.org/10.1080/01431161. 2017.1390272.

McFeeters, S.K., 1996. The use of the normalized difference water index (NDWI) in the delineation of open water features. Int. J. Remote Sens. 17, 1425-1432.

Mohammady, M., Moradi, H. R., Zeinivand, H., & Temme, A. J. A. M. (2015). A comparison of supervised, unsupervised and synthetic land use classification methods in the north of Iran. International Journal of Environmental Science and Technology, 12(5), 1515-1526. https://doi.org/10.1007/s13762-014-0728-3.

Mundia, C. N., Aniya, M. (2005). Analysis of land use/cover changes and urban expansion of Nairobi city using remote sensing and GIS. International Journal of Remote Sensing, 26(13), 2831-2849.

National Academy of Sciences (NAS), 1974 . The Effects of Herbicides in South Vietnam, Part a - Summary and Conclusions. National Academy of Sciences, Washington.

Nguyen, H.H., McAlpine, C., Pullar, D., Johansen, K., Duke, N.C., 2013. The relationship of spatial – temporal changes in fringe mangrove extent and adjacent land use: Case study of Kien Giang coast, Vietnam. Ocean and Coastal Management 76, 12-22.

Onuf, C.P., J.M. Teal and I. Valiela. 1977. Interactions of nutrients, plant growth and herbivory in a mangrove ecosystem. Ecology 58:514–526.

Ogilvie, A., Belaud, G., Delenne, C., Bailly, J.S., Bader, J.C., Oleksiak, A., Martin, D., 2015. Decadal monitoring of the Niger Inner Delta flood dynamics using MODIS optical data. J. Hydrology 523, 368-383.

Ouma, Y.O., Tateishi, R., 2006. A water index for rapid mapping of shoreline changes of five East African Rift Valley lakes: an empirical analysis using Landsat TM and ETMþ data. Int. J. Remote Sens. 27 (15), 3153-3181.

Pham Thi Anh; Carolien Kroeze; Simon R. Bush; Arthur P.J. Mol (2010). Water pollution by intensive brackish shrimp farming in south-east Vietnam: Causes and options for control. Agricultural Water Management, ISSN: 0378-3774, Vol: 97, Issue: 6, Page: 872-882.

Phan, H., Reniers, A., Ye, T., & Stive, M. (2017). Response in the Mekong deltaic coast to its changing sediment sources and sinks. In T. Aagaard, R. Deigaard, & D. Fuhrman (Eds.), Proceedings of Coastal Dynamics 2017: Helsingør, Denmark (pp. 311-322). [Paper No. 225].

Phan Khanh Linh, Van Thiel De Vries, J. S. M., and Stive, M. J. F. (2015). Coastal Mangrove Squeeze in the Mekong Delta. Journal of Coastal Research, 31(2):233–243.

Prasetya GS, 2006 – The Role of Coastal Forest and Trees in Combating Coastal Erosion. FOA.

Primavera, J.H. & Esteban, J.M.A., 2008. A review of mangrove rehabilitation in the Philippines: successes, failures and future prospects. Wetlands Ecol Manage (2008) 16: 345.

Radhika K., Varadarajan S., 2018. A neural network based classification of satellite images for change detection applications. Cogent Eng 5:1–9.

Rahimi, S., Gholami Sefidkouhi, M.A., Raeini-Sarjaz, M., Valipour, M., 2015. Estimation of actual evapotranspiration by using MODIS images (a case study: Tajan catchment). Archives Agron. Soil Sci. 61 (5), 1-15.

Ricepedia. Vietnam basic statistics. Available from http://ricepedia.org/vietnam.

Sadeghi V., Farnood Ahmadi F., Ebadi H., 2016. Design and implementation of an expert system for updating thematic maps using satellite imagery (case study: changes of Lake Urmia). Arab J Geosci 9:1–17. https://doi.org/10.1007/s12517-015-2301-x

Sam, D.D., Binh, N.N., Que, N.D., Phuong, V.T., 2005. Overview of Vietnam Mangrove Forest. agriculture publisher House, Ha Noi, Vietnam (in Vietnamese).

Samson, M.S., Rollon, R.N., 2008. Growth performance of mangroves at the enhancement sites: need to revisit forest management strategies. AMBIO 37 (4), 234–240.

Saenger, P., and Siddiqi, N.A., 1993. Land from the seas: the mangrove afforestation program of Bangladesh, Ocean and Coastal Management 20, 23-39.X

Scott, J. W., Moore, L.R., Harris, W.M., Reed, M.D., 2003. Using Landsat enhanced thematic mapper tasseled cap transformation to extract shoreline. U. S. Geological Survey, Open file report OF 03-272. Available online at http://pubs.usgs.gov/of/2003/0272/.

Shimizu, A., Takada, H., Koike, T., Takeshita, A., Saha, M., Rinawati, N., 2013. Ubiquitous occurrence of sulfonamides in tropical Asian waters Sci. Total Environ., 452–453, pp. 108-115, 10.1016/j.scitotenv.2013.02.027

Silke Tas., 2016. Coastal protection in the Mekong Delta. Master thesis published by TU Delft. uuid:2f82f861-73e2-4bb3-8332-e51e917e64cd.

Song, C., Woodcock, C.E., Seto, K.C., Lenney, M.P., Macomber, S.A., 2001. Classification and change detection using Landsat TM data: when and how to correct atmospheric effect. Remote Sens. Environ. 75, 230-244.

Spalding M, McIvor A, Tonneijck FH, Tol S and van Eijk P (2014) Mangroves for coastal defence. Guidelines for coastal managers & policy makers. Published by Wetlands International and The Nature Conservancy. 42 p.

Stehman, S., 1996. Estimating the kappa coefficient and its variance under stratified random sampling. Photogrammetric Eng. Remote Sens. 62 (4), 401-407.

Stellman, J.M., Stellman, S.D., Christian, R.,Weber, T., Tomasallo, C., 2003. The extent and patterns of usage of agent Orange and other herbicides in Vietnam. Nature 422, 681-687.

Su L, Gong M, Zhang P, Zhang M, Liu J, Yang H (2017) Deep learning and mapping based ternary change detection for information unbalanced images. Pattern Recogn:2–42

Suzuki, T., Zijkema, M., Burger, B., Meijer, M., Narayan, S., 2011. Wave dissipation by vegetation with layer schematization in SWAN. Coastal Engineering 59 (1), 64-71.

Spalding, M., Kainuma, M., Collins, L., 2010. World Atlas of Mangroves. Earthscan, UK and USA, p. 319.

Syvitski, J.P.M., Saito, Y., 2007. Morphodynamic of deltas under the influence of humans. Global and Planetary Changes, 57, 261-282.

Tanner, E.V.J., Vitousek PM, Cuevas E (1998) Experimental investigation of nutrient limitation of forest growth on wet tropical mountains. Ecology 79:10-22.

Terrados, J., U. Thampanya, N. Srichai, P. Kheowvongsri, O. Geertz-Hansen, S. Boromthanarath, N. Panapitukkul, C.M. Duarte., 1997. The effect of increased sediment accretion on the survival and growth of *Rhizophora apiculata* seedlings. Estuar. Coast. Shelf Sci., 45 (1997), pp. 697–701.

Thieler, E.R., Himmelstoss, E.A., Zichichi, J.L., Ergul, A., 2009. Digital Shoreline Analysis System (DSAS) Version 4.0-An ArcGIS Extension for Calculating Shoreline Change. U.S. Geological Survey Open-File Report 2008-1278.

Thomas, N., Hendrix, C. and Congalton, R. G. 2003. A comparison of urban mapping methods using high-resolution digital imagery.. Photogrammetric Engineering and Remote Sensing, 69: 963–972.

Tian, D and Gong. M (2018) A novel edge-weight based fuzzy clustering method for change detection in SAR images. Inf Sci (Ny) 467: 415–430. https://doi.org/10.1016/j.ins.2018.08.015.

Toang, Y.D., 2017. Rice intensive cropping and balanced cropping in the Mekong Delta, Vietnam — economic and ecological considerations. Ecol. Econ., 132, pp. 205-2012, 10.1016/j.ecolecon.2016.10.013.

Tomlinson PB (1994) The Botany of Mangroves. Cambridge University Press, Cambridge.

Tuan, L.X., Yukihiro, M., Tho, N.H., Dao, P.T.A., 2003. Environmental management in mangrove areas. Environmental Informatics Archives 1, 38–52.

Tuong,T.P.,Kam,S.P.,Hoanh,C.T.,Dung,L.C.,Khiem,N.T.,Barr,J.,Ben,D.C.,2003.Impactof seawaterintrusioncontrolontheenvironment,landuseandhouseholdincomesinacoastalar ea.PaddyWaterEnviron.1,65–73.https://doi.org/10.1007/s10333-003-0015-2.

Tzachi M. Samocha, Lopez, I.M., Jones, E.R., Jackson, S., Lawrence, A.L., 2004. Characterization of intake and effluent waters from intensive and semi-intensive shrimp farms in Texas. Aquaculture Research 35, 321–339.

Valiela, I., Bowen, J.L., York, J.K., 2001. Mangrove forests: one of the world's threatened major tropical environments. BioScience 51 (10), 807-815.

Van, T.T., Wilson, N., Tung, H.T., Quistoudt, K., Minh, V.Q., Tuan, L.X., Dahdouh-Geubas, F., Keodam, N., 2015. Changes in mangrove vegetation area and character in a war and land use change affected region of Vietnam (Mui Ca Mau) over six decades. Acta oecologica 63, 71-81.

Veettil,B.K.,Quang,N.X.,2018.Environmental changes near Mekong Delta in Vietnam using remote sensing. Rendiconti Lincei. Scienze Fisichee Naturali 29, 639 – 647. https://doi.org/10.1007/s12210-018-0695-6.

Veettil, B.K., Quang, N.X., Thu Trang, N.T., 2019. Changes in mangrove vegetation, aquaculture and paddy cultivation in the Mekong Delta: A study from Ben Tre Province, southern Vietnam. Estuarine, Coastal and Shelf Science, 226.

Vescovo, L., Gianelle, D., (2008). Using the MIR bands in vegetation indices for the estimation of grassland biophysical parameters from satellite remote sensing in the Alps region of Trentino (Italy)Advances in Space Research, 41 (2008), pp. 1764–1772.

Wang, L., Sousa, W., Gong, P., 2004. Integration of object-based and pixed-based classification for mapping mangroves with Ikonos imagery. International Journal of Remote Sensing 25, 5655-5668.

Wilson, K. L., Skinner, M. A., Lotze, H. K., 2019. Eelgrass (Zostera marina) and benthic habitat mapping in Atlantic Canada using high-resolution SPOT 6/7 satellite imagery. Estuarine, Coastal and Shelf Science. Volume 226.

Wolanski, E., Spagnol, S., Thomas, S., Moore, K., Alongi, M.D., Trott, L., Davidson, A., 2000. Modelling and visualizing the fate of shrimp pond effluent in a mangrove-fringed tidal creek. Estuar. Coast. Shelf Sci. 50, 85-97.

Wu, S. T., Chen, Y. S., 2016. Examining eco-environmental changes at major recreational sites in Kenting National Park in Taiwan by integrating SPOT satellite images and NDVI. Tourism Management, volume 57, pages 23-36.

Zhang X, Xiao P, Feng X, Yuan M (2017b) Separate segmentation of multi-temporal high-resolution remote sensing images for objectbased change detection in urban area. Remote Sens Environ 201: 243–255. https://doi.org/10.1016/j.rse.2017.09.022.

3

Tidal wave propagation along the Mekong deltaic coast

A two-dimensional, barotropic numerical model was employed to investigate the dynamics of tidal wave propagation in the South China Sea with a particular interest for its characteristics along the Mekong deltaic coast. The study indicates that tidal waves propagate from the Pacific Ocean into the South China Sea mainly through the Luzon Strait (LS), where the K_1 diurnal tide dominates due to a quarter wavelength resonance in this semi-enclosed basin, and that the incoming tidal waves from the Celebes open boundary play a more important role than those from the Andaman and Flores open boundaries. Previous studies have not explained why both adjacent seas including the South China Sea and the Gulf of Thailand are dominated by a diurnal tide, while a semidiurnal tide dominates along the eastern Mekong deltaic coast. By means of Green's law, continental shelf tidal resonance theory and standing wave theory, this study clarifies that the large amplified M_2 semidiurnal amplitude leading to a prevailing mixed semidiurnal tide is caused not only by the shoaling effect and the continental shelf oscillation resonance phenomenon but also by the position on the standing wave anti-node line. Moreover, the finding of radial tidal currents occurring along the southern Mekong estuarine coast has not been revealed in earlier studies. Based on a number of numerical, geometrically schematised experiments, we suggest that the interaction between the large amplified amplitude near the shoreline associated with the adjacent low amplitude band system, causing convex hydraulic gradients of tidal amplitude due to basin geometry as well as

This chapter has been published in *Estuarine, Coastal and Shelf Science*, Phan et al. (2019)

sloping topography, is the mechanism for developing these radial tidal current systems. The results reveal that wind monsoon climate could cause either damped or amplified tidal amplitudes around the Mekong deltaic coast of which approximately 2-3 cm is due to the changing atmospheric pressure, the tangential stress of wind over the water surface and wind enhanced bottom friction. Also, this study suggests that the tidal generating forces should be considered to achieve accurate model results depending on the geographical region of interest. Findings achieved from this study contribute to a deeper insight of tidal wave propagation from a deep ocean to a shallow flat basin similar to the South China Sea and its Mekong deltaic coast.

3.1 Introduction

Most delta areas are controlled by three main factors, i.e. sediment input, wave action and tidal action (Galloway, 1983), while the relative importance of these factors may differ. The Mekong Delta may historically be well classified as a tide-dominated delta but the more western parts seem to be rather wave-dominated. This is probably reflected in the classification of Davis & Hayes (1984) where the coastal Mekong Delta is classified as a mixed-energy (tide-dominated) environment affected by the flow regime of the Mekong River and its sediment load, the tidal regimes of the South China Sea (SCS) and the Gulf of Thailand (GoT), coastal currents driven by dominated monsoon winds and the related wave conditions (Delta Alliance, 2011). While several studies of wave processes along the Mekong deltaic coast (MDC) were conducted (Xue et al., 2012; Hein et al., 2013; Tas., 2016;), tidal characteristics on the Mekong shelf have hardly been studied. Because the Mekong Delta shelf is a transitional region between the deep sea of SCS and the shallow sea of GoT, the behaviour of tidal wave propagation along the MDC is distinctive and complicated. Being one of the key factors in controlling morphological processes of the MDC, it is necessary to achieve good understanding of the principal mechanisms of tidal wave propagation on the Mekong deltaic shelf from the SCS and the GoT.

The Taiwan Strait in the North, the Luzon and Palawan Islands in the East and the GoT in the Southwest and Kalimantan in the South surround the SCS. Co-oscillating tides mainly controlled by tidal wave propagation on the Pacific Ocean and the Indian Ocean influence tidal wave characteristic in the SCS. The Pacific Ocean tides spread the SCS through the Luzon Strait and the Celebes Sea, whereas the Indian Ocean tides influence the SCS through the Andaman, Lombok and Flores Seas. However, previous studies did not almost pay attention on different important levels of these open boundaries to the tidal wave system in SCS as well as MDC.

Some earlier studies on tidal characteris in SCS comprise evaluations of tidal harmonic constituents using observation stations by Yu (1984), using Topex/Poseidon (T/P) altimetry data by Yanagi et al. (1997) and/or using numerical models by Ye and Robinson (1983), Fang et al. (1994, 1999), Zu et al (2008). Several studies have shown that tidal waves propagate into the SCS mainly through the LS, and that several amphidromic systems exist on their continental shelves (Yanagi et al., 1997; Ye and Robinson,1983 and Fang et al.,1994, 1999). Although there are numerous studies on tidal characteristic in the SCS, only a few studies considered on the tidal wave evolution in the shallower Southern Vietnam continental shelf, including the MDC. At the mouths of the Mekong River, the maximum and mean tidal ranges are 3.8 m and 2.5 m, respectively (Saito, 2015). The average tide range decreases with distance upstream (Gagliano & McIntire, 1968). All studies found that the tide is mainly diurnal in the whole South China Sea even including the Sunda Shelf and the GoT, while semi-diurnal tides dominate mostly in the region of freshwater influence (ROFI) of the MDC between the Vung Tau and Tran De branches (Nguyen et al., 1998). Zu (2008) suggested that the shoaling effect on the shallower continental shelf of the Mekong region is causing the M_2 tidal amplitude to increase to nearly 1 m. However, the K_1 diurnal tide is amplified less than the M_2 semi-diurnal tide with an amplitude of only some 0.75 m in the MDC (Fang et al., 1998) even though the tidal progressive wave in the SCS is dominated by the K_1 diurnal component. Therefore, the reason why the semidiurnal

tide dominates the tidal wave system in the region of the Mekong river mouth has not been adequately explained to date.

In most previous numerical studies of hydrodynamics in the SCS and MDC, a tidal open boundary forcing at Luzon Strait is often introduced to force tides in this region. The effect of tidal generating forces on the tidal wave system in the SCS as well as along the MDC has not been considered. The SCS is a semi enclosed shallow sea and its massive body of water is nearly 5 km in depth with a surface area of 3.5 million km^2. Therefore, the contribution of the gravitational forces to the tidal wave motion increases considerably and it is necessary to investigate to what extent tide generating forces (TGF) influence the tidal wave propagation in the SCS and whether the role of tide generating forces is important for the tidal wave propagation along the MDC.

Tides can also be affected by local wind and weather patterns. The wind driven contribution to flow and water level changes the tidal amplitude (Wijeratne et al., 2012). The monsoon winds in the SCS are caused by the influence of the trade winds and the seasonal change between the location of the earth and the sun. The East Asian monsoons cause strong seasonal climatic variations in the Mekong Delta (Hordoir et al., 2006). Winds are coming mostly from northeast directions in the winter monsoon season from November to April and southwest winds prevail during the summer monsoon. Annual wind speeds have been recorded from 1999 to 2008 by the Southern Regional Hydro-Meteorological Center (Unverricht et al., 2014) at Vung Tau station ranging from 7 to 9 m/s and in Bac Lieu from 6 to 8 m/s. Under stormy conditions wind speeds can reach 20–30 m/s (Institute of Strategy and Policy on natural resources and environment ISPONRE., 2009). The maximum wind stress occurs along the southeastern coast of Vietnam in both monsoon seasons (Unverricht et al., 2014). Although previous studies (eg. Wyrtki, 1961) agree that the circulation of the SCS is affected mostly by monsoon winds, these studies do not distinguish the different effects between the north east monsoon and the south west monsoon to tidal wave systems. Therefore, it is necessary to clarify the role of wind monsoon climate influencing the tidal wave propagation in the Mekong Delta. The mechanisms of tidal wave propagation in the Mekong Delta shelf are revealed with the aid of the high-resolution process based model Delft3D.

In this study, a large-scale model covering the domain of SCS is setup, with a special interest in the South Vietnam Sea, to gain fundamental insight into the mechanisms of the overall tidal wave propagation in the SCS with specific attention for the MDC. After verification of the model with regard to the co-tidal patterns and tidal current ellipses of the main tidal components, the residual currents and the geographical distribution of tidal types, a sensitivity analysis of the open boundaries is conducted. Effects of several factors including wind climate monsoon, tidal generating forces and river discharges are examined using numerical experiments of the tidal wave propagation.

3.2 Numerical model

The investigation of tidal wave dynamics in the South China Sea as well as Mekong deltaic coast is implement by using the process based model of Delft3D. This section presents the set up as well as the validation of the model.

3.2.1 Model set up

The depth-averaged tidal dynamics model for the whole SCS has been constructed using Delft3D-FLOW, which includes the shallow water equations, the continuity equations and the transport equations for conservative constituents (Lesser et al., 2004).

The details of the numerical schemes can be found in the Delft3D-FLOW user's manual (Deltares, 2014). The current model ranges from 96°-126°E and from 8°S -24°N with flexible orthogonal mesh features with grid cell sizes of nearly 22km near the offshore boundaries and gradually reducing to 4km around the MDC as shown in Figure 3.1. The finer grids are necessary to resolve the topography needed for an accurate simulation. A total of 8 primary tidal constituents (O1, K1, P1, Q1, M2, S2, K2, N2) derived from 15 years of Topex-Poseidon and Jason-1 satellite altimetry (Gerritsen et al., 2003) adjusted to GMT 7+ have been applied for tidal simulations at 8 main boundaries, viz. Taiwan Strait, Luzon Strait, Celebes Zee, Flores Zee, Sape Strait, Lombok Strait, Sunda Strait and Andaman Zee.

The bathymetry data shown in Figure 3.1 are obtained from the General Bathymetric Chart of the Oceans (GEBCO) bathymetry database [IOC, IHO, and BODC, 2003] with 30 arc-second grid resolution. Higher resolution bathymetry data along MDC are obtained from a bathymetry survey of the MDC in 2009 and 2010 in the context of a Vietnam Government project (SIWRR., 2010). The Manning bed friction coefficients selected after model calibration are 0.026 $m^{-1/3}s$ globally with some local values of n=0.015 $m^{-1/3}s$ on the Vietnamese shelf and a value of n=0.5 $m^{-1/3}s$ across the archipelagos separating the Sulu Sea from the SCS and the Celebes Sea, accounting for the effect of partly unresolved islands and underwater ridges. As the model domain covers a large area and the water depth of several sections is relatively deep, the TGF are included in this model and calculated including the equilibrium tide and the earth tide. In the model, the TGF of 10 tidal constituents (M_2, S_2, N_2, K_2, K_1, O_1, P_1, Q_1, MF, and MM) are considered. The six branches of the Mekong River are included as river boundaries with hourly discharges. The value for the horizontal eddy viscosity that is employed as a calibration parameter of Delft3D Flow depends on the flow and the grid size used in the simulation. Because of the large area with grid sizes of kilometers, the horizontal eddy viscosity is specified at 250 m^2/s (Gerritsen et al., 2003). For the shallow flat areas in the domain of the MDC, the process of drying and wetting is considered in this numerical model (Stelling and van Kestereren., 1994) . Computational grids are labelled either wet or dry by evaluating the total water depth at a grid cell or cell boundary with a threshold depth δ (in this study δ = 0.01m). The model was set up with zero initial conditions. The time step of the simulation is 3 minutes. The first seven days are applied as a spin-up period and neglected in the analysis.

3.2.2 Model results validation

The simulation is carried out for the whole year of 2014 using a time step of 3 minutes at zero initial conditions. In the whole SCS, along the MDC on the southern Vietnam shelf, 41 representative tidal stations located throughout the regions of SCS and MDC were selected for model verification. In order to look separately at amplitude and phase errors in individual tidal constituents, we use the vector difference to assess the combined effect of these errors over selected observations. Beside the root mean square error method is employed for the assessment of this tidal dynamics model as well.

$SVD_k = \sum_{s=1}^{s=Smax} VD_{k,s}$

$VD_{k,s} = \sqrt{(A_{c,k}cosG_{c,k} - A_{o,k}cosG_{o,k})^2 + (A_{c,k}sinG_{c,k} - A_{o,k}sinG_{o,k})^2}$

Where $A_{c,k}$, $G_{c,k}$, $A_{o,k}$, $G_{o,k}$ are the computed and observed astronomical amplitude and phase of tidal constituent k at stations s.

The RMSE of the complex amplitude is $\sqrt{\frac{1}{2N}\sum_{i=1}^{N}|A_{Si} - A_{Oi}|^2}$

Where N is the number of the observation stations; A_{Si} and A_{Oi} are the model simulated and observed amplitude at station i, respectively.

3

Computed astronomical amplitudes and phases are analysed by a tidal harmonic analysis program called Delft3D-TIDE tool. Delft3D-TIDE developed by Deltares is capable of analysing local water level or current data of at least one month to separate the astronomical part from the meteorologically induced part of the observation. The astronomical tide observed in oceans and seas is directly or indirectly the result of gravitational forces acting between the sun, moon, and earth. The influence of other celestial bodies on a yearly time-scale is negligibly small. The observed tidal motion can be described in terms of a series of simple harmonic constituent motions, each with their own characteristic frequency (angular velocity). The amplitudes A and phases G of the constituents vary with the positions where the tide is observed. The general formula for the astronomical tide is:

$$H(t) = A_0 + \sum_{i=1}^{k} A_i F_i \cos(w_i t + (V_0 + u)_i - G_i)$$

Where: H(t): water level at time t; A0: mean water level over a certain period; K: number of relevant constituents; I: index of a constituent; Ai: local tidal amplitude of a constituent; Fi: nodal amplitude factor; Wi: angular velocity; $(V0 + u)_i$: astronomical argument; Gi: improved kappa number (=local phase lag)

The Delft3D-TIDE tool is formulated in terms of k relevant constituents, a total of (2k +1) unknowns A0, Ai and Gi must be determined (or (2k +2) unknowns, if an additional term Bt is included). As a result of non-resolvable very long period constituents or non-astronomical phenomena, the mean water level may vary slowly. To take account of such motions, if present, B_t is included in the general formula for the astronomical tide, representing a trend. This is realised by minimisation of the quantity: $\sum(W(t) - H(t))^2$ using a least-squares technique.

The harmonic constants of the water level from 41 observation stations (Figure 3.1) are collected from the International Hydrographic Organization (IHO) tidal dataset, published data by Fang (1999) and Zu (2008), data from permanent stations of Vietnam Southern Regional Hydrometeorological Center as well as from the Global Tide Model. The Global Tide Model developed by Technical University of Denmark Space is available on a 0.125x0.125 degree resolution grid for the major 10 constituents in the tidal spectra. The model is utilizing the latest 17 years of multi-mission measurements from TOPEX/Poseidon, Jason-1 and Jason-2 satellite altimetry. The computed and observed harmonic constants are listed together for comparison. Furthermore, other four temporary measurements stations along the MDC (Table A.2) collected from national projects of Vietnam government are employed for validation of tidal currents simulations (ICOE., 2011, ICOE., 2014, SIWRR., 2016). The SVD and RMSE are generally small as shown in Table 1. Besides, the tidal currents ellipses in the computed data agree well with the

observed data in the magnitude and direction. Hence, the model is used to investigate the tidal dynamics.

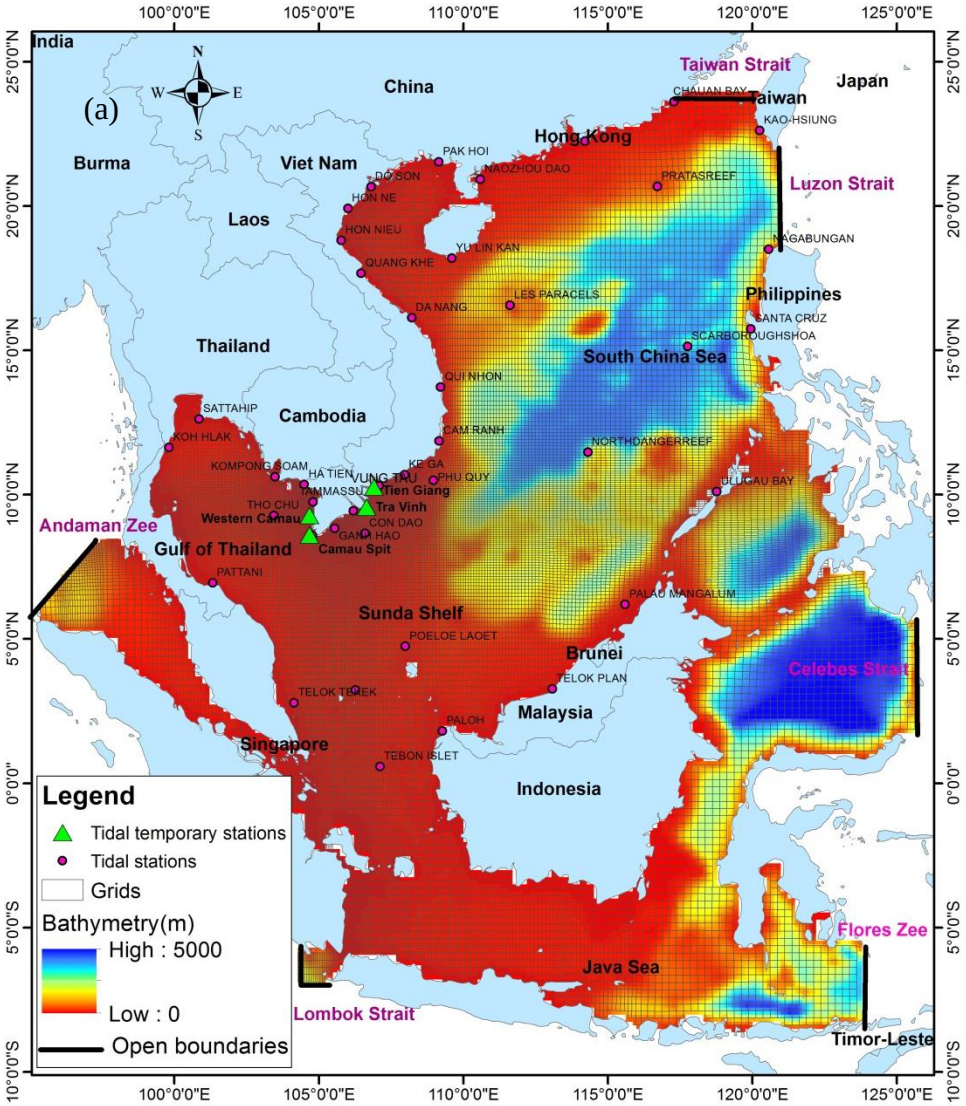

Figure 3.1: Bathymetry, model setup and location of tidal data stations

Table 3.1: Comparison of the harmonic constants between observed and calculated results for M_2 constituent

No	Station name	LONG	LAT	M2						
				Observation		Calculation		dH	dG	VD
				Amp A (cm)	Phase G (deg.)	Amp A (cm)	Phase G (deg.)	(cm)	(deg.)	(cm)
1	YU LIN KAN	109.606	18.19	20.3	303	21.6	312	-1.26	-9	3.5
2	PAK HOI	109.145	21.529	38.3	192	42.6	201.3	-4.28	-9.3	7.8
3	DO SON	106.808	20.667	5.4	76	9.2	81	-3.79	-5	3.8
4	HON NE	106.006	19.918	26.4	36	31.2	45.6	-4.81	-9.6	6.8
5	HON NIEU	105.777	18.81	30.3	31	35.3	40.1	-4.95	-9.1	7.2
6	QUANG KHE	106.464	17.671	17.6	41	23	39.4	-5.37	1.6	5.4
7	DA NANG	108.214	16.127	17.2	330.1	13	324	4.21	6.1	4.5
8	QUI NHON	109.212	13.732	17.3	321.1	10.3	316.7	6.96	4.4	7
9	CAM RANH	109.159	11.858	19.1	329.1	12.9	323.5	6.23	5.6	6.4
10	PHU QUY	108.967	10.497	18.9	345.6	21.1	336.2	-2.15	9.4	3.9
11	KE GA	107.969	10.689	36.4	23	37.9	24.5	-1.47	-1.5	1.8
12	VUNG TAU	107.086	10.305	79.2	65.1	70.9	68.9	8.35	-3.8	9.7
13	CON DAO	106.593	8.656	80	81.1	75	90.7	5	-9.6	13.9
14	MY THANH	106.193	9.432	95	86.39	90.2	92	4.8	-5.6	10.3
15	GANH HAO	105.458	9.037	108	118	101.3	124.3	6.67	-6.3	13.3
16	CA MAU	104.78	8.58	15	97	10.7	101	4.29	-4	4.4
17	TAMMASSU	104.796	9.006	10.5	135	15.3	143	-4.83	-8	5.1
18	HA TIEN	104.494	10.35	9.8	119	12.5	127.1	-2.7	-8.1	3.1
19	THO CHU	103.444	9.272	3	23	6.3	22.4	-3.3	0.6	3.3
20	KOMPONG SOAM	103.483	10.62	11.3	35	15.3	53.7	-4	-18.7	5.9

21	SATTAHIP	100.859	12.622	20.7	163.1	12.6	171.3	8.06	-8.2	8.4
22	KOH HLAK	99.245	10.427	5.1	168.4	7.2	159.1	-2.06	9.3	2.3
23	PATTANI	101.325	6.943	21	312.1	20.5	310.2	0.5	1.9	0.9
24	TELOK TEKEK	104.144	2.785	52.9	274.6	40.1	269.1	12.77	5.5	13.5
25	TEBON ISLET	107.118	0.582	5	204.8	8.6	192.1	-3.56	12.7	3.8
26	SELAT PENINTING	106.263	3.225	13	267.1	9.6	258.8	3.42	8.3	3.8
27	POELOE LAOET	107.992	4.741	9	85	16.4	79.5	-7.37	5.5	7.5
28	PALOH	109.275	1.807	60	106.4	40.8	99.8	19.2	6.6	20
29	TELOK PLAN	113.085	3.264	20.1	54.1	28.5	48.2	-8.44	5.9	8.8
30	PALAU MANGALUM	115.592	6.198	23.5	320.1	24.4	311.3	-0.93	8.8	3.8
31	ULUGAU BAY	118.77	10.104	20	304.1	17	291.3	3	12.8	5.1
32	SANTA CRUZ	119.948	15.739	11.7	263.1	15.5	272.8	-3.8	-9.7	4.4
33	NAGABUNGAN	120.56	18.498	7.6	191.8	9.6	210.8	-2.04	-19	3.5
34	KAO-HSIUNG	120.252	22.618	15.9	236.7	19.4	243.9	-3.45	-7.2	4.1
35	CHAUAN BAY	117.292	23.609	75.3	14.3	55.1	22.2	20.2	-7.9	22.1
36	HONGKONG	114.207	22.249	40.4	267.9	30.2	273.4	10.19	-5.5	10.7
37	NAOZHOU DAO	110.589	20.927	78.8	313.1	84.7	330.4	-5.94	-17.3	25.3
38	NORTHDANGERREEF	114.31	11.469	20	298.1	19.2	303.4	0.75	-5.3	2
39	SCARBOROUGHSHOA	117.765	15.137	20	305.1	15.9	290	4.06	15.1	6.2
40	LES PARACELS	111.617	16.557	16.8	297	18.3	298.3	-1.55	-1.3	1.6
41	PRATASREEF	116.716	20.678	14.2	257.5	11.8	250.5	2.44	7	2.9
Average SVD										7
RMSE								6.7	8.8	

3.3 Results

This section presents the results of the diurnal and semi-diurnal tidal propagation through the co-tidal charts, tidal currents ellipses, residual tidal currents as well as tidal character by the form factor F. Next, a sensitivity analysis was conducted of the various tidal wave source boundaries controlling tidal wave system in MDC.

3.3.1 Cotidal charts

a) The semi-diurnal tides

The co-amplitude and co-phase lines of the semidiurnal tides in Figure 3.2 are obtained from the calculated tidal harmonic components. The M_2 tide propagates mainly southwestward from the Pacific Ocean through the Luzon Strait into the SCS as a progressive wave and a minor part of the M_2 tide turns northward into the Taiwan Strait (TS) as a Kelvin wave. During the propagation, a small branch of it propagates northwestwards into the Gulf of Tonkin, while its main part continues to propagate southwestwards. When the tidal wave reaches the area adjacent to the southwest of Vietnam, part of it turns into the GoT and another part spreads southwards to the Sunda Shelf. The results show that the M2 amplitude is generally small (0.18-0.19 m) in the central part of the SCS with a wave speed of nearly 160-180m/s which can be valued from c=L/t, where L is the distance between two adjacent co-phase lines and t is time duration which wave travels between those two co-phase lines. Meanwhile, the amplitudes in areas including TS, the south of Guangdong around Leizhou Peninsula, the northwest coast of Kalimantan, the south of the Vietnam, and around the western and southern parts of the Malay Peninsula are more than 1m.

A nodal band can be observed along a line roughly corresponding to the axis of the GoT and spreading to the area between Singapore and the west of Kalimantan (Indonesia). The study area is close to the equator leading to a weak Coriolis force. The evidence of this phenomenon is the unusual clockwise amphidromic system of the semidiurnal tide M_2 in the mouth of the Gulf of Thailand (Yanagi and Takao, 1980), as according to the theory it should have a counter-clockwise rotation in the northern hemisphere. The inertia period Ti ($=2\pi/f$, f; the Coriolis parameter $= 2\omega\sin\varphi$, ω; the angular velocity of the earth's rotation, φ; the latitude = 7°N in this case) of the Sunda shelf is 98.5 hours. The Rossby deformation length λ ($=gH/f$) of the shelf is 1580 km with the average depth of the Sunda shelf being roughly 100m. Semi-diurnal and diurnal tidal periods are therefore much shorter than the inertial period and the width of the Sunda shelf of approximately 950km is narrower than the Rossby deformation length. These facts suggest that the Coriolis force on the Sunda shelf does not seriously affect the tidal phenomena. Therefore the condition is not favourable for a Kelvin wave tide to occur, especially looking at the pattern of the tidal wave propagation onto the Sunda shelf in the same phase.

The M_2 tide is amplified on the southern Vietnam shelf up to 1.1m at the coastal zone of Bac lieu Province. When the M_2 tide from the deep SCS travels into shallower water in coastal southern Vietnam (CSV), the celerity will decrease which results in a concentration of energy and thus an increase in tidal amplitude called shoaling. The average water depth of the SCS is about 2500m and the continental shelf area of Southern Vietnam is about 100m. Green's law expresses the increase in amplitude as the wave shoals toward the coast:

$$A_s = \left[\frac{D_d}{D_s}\right]^{1/4} A_d \quad (1)$$

Where: A: the amplitude of tide
D: the water depth
s, d: shallow (coastal zone) and deep water, respectively.

With an average amplitude of M_2 in SCS of nearly 0.18m, the average amplitude of M_2 in the CSV should be approximately 0.4m due to the shoaling effect from Eq (1). However, the average M_2 tide amplitude occurs to be about 0.9m-1.0m in this region, exceeding the amplitude value due to the shoaling effect. Therefore, this larger amplified M_2 amplitude is triggered by not only the shoaling effect but also by another effect viz. resonance. According to the theory of Clarke and Battisti (1981), continental shelf tidal resonance occurs when the shelf scale L is approximately equal to the shelf width:

$L \approx g\alpha/(\omega^2 - f^2)$ (2)

Where:

α: the shelf bottom slope based on Vietnam southern shelf bathymetry = 0.00067 (GEBCO).

ω: M_2 tidal frequency = 1.405×10^{-4} s^{-1},

f: the Coriolis parameter = $2\omega_e \sin ø = 0.228 \times 10^{-4}$ s^{-1}, ω_e: the angular velocity of the earth's rotation, ø: latitude = 9°N in this region.

The shelf scale L calculated by Eq (2) is nearly 340 km, which is roughly equal to the southern Vietnam shelf width of 350 km, hence the semidiurnal resonance effect of M_2 occurs. Therefore, the M_2 amplitude amplification up to 1.1 m at Bac Lieu Province's coast is not only due to the shoaling effect but also due to the continental shelf tidal resonance phenomenon. Both these phenomena cause a prevailing semidiurnal tide along the eastern MDC enclosed by diurnal tide in the SCS and GoT. The propagation of S_2 tide shown in Figure A.1 is similar to that of M_2 tide, but the amplitude of S_2 is much smaller than that of M_2.

b) Diurnal tides

Like the M_2 tide, the K_1 tide mainly propagates into the SCS from the Pacific through the LS (Figure 3.2). The rotation direction of the K_1 tide in the GoT is opposite to that of the M_2 tide due to the particular M_2 tidal frequency as well as due to the influence of the Coriolis force on the K_1 tidal wave being larger than that on the M_2 tidal wave as a result of its longer period (Yanagi and Takao, 1998). Some areas with high K_1 amplitudes are located on the Gulf of Tonkin (about 0.7–0.9 m), in the northern part and the mouth of the GoT and at the south of the Kalimantan Strait (about 0.6 m). In contrast to the condition of the M_2 tide, the amplitude of K_1 is noticeably increased in the SCS basin (about 0.3–0.4m) after spreading from the Pacific (about 0.1–0.15m) through the LS. Therefore, it is suggested that the amplification of K_1 is caused by the resonance in the SCS. The natural oscillation period of the SCS is derived from the following equation for a semi-closed basin (Proudman, 1953):

$$T_i = \frac{4L_b}{(2i-1)\sqrt{gH}} \quad (3)$$

Where i stands for the mode number, *Lb* (=2700 km) denotes the length of SCS from the Luzon Strait to the eastern Malaysian Peninsula, g (=9.81 ms^{-2}) is the gravitational

acceleration and H (=1700m) represents the mean depth of the SCS. The natural oscillation period of the SCS is 23.2h hours close to the K1 diurnal period of 23.9h. The resonance in the SCS is also found in the O_1 diurnal period of 25.8h (Figure A.1).

Moreover, the resonance phenomenon also amplifies the diurnal tide significantly in the Gulf of Tonkin and the GoT. The inertial period *Ti* (=2π/*f*, *f*; the Coriolis parameter = 2ωsinφ, ω; the angular velocity of the earth's rotation, φ; the latitude = 19.5°N in this case) of the Gulf of Tokin is 35.9 hours. The Rossby deformation length λ (= *gH* /*f*) of the gulf is 455 km. Both semi-diurnal and diurnal tidal periods are much shorter than the inertial period and the width of the gulf is narrower than the Rossby deformation length in the Gulf of Tonkin. These facts suggest also that the Coriolis force in the Gulf of Tokin does not seriously affect the diurnal tidal phenomena. The length and mean depth of the Gulf of Tokin are approximately 520 km and 50 m, respectively. The natural oscillation periods along the Gulf of Tonkin calculated from Eq (3) is 26.1 hours close to O_1 diurnal period of 25.8 hours.

The GoT is situated in the southwestern part of the SCS and the length from the shelf edge to the head of the gulf, *L*, is about 1,450 km; and its average depth, *H*, is about 55 m. Similarly, the natural oscillation periods along a semi-closed basin of the GoT from Eq. 3 are T_1= 69.4 hours, T_2= 23.1 hours, and T_3= 13.9 hours and nearly equal to the K1 diurnal period. Although the diurnal tide controls both the Gulf of Tokin and the GoT, the O_1 diurnal tide and K_1 diurnal tide dominate in the Gulf of Tokin and the GoT, respectively.

In summary, the study investigated diurnal and semi-diurnal tidal dynamics in the SCS and MDC. The study reveals the semi-diurnal amplitude amplification at the eastern MDC is not only due to the shoaling effect but also due to the continental shelf tidal resonance phenomenon. Moreover, it illuminates the resonance phenomenon of diurnal tide due to nearly equal natural oscillation period in the semi-basin of SCS.

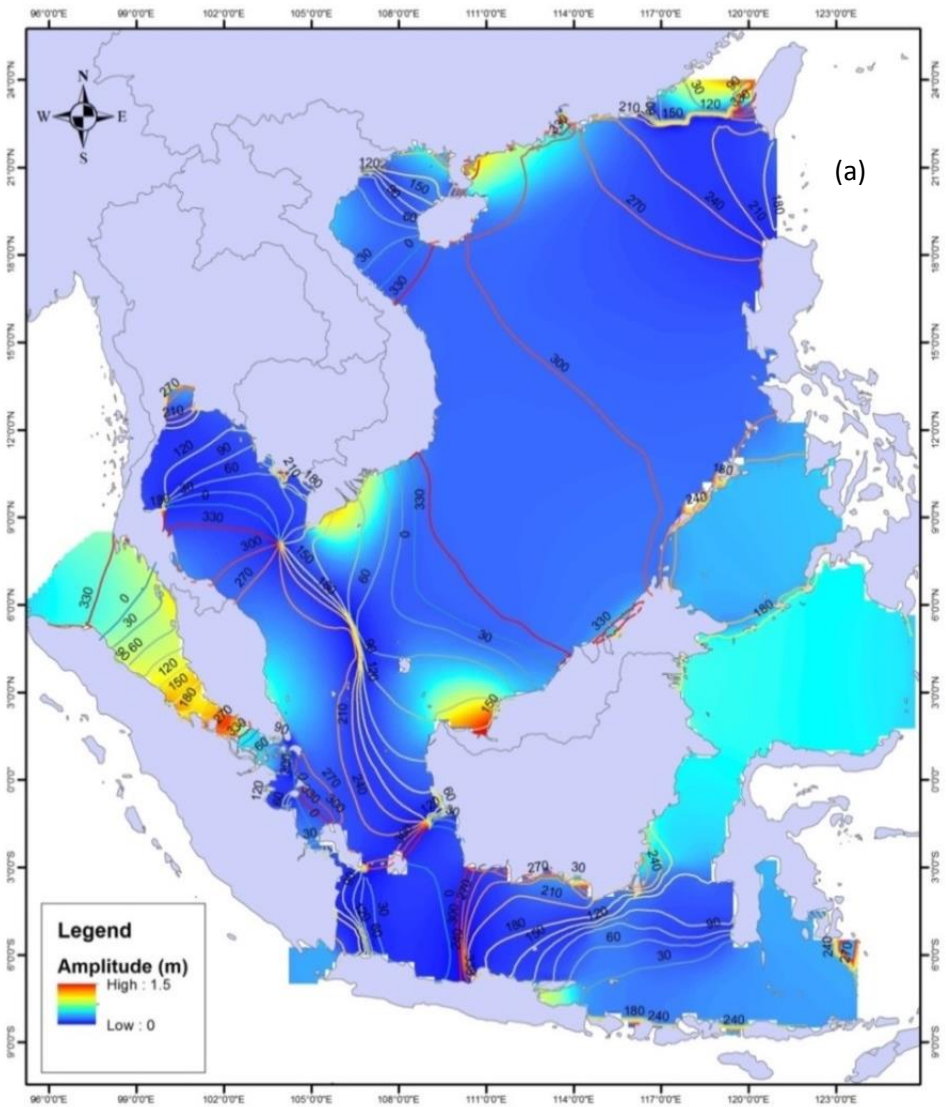

Figure 3.2: Co-tidal charts of semi-diurnal M_2 (a) and diurnal K_1 (b)

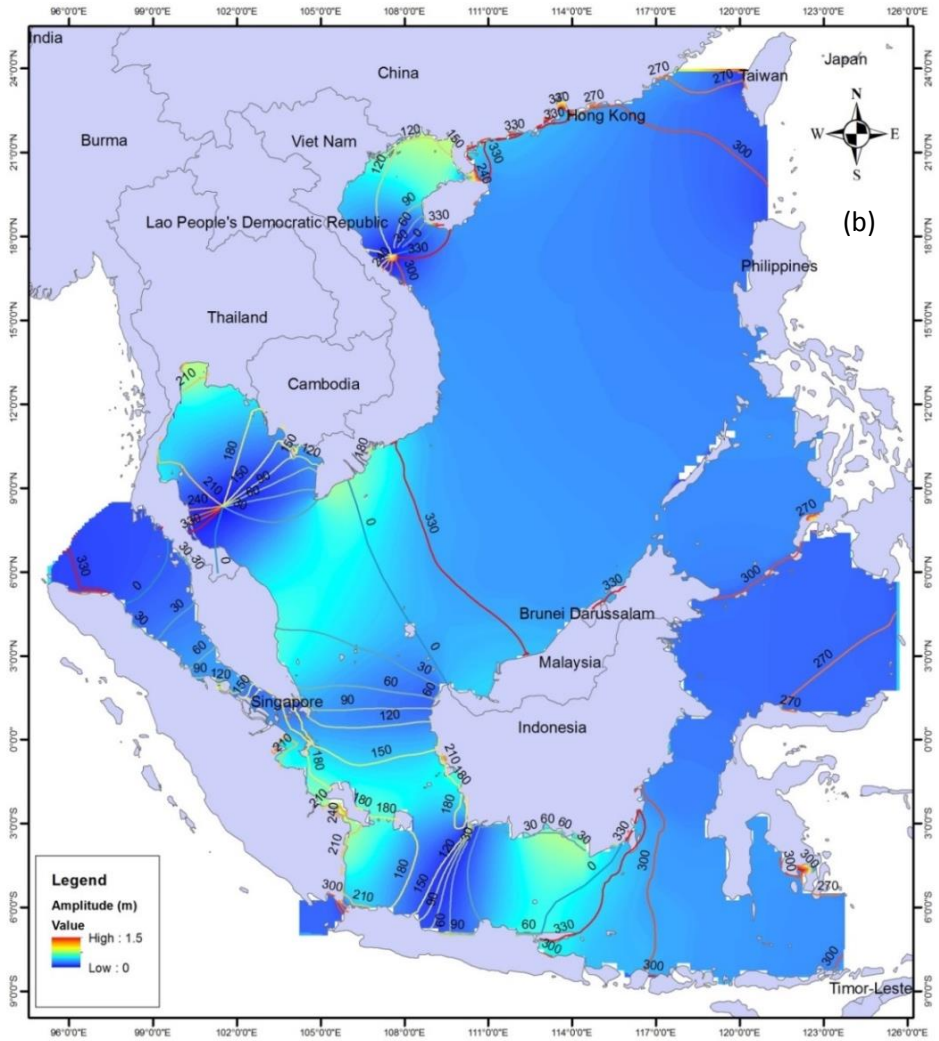

Figure 3.2, continued.

3.3.2 Tidal currents field and residual currents

A common investigative tool for tidal currents is a plot of tidal current vectors. Over a tidal cycle, the current vectors typically trace out a tidal ellipse. Figures 3.3a and b shows the simulated tidal ellipses of the M_2 and K_1 tidal constituents along the Southern Vietnam Coast. The tidal current ellipses of the M_2 tide indicate strong currents on the eastern coast of the Mekong Delta amounting to approximately 35-45 cm/s, while weak currents take place on the western coast. It can be clearly seen that large tidal currents occur in places with large tidal amplitudes.

Moreover, the tidal ellipses in the region off the Mekong River mouth are rectilinear and have a strong cross-shore component, which may be related to a standing wave.

However, the tidal ellipses in the south of the Mekong River mouth are broader and have an alongshore component. This shape rather corresponds to a progressive wave. In contrast to the tidal current ellipses of the M_2 tide, the tidal current ellipses of K_1 represent rather weak currents both on the eastern and western Mekong Delta coast. In contrast, both tidal current ellipses of M_2 and K_1 show rather strong currents and rectilinear shapes on the Camau peninsula.

On the other hand, according to tidal current fields in the flood tide and ebb tide from the Figure 3.3c and d, it seems that a radial tidal current field exists to the south of the Mekong river mouth and Baclieu is the focal point of the converging and diverging currents. This radial tidal current phenomenon also occurs at other places in the world, for instance at the Jiangsu coast in China, which has a larger strength of the radial tidal current velocities compared with the MDC. Su (2015) showed that radial tidal currents in Jiangsu coast are controlled by the special local convergent tidal wave pattern from the meeting of the rotating tidal wave and the incident tidal wave. Furthermore, based on analyzing tidal current system, Peng (2015) suggested that the radial tidal currents are able to appear in a basin including the basin length larger than the width, a depth variation or an oblique tidal wave.

Tide-induced residual currents always play a key role in the oceanic processes, especially in the shallow coastal regions (Lee et al., 2011); the tide-induced residual current fields are also computed and shown in Fig. 3e. It can be found that the residual current increases mainly toward the southwest of the shallow MDC and is strongest along the Camau peninsula, amounting roughly to 10-15cm/s. The finding of the tide-induced residual current with a direction from northeast to southwest along the eastern MDC from this numerical model is in accordance with previous geological studies (Nguyen et al,. 2000, Ta., 2002, Unverricht et al., 2013). A part of the tidal currents continues to flow toward the southwest but the main part of those tidal currents are oriented toward the GoT with diminished magnitude. Based on the distribution of the residual currents combined with the tidal current ellipses of the M_2 semidiurnal tide a standing wave in the region off the Mekong and a corresponding progressive wave in the south of the Mekong River mouths are apparent.

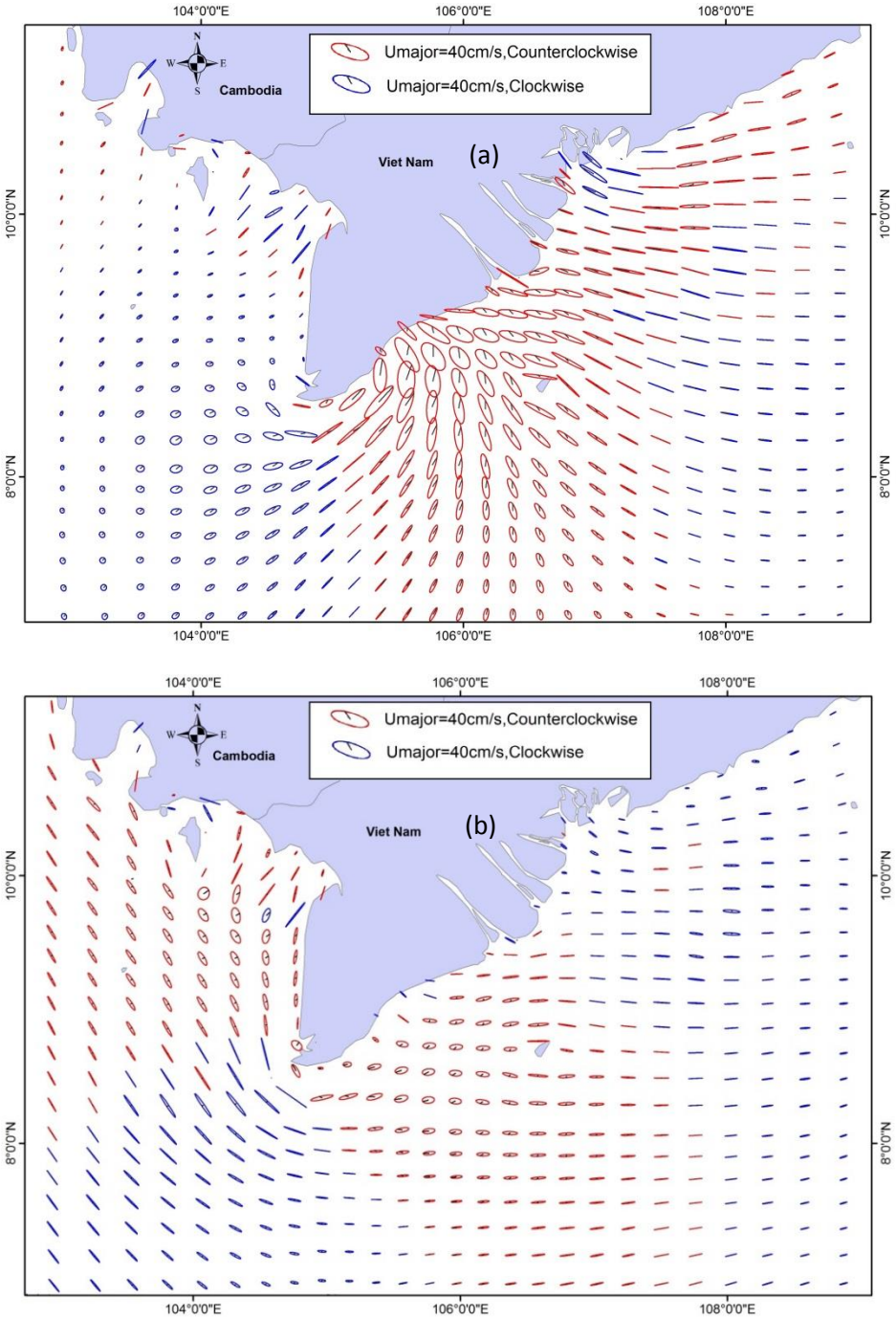

Figure 3.3: Tidal currents in the the tidal current ellipses of M_2 (a), K_1 (b), flood tide (c), the ebb tide (d) and tidal induced residual currents (e).

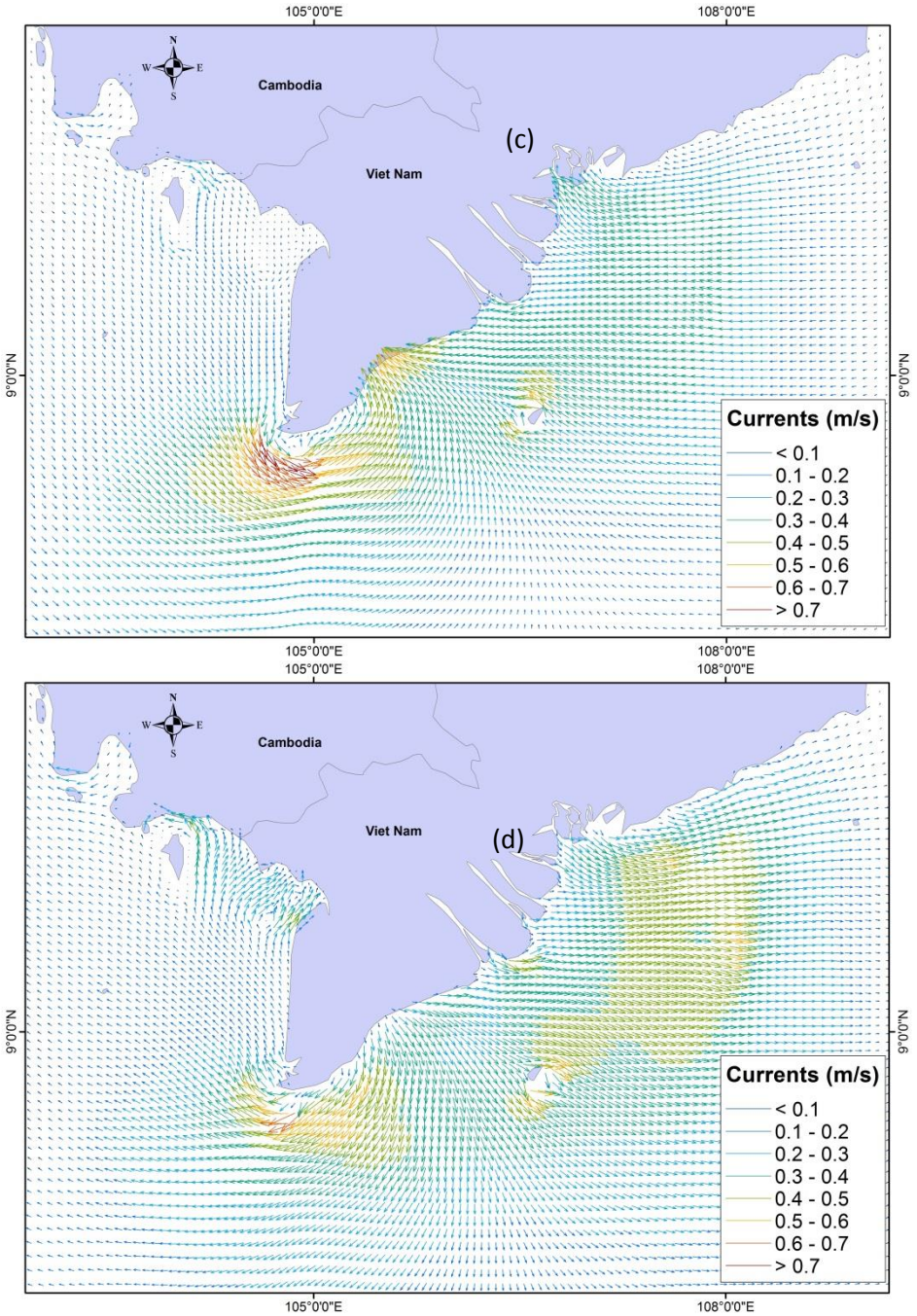

Figure 3.3, continued.

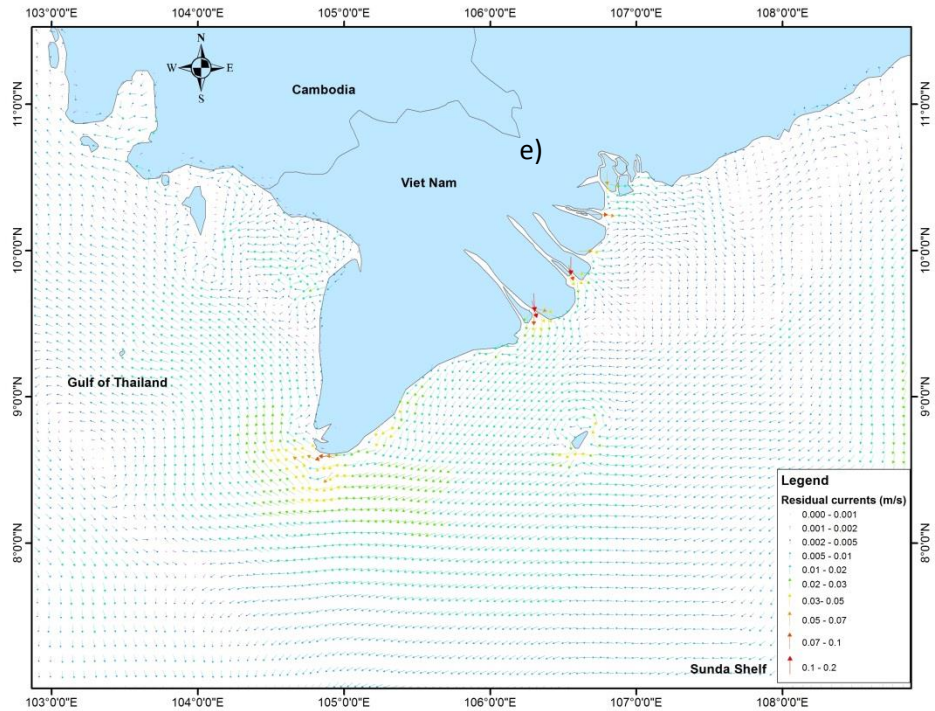

Figure 3.3, continued.

3.3.3 Geographical distribution of tidal characteristics

Classification of the type of tide is based on characteristic forms of a tide determined by the local relationship of the semidiurnal and diurnal tidal constituents. Tide types may be quantitatively classified (e.g., Defant 1961) by the amplitude ratio (F ratio) of:

$$F = (K_1 + O_1) / (M_2 + S_2)$$

K_1, O_1, M_2, S_2 are the principal lunar diurnal constituents, the principal solar diurnal constituent, the principal lunar semidiurnal constituent and the principal solar semidiurnal constituent, respectively. If the ratio is less than 0.25, the tide is classified as semidiurnal; if the ratio is from 0.25 to 1.5, the tide is classified as mixed, mainly semidiurnal; if the ratio is from 1.5 to 3.0, the tide is classified as mixed, mainly diurnal; if the ratio is greater than 3.0, the tide is classified as diurnal.

The results show that the tidal waves in the SCS are greatly affected by the depth and shape of the basins in which they propagate. The natural oscillation period of the various basins for the main tidal constituents are producing zones with predominantly diurnal tides and zones with predominantly semi-diurnal tides. Figure 3.4 indicates that mixed diurnal tides dominate in the SCS, while there are some rare regions where a semidiurnal tide dominates due to the natural oscillating period of SCS close to the diurnal period. A pure prevailing diurnal tide is only found in the GoT, the Gulf of Tonkin, waters between Sumatra and Borneo and the south-west of Luzon Strait due to local conditions. These

findings are in contrast with the results from Yanagi (1997) claiming that a pure diurnal tide dominates in the whole SCS. Besides, this study improves the tidal classification on the western MDC by Wyrtki (1961). These authors propose that a mixed diurnal tide dominates on this coast, but in reality the tide is purely diurnal.

Figure 3.4 shows that semi-diurnal tides dominate in the regions such as Malacca Strait connected directly to the Indian Ocean, Taiwan Strait linked to the East China Sea and South West in GoT. Mixed semi-diurnal tides exist in south of Guangdong, the northwest coast of Kalimantan, the southwest of Thailand and the continental shelf of the Mekong Delta. All above regions are shallow continental shelves with concave coastlines, which are significant factors to increase the M_2 tidal semidiurnal amplitude due to the natural oscillation period of these basins close to the semi-diurnal period.

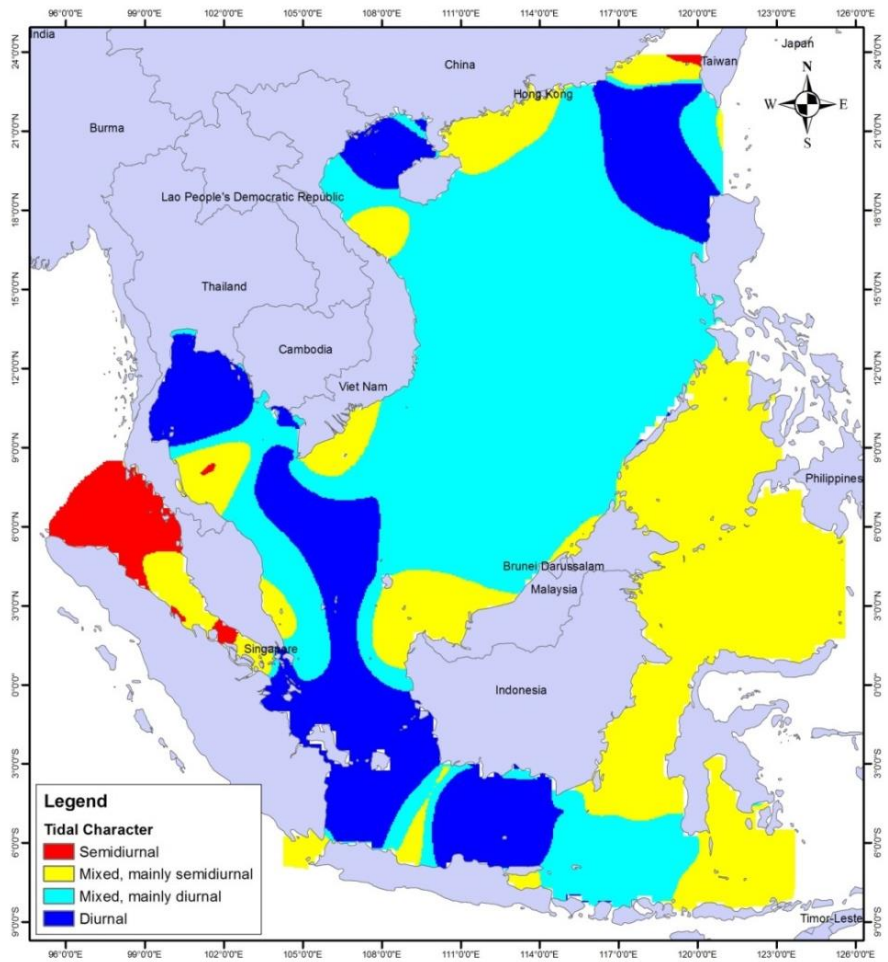

Figure 3.4: Tidal character in the South China Sea

3.3.4 Sensitivity analysis of tidal open boundaries

Tidal oscillations in the SCS are mainly co-oscillating tides forced by tidal wave motions on the Pacific Ocean and the Indian Ocean. The Pacific Ocean tides reach the SCS not only through the Luzon Strait but also through the Celebes Sea, while the Indian Ocean tides reach the SCS through the Andaman, Lombok and Flores Seas. Therefore, the importance of all tidal wave sources towards tidal characteristics in MDC needs to be investigated. A sensitivity analysis was conducted of the various tidal wave source boundaries including Andaman Sea, Flores Sea and Celebes Sea controlling tidal wave system in MDC.

Figures 3.5a, c and e show the calculated differences of phases and amplitudes for the M_2 tide when excluding the Andaman, Flores and Celebes open boundaries. When excluding the Andaman and Flores boundaries, the change of the M_2 amplitude around the MDC is roughly 1 to 2 cm, increasing to 5 to 8 cm nearby Camau spit. Meanwhile, the boundary at Celebes strongly influences the eastern coastal Mekong regions with differences for the M_2 semidiurnal amplitude reaching as high as 15cm. The differences of the co-phase lines are also limited in the case of excluding the Andaman and Flores boundaries. Meanwhile there are significant differences of the co-phase lines, roughly 30-40 minutes, south of the Mekong river mouth when excluding the Celebes boundary condition. The position of the amphidromic point shows a small change in the GoT, while the amphidromic point excluding the Flores boundary seems to be stationary. Comparison between the three open boundaries of Andaman, Flores and Celebes, the Celebes open boundary has the strongest effect on the semidiurnal tide in the coastal Mekong region, while the role of the Flores boundary is almost negligible. Figures 3.5b, d and f indicate the simulated changes of phases and amplitudes of the K_1 tide as a result of eliminating Andaman, Flores and Celebes open boundaries, respectively. Like for the M_2 semidiurnal tide, the incoming K_1 semidiurnal tidal wave from the Celebes Sea influences the MDC more strongly compared with the Andaman and Flores open boundaries. The differences of the K_1 diurnal amplitudes and co-phase lines for a closed Celebes boundary are definitely significant, reaching 25 cm and over 2 hours, respectively. Meanwhile, the K_1 tidal wave propagation from the Andaman and Flores boundaries is smaller than that from the Celebes boundary to the coastal Mekong region with a difference of the K_1 diurnal amplitude of roughly 5-10cm. While the tidal wave from the Flores Sea affects the change of co-phase lines of K_1 diurnal component with an average of about 35 minutes, the effect of Andaman Sea to K_1 tidal wave system in MDC is negligible. The results illustrate that the tidal incoming wave from the Celebes open boundary also plays an important role in the tidal wave system in the Mekong coastal region; hence it should not be neglected in simulating tidal wave propagation in the SCS in general and on the MDC in particular.

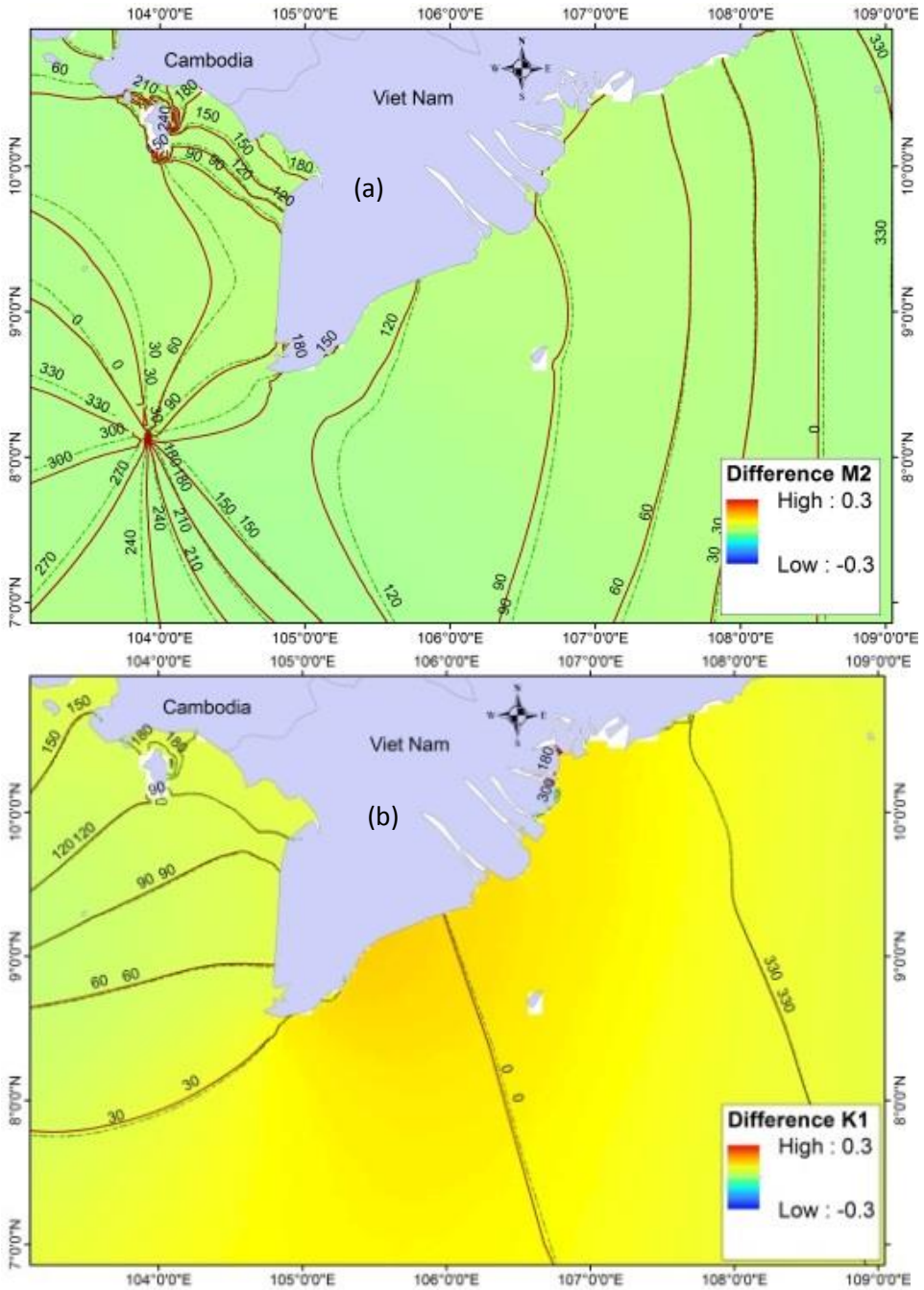

Figure 3.5: Phase and amplitude difference of M_2, K_1 if ignoring Andaman (a,b), Flores (c,d), Celebes (e, f) boundaries, respectively, with brown solid and dashed green lines represent the co-phase lines of case original condition and case of excluding boundary

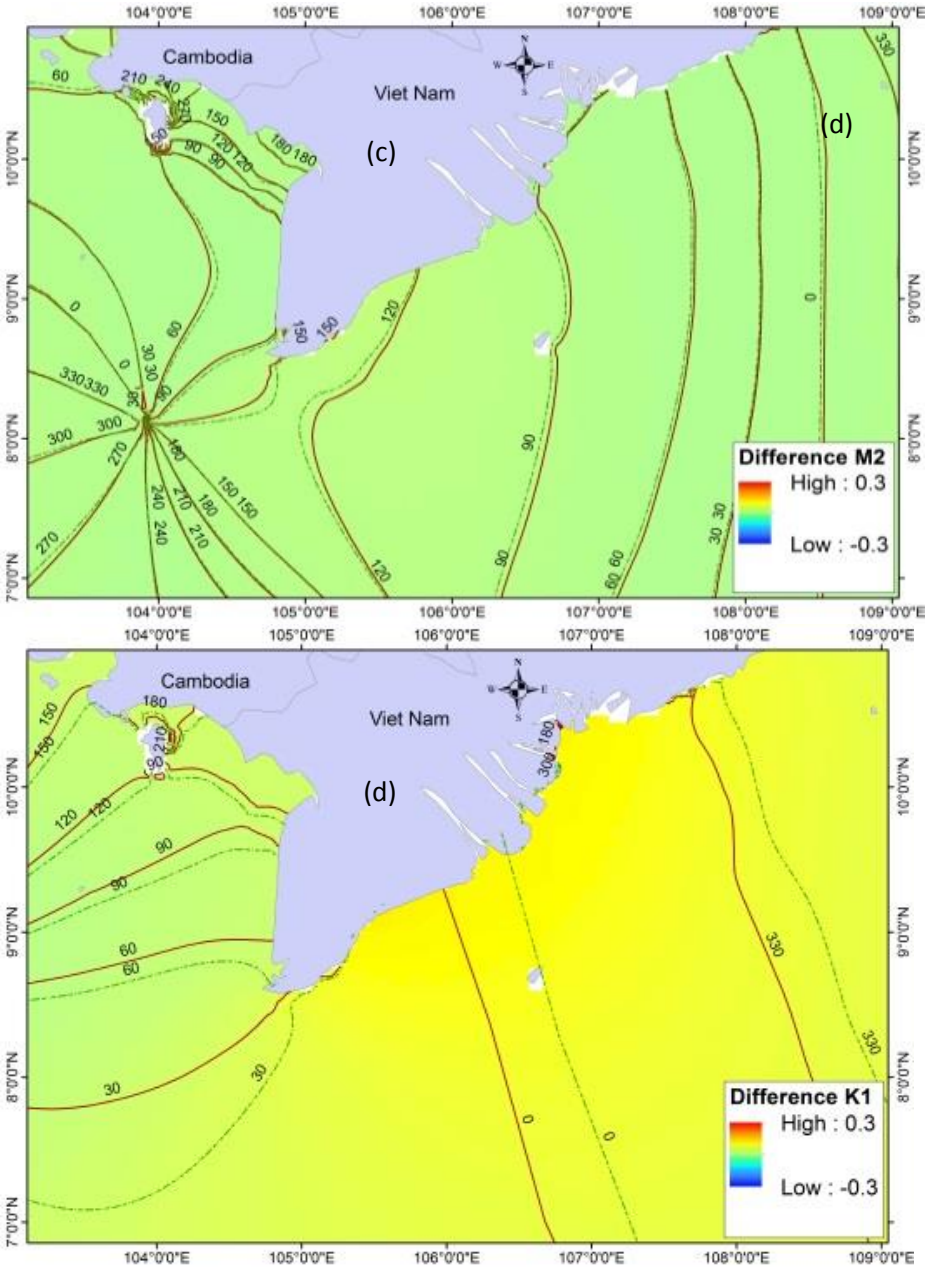

Figure 3.5, continued.

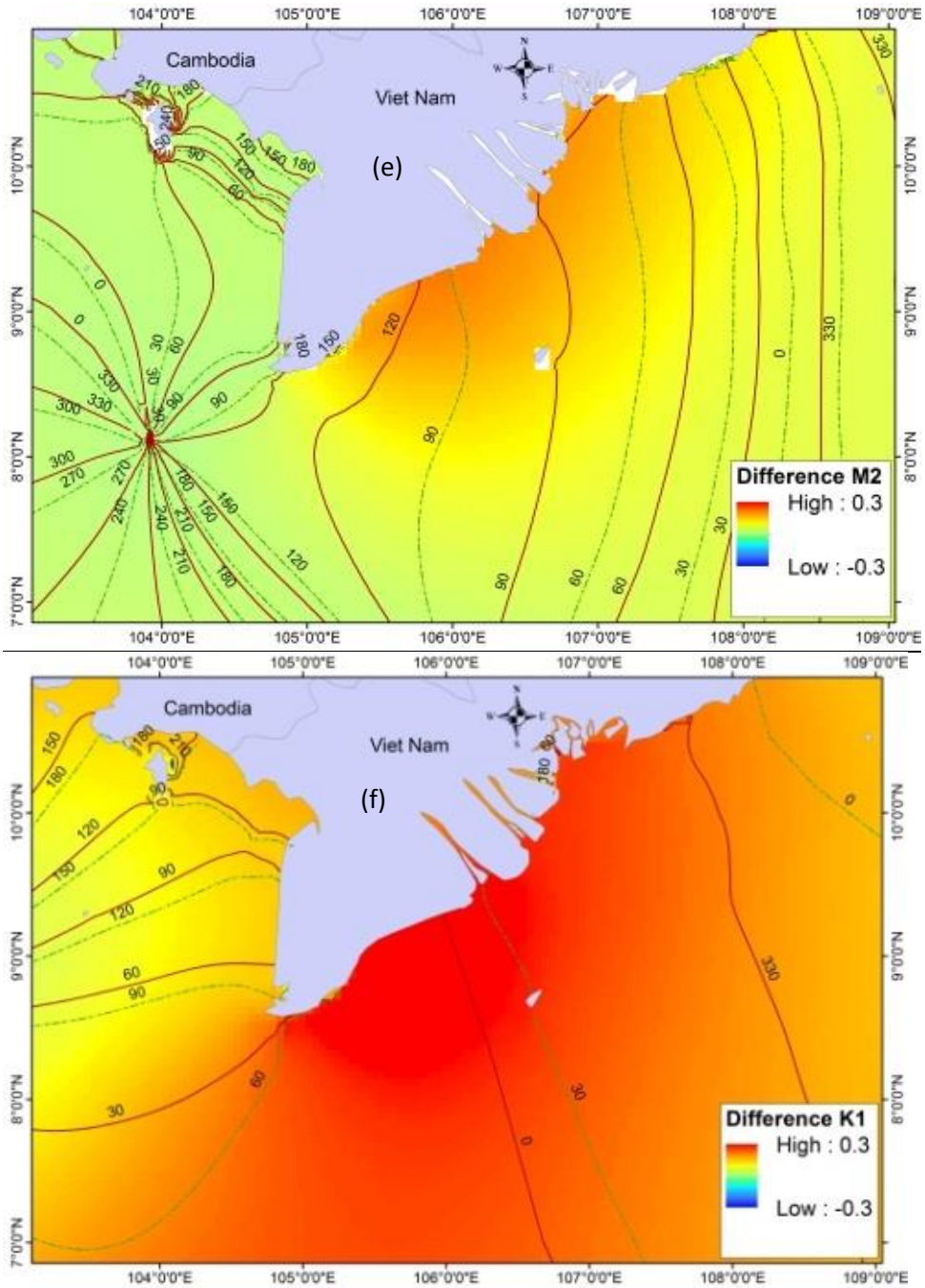

Figure 3.5, continued.

3.4 Discussion

3.4.1 The shoaling and resonance effect

Although the shoaling and resonance processes are explained through the theoretical analysis of section 3.1.1, idealized numerical experiments were established to more firmly demonstrate these effects. The schematization concerns the use of three simplified topographies including a quasi-original case (Figure 3.6a), the narrow Mekong deltaic shelf case (Figure 3.6b) and the flat Mekong deltaic shelf case (Figure 3.6c). Inspired by the results of the sensitivity analysis, the tidal wave system on the Sunda Shelf can be considered to be similar to the tidal wave propagation in a semi-enclosed basin because of the weak role of the Andaman and Flores open boundaries. The simplified models were forced at the open boundary of the SCS with an M_2 tidal amplitude and phase of 0.18m and 300° respectively. Figure 3.6b and 3.6e show that the wide scale of Mekong deltaic shelf significantly influences the resonance phenomenon. The M_2 amplitude decreases considerably along the MDC when the Mekong deltaic shelf is made narrower. Furthermore, figure 3.6c and 3.6f elucidate the importance of the topography for the effects of shoaling and tidal resonance when changing the slope as well as the length of schematized shelf. With a flat topography equal to that of the Mekong deltaic shelf, the M_2 amplitude along the MDC is no longer amplified.

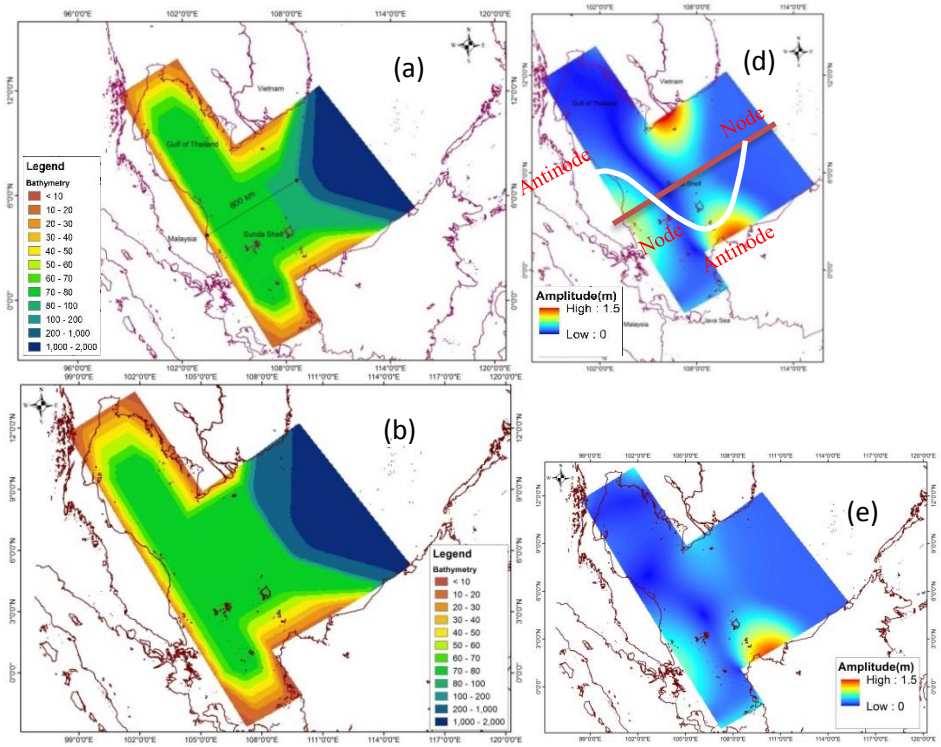

Figure 3.6: Schematised experiments including topography and M2 co-amplitude charts of the quasi-original case (a) (d), the narrow shelf case (b) (e) and the flat topography of Mekong deltaic shelf case (c) (f), respectively.

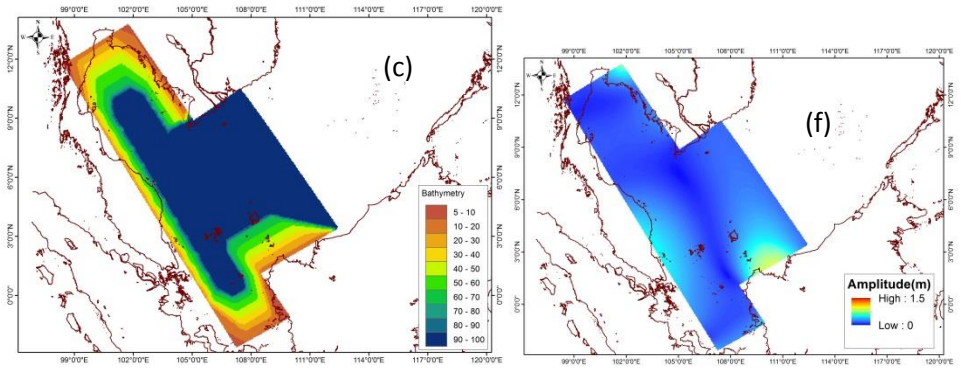

Figure 3.6, continued.

3.4.2 Radial tidal currents

Based on the flood and ebb current fields as well as the tidal current ellipses (Figure 3.3a, b, c, d), it is hypothesized that the interaction between the nearshore amplified amplitude and the offshore low amplitude due to the basin geometry and the shallow, sloping topography creates convex hydraulic gradients leading to radial tidal currents on the Mekong deltaic shelf. To deepen our insight in processes controlling the radial tidal current in the south of Mekong estuaries, schematised experiments were developed with different simplified geometry including the quasi-original case as section 3.4.1 (Figure 3.6a), an extended GoT case (Figure 3.7a) and an extended SCS case (Figure 3.7b). Establishing these experiment cases is to examine how the radial tidal currents alter when changing the magnitude of convex hydraulic gradients by varying the basin geometry. The schematised models were forced at the open boundary at SCS with M_2 tidal amplitude and phase of 0.18m and 300^o respectively as in the reality.

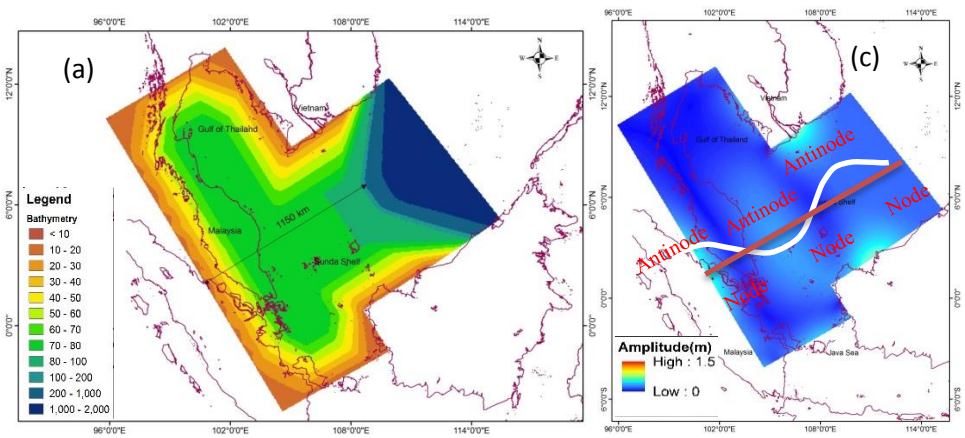

Figure 3.7: Schematised experiments including topography and M_2 co-amplitude charts of the extended Gulf of Thailand case (a, c) and the extended South China Sea case (b, d), respectively.

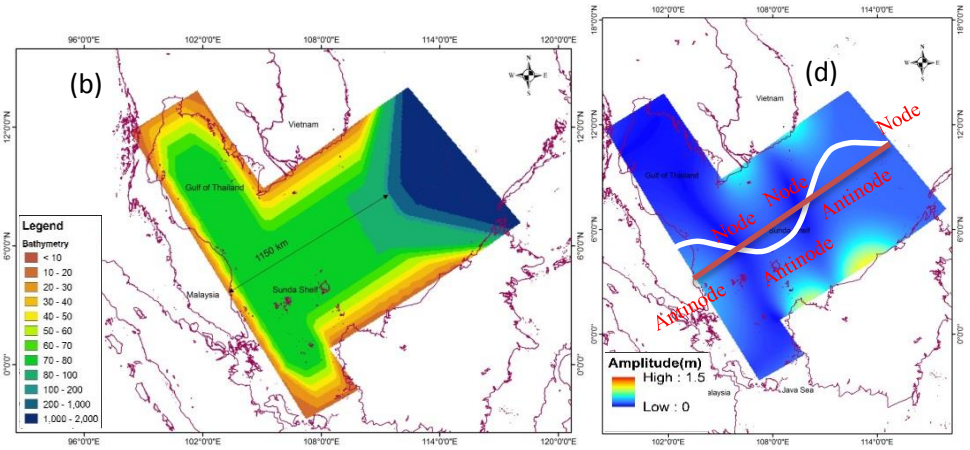

Figure 3.7, continued.

When the incident tidal wave from the SCS propagates to the Sunda Shelf and meets the reflected tidal wave from the western end of the Malaysian coast, this results in a standing wave in this semi enclosed area:

$$\eta(x,t) = \frac{1}{2}\frac{a}{coskL_b}\left[\underbrace{\cos(\omega t - k(x - L_b))}_{incident\ wave} + \underbrace{\cos(\omega t + k(x - L_b))}_{reflected\ wave}\right] = a\frac{\cos(k(L_b - x))}{coskL_b}cos\omega t$$

Where η is surface elevation at location x in a certain moment t along basin length L_b; α, ω, k are tidal amplitude, angular frequency, wavenumber. The amplitude of the tidal elevation along the basin varies according to cos (k(L_b-x)). The amplification occurs for basins with a basin length equal to an uneven multiple of a quarter wavelength.

The basin length L_b from the Sunda Shelf edge to the Malaysian coast is roughly 800 km with a mean depth of 55m. The wavelength L of M_2 in this region equals 1040 km; hence the basin length L_b is nearly three quarters wavelength M_2. Therefore, the Malaysian coast, the MDC and west Kalimantan are located at the antinodes of the standing tidal wave. In contrast, the area in between the MDC and the Malaysian coast is on a node of the standing tidal wave (Figure 3.6d). Similarities in cases of extended GoT and SCS, standing tidal waves are produced and this leads to the nodes and antinodes systems in this basin (Figure 3.7c and d). Specifically, the enlarged amplitude on the Mekong deltaic shelf is caused by shoaling and resonance effects due to the basin geometry, by the depth varying topography and by the position on the anti-nodal line of the standing wave.

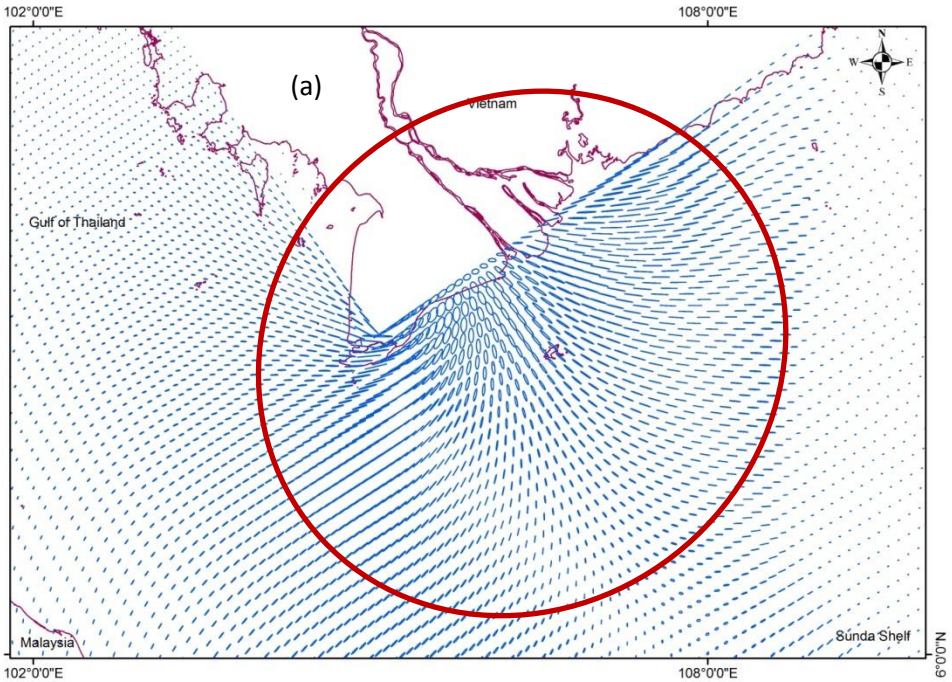
102°0'0"E
108°0'0"E
(a)
Vietnam
Gulf of Thailand
Malaysia
Sunda Shelf
6°0'0"N
102°0'0"E
108°0'0"E
N
W
E
S

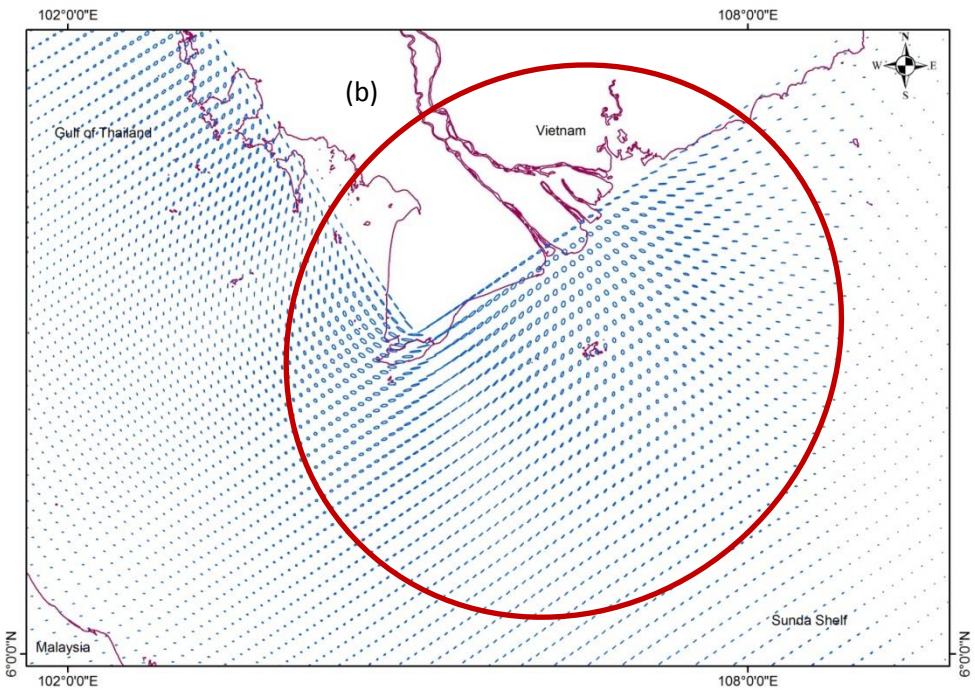
102°0'0"E
108°0'0"E
(b)
Gulf of Thailand
Vietnam
Malaysia
Sunda Shelf
6°0'0"N
102°0'0"E
108°0'0"E
N
W
E
S

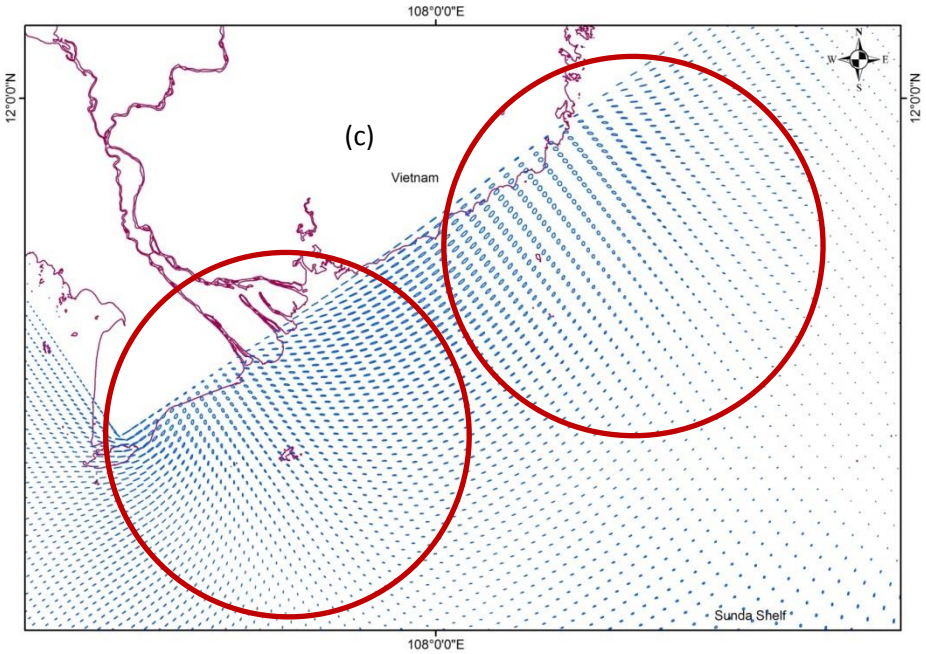

Figure 3.8: Radial tidal currents for quasi-original case (a), extended Gulf of Thailand case (b) and extended South China Sea case (c).

Figures 3.8a, b and c present the computational results of radial tidal currents in the schematised cases for the quasi-original geometry, the extended GoT and the extended SCS. Clearly, radial tidal currents occur in all three cases and there are only minor differences in locations as well as of magnitude for different basin geometries. Although the radial tidal currents compared to the quasi-original case are weaker, the radial tidal currents system are still present rather clearly in the extended SCS and GoT cases as shown in Figures 3.8b and c. Figures 3.6d, 3.7c and 3.7d indicate that there are hydraulic gradients of convex form due to the large amplified amplitude nearshore and the low amplitude offshore. In conclusion, the responsible mechanisms for developing the radial tidal current system on the Mekong deltaic shelf are the convex hydraulic gradients of tidal amplitude due to the basin geometry and the depth varying topography.

3.4.3 Wind monsoon climate

While the tilting of the Earth produces climate seasonality, monsoon climate systems are a consequence of the land-sea temperature differences affected by solar radiation (Huffman et al., 1997). The monsoon climate is an atmospheric flow over Asia and is greatly variable depending on the Siberian High and the Arctic Oscillation (Wang et al., 2012). The Southeast Asian countries are controlled by the monsoon climate, which is charaterized by a large-scale seasonal reversal of the wind system (Serreze and Barry, 2010). The two main monsoon regimes are specifically named the northeast monsoon (winter monsoon) from November to April and the southwest monsoon (summer monsoon) from late May to September. Furthermore, October is the transition month from the

southwest to northeast monsoon seasons (Cruz et al., 2012). Sea level in the oceans varies considerably as a result of wind stress forcing (Wyrtki., 1975; Qiu and Chen 2006). Hence, this study investigates the effect of wind monsoon climate system to the change of tidal wave propagation pattern. In this study, the wind monsoon climate data are collected from NOAA/NCEP in the period of 2011 to 2014 with the winter monsoon case from November to April and the summer monsoon case from May to October.

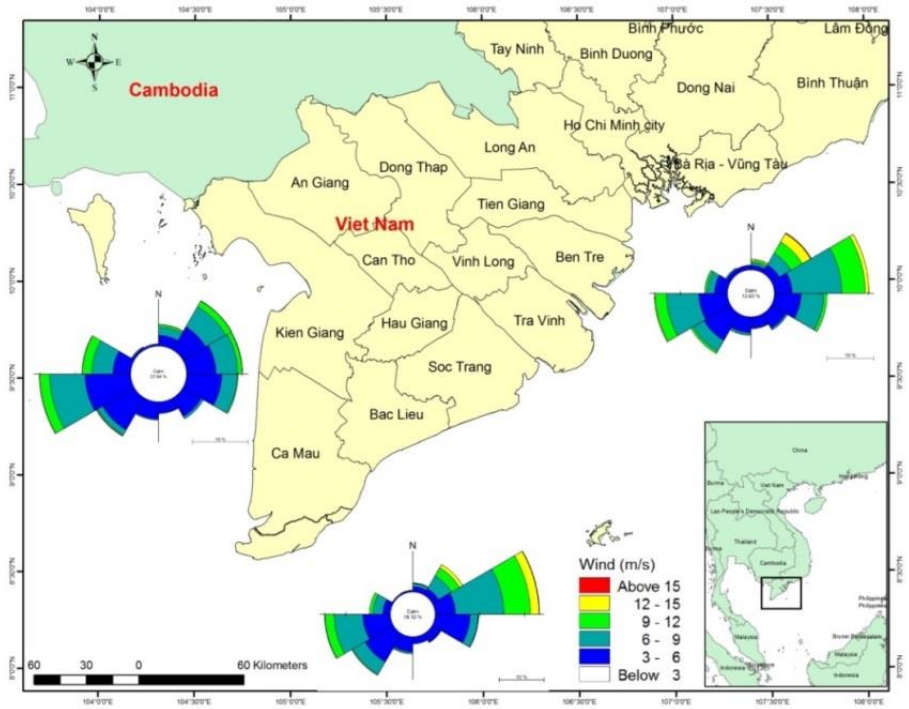

Figure 3.9: Wind rose maps in Mekong deltaic coast.

Fluctuations of sea level are superimposed upon regular tidal oscillations. In addition to the temporary and often dramatic variations in sea level due to tsunamis, hurricanes and other storms, variations in the predicted sea level frequently occur in association with the regular path of cyclonic disturbances across the coastal waters. These changes in sea level may be attributed in part to modifications to the changing atmospheric pressure and in part to the build-up or reduction of water at the coast due to the tangential stress of wind over the water surface. The pressure gradients in the horizontal momentum equations for water of constant density are computed by:

$$\frac{1}{\rho}P_x = g\frac{\partial \zeta}{\partial x}\ ,\quad \frac{1}{\rho}P_y = g\frac{\partial \zeta}{\partial x}$$

Where ρ is the density of water, respectively, P_x and P_y are the horizontal pressure terms in the Cartesian horizontal x, y direction, ζ is water level above some horizontal plane of reference, g is acceleration due to gravity.

The steady state effect of wind stress on the free surface, wind is implemented as a uniform shear stress, based on the wind data available from NOAA included in the momentum equations. Wind stress magnitudes (Stuart., 1988) are computed from:

$$|\overrightarrow{\tau_w}| = \rho_\alpha C_d U_{10}^2$$

Where in ρ_α is the density of air (kg/m^3), U_{10} the wind speed 10 m above the free surface (m/s) and C_d the wind drag coefficient.

Besides, Ruessink et al. (2006) indicated that wind driven flow increased friction over the flood period of a tidal cycle more than it decreased friction over the ebb period, thus raising the friction over the tidal cycle and decreasing the tide current range. Changes in the bottom stress influencing tidal elevations and currents in a shallow sea during prevailing wind are shown by Jones and Davies (2008).

Figure 3.10a and b show the difference of M_2 semidiurnal tidal amplitudes and co-phase lines between original condition and wind climate monsoon condition. The results in the winter monsoon climate show that atmospheric forcing attenuates the M_2 tidal amplitude down to 2.5 cm at Soc Trang Province on the eastern MDC, meanwhile the difference of the M_2 tidal phase is insignificant, viz. only 3-4 minutes. In the summer monsoon, the M_2 tidal amplitude is similarly damped until roughly 2 cm by wind forcing from a dominant southwest direction. The range of the M_2 tidal amplitude attenuation in the summer monsoon moves southward compared with the winter monsoon as a result of the seasonal difference of wind strength and atmospheric pressure due to the wind monsoon climate.

Similarly, the change of the K_1 semidiurnal tidal amplitudes and co-phase lines between the original condition and the wind climate monsoon condition are shown in Figures 3.10c and d. Different from the M_2 semidiurnal tide, the K_1 diurnal tide is attenuated by an average of 1-2cm in the western MDC due to the distribution of tidal characteristics around the MDC. The largest damped K_1 diurnal amplitude amounts to 2.5-2.6 cm along the Kiengiang coast in both the winter and summer monsoon climate. Like for the M_2 tide, the difference of K_1 tidal phases is minor, i.e. only 8-10 minutes. Therefore, the influence of the wind climate monsoon through the wind stress on the surface as well as the bed stress varies from region to region. The monsoon climate influences rather strongly on the semidiurnal tide in the eastern MDC, in contrast, the diurnal tide is affected quite considerably by the monsoon climate in the western region of Mekong Delta.

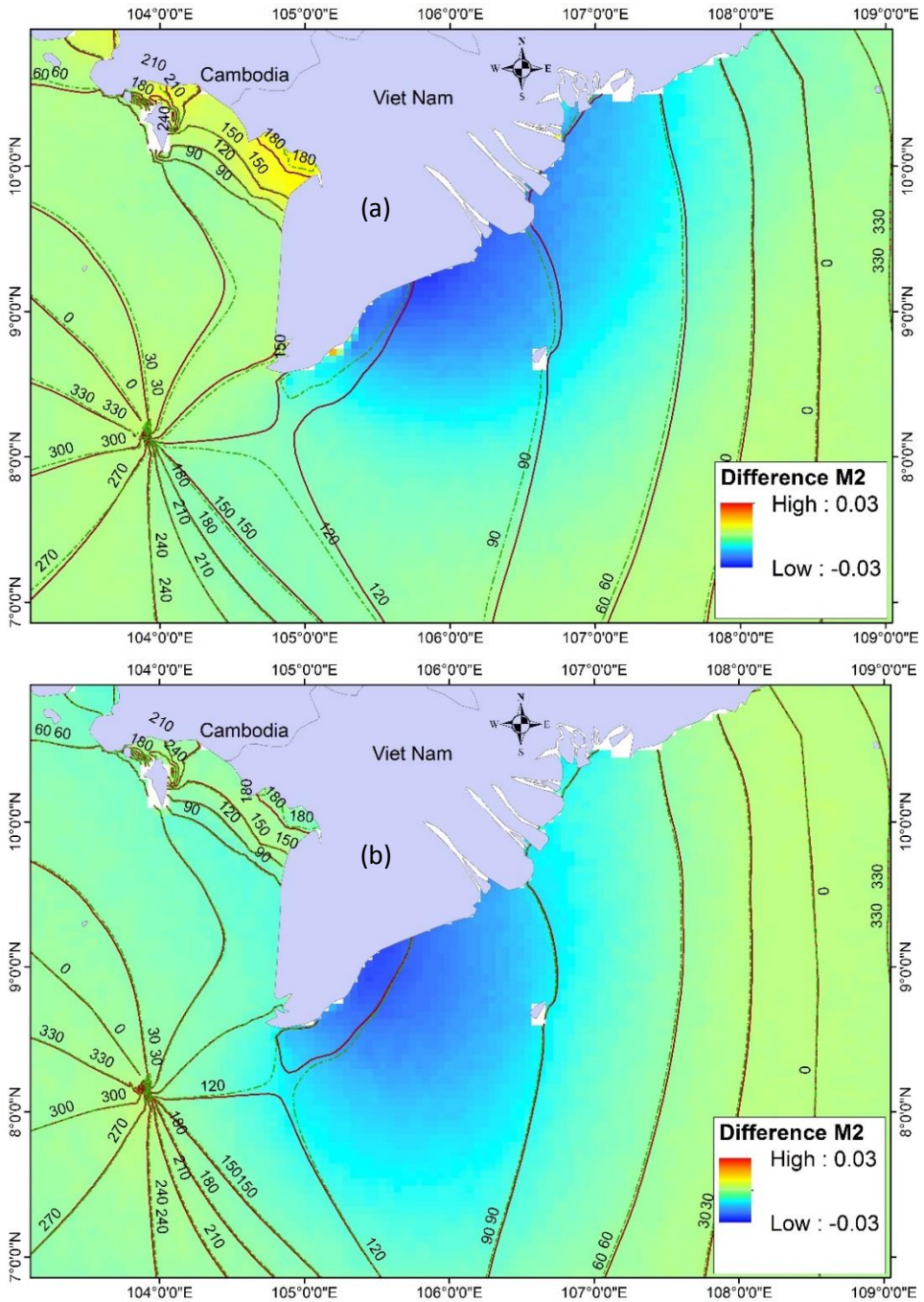

Figure 3.10: Phase and amplitude difference of M_2, K_1 in case of wind climate monsoon in winter (a, c) summer (b, d), solid brown and dashed green lines represent the co-phase lines of case original condition and case of wind monsoon climate.

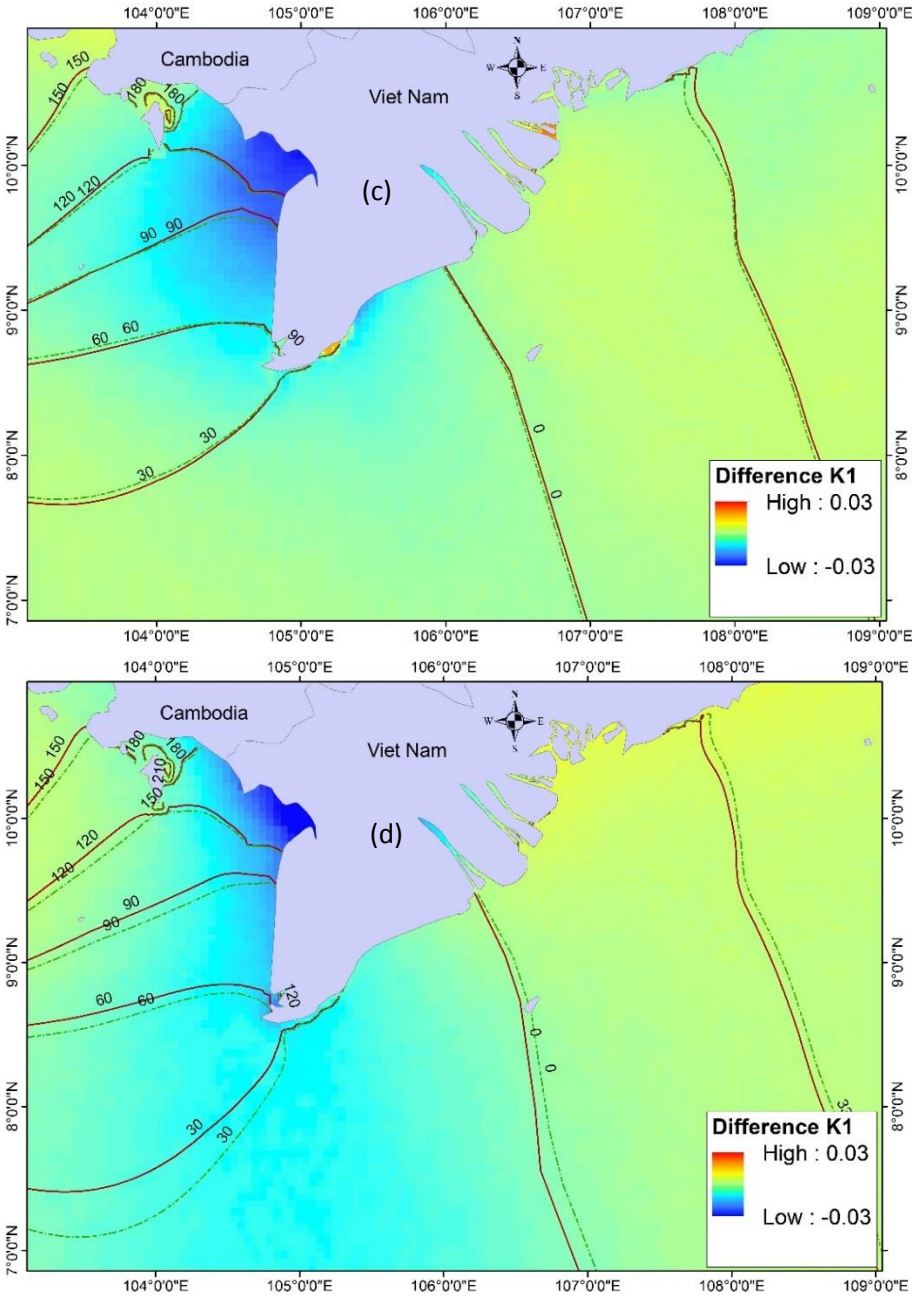

Figure 3.10, continued.

3.4.4 Tide generating forces

Numerical models of tidal motion in coastal seas generally do not account for the direct local influence of the tide generating forces (TGF). The amount of water mass in these models is relatively small and the effect of these forces on the flow can be neglected. For coastal areas, the prescription of tidal forcing along open boundaries is sufficient in generating the appropriate tidal motion. In most numerical studies of tides in the Mekong coastal region, tidal open boundary forces (TOBFs) have been used to force tides and TGF has often been neglected. However, depending on the relative phases and magnitudes of the TOBF and TGF forcing, the interaction of different forcing components may lead to tides amplified or damped in continental shelf seas such as Bass Strait in Australia (Wijeratne et al., 2012), Gulf of Tartary in Japan (Odamaki, 1989), or Yellow Sea in China (Su et al., 2015). Because the water body in the semi-closed basin of SCS is even larger than in the above mentioned sea regions, the contribution of the gravitational forces on the water motion should be considered to generate an accurate tidal motion in the SCS and relevant to the MDC. The intervention between TGF and TOBF forcing enlarges and diminishes the tidal amplitude (Gouillon et al, 2010). The sea level of two tidal waves from TOBF and TGF of the same frequency can be expressed as:

$$\eta(t) = \eta_g(t) + \eta_o(t) = \alpha_g \cos(\omega t - \theta_g) + \alpha_o \cos(\omega t - \theta_o)$$

Where η is the sea level at time t; g, o denotes the TGF case and TOBF case, respectively; α is the selected component's amplitude; ω is the selected tidal component's frequency; and θ is the selected tidal component's phase.

In the case denoted noTGF, the TGFs are ignored and the results are compared with the quasi-original condition case (OC) to examine the effect of TGF on the tidal motions. Figures 3.11a and b show the calculated differences of phase and amplitude of the M2 semidiurnal tide and K_1 diurnal tide between the cases OC and noTGF. Generally, the TGF influences the tidal wave system on the eastern MDC more than on the western MDC for both the M_2 and K_1 tidal components. For the M_2 tidal wave system, the change of the amplitude is relatively significant for the coastal eastern region of Mekong Delta amounting approximately 5-8cm, while the change of amplitude is only 1-1.6cm in the western region. There is a relatively minor difference in the co-phase lines of the M_2 semidiurnal tide being roughly 10-15 minutes and in the position of the amphidromic point in the GoT that moves northwest over a distance of roughly 30km. In the K_1 tidal wave system, changes of the amplitude on eastern and western MDC are on average 5 cm and 2 cm, respectively. The change of the co-phase lines of the K_1 diurnal tide is relatively significant compared to the M_2 tide with a co-phase difference of nearly 40-45 minutes. In conclusion, whether to include the TGF depends on the geographical region of interest.

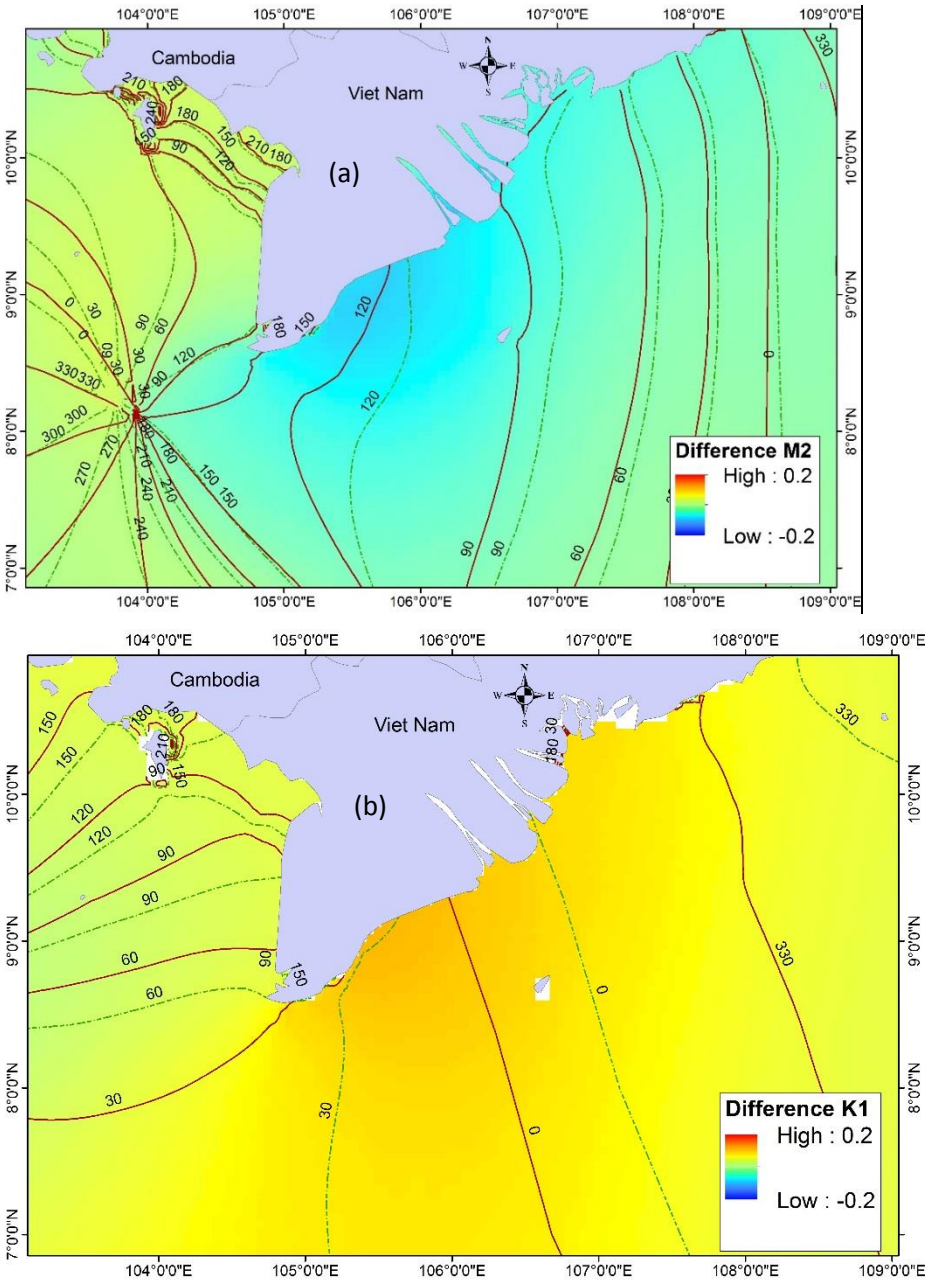

Figure 3.11: Phase and amplitude differences of M_2 (a), K_1 (b) in case of excluding TGF; solid brown and dashed green lines represent the co-phase lines of case original condition and case noTGF.

3.5 Conclusions

A two-dimensional tidal model is constructed with high resolution to allow the simulation of accurate tidal wave propagation in the South China Sea (SCS, also known as the East Sea) as well as along the Mekong Deltaic Coast (MDC). According to the validation of the simulated tidal modelling, this model shows a good capability to reproduce the tidal wave system in the SCS and along the MDC. The mechanism of tidal wave propagation along the MDC is numerically investigated in detail for the M_2, S_2, K_1, O_1 tidal components that earlier studies have not considered.

The results indicate that the semidiurnal and diurnal tides propagate in the SCS mainly through the Luzon Strait. Meanwhile a small part of it moves to the Gulf of Tokin, mostly continuing to flow toward the southwest. After the tidal wave reaches the Sunda Shelf edge, a part of its turns into the GoT and another part spreads southwards to the Sunda Shelf end and Java Sea.

This study reveals that the tidal current ellipses of the M_2 tide indicate strong currents occurring on the eastern coast of the Mekong Delta, while weak currents occur on the western coast. Moreover, radial tidal currents are found to occur near the southern Mekong River mouths, which have never been documented before. A series of numerical, geometrically and topographically schematised experiments were conducted to reveal the mechanisms responsible for establishing this radial tidal current system. Based on the result of these experiments, it is hypothesized that convex hydraulic gradients resulting from the spatial variation of the tidal amplitude due to basin geometry and depth varying topography leads to the formation of the radial tidal current system.

This study also shows that the tidal induced residual current increasing in the southeast ward of shallow coastal region of Mekong Delta is strongest along the Camau peninsula amounting to roughly 10-15cm/s. This result will help understanding morphodynamic process along the MDC. Besides, an improved geographical distribution map of tidal characteristics in the whole SCS was developed by this study.

A sensitivity analysis illustrates that the tidal incident waves from the Andaman and Flores open boundaries influence the tidal wave system in the coastal Mekong region weakly, while the tidal incoming wave from the Celebes open boundary plays an important role. It is concluded that the tidal open boundary at Celebes should not be neglected in simulating the tidal wave propagation in SCS in general and the MDC in particular.

The natural oscillation periods of the Gulf of Tokin, the GoT and the SCS are found to be more or less of diurnal. Although both the SCS and the GoT are dominated by diurnal tides, semidiurnal tides dominate in the eastern MDC, which is enclosed by those seas. Most previous studies have not explained this remarkable characteristic. By means of Green's law, the formula of Clarke and Battisti (1981) and the theory of standing wave, this study demonstrates that the large amplified M_2 semidiurnal amplitude leads to a prevailing mixed semidiurnal tide caused by not only the shoaling effect and the oscillation resonance phenomenon on this continental shelf but also by its position on the anti-node line of the standing wave.

For the first time, the effect of the wind monsoon climate on the tidal wave system in this region is investigated. The results reveal that atmospheric forcing of the monsoon climate could cause damped or amplified tides along the MDC. The monsoon climate influences rather strongly on the M_2 semidiurnal tide system in the eastern MDC,

meanwhile the monsoon climate controls the K_1 diurnal tide in the western region of Mekong Delta.

Inclusion of the TGFs influencing the tidal wave system on MDC has not been considered before. Based on results of this study, it is suggested that the TGFs need to be considered for accurate model simulation depending on the geographical region of interest. Our findings contribute to understanding the processes of tidal wave propagation from the deep ocean into the SCS and to the shallow flats of the MDC. The present study employed a two-dimensional model with the depth-averaged tidal dynamics, other effects such as baroclinic forcing is excluded to calculate tidal wave propagation. Hence, 3D models could be considered to achieve an even higher accuracy of tidal wave propagation along the MDC.

REFERENCES

Clarke, A. J., and Battisti, D. S., 1981The effect of continental shelves on tides, Deep Sea Res., 28A, 665-682.

Cruz, F.T., Narisma, T.G., Villafuerte, M. Q., Cheng, K.U.C., Olaguera, L.M., 2012. A climatological analysis of the southwest monsoon rainfall in the Philippines Atmospheric Research, 122 (2012), pp. 609-616.

Davis Jr., R.A., Hayes, M.O., 1984. What is a wave-dominated coast. Marine Geology 60: 313-329.

Delta Alliance, 2011. Mekong Delta Water Resources Assessment Studies – Vietnam-Netherlands Mekong Delta Masterplan Project. http://wptest.partnersvoorwater.nl/wp-content/uploads/2011/08/WATERRESOURCESfinaldraft.pdf, accessed 17.04.2013.

Deltares, 2014. User manual, Delft3D Flow, Deltares, Delft, the Netherlands.

Defant, A., 1961. Physical Oceanography, volume II. Pergamon Press, Oxford, 598 pp.

Fang, G., Cao, D., Huang, Q., 1994. Numerical modeling of the tide and tidal current in the South China Sea. Acta Oceanologica Sinica 16 (4), 1–12.

Fang, G., Kwok, Y. K., Yu, K., Zhu, Y., 1999. Numerical simulation of principal tidal constituents in the South China Sea, Gulf of Tokin and Gulf of Thailand. Continental Shelf Research 19, 845-869.

Gagliano, S.M., McIntire, W.G., 1968. Reports on the Mekong Delta. Coastal Studies Institute, Louisiana State University Technical Report 57, 144 p.

Gao, X., Wei, Z., Lv, X., Wang, Y., Fang, G., 2015. Numerical study of tidal dynamics in the South China Sea with adjoint method. Ocean modelling 92, 101-114.

Galloway, W.E., Hobday, D.K., 1983. Delta Systems. In: Terrigenous Clastic Depositional Systems. Springer, New York, NY.

Gerritsen, H., E.J.O. Schrama and Van der Boogaard, H.F.P., 2003. Tidal model validation of the seas of South East Asia using altimeter data and adjoint modelling. Proc. 30th IAHR Congress, Thessaloniki, 2003, Vol. D, pp. 239-246.

Gouillon, F., Morey, S. L., Dukhovskoy, D.S., O'Brien, J.J., 2010. Forced tidal response in the Gulf of Mexico/ Journal of Geophysical Research Oceans 115 (C10050).

Hein, H., Hein, B., Pohlmann, T., 2013. Recent sediment dynamics in the region of Mekong water influence. Global and Planetary Change 110, 183-194.

Huffman, G. J., Adler , R. F., Arkin, P., Chang, A., Ferraro, R., Gruber, A., Janowiak, J., McNab, A., Rudolf,B., Schneider, U., 1997. The Global Precipitation Climatology Project (GPCP) combined precipitation data set. Bull. Am. Meteorol. Soc., 78:5–20.

Hordoir, R., Polcher, J., Brun-Cottan, J.-C., Madec, G., 2006. Towards a parametrization of river discharges into ocean general circulation models: a closure through energy conservation. Climate Dynamics 31 (7–8), 891–908.

Institute of Coastal and Offshore Enginerring (ICOE), 2011. Vietnam government project of study on sedimentation and erosion in the along Camau spit, Vietnam. http://icoe.org.vn/index.aspx?aac=CLICK&aid=ARTICLE_DETAIL&ari=3097&lang=1&menu=de-tai--du-an-cac-nam&mid=178&parentmid=1002&pid=1&storeid=0&title=nhiem-vu-khcn-nam-2011 (inVietnamese).

Institute of Coastal and Offshore Enginerring (ICOE), 2014. Province project of morphodynamics in coastal zone of Tra Vinh Province, Vietnam. http://icoe.org.vn/index.aspx?aac=CLICK&aid=ARTICLE_DETAIL&ari=3100&lang=1&menu=de-tai--du-an-cac-nam&mid=178&parentmid=1002&pid=1&storeid=0&title=nhiem-vu-khcn-nam-2014 (in Vietnamese).

Institute of Strategy and Policy on natural resources and environment (ISPONRE), 2009. Vietnam Assessment Report on Climate Change. 127.

Jones, J.E., Davies, A.M., 2008. On the modification of tides in shallow water regions by wind effects. Journal of Geophysical Research-Oceans 113 (C05014). http:// dx.doi.org/10.1029/2007JC004310.

Lee, S., Lie, H. J., Cho, C. H., Kang, S. K., Teague, W. J., Chang, K., Song, K. M. & Oh, K. H., 2011. Vertical structure of the M2 tidal current in the Yellow Sea. Ocean Sci. J. 46 (2), 73‑84.

Lesser, G.R, Roelvink, J.A., van Kester, J.A.T.M and Stelling, G.S., 2004. Development and validation of a three-dimensional morphological model. Coastal Engineering, 51, 883-915.

Mekong River Commission, 2010. State of the basin report 2010 Vientiane: Mekong River Commission.

Nguyen, K. D., Guillou, N. and Pham, N. N., 1998. A 3-D numerical study of the tidal circulation in the Mekong Delta Coastal Zones, Vietnam. International Workshop on the Mekong Delta, 23-27 February 1998, Chiang Rai, Thailand: 57-71.

Nguyen, L.V., Ta, T.K.O., Tateishi, M., 2000. Late Holocene depositional environments and coastal evolution of the Mekong river delta, Southern Vietnam. Journal of Asian Earth Sciences 18 (4), 427–439.

Proudman, J.,1953. Dynamical Oceanography. MethuenandCo. Ltd., London, 409pp.

Odamaki, M., 1989. Co-oscillating and independent tides of the Japan Sea. Journal of the Oceanographical Society of Japan 45 (3), 217-232.

Qiu, B. and S. Chen, 2006: Decadal Variability in the Large-Scale Sea Surface Height Field of the South Pacific Ocean: Observations and Causes. J. Phys. Oceanogr., 36, 1751–1761.

Ruessink, B.G., Houwman, K.T., Grasmeijer, B.T., 2006. Modeling the nonlinear effect of wind on rectilinear tidal flow. Journal of Geophysical Research-Oceans 111(C10002). http://dx.doi.org/10.1029/2006JC003570.

Saito, Y., Nguyen, V. L., Ta, T. K. O., Tamura, T., Kanai, Y., Nakashima, R., 2015. Tide and river influences on distributary channels of the Mekong River delta. American Geophysical Union, Fall Meeting 2015, abstract #GC41F-1148.

Serreze, R.G., Barry, R.G., Chorley, R.J., 2010. Atmosphere, Weather and Climate, Routledge, Oxon.

Su, M., Yao, P., Wang, Z. B., Zhang, C. K, Stive, M. J. F., 2015. Tidal Wave Propagation in the Yellow Sea. Coastal Engineering Journal, Vol. 57, No. 3, 1550008.

Southern Institute of Water Resources Research (SIWRR), 2010. Project for measurements of bathymetry, hydrodynamics in estuaries and coastal zone of Mekong Delta from 2009 to 2010. http://www.siwrr.org.vn/?id=nckh5 (in Vietnamese)

Southern Instiute of Water Resources Research (SIWRR), 2016. Lower Mekong Delta Coastal Zone. http://lmdcz.siwrr.org.vn/?lang=e

Stelling, G. S. and Kester, J. A. T. M. V., 1994. On the approximation of horizontal gradients in sigma co-ordinates for bathymetry with steep bottom slopes. International Journal Numerical Methods In Fluids 18: 915-955.

Stuart D. M., 1988. Coefficients for sea surface wind stress, heat flux, and wind profiles as a function of wind speed and temperature. J. Geophys. Res. **93** (C12): 15467. doi:10.1029/JC093iC12p15467.

Ta, T.K.O., Nguyen, V.L., Tateishi, M., Kobayashi, I., Tanabe, S., Saito, Y., 2002b. Holocene delta evolution and sediment discharge of the Mekong River, southern Vietnam. Quaternary Science Reviews 21 (16–17), 1807–1819.

Tas, S., 2016. Coastal protection in the Mekong Delta. Master thesis. https://repository.tudelft.nl.

Unverricht, D.,Szczucinski, W., Stattegger, K., Jagodzinski, R., Le, X.T., Kwong, L.L.W.,2013. Modern sedimentation and morphology of the subaqueous Mekong Delta, Southern Vietnam. Global and Planetary Change 110, 223-235.

Unverricht, D., Nguyen, T. C., Heinrich, C., Szczucinski, W., Lahajnar, N., Stattegger, K., 2014. Suspended sediment dynamics during the inter-monsoon season in the subaqueous Mekong Delta and adjacent shelf, southern Vietnam. Journal of Ansian Earth Sciences 79, 509-519.

Wang, L., Li, J., Lu, H., Gu, Z., Rioual, P., Hao, Q., Mackay, A.W., Jiang, W., Cai, B., Xu, B., Chu, G., 2012. The East Asian winter monsoon over the last 15,000 years: its links to high-latitudes and tropical climate systems and complex correlation to the summer monsoon. Quaternary Science Reviews, 32, pp. 131-142

Wijeratne, E.M.S., Pattiaratchi, C., Eliot, M., Haigh, I.D., 2012. Tidal characteristics in Bass Strait, southeast Australia. Estuar Coast Shelf Res 114:156–165.

Wyrtki, K.: Physical oceanography of the Southeast Asian waters, Scientific Results of Marine Investigations of the South China Sea and the Gulf of Thailand 1959–1961, NAGA Rep. 2, Scripps Inst. of Oceanogr., La Jolla, California, 195 pp., 1961.

Wyrtki, K., 1975: El Ni˜no–the dynamic response of the equatorial Pacific Ocean to atmospheric forcing. J. Phys. Oceanogr, 5, 572–584

Xue, Z., He, R., Liu, J. P., Warner, J. C., 2012. Modelling transport and deposition of the Mekong river sediment. Continental Shelf research 37, 66-78.

Yanagi, T., Takao, T., Morimoto, A., 1997. Co-tidal and co-range charts in the South China Sea derived from satellite altimetry data.

Yanagi, T., Takao, T., 1998. Clockwise phase propagation of semi diurnal tides in the Gulf of Thailand. Journal of Oceanography, vol. 54, 143-150.

Yao, P., Su, M., Stive, M.J.F., Zhang, C. K., Wang, Z., 2015. Tidal current system in the South Yellow Sea. Cont. Shelf Res.

Ye, A. L., Robinson, I. S., 1983. Tidal dynamics in the South China Sea. Geophys. J. R. astr. Soc 72, 691-707.
Yu, M., 1984. A preliminary study of tidal characteristics in the South China Sea. Acta Oceanologica Sinica 6, 293–300.
Zu, T., Gan, J., Erofeeva, S. Y., 2008. Numerical study of the tide and tidal dynamics in the South China Sea. Deep Sea Research I 55, 137-154.

4

Seasonal nearshore wave climate and longshore sediment transport for the Mekong Delta Coast

This study aims to assess a representative wave climate and the associated longshore wave-driven sediment transport capacity along the Mekong deltaic coast. The wave climate is derived using the state-of-the-art spectral wave model SWAN (Simulating WAves Nearshore). The results show that the wave field evolution on the Mekong deltaic shelf is strongly dominated by the monsoon climate system. While high breaking wave dissipation appears in the estuarine zones in the winter monsoon climate, considerable breaking wave dissipation happens along the western Camau Cape during the summer monsoon climate. The wind fields in the winter monsoon only influence wave fields along the eastern coast because of the limited fetch length on the western coast. The wind system in the summer monsoon climate has a considerable influence on both the eastern and the western coasts. Higher wave heights are found in the northeastern area of the Mekong deltaic shelf, while they decrease towards the southwest and western coast of the Mekong Delta during the winter monsoon. Conversely, significant wave heights on the western shelf are larger compared to the eastern coast in the summer monsoon climate. To quantify the response of shoreline changes of the Mekong Delta to wave conditions under the monsoon climate system, the CERC formula is employed to produce a Longshore Sediment Transport (LST)

This chapter is submitted to Coastal Engineering. Phan, H. M., Ye, Q., Reniers, A. J. H. M., Stive, M. J. F. (2020).

capacity variation. The results reveal that the highest potential LST rates in the whole Mekong deltaic coast take place in front of the Mekong river mouths. The study indicates that the difference in the seasonal potential LST gradients leads to a pattern of erosion and accretion among the coastal areas of the eastern estuarine zones similar to the observations. The findings deepen our understanding of the shoreline evolution of the Mekong Delta in response to the seasonal wave monsoon climate.

4.1 Introduction

The wave fields at the ocean surface generally consist of both swells and wind waves. Nonlinear wave-wave interactions, shoaling, refraction, diffraction, reflection and dissipation affect these surface gravity waves propagating across shallow coastal areas. Knowledge of the wave climate is necessary for various applications, such as the design of coastal structures and sediment transport studies. Because of insufficient buoy observations close to the coastal target region, a numerical wave model is one of the approaches to assess the nearshore wind wave climate. Numerical wave models are very useful for evaluating wave conditions near the coast, allowing for the simulation of wave fields at a much finer spatial resolution than typically sampled in nature. Until today, numerous studies have investigated ocean surface wave characteristics by applying numerical wave models. For instance, Swail et al. (1999) used a global spectral ocean wave model for long-term (40 years) wave hindcasts to analyse the trends and variability of changes in waves. Soomere and Raamet (2011), using the wave modelling (WAM) simulations of wave conditions for 1970–2007, revealed extensive spatial variations in long-term changes in both average and extreme wave heights in the Baltic Sea. Bosserelle et al. (2012) employed the third-generation spectral wave model (WAVEWATCH III) with a 40-year simulation to quantify the interannual variability and longer-term changes in the wave climate around Western Australia. Mirzaei et al. (2013) studied long-term wave transformation tendencies in the southern region of the South China Sea, employing the WAVEWATCH III model to calculate a 31-year wave hindcast. Lv et al. (2014) investigated the wave characteristics by using the SWAN model with the ECMWF (European Centre for Medium Range Weather Forecasts) winds in the Bohai Sea for the period from 1993 to 2012.

The Mekong deltaic shelf is located at the intersection of the deep basin of the South China Sea and the shallow basin of the Gulf of Thailand. The foreshore is very wide due to its extremely gentle slopes in the range of 1:1000-1:2000. Hence, local winds play an important role in generating wave fields in the coastal area of Mekong Delta. The Southeast Asian countries are controlled by a monsoon climate, which is a large-scale seasonal reversal of the wind systems (Serreze and Barry, 2010). The two main monsoon regimes are specifically named based on the direction of the winds: the northeast monsoon (winter monsoon), from November to April, and the southwest monsoon (summer monsoon), from late May to September. Annual wind speeds have been recorded from 1999 to 2008 by the Southern Regional Hydro-Meteorological Center (Unverricht et al., 2014) at Vung Tau station of the southern Vietnam, ranging from 7 to 9 m/s, and in Bac Lieu Province of Mekong Delta, from 6 to 8 m/s. Under stormy situations wind speeds can access 20–30 m/s (Institute of Strategy and Policy on natural resources and environment ISPONRE., 2009). These maximum wind stresses occur regularly along the south-eastern coast of Vietnam in both monsoon seasons (Unverricht et al., 2014). Although previous studies agree that the wave circulation of the Mekong deltaic shelf is affected mostly by monsoon winds, these studies do not distinguish the different effects between the winter monsoon and the summer monsoon to the process of wave transformation from offshore to onshore.

Currently, there are very few studies on wave characteristics in the Mekong deltaic coast. Xue et al. (2012) apply ROMS (Regional Ocean Modeling System) for the coastal ocean circulation and SWAN for the wave height field in the eastern Mekong deltaic coast to simulate the transport and dispersal of Mekong derived sediment during the months of

August and December in 2005. Nevertheless, this study has not evaluated the process of the wave transformation from the lower shoreface zone to the upper shoreface zone in sufficient detail. Tas (2016) used SWAN to translate the offshore boundary conditions into nearshore conditions and the non-hydrostatic, wave-phase resolving model of SWASH conditions (Zijlema et al, 2011) as input in order to calculate the wave transformation up to the western shoreline of the Mekong Delta. Both of the above studies lack wave measurement data to validate the wave models. Furthermore, these studies do not show the importance of the seasonal wind monsoon climate for the wave characteristics in the coastal area of the Mekong Delta.

Figure 4.1: Wave propagation on a typical shallow Mekong deltaic beach, showing very gently sloping, wide breaker zones.

The coastal area of the Mekong Delta is a complex coastal system that poses significant challenges to nearshore wave modeling. In general, the numerical wave models can be structured in models based on the spectrum concept (phase averaged), as well as on models based on the momentum concept (phase resolving). Because the phase resolving models exclude wind input, these are unsuitable for the present application on the Mekong deltaic shelf since the region is significantly affected by the wind monsoon climate. For applications on these larger scales, phase averaged models should be used, and SWAN is an example of such a model. The spectral wind wave model SWAN is widely used for the computation of wave fields over shelf seas, coastal areas and shallow lakes (Booij, 1999; Westhysen, 2009). Gorrell et al. (2011) employed SWAN to calculate the evolution of gravity waves moving 11 km from 550 m water depth to the coastline over complicated nearshore topography at Scripps Canyon. Mulligan et al. (2008) used SWAN to investigate the evolution of the wave field in the coastal Lunenburg bay. Besides, wave processes are responsible for large oscillatory fluid motions, which drive currents, sediment transport and bottom change. Nowadays, over 60% of the shoreline of the Mekong deltaic coast is facing extreme erosion and one of the important causes is wave action. Therefore, a comprehensive understanding of the characteristics of waves in the coastal area of the Mekong Delta is important and necessary. In order to achieve the goal of this study, the spectral wind wave model SWAN is employed to understand wave transformation under wind climate monsoon conditions.

Complicated coastal processes taking place at various temporal and spatial scales lead to shoreline changes (Stive et al, 2002). The action of waves approaching the coast at an angle produces the potential longshore sediment transport computation. The wave-driven

longshore sediment transport depends, amongst other things, on the hydrodynamics in the breaker zone and on the specific sediment properties. The study for the quantification of physical processes that drive the coastal Mekong Delta evolution, such as hydrodynamics and resulting potential longshore sediment transport (LST), is rather scarce. Furthermore, these processes take place over multiple spatial and temporal scales and are extremely difficult to accurately describe and quantify. Hence, as a result, these processes are still not well understood.

Parametric equations driven by a regional wind climate can help provide a quantitative tool to assess longshore transport trends along the coast, explain observed shoreline changes, and provide support in predicting future responses. Nowadays, there are the various formulations available to calculate potential LST rates for a beach; the CERC formula (CERC 1984) is one of them. The widely used CERC formula is used to hindcast the possible evolution of the coastal Mekong Delta (Martinho et al. 2009). The bulk longshore transport provides the total transport over the entire width of the littoral zone. Apparent advantages of the bulk transport formula are robustness and easy to calibrate and apply (Bosboom and Stive., 2013). The current study clarifies the wave characteristic transformation on the Mekong deltaic shelf, especially under a wind monsoon climate. The resulting wave characteristics at the initial breaking zone are used to investigate the potential LST rate, which consecutively helps to understand evolution of the delta in response to the local wave climate.

4.2 Data and Methodology

4.2.1 Wave transformation model description

The SWAN is a third-generation wave model based on the action density balance equation. The theoretical and numerical background of SWAN was described in Holthuijsen et al. (1993), Ris et al. (1999), Booij et al. (1999), and Zijlema and Van der Westhuysen (2005). The SWAN model calculates the development of a sea state by means of action density $N(\sigma,\theta)$ rather than by means of variance density $E(\sigma,\theta)$, since, in the presence of currents, action density is conserved while variance density is not. In the SWAN model the process of the action density (N) is governed through the action balance equation as follows:

$$\frac{\partial}{\partial t}N + \frac{\partial}{\partial x}(c_x N) + \frac{\partial}{\partial y}(c_y N) + \frac{\partial}{\partial \sigma}(c_\sigma N) + \frac{\partial}{\partial \theta}(c_\theta N) = \frac{S(\sigma,\theta,x,y,t)}{\sigma} \quad (1)$$

$$S_{tot} = S_{in} + S_{wc} + S_{nl4} + S_{bot} + S_{brk} + S_{nl3} \quad (2)$$

The terms on the left-hand side of (1) represent the kinematic part including, respectively, the change in wave action over time, the propagation of wave action in geographical space (with C_g the wave group velocity vector and U the ambient current), depth and current-induced refraction (with propagation velocity c_θ in directional space θ) and the shifting of the relative radian frequency σ owing to variations in mean current and depth (with the propagation speed c_σ). The righ side of (1) denotes processes that generate, dissipate or redistribute wave energy, specified by (2). These include the deep

water processes of wind input (S_{in}), white-capping dissipation (S_{wc}), quadruplet nonlinear interaction (S_{nl4}), and the shallow water processes of bottom friction dissipation (S_{bot}), depth-induced breaking (S_{brk}) and triad nonlinear interaction (S_{nl3}).

Wave characteristics in the Mekong deltaic shelf are strongly influenced by the wind of the monsoon climate. The transfer of wind energy to the waves is described with the sum of linear and exponential growth (Miles, 1957):

$$S_{in}(\sigma,\theta) = \alpha + \beta E(\sigma,\theta)$$

Where α, β depend on wave frequency and direction as well as wind magnitude and direction. In which α is the coefficient of initial wave growth, described by an empirical expression of Caveleri and Malanotte-Rizzoli (1981), and β is the coefficient of the exponential wave growth taken from Komen et al. (1984).

Beside a part of the energy is then redistributed over frequencies, but most of it is dissipated by white capping through the following formulation of Hasselmann (1974):

$$S_{ds,w}(\sigma,\theta) = -\tau\tilde{\sigma}\frac{k}{\tilde{k}}E(\sigma,\theta)$$

Where $S_{ds,w}(\sigma,\theta)$ is white-capping dissipation, τ is a steepness dependent coefficient which is estimated by closing the energy balance of the waves in a fully developed condition depending on the wind input, k is the wave number, θ is directional space, E(σ,θ) is variance density and $\tilde{\sigma}$ and $\tilde{k}$ denote a mean frequency and a mean wave number, respectively.

The domain covers the entire Mekong deltaic coast from 103°10'E to 109°10'E of longitude and from 7°40'N to 11°30'N of latitude shown in Figure 4.2. The domain was discretized with a curvilinear grid of 464×227 nodes in spherical coordinates. The directional wave energy density spectrum function was discretized using 36 directional bins and 48 frequency bins between 0.05 Hz and 2.0 Hz. The numerical scheme was first order backward in space and applied the backward in time (BSBT) scheme.

The model was executed in the third generation, nonstationary mode with spherical coordinates to accurately predict the wave conditions in the coastal region. Both linear and exponential wind input growths were included in the model. The formulation for parameterization of wind input , built by Komen et al. (1994) for the exponential growth of wind input, and the linear wave growth term, defined by Cavaleri and Malanotte-Rizzoli (1981), were used in the model. Dissipation due to depth-induced wave breaking is treated by the Battjes and Janssen (1978) spectral formulation with α=1 (proportionality coefficient of the rate of dissipation) and γ=0.73 (breaker index), bottom friction is determined applying the JONSWAP formulation with a friction coefficient of C_{JON}=0.067 m2 s−3, and the Komen et al. (1984) formulation for white-capping is applied with C_{ds}=2.36×10−5. In very shallow waters, triad wave-wave interactions transfer energy from lower frequencies to higher frequencies, often resulting in higher harmonics. Hence, triad wave interactions were activated using the default setting for the Lumped Triad Approximation (LTA) (Eldeberky and Battjes, 1996) with a tunable proportionality coefficient α_{EB}=0.1.

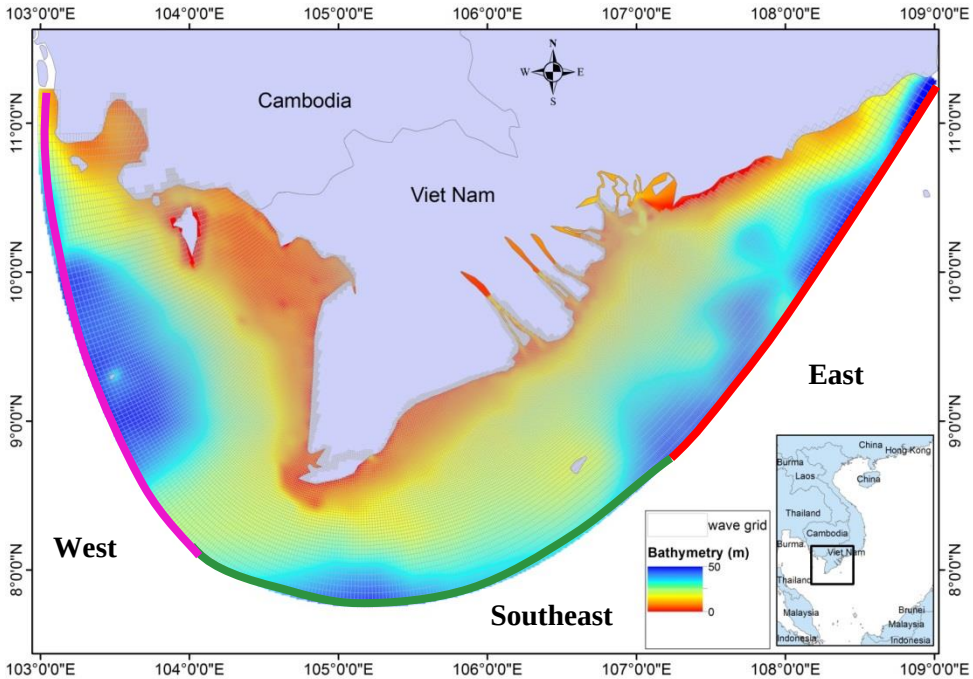

Figure 4.2: Model grid, boundaries (the east, southeast and west boundaries in red, green and purple colors, respectively) and bathymetry in the study area.

4.2.2 Longshore Sediment Transport

Despite the various formulas available to calculate LST rates for a beach (CERC 1984; Kamphuis 1991), estimating LST with reasonable accuracy requires intensive measurements to validate the selected approach for a specific study area; collecting sufficient data to ensure applicability throughout the seasons is an even bigger challenge. Relationships, such as the widely used Coastal Engineering Research Center (CERC) formula and variations of it, have received criticism over time, despite several modifications and variations attempting to incorporate more processes. The selection, therefore, of an arbitrary value for the proportionality constant K in the equation is left to the user and can be a function of many processes that cannot always be described in one parameter (Reeve et al. 2004). Some of these variations included incorporation of a beach slope (Komar 1997), or a modification to compute K as a function of sediment grain size (King 2005), sediment fall velocity (Baba and Komar 1981), and wave breaker angle and height (Lima et al. 2001). Smith et al. (2009) also showed that there are significant departures and disagreements between different methods of estimating longshore transport rates as a function of breaker type. Recently, Mil Homens (2016) optimised the calibration coefficients in the predictive ability for three of the most commonly used bulk LST formulas, including CERC, Kamphuis and Bayram, by using a least squares optimization algorithm.

Despite the lack of measurements to validate or select an appropriate coefficient, the CERC formula can be used to infer relative, rather than absolute, rates of transport via differencing to produce gradients to help explain barrier evolution (Martinho et al. 2009).

Parametric equations driven by regional wind climates can help provide a qualitative tool to assess longshore transport trends along the barrier chain, explain observed migration patterns and shoreline changes, and aid in predicting future responses(s). The CERC formula is based on the assumption that the LST rate is directly proportional to the alongshore component of wave power (Bosboom and Stive, 2013). Considering values at the breaker line and using significant wave height, one form of the CERC LST rate is given by:

$$S = \frac{K}{16(s-1)(1-p)}\sqrt{\frac{g}{\gamma}}\, sin2\varphi_b H_b^{2.5}$$

Where S is the longshore sediment transport rate (expressed in m3/s), K=0.37 is the dimensionless empirical proportionality constant, which is derived from the US Army Corps of Engineers (CERC 1984), s is the relative density of the sediment ρ_s/ρ, p is porosity, g is gravitational acceleration, γ=0.73 is breaker index, which is taken from Battjes and Stive (1985), φ_b is the wave angle of incidence, H_b is the wave height at breaking. The sediment porosity p is calculated from the sediment grain size, based on the relationship as proposed by Boucher et al. (2009).

The inputs for any bulk longshore sediment formula are the breaking wave parameters, which can be estimated using the hind-cast wave dataset available for the shallow-water conditions. This process becomes computationally expensive when a very fine resolution is considered on seasonal to inter-annual scales. To overcome difficulties presented by the spatio-temporal scheme of this study, it is preferable to use empirical breaking wave predictor formula instead of any numerical model (Almar et al., 2014).

The incipient breaking wave heights are achieved by implementing the energy flux conservation equation (1) and Snel's law (3), both equations derived from local water to the break point. The two equations are as follow:

$H_o^2 C_{go} \cos\theta_o = H_b^2 C_{gb} \cos\theta_b$ (1)

$$H_b = H_o \sqrt{\frac{C_{go}}{C_{gb}}} \sqrt{\frac{cos\theta_o}{cos\theta_b}} \quad (2)$$

Where the wave angle at breaking point:

$$\frac{\sin\theta_o}{C_o} = \frac{\sin\theta_b}{C_b} \quad (3)$$

$$\theta_b = \arcsin\left(\frac{C_b}{C_o}\sin\theta_o\right) \quad (4)$$

Where H is wave height; θ is wave angle; C_g and C are group speed and phase speed, respectively; subscripts o and b are local water and the break point, respectively.

The above equations are solved using the following iterative steps:

- Estimate a breaker water depth, h_b
- Determine the shoaling coefficient $K_{sh}=\sqrt{\frac{C_{go}}{C_{gb}}}$
- Determine θ_b using function (4)

- Compute wave height H_b at breaker water depth h_b from function (2)
- Check whether $H_b/h_b \approx \gamma=0.73$. If yes: stop; if no: return step 1 with better estimate of h_b

Where H_o, θ_o, h_o are derived from the output of SWAN.

4.2.3 Data

a) Wind data

The output of the wave model depends on the choice and the availability of the input wind field products, particularly during fair weather periods. The study used two different wind field products from the U.S. National Oceanic and Atmospheric Administration (NOAA) including Global Forecast System (GFS) Atmospheric Model and Blended Global Sea Winds with Climatological Monthly Means. The quality of the wind data used to force a wave model is a critical first-order control for the wave model outcome. It has been clearly demonstrated by Cavaleri (1994) that the empirical relation between significant wave height (Hs) and wind speed square (U10) for a fully-developed wind sea amplifies the error in Hs relative to the error in U10.

GFS is the weather prediction model built by the U.S. National Centers for Environmental Prediction (NCEP). The entire globe is covered by a GFS grid at a base horizontal resolution of 18 miles (28 kilometers) between grid points, which is used by operators to forecast weather up to 16 days in the future. GFS wind data are used for the validation of wave modeling in 2012 and 2017.

The Blended Sea Winds dataset developed by NOAA's National Centers for Environmental Information (NCEI) contains globally gridded, high-resolution ocean surface vector winds and wind stresses on a global 0.25° grid, and various temporal scales of six-hourly, daily, monthly, and 11-year (1995–2005) climatological monthlies. The wind speeds were generated by blending observations from multiple satellites: the Defense Meteorological Satellites Program's (DMSP) SSM/I; the Tropical Rainfall Measuring Mission (TRMM) Microwave Imager (TMI); QuikSCAT and the Advanced Microwave Scanning Radiometer-Earth Observing System (AMSR-E). The wind directions are from the NCEP's Department of Energy (DOE) Reanalysis 2 and are interpolated onto the blended speed grids. The Blended Sea Winds data are employed for wind input with climatological monthly means to simulate the seasonal wave climate.

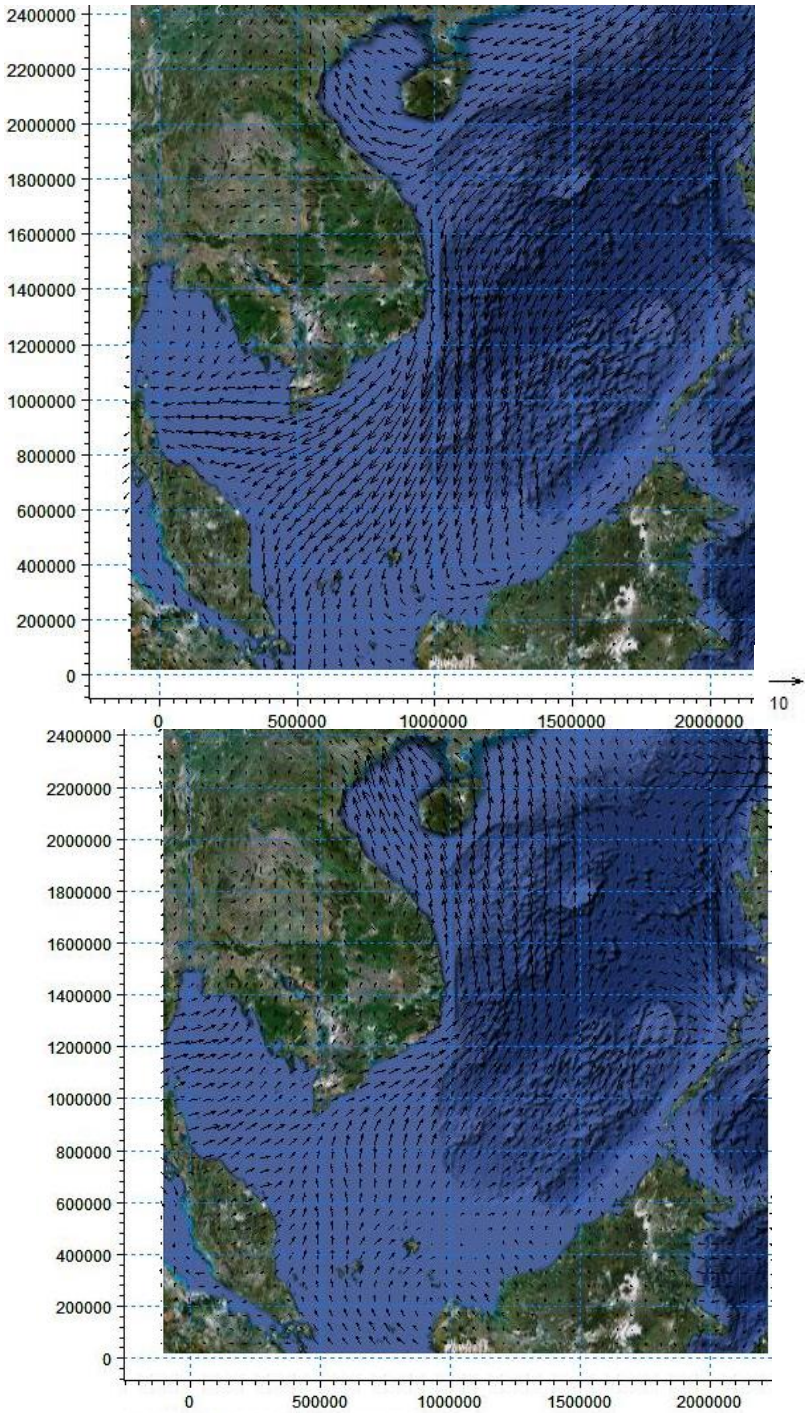

Figure 4.3. Wind field (m/s) in winter (above) and summer monsoon (below) in the Southeast Asia

b) Wave data

The Mekong deltaic shelf is influenced by the wind monsoon climate; hence the validation of wave modeling is carried out both for the winter and the summer monsoon cases. Wave records for the summer monsoon validation were collected from a national research project, conducted by the Vietnam Institute of Coastal and Offshore Engineering, at Camau station in 2012 (Figure 4.7). Wave records from Tiengiang station, resulting from international research projects in terms of Lower Mekong Delta Coastal Zones in 2017 (LMDCZ, 2018), were employed for the winter monsoon climate (Figure 4.7). Due to the lack of permanent buoy data in the study area, data from the global numerical model NOAA Wave Watch III was used for the boundaries of wave modeling. WAVEWATCH III (Tolman 1999) is a third-generation wave model, developed at NOAA/NCEP in the spirit of the WAM model (Komen *et al.* 1994), an advanced development of WAVEWATCH, built at Delft University of Technology (1991), and WAVEWATCH II, developed at NASA's Goddard Space Flight Center. Hind-casts from global wave generation models have been validated and shown to well reproduce the overall wave climate.

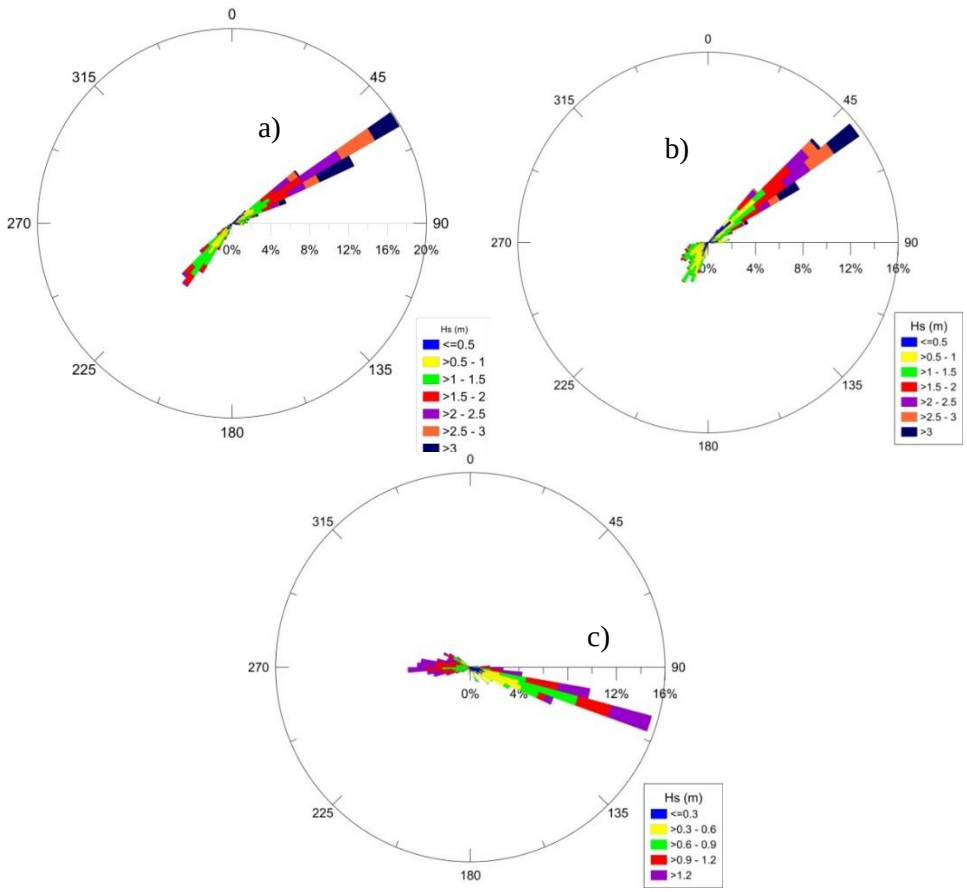

Figure 4.4: Wave roses at boundaries in the east (a), southeast (b) and west (c) Mekong deltaic shelf

c) Bathymetry

Bathymetric information for the SWAN model were achieved from GEBCO (General Bathymetric Charts of the Ocean), given by the British Oceanographic Data Centre (BODC) at a resolution of 30 arc-seconds in both latitude and longitude. The bathymetry for the study area is shown in Figure 4.2. Higher resolution bathymetry data along the Mekong deltaic coast are obtained by a bathymetry survey of the Mekong deltaic coast in 2009 and 2010 by the Vietnamese Government (SIWRR, 2010).

d) Sediment properties

For the study area, a large number of soil samples were collected and their sediment properties were assessed as part of the project of LMDCZ (2018). The variations in sediment grain-size and relative density along the Mekong Delta are shown in Figure 4.5. Along the estuary zone, coarser sand was observed with a grain-size ranging from fine to medium. A large area of fine-grained sediments (mainly fine sand) was detected along the East coast. The large sand patch, originally located near Bac Lieu, is found further downstream toward southern Ca Mau. Fine silt was found along the West coast, while coarse sand was found at several offshore locations.

The estuary zones, from Cua Tieu to Dinh An, are influenced by a strong river runoff and fine sediment discharges. Off the Dinh An and Tran De river mouths, a range of mixed sediments are found, ranging from fine silt to very fine sand, but mostly consisting of coarse silt sediment. Elsewhere in this area, sediments are composed of sand mixtures, ranging from very fine to medium sand, with fine sand being dominant (Figure 4.5). Along the East and the West coast, south of the Tran De river mouth to Rach Gia, most seabed sediments consist of fine silt grain-sizes. There are smaller patches with fine sand near the cape of Ca Mau in front of the Bo De river mouth and near Ha Tien.

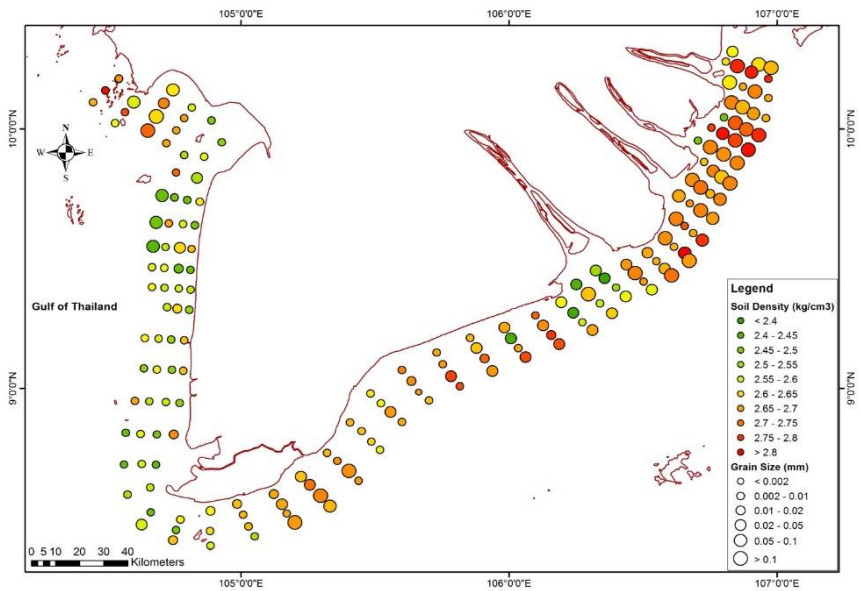

Figure 4.5: Distribution of soil density and grain size along the Mekong deltaic coast (LMDCZ, 2018)

4.3 Results and discussion

This section firstly shows the validation of model through wave height and wave period between computed and observed data. Secondly, wave characteristics in the Mekong deltaic coast including wave height, wave spectrum and wave dissipation are analysed and discussed. Finally, the seasonal and annual potential longshore sediment transport are presented and discussed.

4.3.1 Validation

In this study, the differences between the simulations (sim) and the observations (obs) of n number of observations are assessed through performance indicators, such as Bias, Root Mean Square Error (RMSE), Scatter Index (SI), for two temporary measurements along the Tien Giang (LMDCZ., 2018) and the Ca Mau (ICOE., 2016) coasts (Figure 4.7).

Bias is a statistical quantity that indicates the average difference between model output and the in-situ measurement. The Bias-value reveals the general trend in the model performance and allows to conclude whether the model consistently over- or under predicts the measurements:

$$Bias = \frac{1}{n}\sum_{i=1}^{n}(obs - sim)$$

The RMSE is an absolute measure of the goodness-of-fit between the model data and the buoy measurements. It is inferred that the lower the value of RMSE, the better the fit of data between model and observations:

$$RMSE = \sqrt{\frac{1}{n}\sum_{i=1}^{n}(sim - obs)^2}$$

The SI is expressed in percentages as a measure and indicates how close the results of the computation model and experiments are. The scatter index does not show general trends, but assesses the average model performance:

$$SI = \frac{RMSE}{\overline{obs}}$$

where $\overline{obs}$ is the mean of the observations.

The results of the model validation shown in Figure 4.6 and Table 4.1 indicate that the model is sufficient for our study.

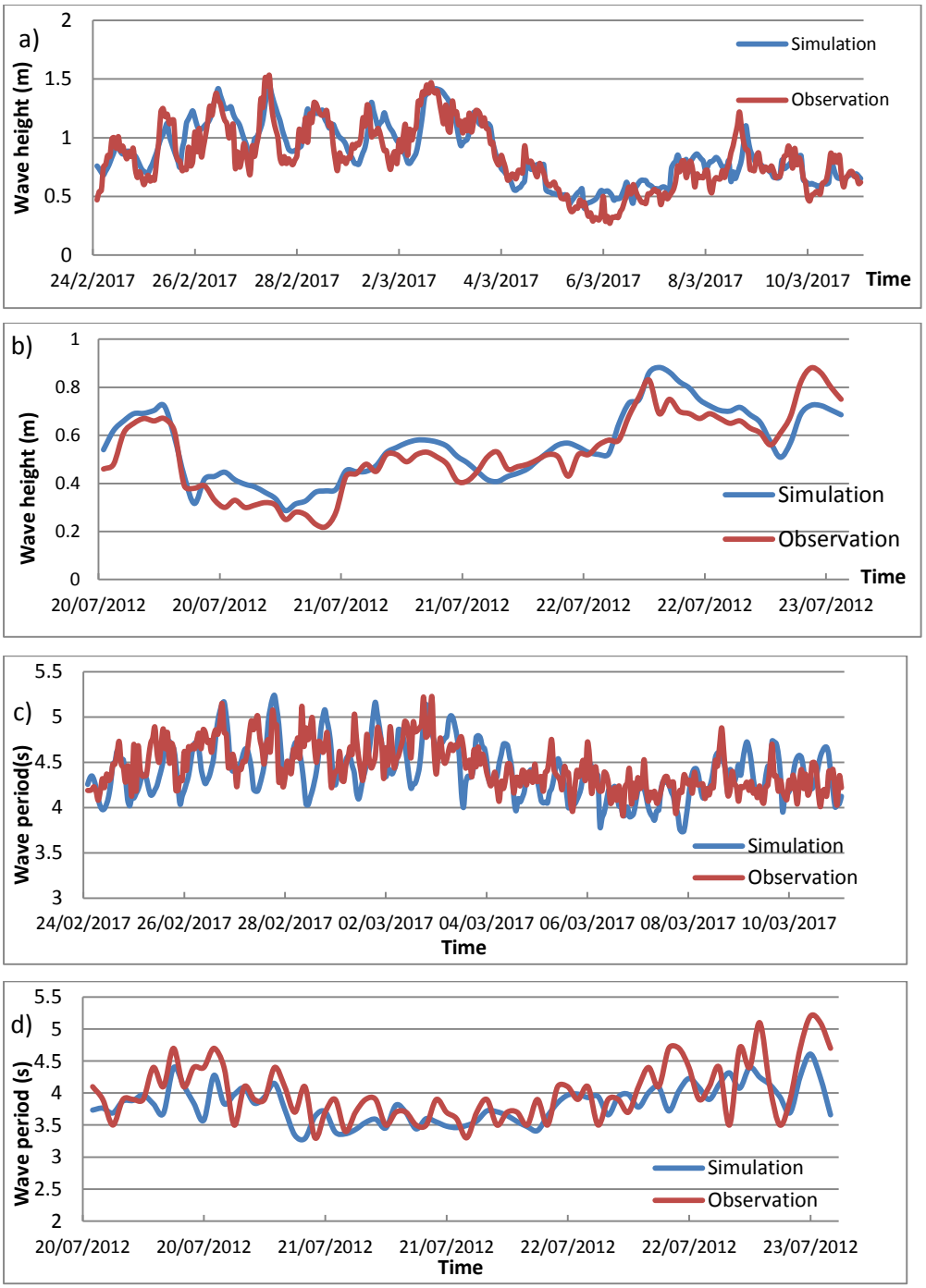

Figure 4.6: The simulation and observation results of wave height and wave period in Tien Giang (measurement 1, a-c) and Ca Mau (measurement 2, b-d)

Table 4.1: Results of the model validation for wave height (m) and wave period (s)

	Stations	Bias	RMSE	SI
Wave height (m)	**Measurement 1**	0.033	0.147	0.177
	Measurement 2	-0.038	0.061	0.116
Wave period (s)	**Measurement 1**	0.14	0.64	0.15
	Measurement 2	0.18	0.47	0.12

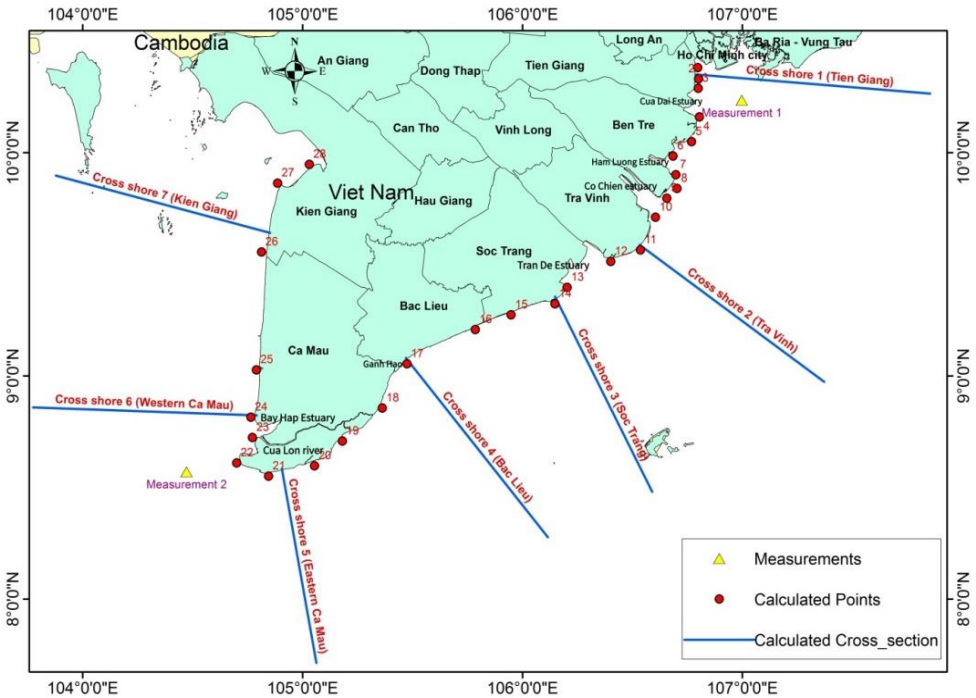

Figure 4.7: The measurement locations, the extracted points and cross-sections.

4.3.2 Wave characteristics

Seasonal averages were determined by combining the December-January-February monthly mean for the winter monsoon climate and June-July-August for the summer monsoon climate over a period of 10 years. The evolution of wind-swell wave peaks in the observed energy spectrum at sites in the cross-shore profiles along the Mekong deltaic shelf is shown in Figure 4.9.

a) Wave height

Figure 4.8a, b and Figure 4.9a, b show the seasonally averaged spatial distribution and cross-shore profiles of the significant wave height, respectively, over the Mekong deltaic shelf during 10 years (1995- 2005) in the winter and summer monsoon climate. The wave height decreases gradually from the north-rastern Mekong deltaic shelf at 2.5-3 meter to the coast and to the west, where the values are only 0.4-0.5 meter lower due to the effect of winter monsoon climate coming from the north-east. Contrary to the winter monsoon climate, a significant wave height in the western shelf is roughly 1.3-1.8 meter higher than the significant wave height on the eastern coast during the summer monsoon climate. Along the eastern Mekong deltaic coast, the highest wave height is found in the cross-shore profile of 2 at Tra Vinh Province, meanwhile, the lowest wave height occurs in the cross-shore profile of 4 at Bac Lieu Province (Specific cross-shore profiles shown in Figure 4.7). Due to shallow water in the Mekong deltaic shelf, the breaker zone starts taking place quite far from the onshore, roughly at 1 to 5 km.

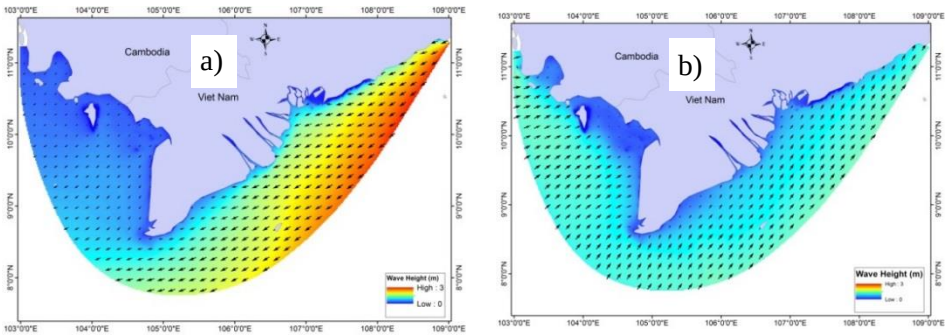

Figure 4.8: The wave field evolution in the Mekong deltaic coast under winter (a) and summer (b) monsoon climate.

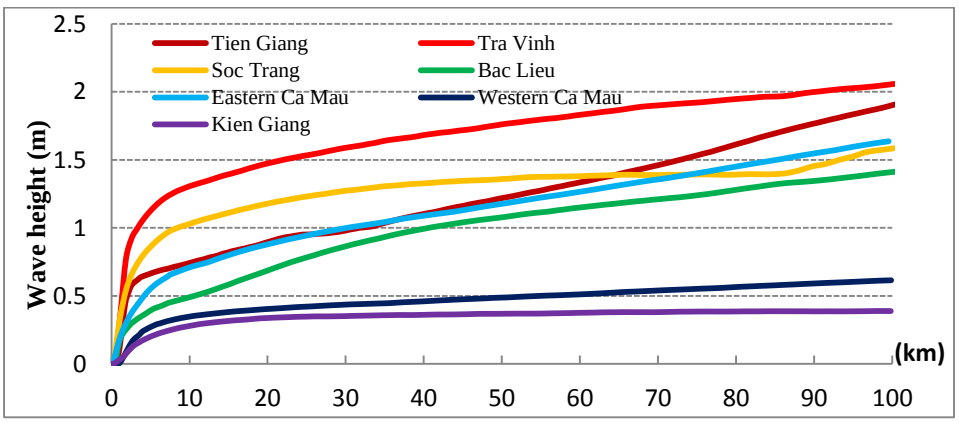

Figure 4.9: Wave height transformation in the cross-shore profiles along the Mekong deltaic shelf in the winter (above) and summer (below) monsoon climate.

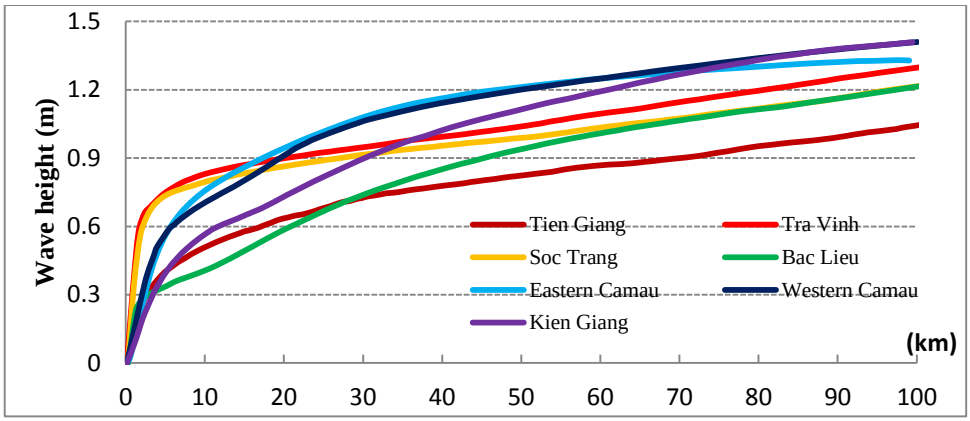

Figure 4.9: Wave height transformation in the cross-shore profiles along the Mekong deltaic shelf in the winter (above) and summer (below) monsoon climate.

b) Wave spectrum

For the analysis of some other aspects concerning the effect of the bottom topography on waves in the Mekong deltaic shelf, a wave spectrum transformation is considered. The evolution of wind swell wave peaks in the observed energy spectrum at sites in the cross-shore profiles along the Mekong deltaic shelf is shown in Figure 4.10. The variance density as a function of frequency is represented with solid lines at various locations. The definition of the variance density spectrum E(f) is as follows:

$$E(f) = \lim_{\Delta f \to 0} \frac{1}{\Delta f} \frac{1}{2} \overline{a^2}$$

Where a and f are wave amplitude and frequency.

For most of the sites located about 100km from the onshore, the energy spectrum of the swell peak is larger than its wind-sea peak in the eastern Mekong Delta in the winter monsoon climate. When the wave propagates closer to the Mekong deltaic coast, the energy spectrum of the wind and the swell sea peak fall due to the effect of dissipation. Furthermore, the rate of the reduced wave energy of a lower frequency of swell is higher than a higher wave frequency when waves move towards shallower water, because in shallow water the orbitals of the waves with a lower frequency reach down as far as the waves with a higher frequency and thus "feel the bottom" quite as much. Therefore, the energy spectrum of a swell peak decreases more quickly than its wind peak as waves travel to the Mekong deltaic coast. Wind magnitude and direction distribution, contrary to the winter monsoon climate, lead to a larger wave energy in the western Mekong deltaic shelf in the summer.

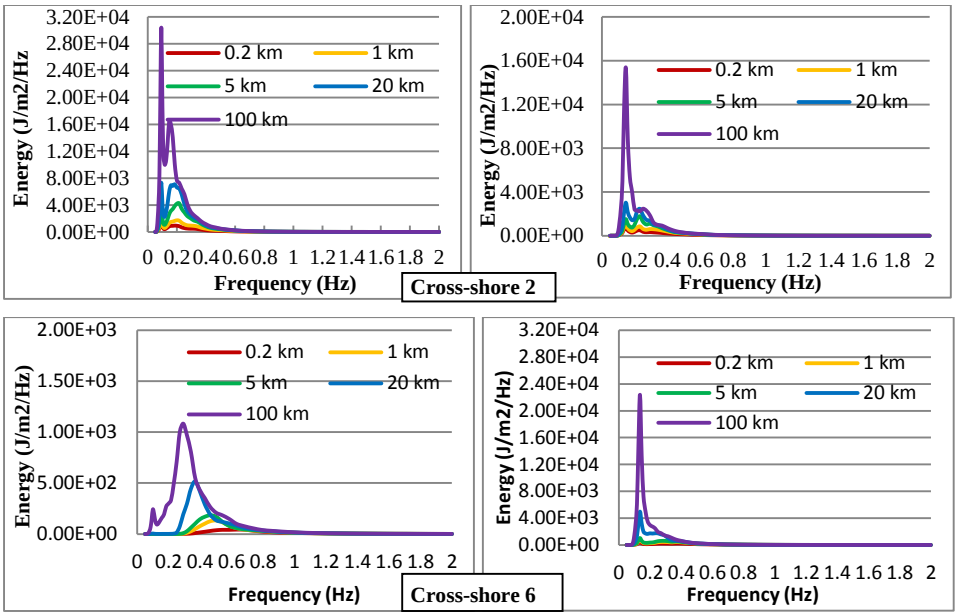

Figure 4.10: The transformation of the wave energy spectra in cross-shore profiles along the Mekong deltaic coast under winter (left column) and summer (right column) monsoon climate.

c) Dissipation

As soon as waves propagate over the shelf, the process of wave energy transformation takes place, due to non-linear interaction, wind input and wave dissipation. Figure 4.11 indicates the evolution of wave dissipation over the Mekong deltaic shelf under the wind monsoon climate. Compared with the summer monsoon climate, wave dissipation occurs much stronger in the winter monsoon climate. In deeper water, the dissipation process of white capping is dominant and wind input at deep water results in an increase of wave steepness. Part of the energy is then redistributed over frequencies, but most of it is dissipated by white capping through the following formulation of Hasselmann (1974):

$$S_{ds,w}(\sigma,\theta) = -\tau\tilde{\sigma}\frac{k}{\tilde{k}}E(\sigma,\theta)$$

Where $S_{ds,w}(\sigma,\theta)$ is white-capping dissipation, τ is a steepness dependent coefficient which is estimated by closing the energy balance of the waves in a fully developed condition depending on the wind input, k is the wave number, θ is directional space, E(σ,θ) is variance density and $\tilde{\sigma}$ and $\tilde{k}$ denote a mean frequency and a mean wave number, respectively.

Due to distribution of wind monsoon climate, higher wave dissipation occurs on the eastern shelf during the winter monsoon climate and on the western shelf during the summer monsoon climate, respectively. Besides the dissipation of white-capping, the depth-induced dissipation is caused by bottom friction in the continental shelf sea as well, which leads to a higher dissipation of up to 0.7-0.8 N/ms in the north-east of the Mekong deltaic shelf as a result of a higher bottom elevation compared with adjacent areas, as well as leading to the above mentioned white-capping. The bottom friction is influenced by the complicated mechanism of the transfer of energy and momentum from the wave-induced motion of the

water particle to the turbulent boundary at the bottom layer which can generally be represented (Bertotti and Cavaleri, 1994):

$$S_{ds,b}(\sigma,\theta) = -C_{bottom}\frac{\sigma^2}{g^2 sinh^2(kd)}E(\sigma,\theta)$$

Where C_{bottom} is the bottom friction coefficient, g is gravity force, h is wave height, d is water depth, k is the wave number, θ is directional space and σ is wave frequency.

In shallower waters, the presence of the bathymetry results in wave breaking with steeper waves as well. The dissipation of this wave breaking is described by the following function:

$$S_{ds,br}(\sigma,\theta) = -\frac{D_{tot}}{E_{tot}}E(\sigma,\theta)$$

Where E_{tot} and D_{tot} are the rate of dissipation of the total energy due to wave breaking according to Battjes and Janssen (1978). The value of D_{tot} depends on the breaking parameter, proposed by Battjes and Stive (1985), $\gamma=H_{max}/d = 0.73$ (in which H_{max} is the maximum possible individual wave height in the local water depth d)

There clearly is dissipation of wave breaking over the surf zone in front of the shoreline of Mekong Delta. In the winter monsoon climate, a higher dissipation of wave breaking occurs in the estuaries zones since the breaking wave height is still quite large in this area. However, higher dissipation takes place along the western Camau Cape during the summer monsoon climate.

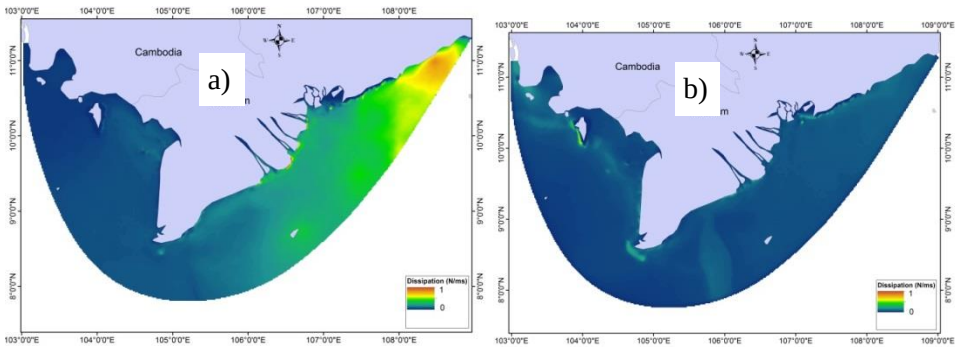

Figure 4.11: The distribution of wave dissipation along the Mekong deltaic shelf under winter (a) monsoon climate and summer (b) monsoon climate.

4.3.3 Potential longshore sediment transport

LST occurs when waves approach the coast at an angle. Research efforts on the improvement of bulk LST equations have continued; yet there is no general consensus on the choice of a formulation. There is, for instance, the CERC formula of the bulk longshore transport, widely applied by coastal engineers. This formula is mainly used due to its applicability in regions with limited observations. Moreover, the CERC formula has been tested and successfully been applied to similar coastal environments and is found to provide results in close agreement with process-based models (Almar et al., 2014). Using the long-term wind climate analysis, wind probability was determined for two areas

covering the eastern and western parts of the Mekong deltaic shelf. The seasonal and annual LST calculations, with 28 sites along the Mekong deltaic coast (Figure 4.7), are shown in Figure 4.12 (positive LST values show the direction from the north-east to the south of the Camau spit and then to the north). Moreover, the LST gradients (in m3/m/year) were also computed along the Mekong deltaic coast under the wind/winter monsoon climate and were used to identify potential locations of erosion or accretion. This was accomplished by differencing the LST rate and dividing it by the segment distance. The potential erosion/accretion rates, shown in Figure 4.13, are calculated by the potential LST gradients along the Mekong deltaic coast dividing the proposed average closure depth for very shallow water depth. Closure depths along the Mekong deltaic coast are calculated by using the Hallemeier equation (1981). Due to different wave characteristics on the spatial scale, the potential LST and erosion/accretion rate are separately analysed and discussed for the eastern and western Mekong deltaic coast.

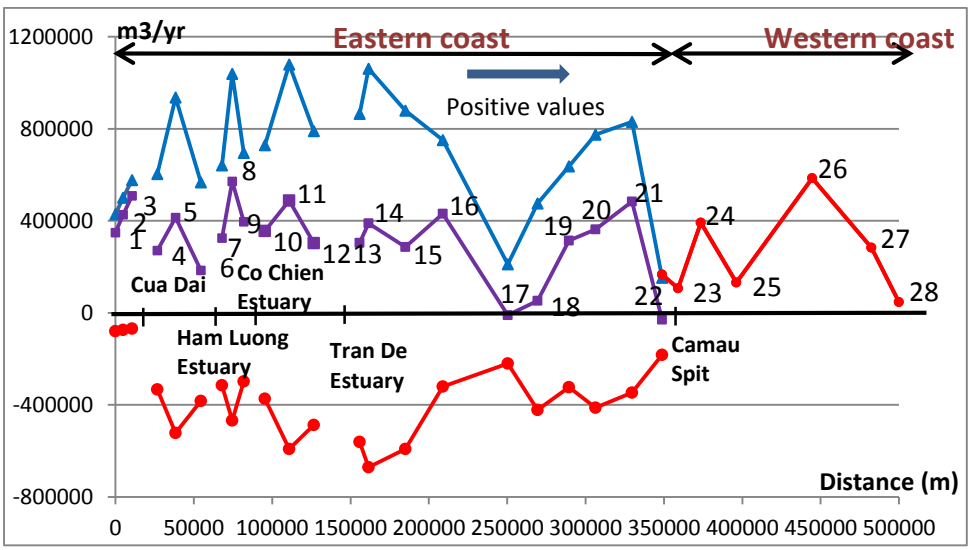

Figure 4.12: Annual LST rate along the Mekong deltaic coast. Blue, red, purple lines are referred to winter monsoon, summer monsoon and net LST rates, respectively.

a) The eastern Mekong deltaic coast

Due to the dominant offshore wave propagation directions in the winter monsoon climate, the trend of the littoral drift along the eastern coast of the Mekong Delta is towards the south-west. In the estuarine area, the highest sediment transport rate is approximately up to $1.1x10^6$ $m^3/yr.$ at Tra Vinh Province as a result of deep bathymetry in this area. In the south of the Mekong estuaries, the sediment transport rate decreases gradually from $1.06x10^6$ $m^3/yr.$ to the lowest rate at $211x10^3$ $m^3/yr.$ towards the southwest, almost as far as Ganh Hao estuary. More specifically, there are variations of LST gradients in this coastal area which mainly depend on the magnitude of the breaking wave height and its incident angle, shown in Figure 4.12. The lowest LST rate in this zone occurs at Ganh Hao estuaries (Bac Lieu Province), which has a minor breaking wave height due to a shallower bathymetry compared with the adjacent areas on the shelf.

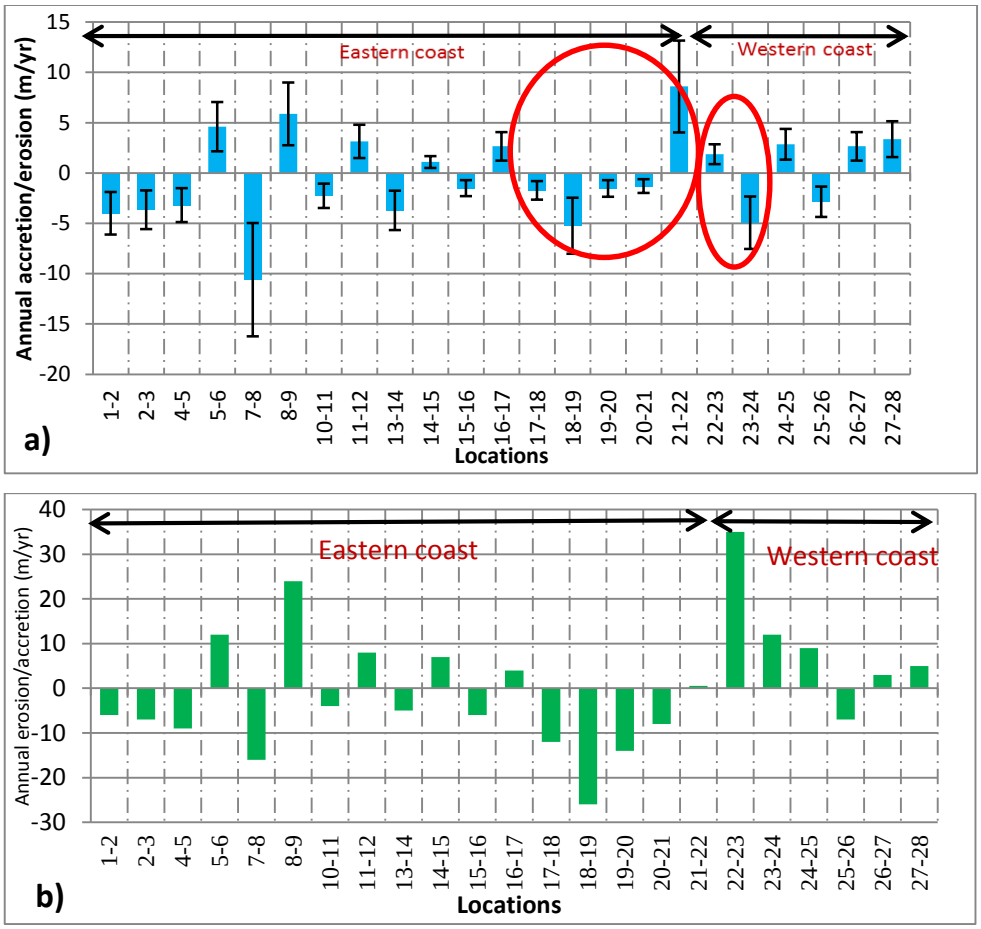

Figure 4.13: The annual erosion/accretion processes along the Mekong deltaic coast between the calculation from the potential LST gradients (a) with error bars of 53% (Mil-Homens et al, 2013) and the observations (b).

However, the direction of the LST in the eastern Mekong Delta is completely opposite during the summer monsoon climate; i.e. towards the north-east because the dominant offshore wave propagation directions are north-north east and north east. In general, the magnitude of LST rate is lower than its magnitude in the winter monsoon climate along this Mekong deltaic coast. On the southern coast of the Mekong river mouths, the lowest LST rate occurs at Bac Lieu Province. Meanwhile, the highest LST rate in the eastern Mekong deltaic coast moves to the south of the Mekong estuaries at Soc Trang Province.

In the Mekong estuaries, there is a reverse variation of LST gradients between two seasons under the monsoon climate, however, the trend of the LST gradient in the winter monsoon climate controlled the annual net LST along the Mekong deltaic coast due to the stronger wind as shown in Figure 4.13. This imbalance in the seasonal LST leads to the same pattern in the coastal areas of the eastern estuarine zones, including Ben Tre and Tra

Vinh provinces: the yearly net LST gradient increases in the north-east areas and decreases in the south-west areas. Therefore, in the estuary areas, the erosion occurs in the coastal north-east zones, meanwhile, the accretion takes place in the coastal south-west zones, consistent with the shoreline change analysis of Phan et al. (2017) as shown in Figure 4.12.

Due to the dominant winter monsoon climate, the annual LST gradients along this Mekong deltaic coast are controlled by the pattern of the winter LST gradients. Along the southern coast of the Mekong river estuaries from Soc Trang Province to Camau Cape, there is a different pattern of LST gradients between two zones from Tran De estuary to Ganh Hao estuary (TD-GH) and from Ganh Hao estuary to Ca Mau Cape (GH-CM). While the increase and decrease of annual net LST gradients intersperse with each other in the coastal zone of TD-GH, annual LST gradients increase along the coastal area of GH-CM. Therefore, it leads to the erosion phenomenon with a long distance of GH-CM as shown in Figure 4.12. On the other hand, due to receiving sediment sources directly from the Mekong river, although LST gradients in the estuaries areas are higher than LSR gradients in the southern coast, its erosion level is lower compared with the erosion phenomenon in the southern coast as shown in Fig.14b. Furthermore, there is quite a large difference between the annual erosion/accretion processes along the Mekong deltaic coast between the calculation from the potential LST gradients and the observations in the section within point 17-22. The possible reasons come from (1) the significant role of strong tidal currents in the coastal zone of GH-CM (Phan et al., 2019), (2) the effect of Cua Lon river and numerous other channels connected between the East Sea, which has a high tidal amplitude, and the West Sea having a very low tidal amplitude in Ca Mau Province (Phan et al., 2019), (3) the wind monsoon induced currents, (4) relative sea level rise including sea level rise and subsidence (Phan et al., 2017; Erban, et al., 2014), (5) the quicker reaction of the upper shoreface with respect to forcing conditions than the lower shoreface (Stive and de Vriend, 1995).

b) The western Mekong deltaic coast

Contrary to the eastern Mekong Delta, the potential LST rate in the western Mekong deltaic coast is dominated by the summer monsoon climate into the direction towards the North. Because of lower summer monsoon winds, the potential LST rate in this zone is moderately small, averaging approximately 260×10^3 m^3/yr. Due to a limited fetch length, the breaking waves have nearly been absent in the surf zone of the western Mekong deltaic coast, therefore, the wave-induced LST rate is extremely low (neglected) for the period of the winter monsoon climate shown in Figure 4.15b. The declining process of the annual net LST occurs in two areas, including the western Camau Cape and the end area of the western coast, which leads to sedimentation locally. Meanwhile, the LST rise at 586×10^3 m^3/yr. in the center of the western coast, is resulting in the erosion phenomenon. Although, the annual net LST gradients also increase to 19 m^3/m/yr. in the area of Bay Hap estuary (section points 23 - 24), which means there would be erosion in this area, due to several causes a high accretion rate actually happens. First of all, this estuarine area is supplied by sediment from the Bay Hap and Cua Lon rivers. Secondly, after sediment is brought to the western nearshore of the Ca Mau spit by the winter monsoon climate, the summer monsoon climate carries the sediment to the western coast of Ca Mau spit. This second reason leads to the "error" of accretion between section 21-22 and section 22-23. The above results in the western coast also agree with the analysis of shoreline change using remote sensing by Phan et al (2017).

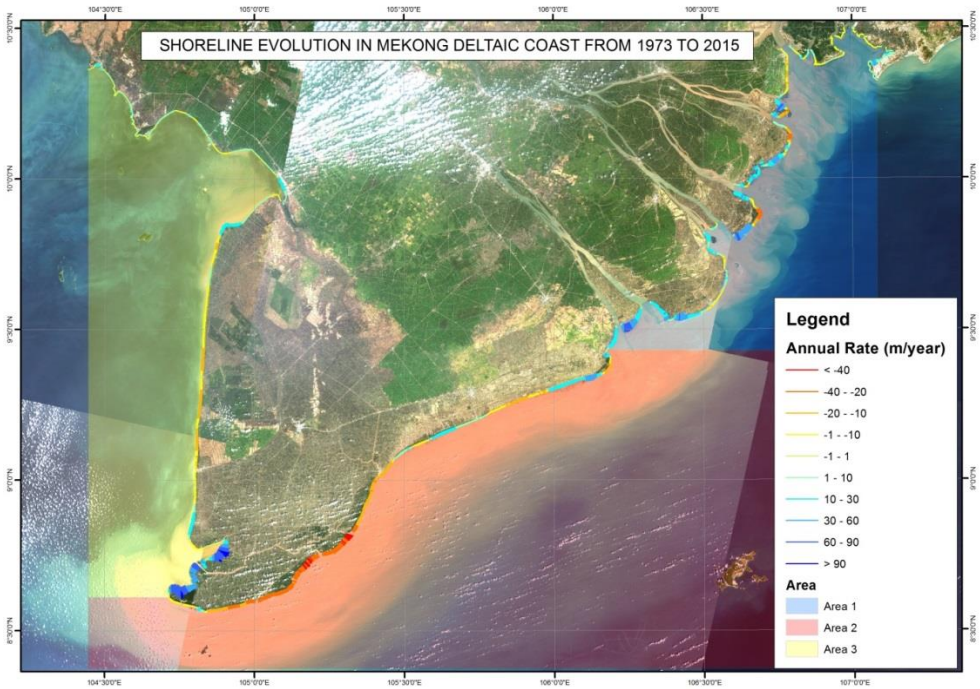

Figure 4.14: The shoreline evolution along the Mekong deltaic coast over 43 years (Phan et al., 2017)

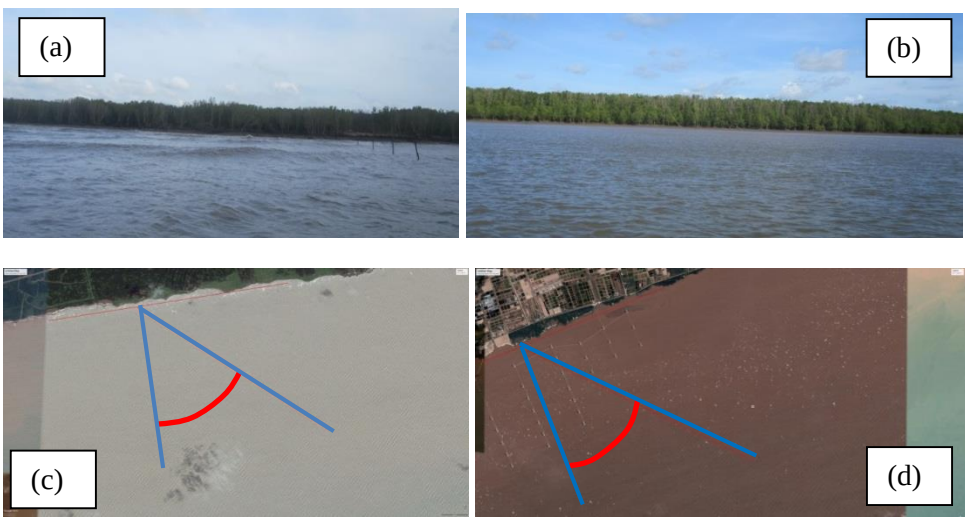

Figure 4.15: The wave fields in the eastern (a) and western (b) Ca Mau Province during the winter monsoon climate in Nov. 2014. The wave field (wave angle in red colors) was collected from google earth in Bac Lieu (c) and the eastern Camau (d) during winter monsoon climate.

4.4 Conclusions

This study analysed the nearshore wave climate characteristics and the corresponding potential longshore sediment transport rates, as well as shoreline evolution along the Mekong Deltaic Coast. The evolution of the wave fields over the Mekong deltaic shelf was investigated by numerical modelling using the spectral wave model SWAN. A comparison between field observations and numerical simulations showed SWAN to perform reasonably well on the wave field transformation on the Mekong deltaic shelf. The widely used CERC formula is employed to analyse the potential longshore sediment transport both seasonally and annually.

The wave field evolution in the Mekong deltaic shelf is significantly controlled by the wind monsoon climate. Higher wave heights are found in the north east area of the Mekong deltaic shelf and these decrease to the south-western and western coast of Mekong Delta in the winter monsoon. Opposite to the winter monsoon climate, significant wave heights on the western shelf are generally higher than the wave height on the eastern coast during the summer monsoon climate. While the wind fields during the winter monsoon climate only influence wave fields on the eastern coast, the wind system during the summer monsoon climate rather remarkably affects both the eastern and western coasts.

The study reveals that when the waves propagate closer to the Mekong deltaic coast, the energy spectra of the wind and swell sea peaks fall, due to the effect of dissipation. Also, the rate of reducing wave energy of lower frequencies of swell is higher than that of higher wave frequencies, in particular when waves move to shallower water since the waves with a lower frequency feel the bottom more strongly. The depth-induced dissipation of waves is found along the north east of the Mekong deltaic shelf. While the high dissipation of wave breaking occurs in the estuarine areas in the winter monsoon climate, large dissipation takes place along the western Camau Cape during the summer monsoon climate.

Similar to the wave field evolution, due to the effect of the wind monsoon climate on the Mekong deltaic shelf, the annual net LST gradients along the eastern coast are controlled by the pattern of the winter LST gradients, while the annual net LST gradients in the western region are dominated by the summer LST gradients. The study indicates that the gradients in the seasonal LST result in a similar pattern of the erosion and accretion phenomenon in the coastal areas of the eastern estuarine zones as observed. On the other hand, the study shows that potential LST gradients in the estuarine areas are higher than LSR gradients on the south eastern coast, whereas shoreline retreat in the south eastern region occurs more seriously in reality. The probable causes for this phenomenon include: (1) sediment input from the Mekong river, (2) the effect of strong tidal currents in the coastal zone of GH-CM, (3) the role of the Cua Lon river and abundant other channel systems linking the East and West Seas, (4) the wind monsoon induced currents which should be considered in the future.

References

Almar, R., Du Penhoat,Y., Hounkonnou, N., Castelle, B., Laibi,R., Anthony, E., Senechal, N.,Degbe, G., Chuchla, R.,Sohou, Z., Dorel,M., 2014. The Grand Popo experiment, Benin. J.Coast.Res.70,651–656 (Special issue).

Baba, J., Komar, P.D., 1981. Measurements and analysis of settling velocities of natural quartz grains. J Sediment Petrol 51:631–640.

Bailard, J.A., 1981. An energetics total load sediment transport model for a plane sloping beach. J Geophys Res 86C:10983–10954.

Battjes, J.A., Janssen, J.P.F.M., 1978. Energy loss and set-up due to breaking of random waves. In: Proceedings of 16th International Conference on Coastal Engineering, ASCE, pp. 569–587.

Battjes, J. A. and M. J. F. Stive, 1985: Calibration and verification of a dissipation model for random breaking waves. J. Geophys. Res., 90 (C5), 9159–9167.

Bertotti, L. and Cavaleri, L. Accuracy of wind and wave evaluation in coastal regions, Proc. 24th Int. Conf. Coastal Engineering, ASCE, pp. 57-67, 1994

Booij, N., R. C. Ris, and L. H. Holthuijsen, 1999: A third generation wave model for coastal regions, Part I, Model description and validation. J. Geophys. Res., 104 (C4), 7649–7666.

Boucher M., Favreau G., Vouillamoz J.M., Nazoumou Y., Legchenko A., 2009. Estimating specific yield and transmissivity with magnetic resonance sounding in an unconfined sandstone aquifer (Niger) Hydrogeol. J.;17:1805–1815. doi: 10.1007/s10040-009-0447-x.

Bosserelle, C., Pattiaratchi, C.B., Haigh, I., 2012. Inter-annual variability and longer-term changes in the wave climate of Western Australia between 1970 and 2009. Ocean Dyn. 62, 63–76.

Cavaleri, L., Malanotte-Rizzoli, P., 1981. Wind wave prediction in shallow water: theory and applications. Journal of Geophysical Research 86 (C11), 10961–10973.

Cavaleri, L., 1994. Applications to wave hindcasting and forecasting; Chapter IV; In: Dynamics and Modeling of Ocean Waves, Cambridge University Press, UK, 532p.

CERC, 1984. Shore Protection Manual. Vols I and II. Coastal Engineering Research Center. U.S. Army Corps of Engineers, Washington, DC. U.S. Government Printing Office, Vicksburg.

Eldeberky, Y., Battjes, J.A., 1996. Spectral modeling of wave breaking: application to Boussinesq equations. Journal of Geophysical Research 101 (C1), 1253–1264.

Erban, L. E., Gorelick, S. M., Zebker, H.A., 2014. Groundwater extraction, land subsidence and sea level rise in the Mekong Delta, Vietnam. Environmental Research Letters. 9 (2014) 084010 (6pp)

Gorrell, L., Raubenheimer, B., Elgar, S., & Guza, R. T., 2011. SWAN predictions of waves observed in shallow water onshore of complex bathymetry. *Coastal Engineering*, *58*(6), 510–516. https://doi.org/10.1016/j.coastaleng.2011.01.013.

Hallermeier, R. J., 1981. A Profile Zonation for Seasonal Sand Beaches from Wave Climate. Coastal Engineering, Vol. 4, 253-277.

Hasselmann, K., 1974. On the spectral dissipation of ocean waves due to white- capping. Boundary-Layer Meteorology 6 (1–2), 107–127.

Holthuijsen, L.H., Booij, N., Ris, R.C., 1993. A spectral wave model for the coastal zone. In: Proceedings 2nd International Symposium on Ocean Wave Measurement and Analysis, New Orleans, Louisiana, July 25–28, New York, pp. 630–641.

Institute of Coastal and Offshore Enginerring (ICOE), 2016. Research project of coastal processes along the Ca Mau http://icoe.org.vn/index.aspx?aac=CLICK&aid=ARTICLE_DETAIL&ari=3100&lang=1&menu=&mid=0&parentmid=0&pid=1&title=nhiem-vu-khcn-nam-2014

João Mil-Homens, Roshanka Ranasinghe, J.S.M. van Thiel de Vries, and M.J.F. Stive., 2013. Re-evaluation and improvement of three commonly used bulk longshore sediment transport formulas. Coastal Engineering, 75:29–39. ISSN 0378-3839. doi: 10.1016/j.coastaleng.2013.01.004.

Judith Bosboom and Marcel J. F. Stive, 2013. Coastal dynamics 1. ISBN 978-90-6562-286-0.

Kamphuis, J.W., 1991. Alongshore sediment transport rate. J Waterway Port Coast Ocean Eng 117:624–641.

King, D. B. Jr., 2005. Influence of grain size on sediment transport rates with emphasis on the total longshore rate. US Army Corps of Engineers ERDC/CHL CHETN-II-48. http://chl.erdc.usace.army. mil/library/publications/chetn/pdf/chetn-ii-48.pdf

Komar, P. D., 1998. Beach Processes and Sedimentation. Prentice Hall Inc., New Jersey (544–545).

Komen, G. J., Hasselmann, S., Hasselmann, K., 1984. On the existence of a fully developed windsea spectrum. Journal of Physical Oceanography 14, 1271–1285.

Komen, G. J., Cavaleri, L., Donelan, M., Hasselmann, K., Hasselmann, S., Janssen, P.A.E.M., 1994. Dynamics and Modelling of Ocean Waves. Cambridge University Press, 554.

Larson, M., Hoan, L.X., Hanson,H., 2010.A direct formula to compute wave properties at incipient breaking. J. Waterw. Port Coast. OceanEng. 136(2),119–122.

Lima, S. F., Almeida, L. E. S. B., Toldo, E.E. Jr., 2001. Estimate of longshore sediments transport from waves data to the Rio Grande do Sul coast. Pesquisas 48:99–107

LMDCZ., 2018. Lower Mekong Delta Coastal Zones Project. http://lmdcz.siwrr.org.vn/?lang=e

Lv, X., Yuan, D., Ma, X., Tao, J., 2014. Wave characteristics analysis in Bohai Sea based on ECMWF wind field. Ocean Eng. 91, 159–171.

Martinho, C.T., Dillenburg, S.R., Hesp, P., 2009. Wave energy and longshore sediment transport gradients controlling barrier evolution in Rio Grande do Sul, Brazil. J Coast Res 25(2):285–293.

Mirzaei, A., Tangang, F., Juneng, L., Mustapha, M.A., Husain, M.L., Akhir, M.F., 2013. Wave climate simulation for southern region of the South China Sea. Ocean Dyn. 63, 961–977.

Miles, J.W., 1957. On the generation of surface waves by shear flows. Journal of Fluid Mechanics 3, 185–204.

Mulligan, R., Hay, A., and Bowen, A., 2008. Wave-driven circulation in a coastal bay during the landfall of a hurricane, *J. Geophys. Res.*, 113, C05026, doi:10.1029/2007JC004500.

Phan, H., Reniers, A., Ye, T., Stive, M., 2017. Response in the Mekong deltaic coast to its changing sediment sources and sinks. In T. Aagaard, R. Deigaard, & D. Fuhrman (Eds.), Proceedings of Coastal Dynamics 2017: Helsingør, Denmark (pp. 311-322). [Paper No. 225].

Phan, H. M., Ye, Q., Reniers, A. J. H. M., Stive, M. J. F., 2019. Tidal wave propagation along The Mekong deltaic coast. Estuarine, Coastal and Shelf Science, 220, 73-98. https://doi.org/10.1016/j.ecss.2019.01.026

Reeve, D., Chadwick, A., Fleming, C., 2004. Coastal Engineering: Processes, Theory, and Design Practice. Spon Press, Taylor and Francis Group, London and New York.

Ris, R.C., Holthuijsen, L.H., Booij, N., 1999. A third-generation wave model for coastal regions: 2 Verification. Journal of Geophysical Research 104 (C4), 7667–7681.

Serreze, R.G., R.G. Barry, Chorley, R.J., 2010. Atmosphere, Weather and Climate, Routledge, Oxon.

Smith, E. R., Wang, P., Ebersole, B.A., Zhang, J., 2009. Dependence of total longshore sediment transport rates on incident wave parameters and breaker type. J Coastal Res 25:675–683

Soomere, T., Räämet, A., 2011. Long-term spatial variations in the Baltic Sea wave fields. Ocean Sci. 7 (1), 141–150.

Southern Institute of Water Resources Research (SIWRR)., 2010. Project for measurements of bathymetry, hydrodynamics in estuaries and coastal zone of Mekong Delta from 2009 to 2010. http://www.siwrr.org.vn/?id=nckh5 (in Vietnamese)

Swail, V.R., Cox, A.T., Cardone, V.J., 1999. Analysis of wave climate trends and variability. WMO Workshop on Advances in Marine Climatology (CLIMAR99), 8–15 September 1999, Vancouver, B.C. pp. 245–256.

Stive, M.J.F. and De Vriend, H.J., 1995. Modelling Shoreface Profile Evolution. Marine Geology, 126, 235-248. http://dx.doi.org/10.1016/0025-3227(95)00080-I

Stive, M.J.F., Aarninkhof, S.G.J, Hamm, L., Hanson, H., Larson, M.,Wijnberg, K.L., Nicholls, R.J., Capobianco M., 2002. Variability of shore and shoreline evolution. Coast Eng 47(2): 211–235.

Tas, S., 2016. Coastal protection in the Mekong Delta. Master thesis. https://repository.tudelft.nl.

Tolman, H.L., 1991. A third-generation model for wind waves on slowly varying, unsteady and inhomogeneous depths and currents. Journal of Physical Oceanography 21, 782–797.

Tolman, H.L., 1999. User manual and system documentation of WAVEWATCH III version 1.18, NOAA/NWS/NCEP/OMB technical note 166, 100 pp.

Unverricht, D., Szczucinski, W., Stattegger, K., Jagodzinski, R., Le, X.T., Kwong, L.L.W., 2013. Modern sedimentation and morphology of the subaqueous Mekong Delta, Southern Vietnam. Global and Planetary Change 110, 223-235.

Van der Westhuysen, A. J., 2009: Modelling of depth induced wave breaking under finite-depth wave growth conditions. J. Geophys. Res., in press.

WAVEWATCH III. https://polar.ncep.noaa.gov/waves/

Xue, Z., He, R., Liu, J. P., Warner, J. C., 2012. Modelling transport and deposition of the Mekong river sediment. Continental Shelf research 37, 66-78.

Zijlema, M., Stelling, G. and Smit, P., 2011. SWASH: An operational public domain code for simulating wave fields and rapidly varied flows in coastal waters. Coast. Engng., 58, 992-1012.

Zijlema, M., Van der Westhuysen, A.J., 2005. On convergence behaviour and numerical accuracy in stationary SWAN simulations of nearshore wind wave spectra. Coastal Engineering 52 (3), 237–256.

5

Seasonal morphodynamics along the Mekong Deltaic Coast

The Mekong Delta, one of the largest plains in Asia, has been receiving tens of millions of tons of sediments every year.However the Mekong deltaic coast has faced severe erosion in the recent decades, partially due to reduced fluvial sediment supply. This study employed the process-based model of Delft3D to find the mechanisms of sediment transport as well as the processes of alongshore sediment gradients along the Mekong deltaic coast under the monsoon climate system. Due to a considerable difference between the summer and winter monsoon climate, the mechanism of annual residual transport, sediment transport and relevant morphodynamics along Mekong deltaic coast is dominated strongly by the winter monsoon. The study shows that due to the Mekong River mouths system as well as strong natural forces, such as winds, waves and tides during the winter monsoon climate, the process of morphodynamics is more complicated on the eastern Mekong deltaic coast than on its western coast. The study found that not only wave action, but also the effects of wind and tide contribute importantly to the increase of the rate of residual sediment transport (RST) on the eastern coast of Camau, nearly equivalent to the rate of RST on the adjacent coastal areas of the Mekong River estuaries, leading to erosion up to 30-40 m/yr. Such severe erosion has not been explained in earlier studies. Furthermore, the study suggests that the numerous connected channel systems and the occurrence of overwash are partly responsible for the transport of sediment from the eastern Camau coast to the western Camau coast. In addition to the decreased sediment discharge from the Mekong River, relative sea level rise and mangrove squeeze also cause a severe shoreline retreat.

This chapter is submitted to *Estuarine, Coastal and Shelf Science*. Phan, H. M., Ye, Q., Reniers, A. J. H. M., Stive, M. J. F. (2020).

5.1 Introduction

A delta generally occurs where a river carrying sediments flow into an ocean, sea, estuary, lake, reservoir. Conceptual process based models for deltaic deposition include: 1) river-dominated/ influenced, such as the Mississippi, Yellow River, and Po deltas, 2) wave dominated/ influenced, such as the Nile and Danube deltas, 3) tide dominated/ influenced, such as the Amazon, Yangtze, and Fly deltas (Galloway, 1975), and 4) deltas dominated by the combination of the former three processes, such as the Mekong Delta (Ta et al., 2002a,b). The evolution of a deltaic system is a unsteady process and is usually characterized by lobe switching, such as in the Mississippi (Roberts, 1997) and Po deltas (Correggiari et al., 2005), and even changes of a dominant process, such as the transformations in the Mekong Delta (Ta et al., 2002a, Unverricht et al., 2013).

According to the classification of Davis & Hayes (1984) the coasts of the Mekong Delta are a mixed-energy (tide-dominated) environment which is affected by the discharge regime of the Mekong River and its sediment load, the tidal regime of the Vietnamese East Sea and the Gulf of Thailand, as well as by coastal long-shore currents driven by prevailing monsoon winds and the corresponding wave conditions (Delta Alliance, 2011). The resulting Mekong River Delta is bounded by the South China Sea to the east and the Gulf of Thailand to the west. Bore hole studies showed that this delta plain began its progradation around 8000 years ago (Tamura et al., 2009). Over the past 6000 years, tremendous amounts of Mekong River sediment input have allowed the MRD to prograde more than 250 km to the southeast (Nguyen et al., 2000). Recent observations on sediment grain size variations along bore-holes further suggested that the MRD evolution during experienced a phase alteration from a ‘‘tide-dominated’’ to a ‘‘tide and wave dominated’’ condition around 3000 BP (Ta et al., 2002a, 2002b). Today, with 200 new dams to be added to the river basin in the next couple of decades, more significant changes are expected in the MRD hydrological regime, the coastal circulation and in the delta dynamics (Xue et al., 2010).

Figure 5.1: Shoreline retreat along the mangrove coast of Mekong Delta

Earlier studies of sedimentation almost exclusively focused on the Mekong River system and only a few studies focused on the coastal zone of the lower Mekong Delta (Unverricht et al, 2013, 2014; Hein et al, 2013, Xue et al, 2012). Previous geology studies indicate that Mekong-derived sediment has a limited cross-shelf distribution immediately seaward of the distributary-channel mouths, in contrast to an extensive along-shelf, distal deposit extending to the Ca Mau Peninsula (Xue et al., 2010, Xue et al., 2012, Unverricht et al., 2013, Unverricht et al., 2014). Using the numerical modelling of the Princeton Ocean Model, Hordoir et al. (2006) show that the Mekong River plume corresponds to a seasonal cycle and the reverse spread of the Mekong River plume is caused by the monsoon climate; i.e., north-eastward in winter and south-westward in summer. Meanwhile, Xue et al. (2012) points out that a large volume of fluvial sediments was transported and deposited near the Mekong River mouth during summertime. Then, strong wave mixing and coastal currents lead to resuspension and southwestward dispersal of a small fraction of previously deposited sediments in the following winter. Hein et al. (2013) show that the growth of the sub-aquatic delta is still ongoing in or near the river mouths. However, these studies focus mainly on the estuary areas without any attention to sediment dynamics in the south-eastern and western coast of Mekong Delta. Therefore, due to the complex and variable morphology along the full length of the Mekong deltaic coast, the overall sediment dynamics are still insufficiently understood.

Along the entire coastline a complicated dynamic process of accretion and erosion is taking place. In some areas, a loss of land up to 40 m per year due to erosion has been recorded, while in other areas land accretion can reach up to 90 m per year (Phan et al., 2017). The highly dynamic coastline of the Lower Mekong Delta is controlled by a combination of waves, tidal currents, a wind monsoon climate and sediment loads from the Mekong River. The wave processes at the Mekong Delta are controlled by the monsoon winds. The NE monsoon generates the highest waves on the east coast, while the SW monsoon can be held responsible to control the wave climate on the west coast (Bakker, 2017). Phan et al. (2019) showed that strong tidal currents occur along the southern coast up to 0.8-1 m/s, which may trigger the movement of bed sediment(s). Hence, it is necessary to clearly consider and quantify the role of every factor of influence on the coastal environment, including tide, wind and wave influencing the sediment budget along the Mekong deltaic coast.

In Chapter 4 the computed longshore wave driven sediment transport capacity along the Mekong deltaic coast is presented. The results show that the annual rate of erosion/accretion processes along the Mekong deltaic coast due to the wave climate only is lower compared with the observation of satellite images. Hence, the question is what other factors, besides wave impact, control coastline retreat in the coastal area of Mekong Delta. The sediment transport patterns and the associated morphological changes under present day conditions need to be better understood. Therefore, the objective of this study is to obtain a coherent and synoptic picture of the seasonal morphodynamics on the Mekong deltaic coast by using numerical modelling of Delft3D under effects of wind, wave and tide.

5.2 Numerical modelling

5.2.1 Model setup

In this study we applied the process based numerical model of Delft3D to simulate the transport and dispersal of Mekong-derived sediment in 2005. The Delft3D model consists of state- of-the-art modelling components for the hydrodynamics and sediment transport (Delft3D-FLOW module, Lesser et al., 2004) and wind-wave dynamics (Delft3D-Wave module). The model domain has 503 x 213 points ranging from 1°N – 13.5°N and 99°E-116.5°E through flexible orthogonal mesh structures with grid cell sizes of nearly 5 km near the offshore boundaries and regularly decreasing to 0.5 km near the Mekong deltaic coast.

The bathymetry of this study was taken from the General Bathymetric Charts of the Ocean produced by the British Oceanographic Data Centre with a resolution of 30 arc-seconds. Moreover, the bathymetric survey of the Mekong deltaic coast in 2009 and 2010 by the Vietnam Government project (SIWRR, 2010) has been used to create a high resolution bathymetry around the Mekong deltaic coast.

A large number of soil samples along the Mekong deltaic coast were collected and their sediment properties were assessed by the project of the LMDCZ (2018). The variations of sediment grain-size and relative density along the Mekong Delta are shown in Chapter 4. Along the estuary zone, coarser silt was observed with grain-sizes ranging from fine to medium. Off the Dinh An and Tran De river mouths, a range of mixed sediments from fine silt to very fine sand are found, with predominantly coarse silt sediment. A large quantity of the fine-grained sediments (mainly silt) was detected along the south-east coast; fine silt was found along the West coast and coarse sand was found at several offshore locations. According to measurements by LMDCZ (2018), 80-90% of sediment along the Mekong deltaic coast is clay-silt with a size in the order of 10 μm - 20 μm. Wolanski et al. (1996) found a grain size of flocculated sediment of on average 40 μm in the estuaries during the low flow season. Stephens et al. (2017) indicated that median sediment grain sizes range from 5 µm to 20 µm in the Bassac River. Meanwhile, during the high flow season the floc size ranged from 50–200 μm. Based on these observations, the present model included two types of sediments: type 1 and type 2, respectively, representing the cohesive sediment and non-cohesive sediment fractions. A uniform grain size of non-cohesive sediment is 100 μm. Based on the results of the calibration performed by Wolanski et al. (1996) the critical shear stress for erosion and sedimentation was set to 0.4 N/m2 and 1000 N/m^2, respectively. The erosion rate is 3x10^{-5} kg/m^2/s. Furthermore, settling velocities of sediment in fresh and salt water are 0.15 and 0.25 mm/s, respectively. The later value was tested against observations by Wolanski et al. (1998) and McLachlan et al. (2017).

Due to shallow water depths, wind fields play an important role for wave processes along the Mekong deltaic coast. Two wind field products including National Oceanic and Atmospheric Administration (NOAA), namely the Global Forecast System Atmospheric Model and the Blended Global 0.25° Sea Winds with Climatological Monthly Means are used in this study. The Global Forecast System, the weather prediction model built by the NOAA's National Center for Environmental Prediction, is used for model validation, while the Blended Sea Winds dataset developed by NOAA's National Center for

Environmental Information, provides the wind input with climatological monthly means to simulate seasonal climate. On the other hand, wave data in this study used the global numerical model NOAA WAVEWATCH III with a 0.5° grid as boundaries for wave modeling. WAVEWATCH III is an advanced development of the WAVEWATCH model, and WAVEWATCH II, developed at NASA's Goddard Space Flight Center. WAVEWATCH III is a third-generation wave model produced by NOAA/NCEP (Komen et al. 1994). The NOAA WAVEWATCH III model solves the spectral action density balance equation for wave frequency-direction spectra. Hindcasts from these global wave generation models have been validated and shown to reproduce the overall wave climate well in many studies (Li et al., 2016, Zieger et al., 2015).

The river flow and suspended sediment transport time series of the upstream boundary at My Thuan and Can Tho stations were retrieved from the Institute of Coastal and Offshore Engineering and the Southern Institute of Water Resources Research. The flow discharge in the Mekong River follows a seasonal cycle regime, specifically the flood season during May until October and the dry season from November to April. Open boundaries in the deep sea, including the South China Sea and Sunda shelf, were extracted from a total of 8 primary tidal constituents (O_1, K_1, P_1, Q_1, M_2, S_2, K_2, N_2) derived from the tidal wave model of Phan et al. (2019). 15 years of Topex-Poseidon and Jason-1 satellite altimetry (Gerritsen et al., 2003) adjusted to GMT 7 + have been applied for tidal simulations at 8 main boundaries (Phan et al., 2019).

5.2.2 Scenarios

Different scenarios are established to investigate the relative effects of tide, wave and wind on the sediment transport and morphological evolution of the Mekong deltaic coast under the influence of the seasonal and annual monsoon climate. The simulation, considering all three aspects (i.e. tide, wave and wind) together, is taken as the original case. In each new scenario, we change one aspect of these influence factors and keep the other aspects unchanged. The table 5.1 shows scenarios for the simulation of hydrodynamics and sediment transport along the Mekong deltaic coast in detail.

This study used the morphological factor approach in order to reduce the computational effort. The morphological acceleration factor (Roelvink., 2006) is a device used to assist in dealing with the difference in time-scales between hydrodynamic and morphological developments. It works very simply by multiplying the sediment fluxes to and from the bed by a constant factor. For longer-duration morphological simulations the tidal forcing is simplified to a morphologically representative 24.8 hour tidal cycle (Latteux., 1995, Jiao., 2014).

Table 5.1: Scenarios for the simulation.

Scenarios	**Winter**	**Summer**
Tide	✓	✓
Wind	✓	✓
Wave	✓	✓
Tide+Wind	✓	✓
Tide+Wave	✓	✓
Tide + wind + wave	✓	✓

5.3 Results

This section mentions the model validation through comparing suspended sediment concentration indicator between the computed and satellite measured data. Next, the residual flow and sediment transport patterns along the Mekong deltaic coast in the summer and winter monsoon climate are presented. Finally, the alongshore sediment budget is calculated understand the seasonal morphodynamical process along the Mekong deltaic coast.

5.3.1 Model validation

The traditional method to validate the prediction of the suspended sediment concentration is to compare with field measurements including ship surveys and in situ time series. However, this approach is time-consuming and costly, especially in the case of an extremely large area like the Mekong deltaic coast. Therefore, the numerical results of SSC fields are validated with SSC data from satellite images. The European Space Agency produced a 10-year MERIS (Medium Resolution Imaging Spectrometer) climatology (2002-2012), obtaining the information of Suspended Particulate Matter Concentration (kg/m^3), which is supposed to be approximately equivalent to Suspended Sediment Concentration. ENVISAT MERIS is one of 10 sensors used in March of 2002 on board of the polar-orbiting Envisat-1 environmental research satellite including measuring ocean color. The study results of the suspended sediment concentration pattern were compared with the satellite measured Suspended Particulate Matter Concentration in the months of July and December, respectively representing the summer and winter monsoon climate. Although there is still uncertainty in the penetration through water body, the patterns of sediment plume from the remote sensing observations is useful to compared to the simulation. Figure 5.2 shows that the spatial and temporal scales of suspended sediment concentration patterns from the computed model moderately agree with the observations of satellite images. Therefore, the model can be considered to analyse the sediment transport as well as the morphodynamics along the Mekong deltaic coast.

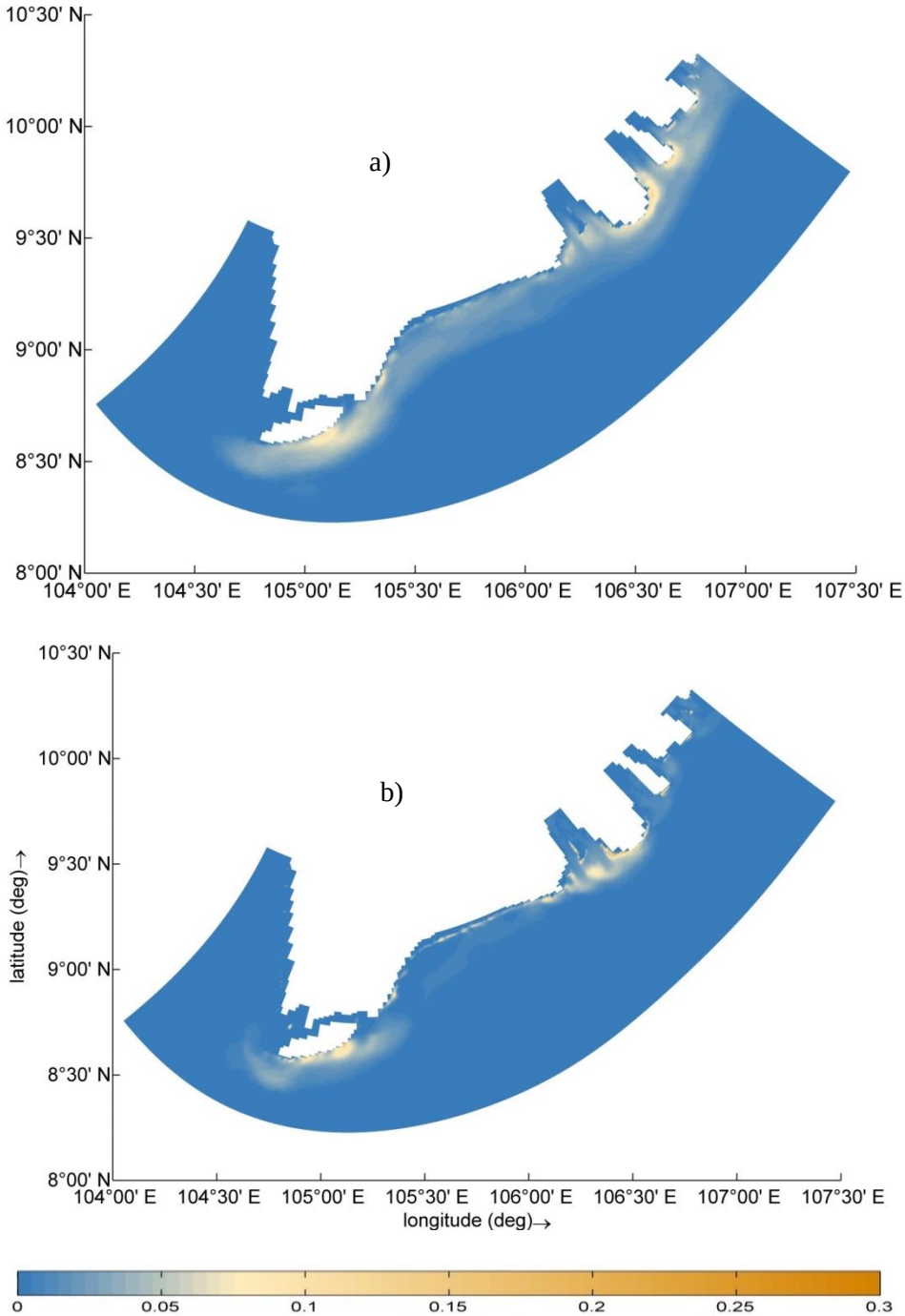

Figure 5.2: The suspended sediment concentration in the simulation and the total suspended concentration in the observation in the winter (a) (c) and summer (b) (d), respectively (kg/m^3)

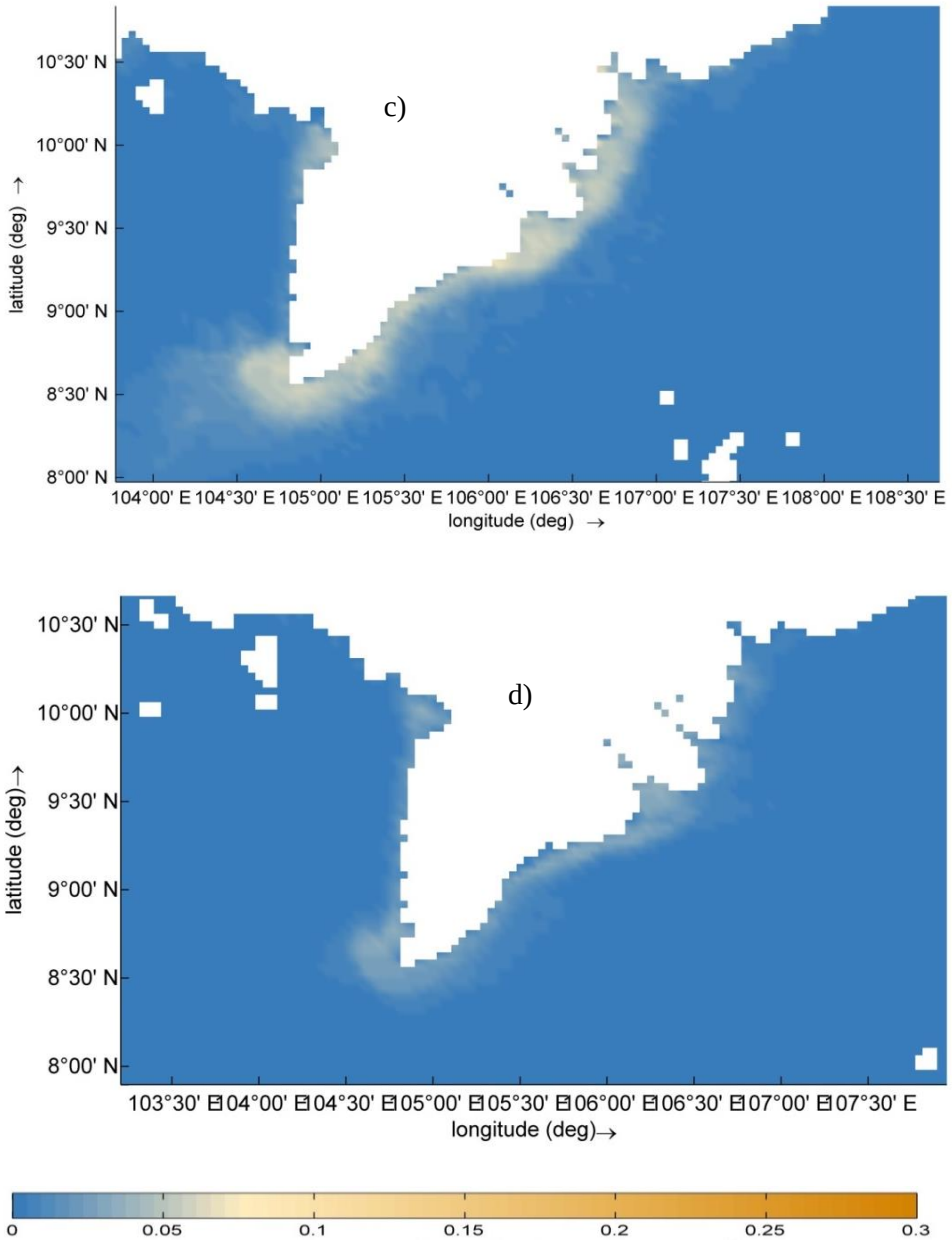

Figure 5.2, continued.

5.3.2 Residual flow patterns

Figure 5.3 shows the residual flow currents patterns along the Mekong deltaic coast in the winter and summer monsoon climate. During winter monsoon climate, while the residual currents prevail in the south-westward direction along the eastern Mekong deltaic coast, it occurs in the southward direction in the western Mekong deltaic coast. Conversely, it takes place in the north-eastward and northward directions along the eastern and western Mekong deltaic coast, respectively, during summer monsoon climate. The magnitude of the residual currents in the winter monsoon climate is considerably higher than its magnitude in the summer monsoon climate. The ebb directed residual flow velocity has a high magnitude in the estuarine areas in both seasons of the monsoon climate, up to 0.2 m/s for the period of the summer monsoon due to high floods from the Mekong River in this season. The residual current flow along the eastern coast of Mekong Delta has a higher magnitude compared with the western coast in the winter monsoon In contrast, the residual currents along the eastern and western Mekong deltaic coast in the summer monsoon are rather equivalent. The residual current velocities in the eastern Ca Mau Province are high compared with adjacent areas.

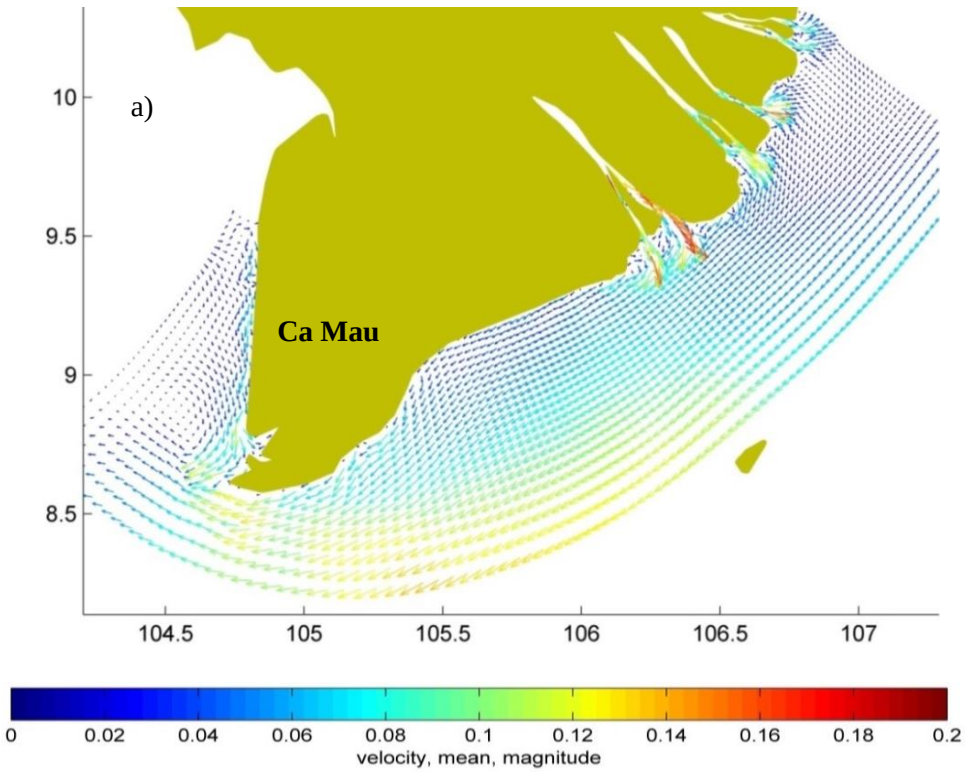

Figure 5.3: Residual flow velocity (m/s) in the winter (a) and summer (b)

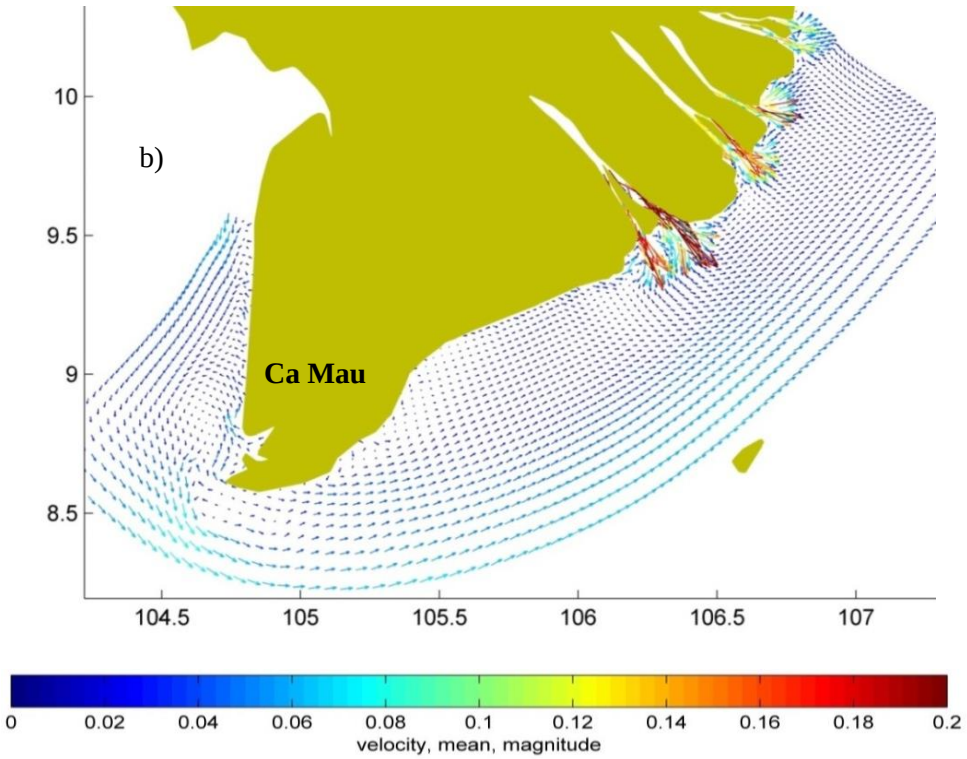

Figure 5.3, continued.

In addition, the study analyses the role of wind, waves and tides influencing the residual flow patterns along the Mekong deltaic coast. The results indicate that the overall distribution of the residual flow patterns is consistently associated with the wind monsoon climate system. Wave action does not significantly impact the residual flow velocity, as shown in Figure 5.4. Therefore, the residual flow pattern in the case of a combined tide and wave climate in the summer seems to be nearly similar to the case when there is only the tide effect as illustrated in Figure B.1, excepting in the surfzone. Figure 5.4 showed that the residual flow is strongly influenced by the wind effect in both seasons, especially on the shelf of Ca Mau Province. In the simulation of a combined wind and tide climate, the residual flow is deflected into a more south-westward direction in the estuary areas during the winter monsoon climate, instead of a southward direction in the case of the tidal effect alone. Also, in the eastern shelf, although tide induced residual flow occurs in the south-westward direction, residual flow takes place in the north-eastward direction when wind action is included. Similarly, along the western Mekong deltaic coast, the residual flow in the case including wind is reversed completely in the southward direction during the winter monsoon climate, while the residual currents in the case of only tide induced effect flow in northward direction. The results of this study indicate that the role of wind action for the residual flow patterns is more significant than of wave action along the Mekong deltaic shelf.

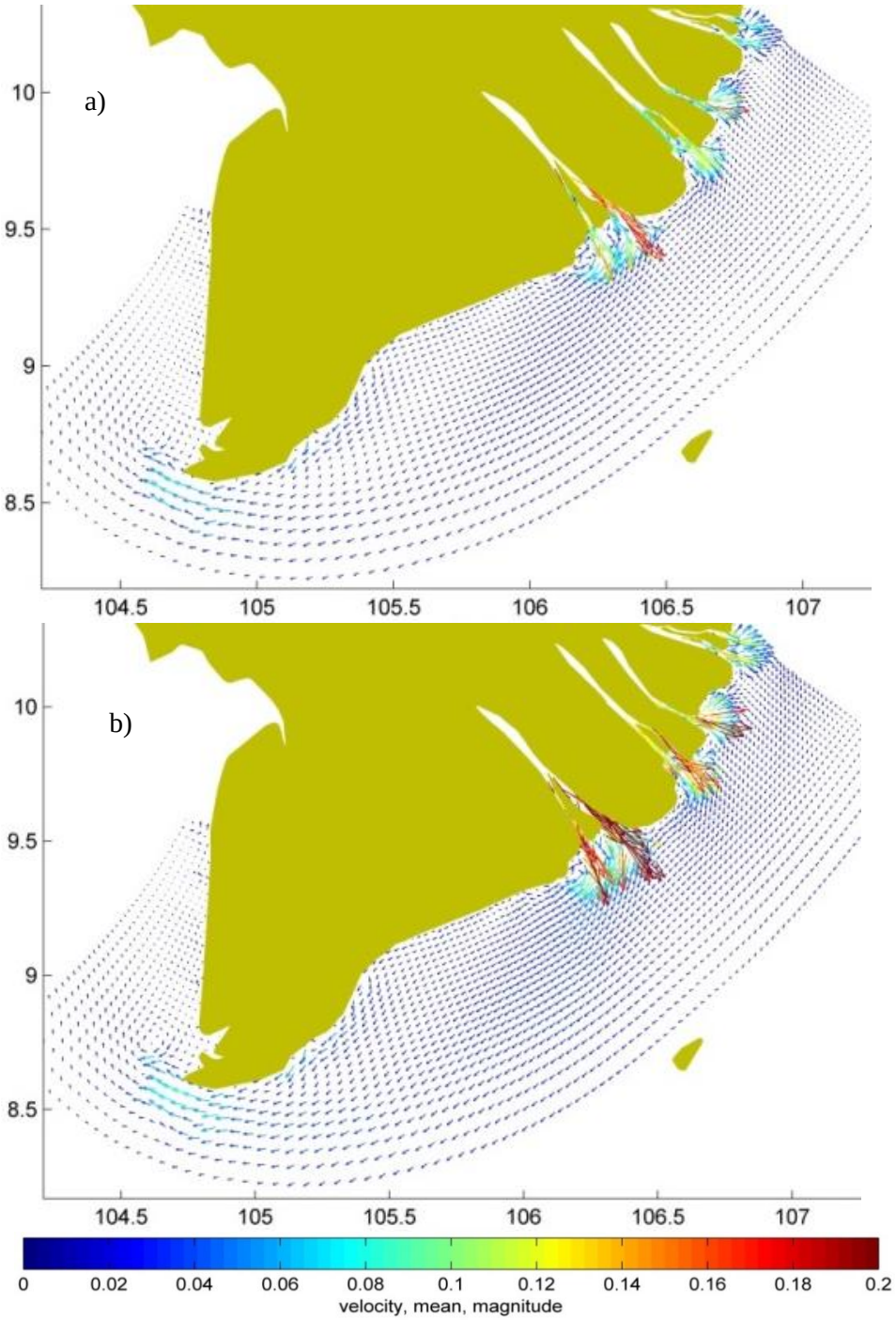

Figure 5.4: Residual flow velocity (m/s) under tide only (a, b), wind only (c, d) and wave only (e, f) effect in the winter and summer, respectively.

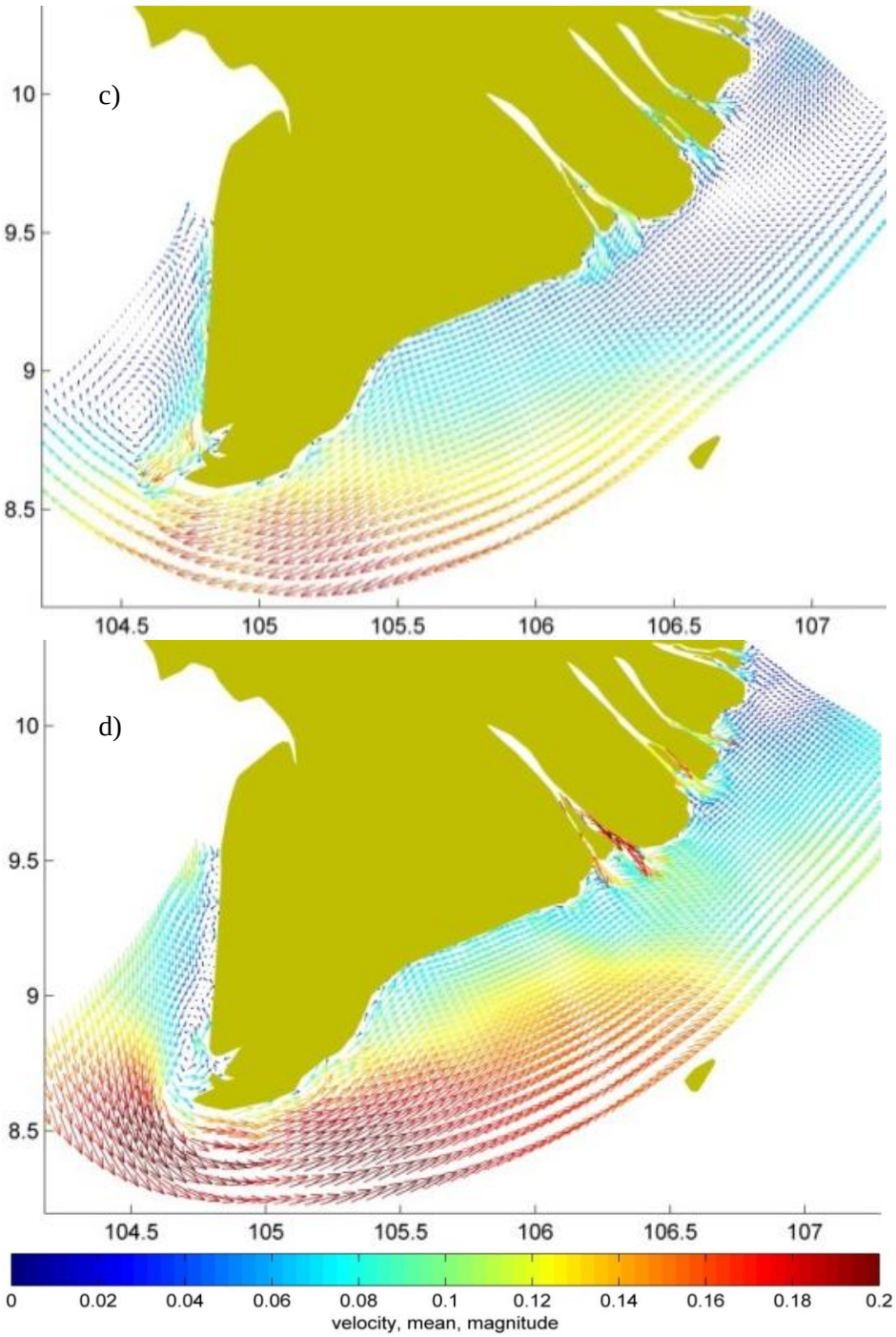

Figure 5.4, continued.

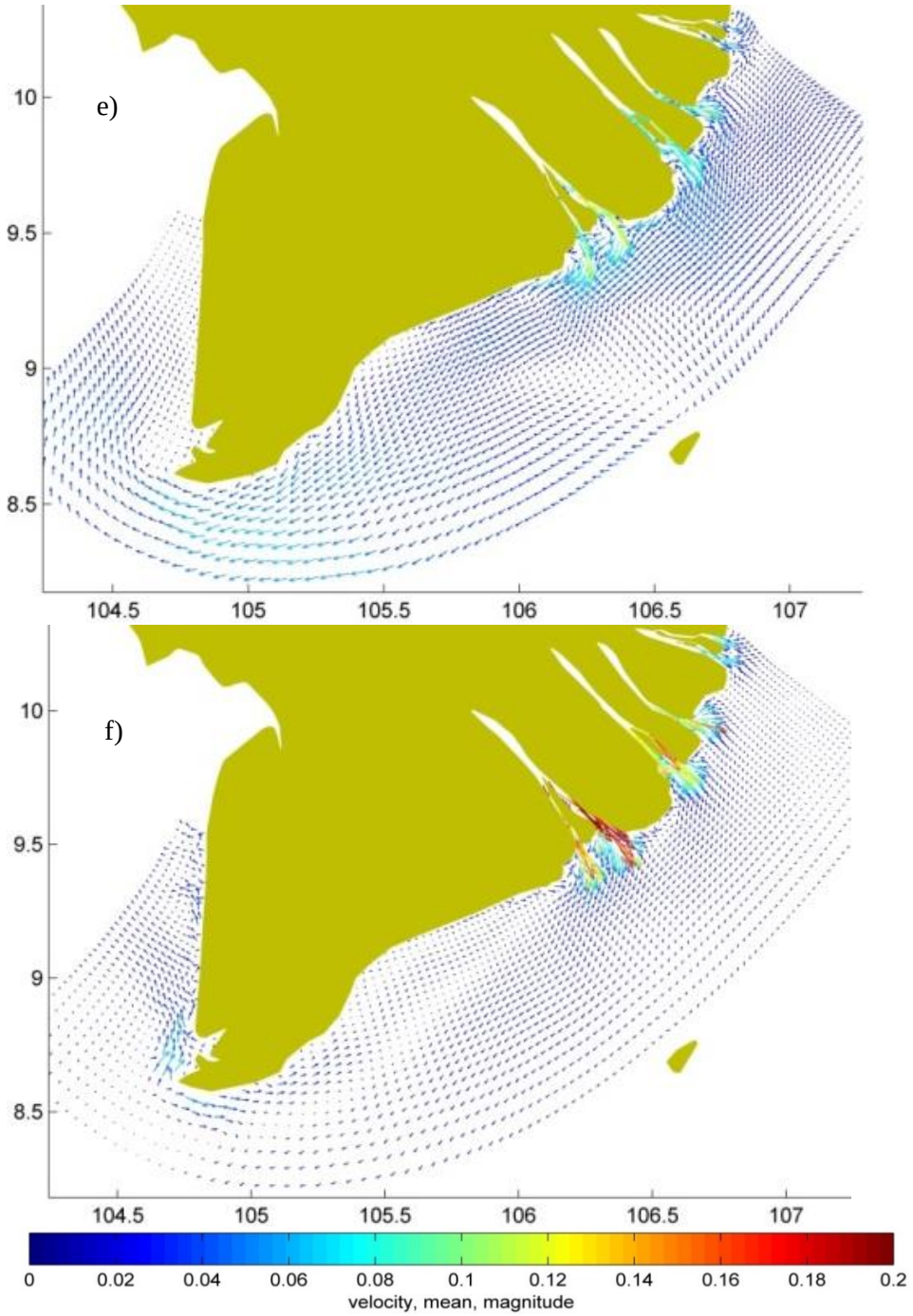

Figure 5.4, continued.

5.3.3 Residual sediment transport patterns

Figure 5.5 shows the Residual Sediment Transport (RST) patterns along the Mekong deltaic coast in the winter and summer monsoon climate. Similar to the residual flow, the RST along the Mekong deltaic coast is influenced strongly by the monsoon climate system. Generally, whereas the sediment transport travels in the south-westward direction during the winter monsoon along the eastern Mekong deltaic coast, it moves in the north and north-eastward direction during the summer monsoon. In the estuarine areas, the sediment transport direction is quite complicated with the large transport along the main inlets of rivers before being deflected into an alongshore direction on the outer edge of the estuaries under the monsoon climate system. Due to the effect of the monsoon climate system, along the eastern Mekong deltaic coast the magnitude of RST in the winter is significantly greater than its magnitude in the summer, except for the estuarine areas owing to the high flow in the Mekong River during this summer season. The study shows that in the winter monsoon strong transports occur up to 8.10^{-5} $m^3/m/s$ in two zones, including the Mekong River mouths as well as adjacent coasts and the eastern coast of Ca mau Province. Meanwhile, high RST only occurs in the estuarine areas during the summer monsoon. On the other hand, the RST is very low along the western coast in both summer and winter season.

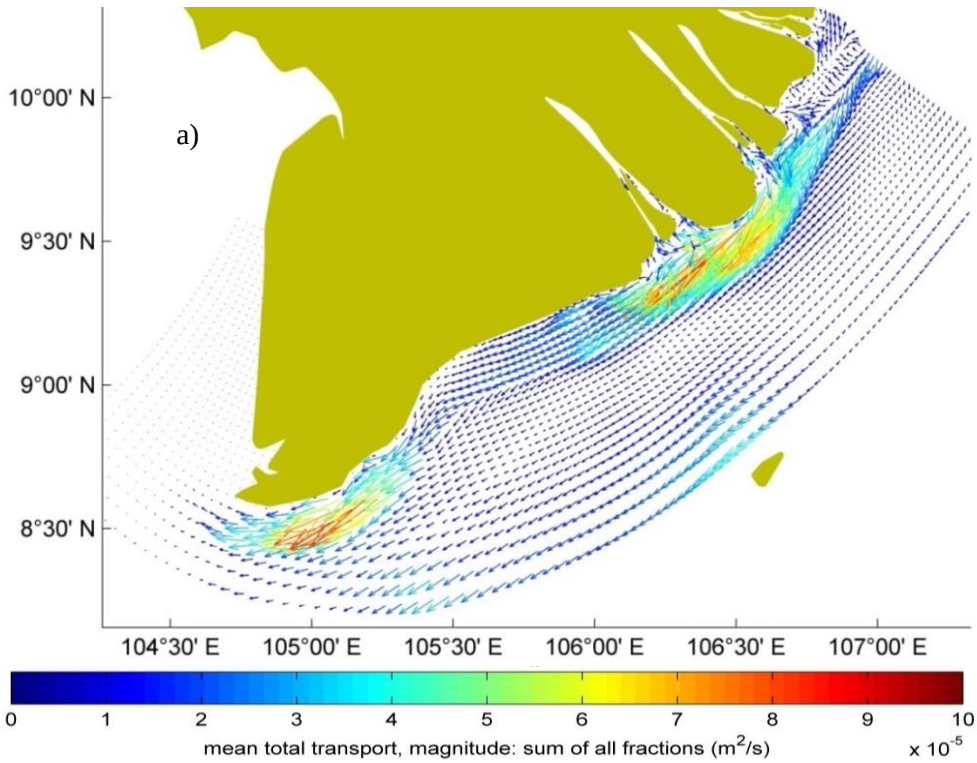

Figure 5.5: Residual sediment transport ($m^3/m/s$) in the winter (a) and summer (b)

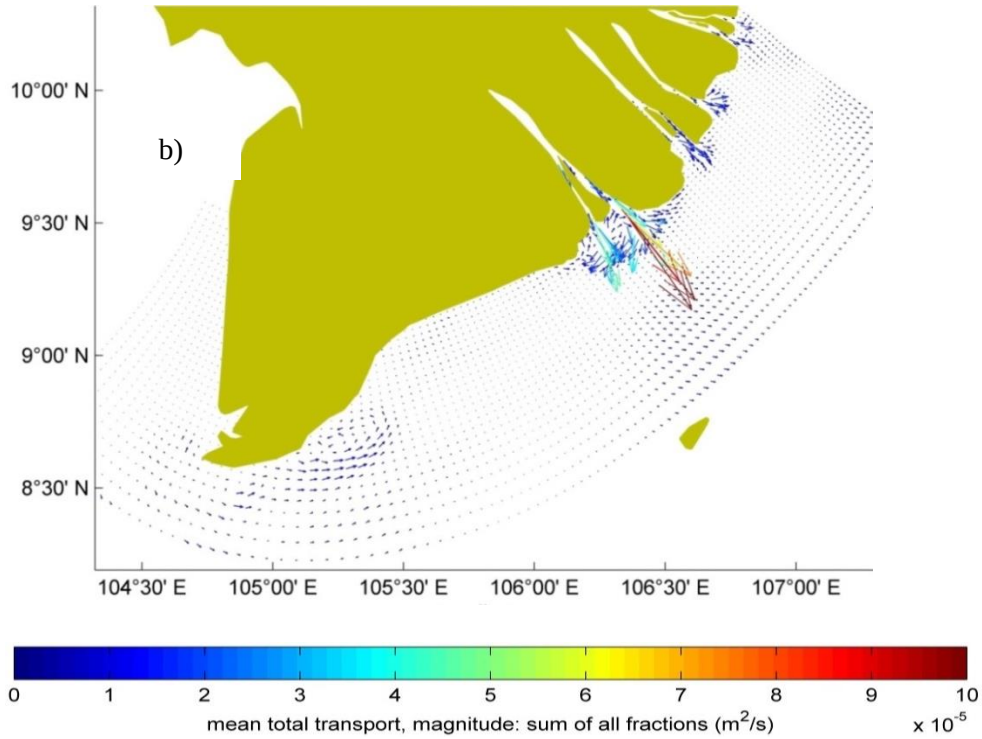

Figure 5.5, continued.

The study also investigates factors of wind, wave and tide controlling the process of RST patterns along the Mekong deltaic coast (Figure 5.6). The results show that while the wind action plays the most important role toward the development of residual flow velocity patterns, wave action significantly influences the RST patterns in both seasons. Tide action can cause the RST in the estuaries and at Camau Cape. In the case of only wave action, the RST in the eastern coast of Camau is less than the RST in the coastal areas of the Mekong River mouths during the winter monsoon case; this result is similar to the study of Phan et al. (2019b). However, when the effect of wind and tide is included, the RST in the eastern coast of Camau increases becoming nearly equivalent to the RST in the coastal areas in the Mekong River mouths. The wind induced currents are mostly insufficient to cause sediment transport in both seasons due to its lower force than its critical shear stress (Figure B.2). However, the role of wind for sediment transport rises when tide induced currents are enough to move and stir bed the sediment (Figure B.2). While the role between wind and tide with respect to sediment transport is complementary during the winter monsoon, their roles are both suppressed during the summer monsoon due to their movement in opposite direction along the eastern coast of Mekong Delta, especially with a high tide induced flow in the eastern coast of Ca mau Province. Finally, the result illustrates a strong wave action dominated RST along Mekong deltaic coast in both seasons, due to the waves producing high sediment stirring and strong wave induced currents.

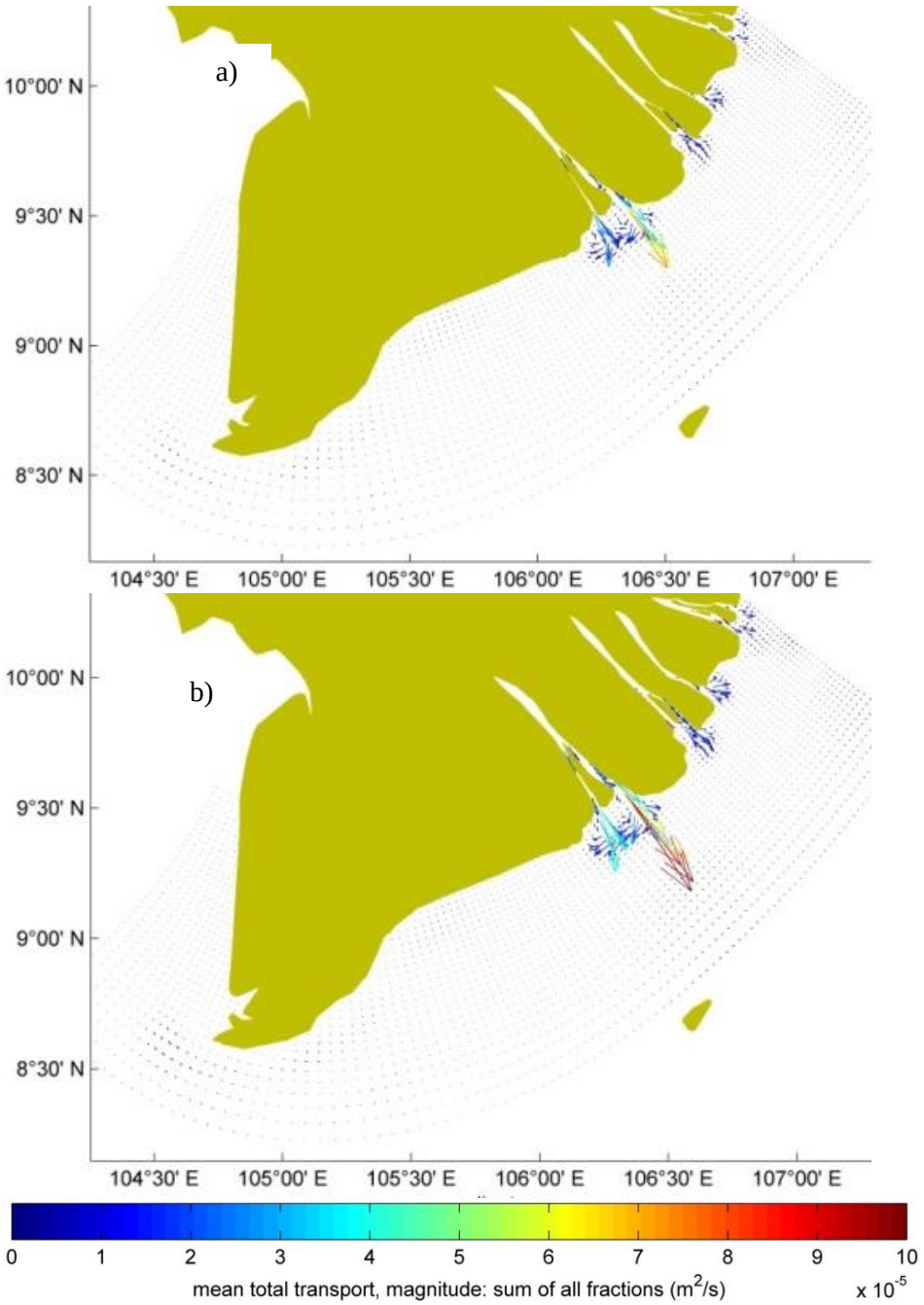

Figure 5.6: Residual sediment transport ($m^3/m/s$) under tide only (a, b), wind only (c, d) and wave only (e, f) effect in the winter and summer, respectively.

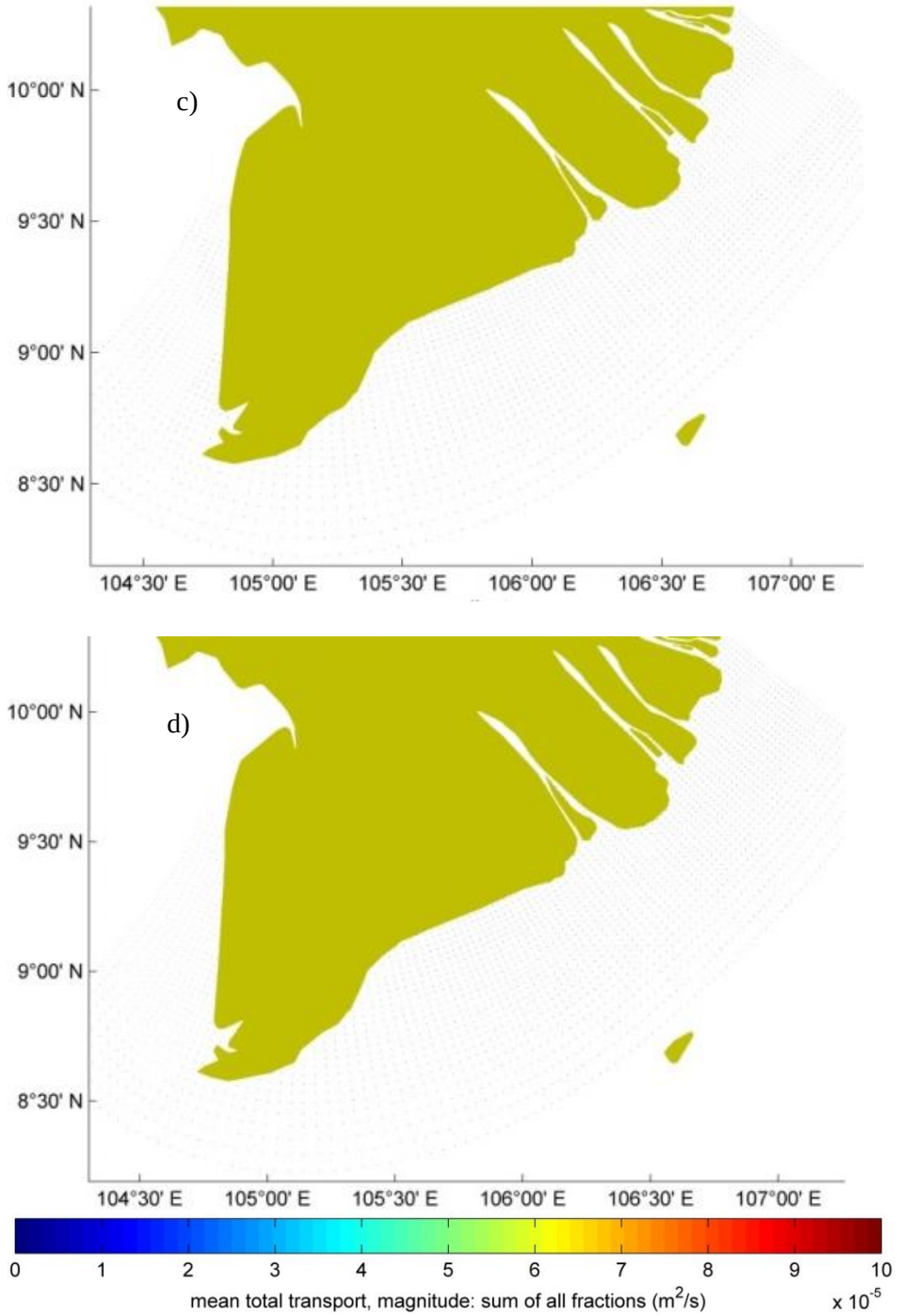

Figure 5.6, continued.

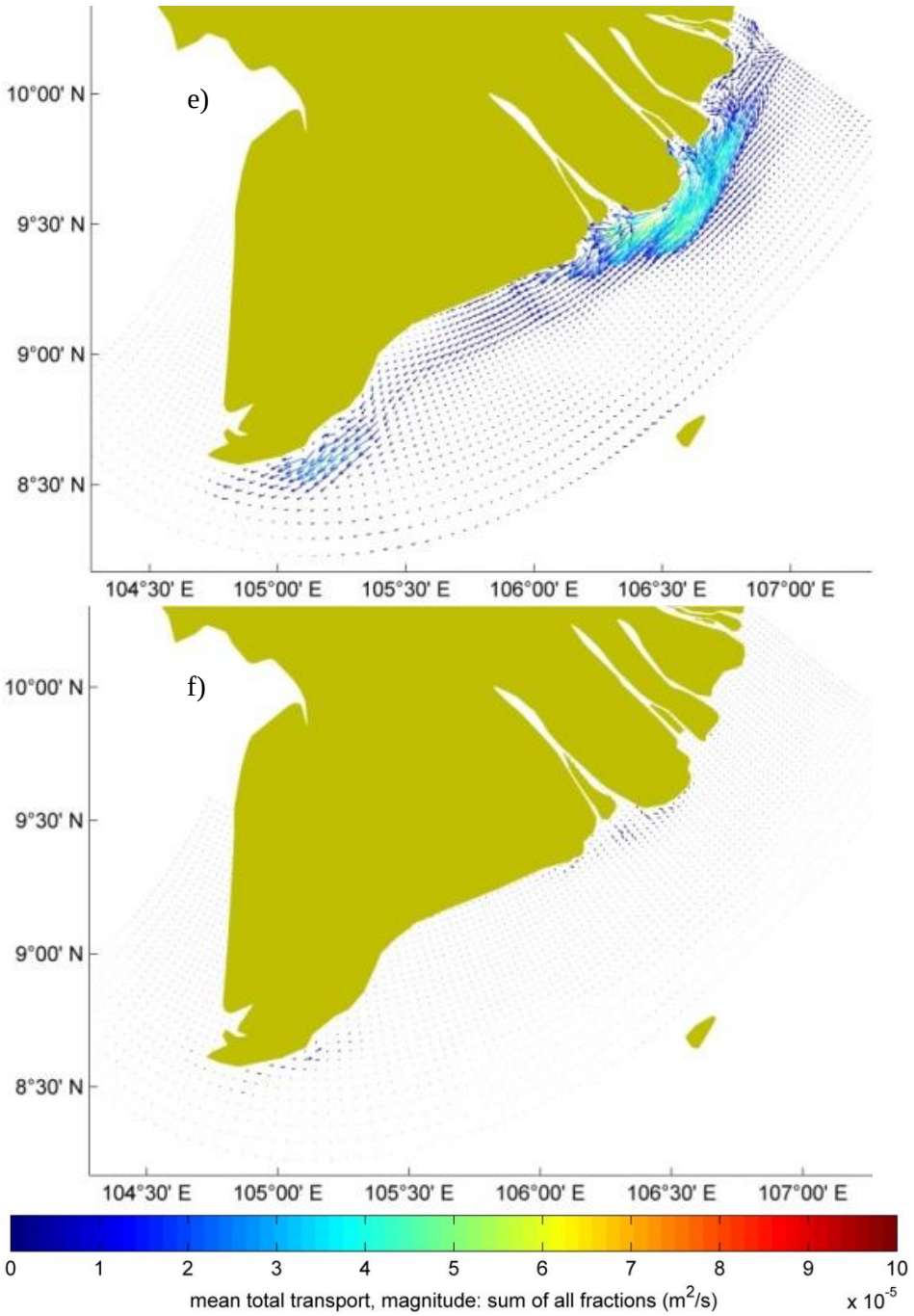

Figure 5.6, continued.

5.3.4 Alongshore sediment budget

In order to understand the morphodynamical process along the Mekong deltaic coast, the alongshore sediment budget is calculated based on sediment coming in and going out between sub-regions through simulated seasonal averaged sediment transports. There is a considerable difference in the magnitude of sediment transport between the summer and winter monsoon period. The mechanism of annual sediment transport and the corresponding morphodynamics along Mekong deltaic coast is dominated strongly by the winter monsoon. The annual sediment input from the Mekong River for Mekong deltaic coast was estimated ranging 45 million to 55 million ton/yr. during 1988 and 2012 (Phan et al., 2017). Floods carrying sediment into the estuaries from the Mekong River occur in the summer monsoon, however most of the sediment deposits in the river mouths due to weak winds and the wave effect in this season. During the winter season, part of the sediment is resuspended and brought in south-westward direction, particularly up to $7x10^{-5}$ $m^3/m/s$ along the coastal area of Tra Vinh Province, owing to strong wind and wave action in the winter monsoon. The value of alongshore sediment flux through the profile 5 in Figure 5.7a and b shows that annually around 11 million ton/yr of sediment moves in south-westward direction. It also means that approximately three-fourth of the fluvial sediments settle down in the estuarine areas. This result of sedimentation in river mouths areas is consistent with an earlier study on the accretion and erosion along Mekong deltaic coast using Remote Sensing technique (Phan et al., 2017).

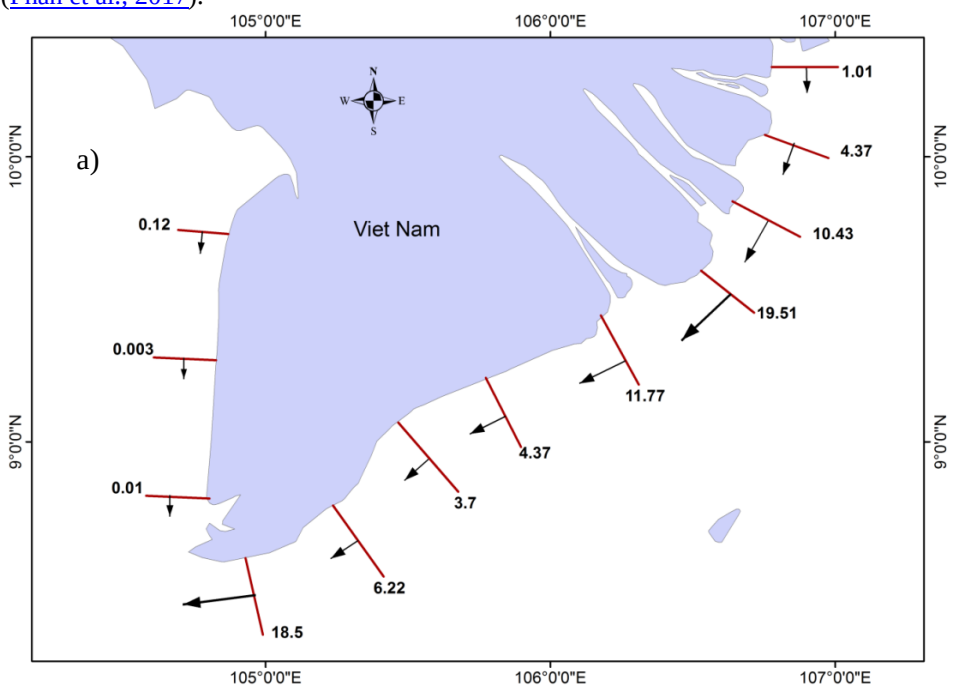

Figure 5.7a, b: Seasonal longshore sediment budget (Mton/yr.) in the winter (a) and summer (b)

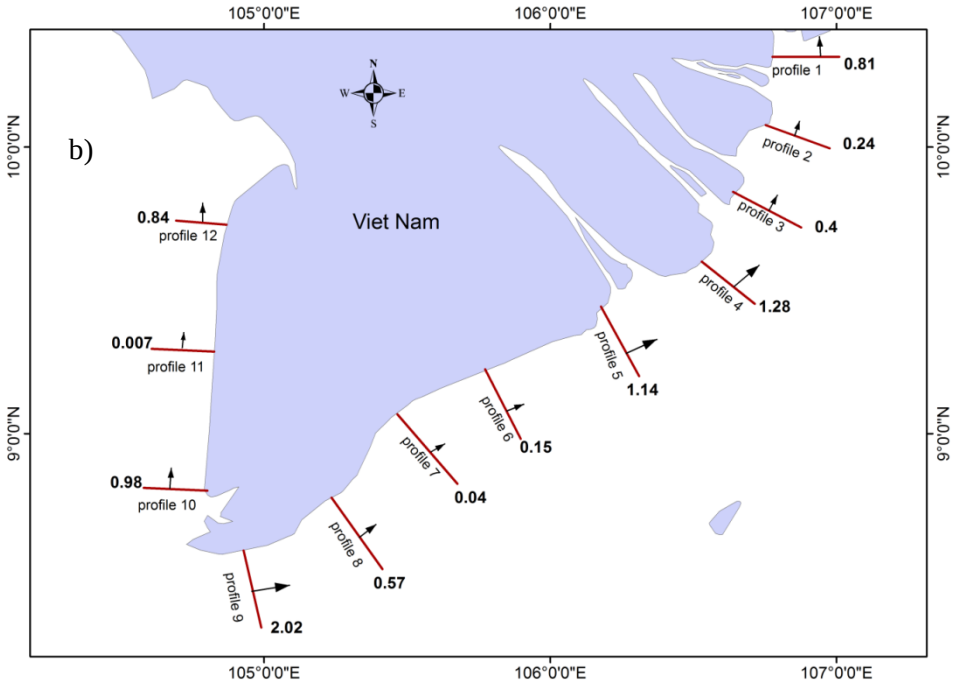

Figure 5.7a, b, continued.

The south-eastern Mekong deltaic coast of, Soc Trang and Bac Lieu Provinces receive roughly 6 Mt/yr and 0.6 Mt/yr of sediment from fluvial sediment of river mouths, respectively. Further south-westward, there is a rapid alongshore sediment transport up to 16 Mt/yr in eastern Ca Mau. Based on the previous analysis in which each factor of wind, wave and tide in relation to sediment transport was included, it can be seen that the mechanism to cause high alongshore sediment transport on the eastern coast of Camau is different from in the Mekong River mouths. While waves play a major role in the alongshore sediment transport off the Mekong River mouths, tide and wind induced currents contribute partly to cause high alongshore sediment transport in the eastern coast of Ca Mau, besides the wave effect. The eastern Camau Province area in between profiles 8 and 9 lost nearly 11 Mt/yr of sediment. The length of this section of coast is approximately 44 km with a proposed closure depth of roughly 6m, hence the average rate of erosion is calculated to result in nearly 27 m/yr. Similarly, the average rate of accretion in the profile 9 and 10 sections is estimated to be roughly 38 m/yr. These results are in accordance with the study on shoreline change using remote sensing (Phan et al., 2017). The sediment transport towards the western Mekong deltaic coast is quite low, approximately 1.0 Mt/yr. through profile 10, due to a weaker effect of wave, wind and tide factors.

5.4 Discussion

The result section showed tide, wind, wave actions control the morphodynamics processes along the Mekong deltaic coast. However, in the recent decades, coastline

retreat has taken place more seriously in the Mekong delta, especially a severe erosion up to 40m/yr in some areas, e.g. eastern coast of Camau province. This section discusses some possible reasons causing this more and more critical erosion phenomenon including the impact of the linking channel and overwash phenomenon toward the erosion in the eastern coast of Camau, the relative sea level rise, coastal squeeze as well as the depletion of fluvial sediment source from Mekong river.

5.4.1 Linking channel and overwash

The average erosion rate in eastern Camau based on coastal processes was calculated above to be 27 m/yr. However, the observed erosion rate is up to over 40 m/yr at the Cua Lon River mouth (Figure 5.8a) creating a concave shoreline. In the previous chapter it was suggested that the Cua Lon river, which connects the East and the West Sea, is able to transport sediment from East to West, creating an additional sediment sink. In order to test this hypothesis, schematised process models were developed including a channel with a depth of 4 m and a width of 500 m, as well as a model without a channel. The schematised bathymetry was smoothed from practical bathymetry and tidal constituents at boundaries were extracted from a previous model. Due to the dominant winter monsoon climate, a constant averaged wind was chosen with a magnitude of 10 m/s and an angle of 75°, and a constant averaged wave height was selected with a magnitude of 2 m and an angle of 75° at the east boundary. Figure 5.8 shows that a high flow velocity and associated sediment transport occurs at the channel mouth in eastern Camau. This is a probable reason for an increased erosion at the coast adjacent to the channel mouth.

The decrease of gradients in the computed net alongshore transport should cause the sedimentation in the profile of 9 section towards Camau headland, however the field and remote sensing observations show a light retreat. The coastal process along Camau cape is similar to the dynamic process of spit, when the coast sharply changes its orientation ending in a curved shape. The sediment source mainly feeds this spit from the erosion of the eastern coast of Camau. The Camau spit in the field is elongating at a very low rate, hence a possible explanation for this situation is the overwash phenomenon from the east sea to the west sea, which is almost like a bay with cross-shore sediment transport. This overwash probably occurs in the Camau spit because of the low land with elevation ranging 0-1m, the numerous channels and the wave effect in north-northeast direction under influence of the summer monsoon climate.

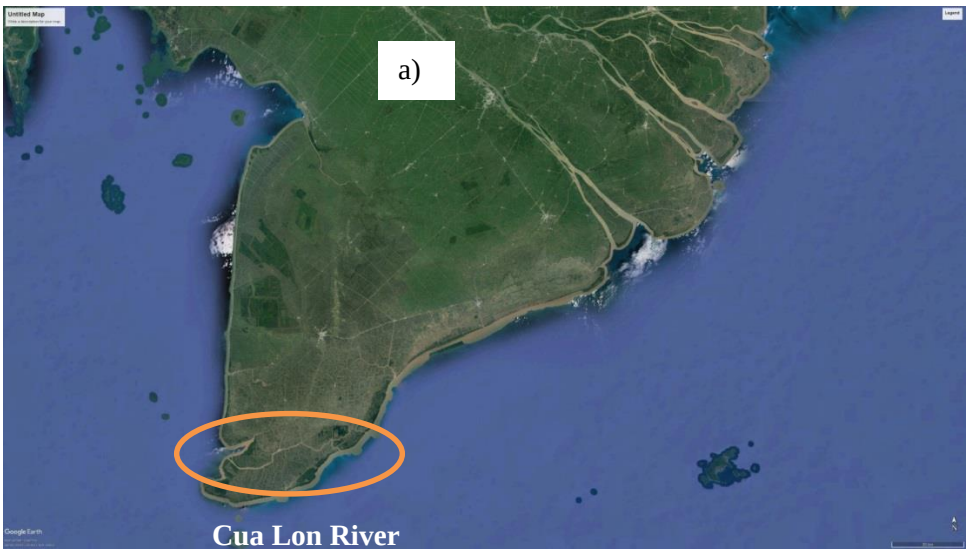
a)
Cua Lon River

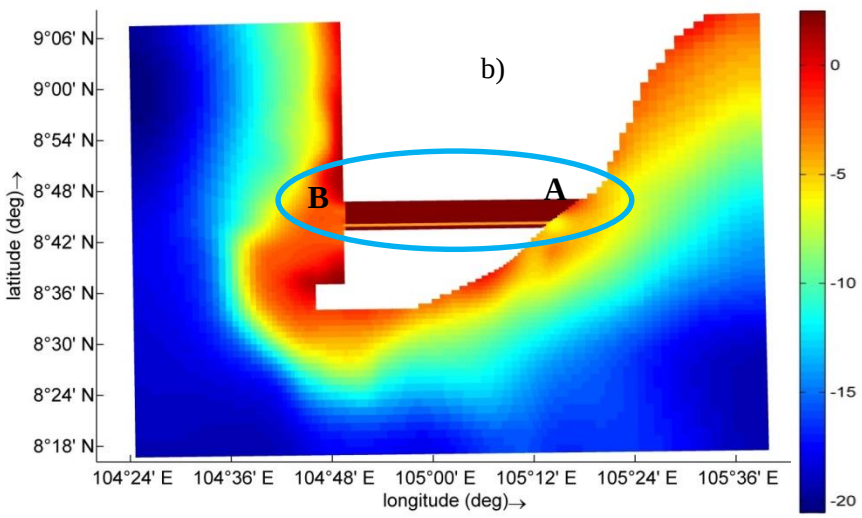
b)
A
B
9°06' N
9°00' N
8°54' N
8°48' N
8°42' N
8°36' N
8°30' N
8°24' N
8°18' N
latitude (deg)→
104°24' E
104°36' E
104°48' E
105°00' E
105°12' E
105°24' E
105°36' E
longitude (deg)→
0
-5
-10
-15
-20

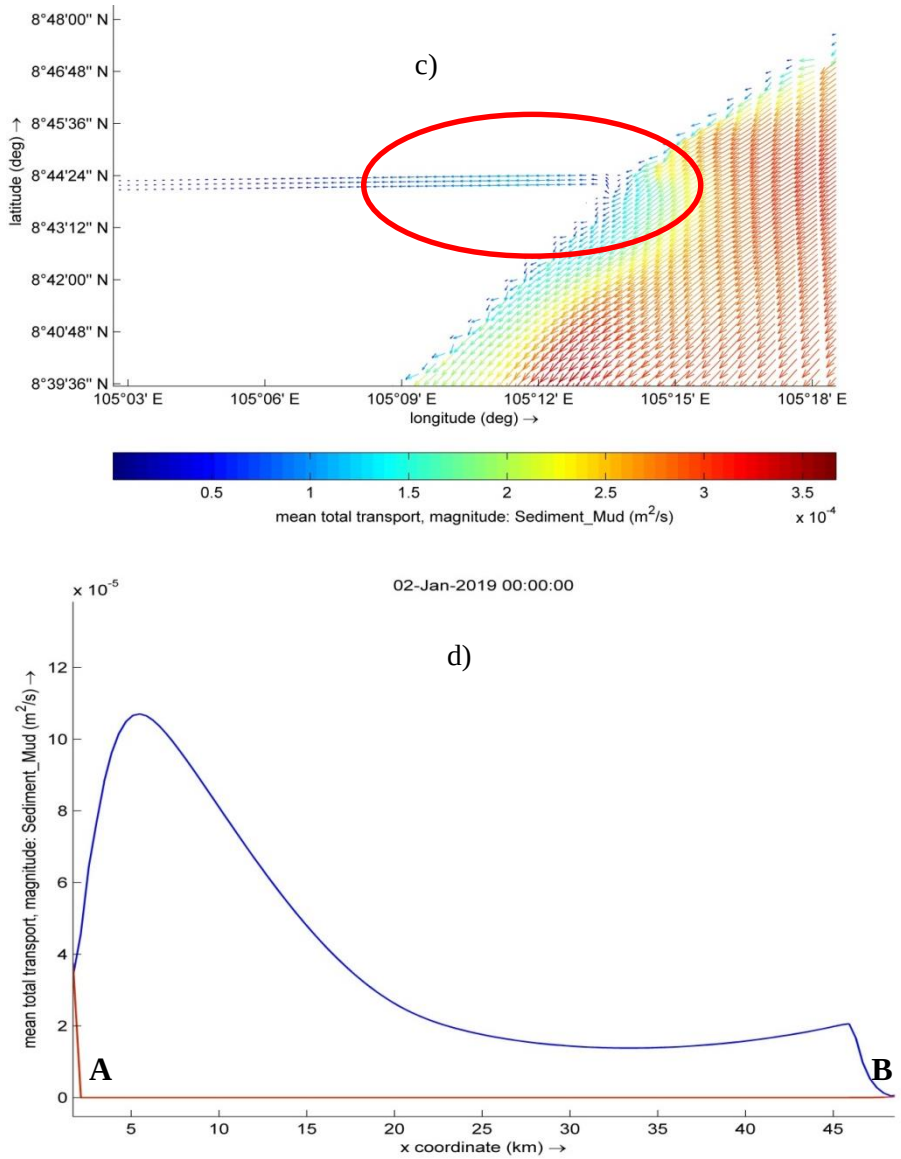

Figure 5.8: Location of Cua Lon river (a), schematised topography (b), residual sediment transports in the horizontal field (c) and along linked channel profile of A-B (d), respectively.

5.4.2 Relative sea level rise and coastal squeeze

Coastal areas of Mekong delta have suffered the severe impact from the sea level rise and the subsidence. The data of Vungtau gauge station from Chapter 2 show that between 1979 and 2007 the HHWL of sea level at this station has risen by 13 cm, e.g. nearly 4.0 mm/year. Besides, rather severe subsidence with an average of 1.6 cm/year is caused

by natural reasons, such as compaction of fresh deltaic deposits, and as a result of human impact, such as groundwater extraction in the Mekong Delta, especially at Ca Mau Peninsula (Erban et al., 2014; Minderhoud et al., 2017). In recent decades the demand for fresh water has significantly risen due to the increase of population and aquaculture. It causes a continuous drawdown of hydraulic heads over the whole delta subsurface and leads to aquifer system compaction. Therefore, with very gentle slope of 1:1000-1:2000, a severe shoreline recession takes place due to a relative sea level rise, i.e. the sum of eustatic sea level rise, natural and human induced subsidence, according to the Bruun rule. This is a probable reason to explain why some coastal areas undergo a light and medium level of erosion ranging 1-10 m/yr., although the sediment transport gradient is levelling and even declining such as coastal areas in Soc Trang, Bac Lieu and western Camau provinces.

An important risk for marine life is loss of habitat due to coastal land claims and relative sea level rise. Coastal land claims often involve construction to protect the land from erosion and/or flooding, and the conversion of mangrove forest to other land cover categories. Relative sea level rise pushes mangroves landward, meaning that the mangrove habitat is squeezed into a narrowing zone where coastal land is claimed and, as a consequence, the phenomenon of coastal mangrove squeeze takes place (Doody., 2004; Doody., 2013). Torio (2013) developed a Coastal Squeeze Index to evaluate the potential of a coastal marsh squeeze and to classify the threatening pressures of various wetlands in the United States and Canada. At present, the coastal Mekong Delta is facing coastal mangrove squeeze by infra-gravity waves and by a sea dike system with a critical width of 140m to maintain a healthy mangrove forest (Phan et al., 2015).

5.4.3 Fluvial sediment source

The sediment flow from the Mekong River is one of several significant elements affecting the morphodynamic process in general as well as the retreat of the Mekong Delta coastline in particular. Measurements of suspended sediment concentration data at Tanchau permanent station show that there is a significant difference among the period of 1988-1995, the period of 1996-2000 and the period of 2001-2012. Between 1988-2012, in the period of 1996-2000 the suspended sediment concentration declined significantly from an average 124 mg/l in period of 1988-1995 to an average 85 mg/l at Tanchau station. In the next periods, there is a slight increase of suspended sediment concentration to 110 mg/l and 115 mg/l in the periods of 2000-2005 and 2005-2012 at Tanchau station. Therefore, the total sediment load of the Mekong River in the Vietnam zone is estimated up to an average ranging from 45 to 55 million ton/year.

Furthermore, combined with Landsat images during flood season, it can be seen easily that the allocated sediment area in the Mekong deltaic coast is estimated at approximately 6000-7000 km^2. According to Linsley et al. (1982), the dry density of most soils varies within the range of 1.1-1.6 g/cm^3, then the amount of the Mekong sediment load supplying for subaqueous delta system is equivalent to a depth average value of 7-8 mm/yr.

Especially, the series of dams built in the upstream area of the Mekong River, Mawan (1993), Dachaoshan (2003), Jinghong (2008), Xiaowan (2013), Nouzhadu (2015) and Xayburi Dam (being implemented), also affect the amount of sediment loads from the Mekong River toward the Mekong deltaic coast. Furthermore, since the U.S. trade embargo was lifted in 1995, a growth in the economy in general and in the construction sector in

particular took place in Vietnam. The Resources and Environment Departments of 7 provinces in the lower Mekong Delta, including Dongthap, Angiang, Bentre, Tiengiang, Travinh, Vinhlong and CanTho provinces, reported an increase in the demand of sand (Fig. 5.10). Sand mining in these provinces aggravated the decrease of sediment loads into the coastal zone. Consequently, the change of the sediment load deposits into the Mekong River influences the morphodynamic process, specifically causing more serious erosion along Mekong deltaic coast. This phenomenon needs to be further clarified in the subsequent research.

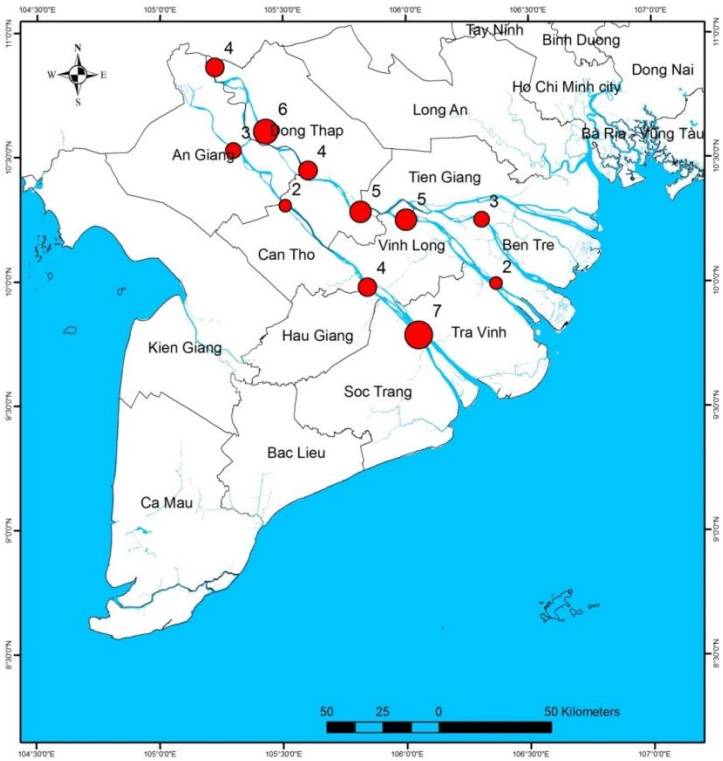

Figure 5.10: Sand mining (Mton/yr) in the Lower Mekong Delta of Vietnam (Bravard et al., 2013)

5.5 Conclusions

The numerical model of Delft3D was employed to provide synoptic estimates for sediment transport rates and gradients and associated sediment budget along the Mekong deltaic coast with factors including wind, wave and tide. The study shows that the distribution of the residual flow patterns is consistent with the monsoon climate system. While the magnitude of residual currents flowing along the eastern coast of the Mekong Delta is higher compared to the currents along the western coast during the winter monsoon, the residual currents in the eastern and western Mekong deltaic coast occurring during the summer monsoon are equivalent. Furthermore, the results demonstrate that the role of wind forcing related to the residual flow patterns is considerably larger than the wave forcing

along the Mekong deltaic shelf. Meanwhile, the tide induced residual currents are low along the Mekong deltaic coast, except along Camau Cape.

Due to the effect of the seasonal monsoon climate system, the scale of residual sediment transport (RST) in the winter is significantly larger than RST along the eastern Mekong deltaic coast in the summer, with the exception of the river mouths due to the flooding in this season. The results reveal that wave action significantly influences the RST patterns in both seasons although its effect for residual currents is negligible. Sediment from the Mekong River is carried to the estuaries by floods and is deposited during the summer monsoon due to a weak wind and wave influence in this season. Roughly one fourth of the fluvial sediments are resuspended and transported in south-westward direction as a result of robust wind and wave effects in the winter monsoon. While waves play a key role in the sediment transport for the Mekong River estuaries, tide and wind induced currents also contribute partly to excessive alongshore sediment transport on the eastern coast of Ca Mau leading to serious erosion in this zone. The amount of sediment moving to the western Mekong deltaic coast is quite low, approximately 1.0 Mt/yr, due to weaker effects of wave, wind and tide factors. However, the inland connecting channel systems and overwash phenomena are suggested to transfer sediment from the eastern coast to the western coast of Camau Province. On the scale of the whole Mekong deltaic coast, the change of the sediment load in the Mekong River as well as relative sea level rise, including eustatic sea level rise, natural and human induced subsidence and mangrove squeeze, are causing serious coastal erosion, especially because of the very gentle profile slopes. This study emphasizes that a better understanding of the mechanism of morphodynamics along the Mekong deltaic coast is obtained by considering the seasonal monsoon climate system.

References

Bakker, S. A., 2017. Coastal prorection in the Mekong Delta. Master thesis. Delft University of Technology.

Bravard, J. P., Goichot, M., Gaillot, S., 2013. Geography of Sand and Gravel Mining in the Lower Mekong River. First Survey and Impact Assessment. 26 | 2013 : octobre 2013/décembre 2013

Correggiari, A., Cattaneo, A., Trincardi, F., 2005. The modern Po Delta system: lobe switching and asymmetric prodelta growth. Marine Geology 222–223, 49–74.

Davis Jr., R.A., Hayes, M.O.,1984.What is a wave-dominated coast. Marine Geology 60: 313-329.

Delta Alliance (2011) Mekong Delta Water Resources Assessment Studies – Vietnam-Netherlands Mekong Delta Masterplan Project. http://wptest.partnersvoorwater.nl/wp-content/uploads/2011/08/WATERRESOURCESfinaldraft.pdf, accessed 17.04.2013.

Doody, J.P., 2004. Coastal squeeze e an historical perspective. Journal of Coastal Conservation 10, 129-138.

Doody, J.P., 2013. Coastal squeeze and managed realignment in southeast England, does it tell us anything about the future? Ocean and Coastal Management 79, 34-41.

Galloway, W.E., 1975. Process framework for describing the morphologic and stratigraphic evolution of deltaic depositional systems. In: Broussard, M.L. (Ed.), Deltas, Models for Exploration. Houston Geol. Soc., Mem. 13, pp. 87–98.

Gerritsen, H., Schrama, E.J.O., Van der Boogaard, H.F.P., 2003. Tidal model validation of the seas of South East Asia using altimeter data and adjoint modelling. Proc. 30th IAHR Congress, Thessaloniki, 2003, vol. D. pp. 239–246.

Hein, H., Hein, B., Pohlmann, T., 2013. Recent sediment dynamics in the region ofMekong water influence. Glob. Planet. Chang. 110, 183–194.https://doi.org/10.1016/j.gloplacha.2013.09.008.

Hordoir, R., Polcher, J., Brun-Cottan, J.-C., Madec, G., 2006. Towards a parametrization of river discharges into ocean general circulation models: a closure through energy conservation. Climate Dynamics 31 (7–8), 891–908.

Jiao, J., 2014. Morphodynamics of Ameland Inlet. Medium-term Delft3D modelling. MSc thesis Delft University of Technology. 10 September 2014.

Latteux, B. (1995). Techniques for long-term morphological simulation under tidal action. Marine Geology, 126(1–4), 129–141. https://doi.org/10.1016/0025-3227(95)00069-B

Le Blanc, R.J., 1975. Significant studies of modern and ancient deltaic sediments. In: Broussard, M.L. (Ed.), Deltas, Models for Exploration. Houston Geol. Soc., pp. 13–85.

Lesser, G.R., Roelvink, J. A., Kester, J. A.T.M., Stelling, G. S.,2004. Development and validation of a three-dimensional morphological model. Coastal Engineering, ISSN: 0378-3839, Vol: 51, Issue: 8, Page: 883-915

Li, N., Cheung, K. F., Stopa, J. E., Hsiao, F., Chen, Y. L., Vega, L., & Cross, P. (2016). Thirty-four years of Hawaii wave hindcast from downscaling of climate forecast system reanalysis. Ocean Modelling, 100, 78–95. https://doi.org/10.1016/j.ocemod.2016.02.001

Linsley, R.K, et al., 1982, Hydrology for Engineers, 3rd ed., McGraw-Hill, New York, N.Y.

LMDCZ., 2018. Lower Mekong Delta Coastal Zones Project. http://lmdcz.siwrr.org.vn/?lang=e

McLachlan, R., Ogston, A., Allison, M., 2017. Implications of tidally varying bed shear stress and intermittent estuarine stratification on fine-sediment dynamics through the Mekong's tidal river to estuarine reach. Cont. Shelf Res. 147, 27–37. http://dx.doi.org/10.1016/j.csr.2017.07.014

Nguyen, L.V., Ta, T.K.O., Tateishi, M., 2000. Late Holocene depositional environments and coastal evolution of the Mekong river delta, Southern Vietnam. Journal of Asian Earth Sciences 18 (4), 427–439.

Orton, G.J., Reading, H.G., 1993. Variability of deltaic processes in terms of sediment supply, with particular emphasis on grain size. Sedimentology 40, 475–512.

Phan, H., Reniers, A., Ye, T., & Stive, M., 2017. Response in the mekong deltaic coast to its changingsediment sources and sinks. In T. Aagaard, R. Deigaard, & D. Fuhrman (Eds.), Proceedings of CoastalDynamics 2017: Helsingør, Denmark (pp. 311-322). [Paper No. 225]

Phan, H. M., Ye, Q., Reniers, A. J. H. M., & Stive, M. J. F., 2019. Tidal wave propagation along The Mekong deltaic coast. Estuarine, Coastal and Shelf Science, 220, 73–98. https://doi.org/10.1016/j.ecss.2019.01.026

Phan Khanh Linh, Van Thiel De Vries, J. S. M., and Stive, M. J. F., 2015. Coastal Mangrove Squeeze in the Mekong Delta. Journal of Coastal Research, 31(2):233–243.

Postma, G., 1990. Depositional architecture and facies of river and fan deltas: a synthesis. In: Colella, A., Prior, D.B. (Eds.), Coarse-Grained Deltas. IAS Spec. Publ., vol. 10, pp. 13–27.

Roberts, H.,1997. Dynamic Changes of the Holocene Mississippi River Delta Plain: The Delta Cycle. Journal of Coastal Research. 13. 605-627.

Roelvink, J.A., 2006. Coastal morphodynamic evolution techniques. Coastal Engineering, 53: 277–287. http://dx.doi.org/10.1016/j.coastaleng.2005.10.015

Ta, T.K.O., Nguyen, V.L., Tateishi, M., Kobayashi, I., Saito, Y., Nakamura, T., 2002a. Sediment facies and Late Holocene progradation of the Mekong River Delta in Ben Tre Province, southern Vietnam: an example of evolution from a tide- dominated to a tide- and wave-dominated delta. Sedimentary Geology 152 (3–4), 313–325.

Ta, T.K.O., Nguyen, V.L., Tateishi, M., Kobayashi, I., Tanabe, S., Saito, Y., 2002b. Holocene delta evolution and sediment discharge of the Mekong River, southern Vietnam. Quaternary Science Reviews 21 (16–17), 1807–1819.

Torio, D. D. and Chmura, G. L. (2014) Assessing Coastal Squeeze of Tidal Wetlands. Journal of Coastal Research: Volume 29, Issue 5: pp. 1049 – 1061.

Unverricht, D.,Szczucinski, W., Stattegger, K., Jagodzinski, R., Le, X.T., Kwong, L.L.W.,2013. Modern sedimentation and morphology of the subaqueous Mekong Delta, Southern Vietnam. Global and Planetary Change 110, 223-235.

Unverricht, D., Nguyen, T.C., Heinrich, C., Szczucinski, W., Lahajnar, N., Stattegger, K., 2014. Journal of Asian Earth Sciences 79, 509-519.

Southern Institute of Water Resources Research (SIWRR)., 2010. Project for measurements of bathymetry, hydrodynamics in estuaries and coastal zone of Mekong Delta from 2009 to 2010. http://www.siwrr.org.vn/?id=nckh5 (in Vietnamese)

Stephens, J.D., Allison, M.A., Leonardo, D.R., Di Weathers, H.D., Ogston, A.S., McLachlan, R.L., Xing, F., Meselhe, E.A., 2017. Sand dynamics in the Mekong River channel and export to the coastal ocean. Cont. Shelf Res. 147, 38–50. http://dx.doi.org/10.1016/ j.csr.2017.08.004.

Xue, Z., Liu, J. P., Ge, Q., 2010. Changes in hydrology and sediment delivery of the Mekong River in the last 50 years: connection to damming, monsoon, and ENSO. Earth Surf. Proccess. Landforms 36, 296-308.

Xue, Z., He, R., Liu, J. P., Warner, J. C., 2012. Modelling transport and deposition of the Mekong river sediment. Continental Shelf research 37, 66-78.

Weise, B.R., 1980. Wave-dominated deltaic systems of the Upper Cretaceous San Miguel Formation, Maverick Basin, South Texas. Report of Investigations107, Texas Bureau of Economic Geology, Austin, Texas, 39 pp.

Wolanski, E., Huan, N.N., Dao, L.T., Nhan, N.H., Thuy, N.N., 1996. Fine-sediment dynamics in the Mekong River estuary, Viet Nam. Estuar. Coast. Shelf Sci. 43, 565–582.

Wolanski, E.,Nhan, N.H., Spagnol, S., 1998. Sediment dynamics during low flow conditions in the Mekong River estuary, Vietnam. Journal of Coastal ResearchVolume 14, Issue 2, Spring 1998, Pages 472-482

Zieger, S., Babanin, A. V., Erick Rogers, W., & Young, I. R. (2015). Observation-based source terms in the third-generation wave model WAVEWATCH. Ocean Modelling, 96, 2–25. https://doi.org/10.1016/j.ocemod.2015.07.014

6

Conclusions and Recommendations

6.1 Conclusions

The main purpose of this thesis is to understand the tide-wind-wave induced hydrodynamics, sediment dynamics and seasonal morphodynamics along the Mekong deltaic coast, specifically in the context of its shoreline and land cover changes. The four main objectives were therefore to investigate:

1. The shoreline and coastal land cover evolution of the Mekong Delta,
2. The tidal wave characteristic along the Mekong deltaic coast,
3. The wave climate and bulk longshore sediment transport along the Mekong deltaic coast,
4. The seasonal morphodynamics of Mekong deltaic coast.

These objectives were achieved using an integrated approach including a theoretical analysis, Remote Sensing techniques, GIS and complex process-based models. In this chapter, the main findings are summarised.

6.1.1 Shoreline and coastal land cover evolution of the Mekong Delta

Detailed spatiotemporal dynamic analysis from the extracted shoreline change of Mekong Delta resulted in the classification of the Mekong deltaic coast into three distinctive areas: the sedimentation in the Mekong river mouths area, the erosion in the south-eastern Mekong deltaic coastal area and the rather stable western coastal area of the Mekong Delta. Generally, sedimentation is still prevailing in most of the Mekong deltaic coast with an average annual accretion of 1.2 km^2. In the period of 1973 to 2015, a net land gain of by average 1.3 km^2/yr. occurred in the Mekong river mouths, with the lowest value of net gain in land at nearly 0.5 km^2/yr. in the period of 2000-2005. The erosion dominated the south-eastern coast with an average net land loss rate of 1.6 km^2/yr., especially in several eastern areas of Ca Mau Province, with an erosion rate up to 40 m/yr. Meanwhile, the net land gain during 43 years was 1.1 km^2/yr along the western coast. This study indicates a fairly close relationship between the shoreline changes in the Mekong deltaic coast itself and the sediment load in the Mekong River. There was a relatively large difference of the coastline change rate among the periods of 1973-1990, 1990-2005 and 2005-present, of which the erosion phenomenon in the period of 1990-2005 was the most serious situation.

Besides, this study showed an in-depth picture of long-term dynamics of mangroves and other types of land cover in the coastal Mekong Delta in Vietnam. The results revealed that a significant decline of land cover, amounting to half the mangrove extent, took place over 43 years, from 185,800 hectares in 1973 to 95,960 hectares in 2015. However, the mangrove extent, dropping to a minimum of 89,650 ha in 2010, also showed a bright signal as the mangrove area increased in the period of 2010-2015, after restoration projects were carried out to limit coastal erosion and loss of mangrove forest. Meanwhile, an outburst of aquaculture took place, initially with only an area of few hectares in 1973, growing to 295,320 ha in 2015 due to the economic benefits of this farming type. Aquaculture is one of the key reasons leading to the critical decline of the mangrove area in the Mekong Delta, specifically aquaculture taking over approximately 2170 ha/yr of mangrove area in the recent 43 years. In this study the loss of mangrove areas in the Mekong Delta due to coastal erosion, viz. a mean loss of over 400 ha/yr, is also quantified.

6.1.2 Tidal wave characteristics along the Mekong deltaic coast

The results pointed out that the semidiurnal and diurnal tides spread in the South China Sea primarily through the Luzon Strait. Meanwhile a part of it moves to the Gulf of Tonkin, mostly continuing to flow in south-western direction. After the tidal wave reaches the Sunda Shelf edge, one turns into the Gulf of Thailand, while another part spreads southwards to the Sunda Shelf end and the Java Sea.

This study reveals that strong tidal current ellipses of the M2 tide occur on the eastern coast of Mekong Delta, while weak currents take place on the western coast and the radial tidal currents appear close to the southern Mekong river mouths. A series of numerical, geometrically schematised experiments were performed to find the mechanism that causes this radial tidal current system. From the result of these experiments, it is assumed that convex hydraulic gradients of tidal amplitude, as a result of basin geometry and depth varying topography, lead to the pattern of the radial tidal current system.

This study shows that the tidal induced residual currents, increasing southeastward of the shallow coastal region of Mekong Delta, appear the greatest along the Camau Cape amounting to approximately 10-15cm/s. Thus, an improved geographical distribution map of tidal characteristics in the entire SCS was established. Furthermore, this work also indicates that the tidal incident waves from the Andaman and Flores Islands' open boundaries weakly affect the tidal wave system in the coastal Mekong region, whereas the tidal wave from the Celebes Islands open boundary has a more important role. Therefore, the tidal open boundary at Celebes should not be ignored in reproducing the tidal wave propagation in the South China Sea in general and in the Mekong Deltaic Coast in particular.

Using approaches of Green's law, the formula of Clarke and Battisti and the theory of standing wave, this study proves that the large amplified M_2 semidiurnal amplitude leads to a prevailing mixed semidiurnal tide in the eastern Mekong deltaic shelf, not only caused by the shoaling effect, the oscillation resonance phenomenon on this continental shelf, but also by the position on the anti-node line of standing wave. This result explains the reason why, while both the South China Sea and the Gulf of Thailand are dominated by diurnal tides, semidiurnal tides take over in the eastern MDC, which is surrounded by those two seas.

The results show that atmospheric forcing in the monsoon climate could produce dampened or intensified tides along the MDC. The wind monsoon climate has a relatively high impact on the M_2 semidiurnal tidal system in the eastern MDC, while the monsoon climate manipulates the K_1 diurnal tide in the western region of the Mekong Delta. Moreover, based on results of this study, it is proposed that the tide generating force needs to be taken into account for a precise model simulation depending on the geographical region of interest.

6.1.3 Seasonal wave climate and bulk longshore sediment transport

Wave field evolution is significantly manipulated by the wind monsoon climate in the Mekong deltaic shelf. Higher wave heights are found in the northeast area of the Mekong deltaic shelf and decrease to the southwest as well as to the western coast of the Mekong Delta in the winter monsoon. Contrary to the winter monsoon, significant wave heights on the western shelf are mostly higher than the wave height on the eastern coast during the summer monsoon. While the wind fields during the winter monsoon just have

an effect on wave fields on the eastern coast, the wind system during the summer monsoon influences the eastern and western coasts together.

The study reveals that once the waves move closer to the Mekong deltaic coast, the energy spectra of the wind and swell sea peaks decrease, owing to the effect of dissipation. Also, the rate of the reduction of the wave energy at lower frequencies of swell is more considerable than that at higher wave frequencies, because the waves with a lower frequency feel the bottom more strongly. The depth-induced dissipation of waves is realized along the northeast of the Mekong deltaic shelf. While the large dissipation of wave breaking occurs in the estuarine areas during the winter monsoon, great dissipation happens along the western Camau Cape during the summer monsoon.

Like the wave field evolution, also owing to the effect of the wind monsoon climate on the Mekong deltaic shelf, the annual net LST gradients along the eastern coast are directed by the pattern of the winter, while the annual net LST gradients in the western region are dominated by the summer pattern. The study points out that the imbalance in the seasonal LST results in a similar pattern of the retreat and accretion phenomenon in the coastal areas of the eastern estuarine zones as detected in satellite images. Additionally, the study shows that potential LST gradients in the estuarine areas are higher than LSR gradients on the south-eastern coast, although shoreline retreat in the south-eastern region actually occurs more seriously. Therefore, other processes are most likely controlling the LST along the Mekong deltaic coast besides wave action.

6.1.4 Seasonal morphodynamics

The study calculated the sediment transport and the sediment budget along the Mekong deltaic coast with physical forcings taking into account wind, wave and tide. The study demonstrates that the distribution of the residual flow patterns is associated with the monsoon climate system. While the residual currents' velocity in the eastern and western Mekong deltaic coast occurring during the period of the summer monsoon are rather equivalent, the magnitude of residual currents' flow along the eastern coast of the Mekong Delta is higher compared to the western coast during the winter monsoon. Also, the wind forcing, affecting the residual flow patterns, is more significant than the wave forcing in the Mekong deltaic shelf. Meanwhile, the tide induced residual currents are really low along the Mekong deltaic coast, excluding the Mekong river mouths and Camau Cape.

Under the effect of the monsoon climate system, the level of the residual sediment transport in the summer is notably smaller than the residual sediment transport in the winter along the eastern Mekong deltaic coast, excepting river mouths areas by reason of the impact of flood from Mekong river in this summer season. The results show that the incoming wave induces significant residual sediment transport patterns in both seasons, especially on the eastern coast, although its force to residual currents is minor. Sediment is transported to the estuaries by the floods from the Mekong river and drops in this area during the summer monsoon due to weak winds and wave influences in this season. Approximately one fourth of these fluvial sediments are resuspended and delivered in south-westward direction as a result of a strong wind and wave effect in the winter monsoon. Whereas waves have a crucial role in the sediment transport off the Mekong river estuaries, tide and wind induced currents also partially cause the development of a high alongshore sediment transport on the eastern coast of Ca Mau leading to a severe coastline retreat in this region. The sediment that travels to the western Mekong deltaic

coast is moderately low (nearly 1.0 Mt/yr) which can be attributed to a weaker influence of wave, wind and tide dynamics. The results from the numerical modelling are consistent with the results of shoreline evolution extracted from satellite images.

Besides, the connected channel and overwash occurrence are assumed as the factors to transport sediment from the eastern coast to western coast of Ca Mau Province. Additionally, the transformation of the sediment flow from the Mekong River, the relative sea level rise including the eustatic sea level rise and the natural and human induced subsidence, as well as mangrove squeeze trigger the high-level risk of coastline retreat.

6.2 Recommendations

The study on tidal wave characteristics along the Mekong deltaic shelf found that the radial tidal currents occur on the south-eastern coast of the Mekong Delta, however it does not create radial sandy ridges, like at the Jiangsu coast of China. The probable reasons are that the tidal range at the Jiangsu coast is quite large with up to 8 meter in the springtide compared with 3.5 meter at the Mekong deltaic coast and leads to high tidal currents speed as well as massive sediment source into this Jiangsu coast. However, both areas have the same shoreline of a concave geographic shape and a convex bathymetry. Therefore, the important role of these radial tidal currents towards the morphodynamics of Mekong deltaic coast needs to be quantified.

The effects of salinity, temperature and wind-induced density stratification are important for the dynamics of coastal processes. This study employed a 2DH barotropic Delft3D modelling method to simulate tides and waves as well as morphodynamical processes. Especially, for the large Mekong river mouths system, non-linear stratification caused by salinity will possibly affect the sediment transport rates as well as the morphodynamics of the estuarine system. Normally, the sum of the barotropic and baroclinic pressure leads to an offshore force on the near-surface layers and an onshore force on the near-bed layer. Therefore, a three- dimensional, baroclinic numerical model is necessary to fully simulate the coastal process in the Mekong Delta.

Currently, the study on factors affecting the coastal morphology of the Mekong Delta nearly exclusively focused on currents, wave from the sea and rarely considered the driving forces from the upstream of the Mekong Delta, such as flow discharge and sediment load. There are probably significant changes in the coastal morphology from the influences of human interventions by dams, diking, embankment and sand mining. Lu and Siew (2006) studied the impact of the Manwan dam, which was the first dam in operation, on the water discharge and the sediment flux in the Lower Mekong River. The authors stated that after the construction of the Manwan dam, the mean monthly sediment concentration has decreased at all stations of the Mekong estuaries, especially a significant decrease at Can Tho city. Therefore, the study on above effects from upstream to the evolution of the Mekong deltaic coast also needs clarification. Furthermore, based on the collected data from 1979 to 2007 at Vungtau gauge station, the sea level rise occurs at nearly 4 mm/yr. as well as subsidence being triggered by natural reasons, as the compaction of young deltaic deposits and human impact as groundwater withdrawal in Mekong Delta is occurring at a rather serious rate of 1.6 cm/year. Erosion up to 10 m/yr. has been taking place at the coastal areas of Soc Trang, Bac Lieu Province as well western Camau, even though the magnitude

as well as the gradient of sediment transport is rather insignificant. Whether relative sea level rise causes this retreat phenomenon is an interesting topic to for furher study.

The hydrodynamic processes of the coastal Mekong Delta are also affected by interference of the average discharge of 1100 m^3/s Saigon-Dongnai river basin via the Soairap mouth. The subaqueous area is supplied sediment discharge of approximately 5 million tons per year. The northern coastal Mekong Delta zone contiguous Soairap mouth not only receives sediment from the Mekong River but also from the Saigon-Dongnai River. Therefore, it is necessary to quantify the contribution of the sediment transport from the Saigon-Dongnai River source to the sediment distribution in the coastal Mekong Delta.

Furthermore, there are multiple flood drainage systems built in the Long Xuyen Quadrangle to transport water from the lower Mekong River to West Sea in order to reduce the flood hazard in the downstream territory. Therefore, the study would be more efficient if the sediment sources from these canals were taken into account for the whole of the Mekong deltaic coast.

Camau Cape is the area where the mechanism of morphodynamics is of most interest, of high impact and in dire need to be understood. It is a transition zone between a high range of the semidiurnal tide in the east and a small range of the diurnal tide in the west, leading to high tidal currents of up to 1 m/s, enough to stir the bed sediment. Furthermore, this area is influenced by strong wind and wave actions in both seasonal climate systems, the winter and summer monsoon, with especially strong winds in cross-shore direction during the summer season. Since the elevation of this land is very low, ranging 0 – 1m, it is necessary to investigate whether these factors could cause a destructive overwash phenomenon.

A

Validation and Results of Tidal Wave Characteristic

Table A.1: Comparison of the harmonic constant between observed and calculated results for four primary constituents

No	Station name	LONG	LAT	S2						
				Observation		Calculation		dH	dG	VD
				Amp (cm)	Phase (deg.)	Amp (cm)	Phase (deg.)	(cm)	(deg.)	(cm)
1	YU LIN KAN	109.606	18.19	6.8	335.2	10.9	326.6	-4.1	8.6	4.3
2	PAK HOI	109.145	21.529	10.6	353	14.7	344.1	-4.1	8.9	4.6
3	DO SON	106.808	20.667	4.3	136	9.9	139.9	-5.6	-3.9	5.6
4	HON NE	106.006	19.918	9.8	142	19.2	137.3	-9.4	4.7	9.5
5	HON NIEU	105.777	18.81	10	114	19.3	118.5	-9.3	-4.5	9.4
6	QUANG KHE	106.464	17.671	5.2	91	7.4	97.3	-2.2	-6.3	2.3
7	DA NANG	108.214	16.127	5.8	10	8.2	5	-2.4	5	2.4
8	QUI NHON	109.212	13.732	7	7	9.9	352.5	-2.9	14.5	3.6
9	CAM RANH	109.159	11.858	8.5	15	10.7	357.2	-2.2	17.8	3.7
10	PHU QUY	108.967	10.497	7.8	36.8	11.2	29.3	-3.4	7.5	3.7
11	KE GA	107.969	10.689	15.8	68	17.4	59.9	-1.6	8.1	2.8
12	VUNG TAU	107.086	10.305	30.7	111	38.5	120.2	-7.8	-9.2	9.5
13	CON DAO	106.593	8.656	28	142	29.1	143	-1.1	-1	1.2
14	MY THANH	106.193	9.432	37	141	41.1	146.7	-4.1	-5.7	5.7
15	GANH HAO	105.458	9.037	39	177	47.5	181.7	-8.5	-4.7	9.2
16	CA MAU	104.78	8.58	8	171	19.3	179	-11.3	-8	11.5
17	TAMMASU	104.796	9.006	2.3	186	6.4	178.1	-4.1	7.9	4.1
18	HA TIEN	104.494	10.35	1.9	214	2.2	218.8	-0.3	-4.8	0.3
19	THO CHU	103.444	9.272	2	54	1.9	61.6	0.1	-7.6	0.3
20	KOMPONG SOAM	103.483	10.62	5.5	93	3.9	99.1	1.6	-6.1	1.7

21	SATTAHIP	100.859	12.622	12.2	225	5	231	7.2	-6	7.3
22	KOH HLAK	99.245	10.427	1.3	217	2.5	205.9	-1.2	11.1	1.3
23	PATTANI	101.325	6.943	4.5	350	8.2	1.2	-3.7	11.2	3.9
24	TELOK TEKEK	104.144	2.785	18.3	327	20.8	304.9	-2.5	22.1	7.9
25	TEBON ISLET	107.118	0.582	3	171.8	8.2	182.4	-5.2	-10.6	5.3
26	SELAT PENINTING	106.263	3.225	6	276	2.5	277.8	3.5	-1.8	3.5
27	POELOE LAOET	107.992	4.741	4	86	8.2	83.9	-4.2	2.1	4.2
28	PALOH	109.275	1.807	25	156.5	31.5	144.7	-6.5	11.8	8.7
29	TELOK PLAN	113.085	3.264	8	26	14.7	37.4	-6.7	-11.4	7.1
30	PALAU MANGALUM	115.592	6.198	10.4	358	12.7	349.6	-2.3	8.4	2.9
31	ULUGAU BAY	118.77	10.104	8	345	15	329.2	-7	15.8	7.6
32	SANTA CRUZ	119.948	15.739	1.7	323	6.1	331.6	-4.4	-8.6	4.5
33	NAGABUNGAN	120.56	18.498	5.8	214.9	2.6	201.2	3.2	13.7	3.4
34	KAO-HSIUNG	120.252	22.618	7.9	81.9	2	92.8	5.9	-10.9	6
35	CHAUAN BAY	117.292	23.609	28	80.4	39.3	84.2	-11.3	-3.8	11.5
36	HONGKONG	114.207	22.249	16.2	298.9	13.4	295.1	2.8	3.8	3
37	NAOZHOU DAO	110.589	20.927	34.9	23	40.4	31.3	-5.5	-8.3	7.7
38	NORTHDANGERREEF	114.31	11.469	10	347	15.2	341.3	-5.2	5.7	5.3
39	SCARBOROUGHSHOA	117.765	15.137	10	340	6.9	331.1	3.1	8.9	3.4
40	LES PARACELS	111.617	16.557	7.7	353	8.3	348.3	-0.6	4.7	0.9
41	PRATASREEF	116.716	20.678	6	267.1	2.7	284.6	3.3	-17.5	3.5
Average SVD										5
RMSE								5.2	9.5	

No	Station name	LONG	LAT	K1						
				Observation		Calculation		dH	dG	VD
				Amp (cm)	Phase (deg.)	Amp (cm)	Phase (deg.)	(cm)	(deg.)	(cm)
1	YU LIN KAN	109.606	18.19	28.5	310	23.4	316.1	5.1	-6.1	5.8
2	PAK HOI	109.145	21.529	86.2	102	79.6	105.2	6.6	-3.2	8.1
3	DO SON	106.808	20.667	67.5	106	59.8	112.5	7.7	-6.5	10.6
4	HON NE	106.006	19.918	54.4	107	49.8	113.7	4.6	-6.7	7.6
5	HON NIEU	105.777	18.81	43.6	113	36.8	122.4	6.8	-9.4	9.4
6	QUANG KHE	106.464	17.671	21.5	111	12.4	134.2	9.1	-23.2	11.2
7	DA NANG	108.214	16.127	19.5	305.7	21.3	304.6	-1.8	1.1	1.8
8	QUI NHON	109.212	13.732	32.9	316.2	22.9	312.3	10	3.9	10.2
9	CAM RANH	109.159	11.858	34.5	307.7	27.7	314.7	6.8	-7	7.8
10	PHU QUY	108.967	10.497	37	305.6	30.2	312.4	6.8	-6.8	7.9
11	KE GA	107.969	10.689	45.3	303	42.8	308.7	2.5	-5.7	5
12	VUNG TAU	107.086	10.305	59.5	327.7	55.2	331.9	4.3	-4.2	6
13	CON DAO	106.593	8.656	59	333.7	52	340.5	7	-6.8	9.6
14	MY THANH	106.193	9.432	64	342	58.2	345.1	5.8	-3.1	6.7
15	GANH HAO	105.458	9.037	67	3	70.1	11.4	-3.1	-8.4	10.5
16	CA MAU	104.78	8.58	33	23	41	31.7	-8	-8.7	9.7
17	TAMMASU	104.796	9.006	18	107	25.8	116	-7.8	-9	8.5
18	HA TIEN	104.494	10.35	26.2	126.7	29.7	135.3	-3.5	-8.6	5.4
19	THO CHU	103.444	9.272	17	89	13.4	91.4	3.6	-2.4	3.6
20	KOMPONG SOAM	103.483	10.62	24.5	141.7	25.6	147.4	-1.1	-5.7	2.7

21	SATTAHIP	100.859	12.622	54.4	185.7	60.4	192.2	-6	-6.5	8.9
22	KOH HLAK	99.245	10.427	40.2	186.7	43.8	197.2	-3.6	-10.5	8.5
23	PATTANI	101.325	6.943	12.2	333.7	10.7	339.1	1.5	-5.4	1.9
24	TELOK TEKEK	104.144	2.785	43	25.2	48.6	36.4	-5.6	-11.2	10.6
25	TEBON ISLET	107.118	0.582	28	129.9	21.6	119.7	6.4	10.2	7.7
26	SELAT PENINTING	106.263	3.225	39	13.7	39.5	27.9	-0.5	-14.2	9.7
27	POELOE LAOET	107.992	4.741	36	349	37	353	-1	-4	2.8
28	PALOH	109.275	1.807	27	357.7	20.6	12	6.4	-14.3	8.7
29	TELOK PLAN	113.085	3.264	42	320.6	36.9	328	5.1	-7.4	7.2
30	PALAU MANGALUM	115.592	6.198	34.1	312.6	30	320.6	4.1	-8	6.1
31	ULUGAU BAY	118.77	10.104	31	312.7	25.8	301.7	5.2	11	7.5
32	SANTA CRUZ	119.948	15.739	25.7	313.7	20.3	321.2	5.4	-7.5	6.2
33	NAGABUNGAN	120.56	18.498	16.5	313.5	11.3	318.7	5.2	-5.2	5.4
34	KAO-HSIUNG	120.252	22.618	16.5	285	19.4	298.5	-2.9	-13.5	5.1
35	CHAUAN BAY	117.292	23.609	32	292.3	27.8	275.4	4.2	16.9	9.7
36	HONGKONG	114.207	22.249	36	299.8	29.1	316	6.9	-16.2	11.4
37	NAOZHOU DAO	110.589	20.927	44	314.7	36.5	332.4	7.5	-17.7	14.4
38	NORTHDANGERREEF	114.31	11.469	20	305.7	26.3	311.3	-6.3	-5.6	6.6
39	SCARBOROUGHSHOA	117.765	15.137	30	330.7	25.4	327.8	4.6	2.9	4.8
40	LES PARACELS	111.617	16.557	26.8	306	22.9	310.7	3.9	-4.7	4.4
41	PRATASREEF	116.716	20.678	27.5	314.9	18.4	312.7	9.1	2.2	9.2
Average SVD										7.4
RMSE								5.7	9.3	

No	Station name	LONG	LAT	O1						
				Observation		Calculation		dH	dG	VD
				Amp (cm)	Phase (deg.)	Amp (cm)	Phase (deg.)	(cm)	(deg.)	(cm)
1	YU LIN KAN	109.606	18.19	28.7	271	27.1	287.8	1.6	-16.8	8.3
2	PAK HOI	109.145	21.529	94.7	51	98.9	64	-4.2	-13	22.3
3	DO SON	106.808	20.667	74.1	48	81.4	61.3	-7.3	-13.3	19.4
4	HON NE	106.006	19.918	69.1	50	63.1	62	6	-12	15.1
5	HON NIEU	105.777	18.81	58.9	54.5	51	69	7.9	-14.5	15.9
6	QUANG KHE	106.464	17.671	26.9	58	34.4	73.3	-7.5	-15.3	11
7	DA NANG	108.214	16.127	12.9	257.4	16.2	251.3	-3.3	6.1	3.6
8	QUI NHON	109.212	13.732	28.5	267.3	27.3	269.6	1.2	-2.3	1.6
9	CAM RANH	109.159	11.858	29.2	267.4	34.4	269.2	-5.2	-1.8	5.3
10	PHU QUY	108.967	10.497	31.3	263.3	30.4	270.4	0.9	-7.1	3.9
11	KE GA	107.969	10.689	37.7	265	37	272.8	0.7	-7.8	5.1
12	VUNG TAU	107.086	10.305	45.2	276.4	45.1	281.3	0.1	-4.9	3.9
13	CON DAO	106.593	8.656	45	290.4	44	296.8	1	-6.4	5.1
14	MY THANH	106.193	9.432	45.1	293	52.4	301.8	-7.3	-8.8	10.4
15	GANH HAO	105.458	9.037	44.7	310	51.4	315.8	-6.7	-5.8	8.2
16	CA MAU	104.78	8.58	19	325	25.1	311.3	-6.1	13.7	8
17	Tammassu	104.796	9.006	11	66	15.5	67.8	-4.5	-1.8	4.6
18	HA TIEN	104.494	10.35	12.8	88	17.6	85	-4.8	3	4.8
19	THO CHU	103.444	9.272	7	55	15.6	62.8	-8.6	-7.8	8.7
20	KOMPONG SOAM	103.483	10.62	18.4	98.4	23.1	100.1	-4.7	-1.7	4.8

21	SATTAHIP	100.859	12.622	42	125.4	48.5	132.9	-6.5	-7.5	8.8
22	KOH HLAK	99.245	10.427	26.8	134.4	31.5	142	-4.7	-7.6	6.1
23	PATTANI	101.325	6.943	7.3	279.4	5.7	287.8	1.6	-8.4	1.8
24	TELOK TEKEK	104.144	2.785	32.2	342.4	35.6	352.4	-3.4	-10	6.8
25	TEBON ISLET	107.118	0.582	27	43.9	28.2	53.6	-1.2	-9.7	4.8
26	SELAT PENINTING	106.263	3.225	29	327.4	32.5	342	-3.5	-14.6	8.5
27	POELOE LAOET	107.992	4.741	29.7	282	34.9	301.2	-5.2	-19.2	12
28	PALOH	109.275	1.807	14	294.7	21.1	294	-7.1	0.7	7.1
29	TELOK PLAN	113.085	3.264	36	268.4	35	277.6	1	-9.2	5.8
30	PALAU MANGALUM	115.592	6.198	31.1	274.4	29.2	272.4	1.9	2	2.2
31	ULUGAU BAY	118.77	10.104	28	266.4	22.9	246	5.1	20.4	10.3
32	SANTA CRUZ	119.948	15.739	21.9	258.4	22.9	273.6	-1	-15.2	6
33	NAGABUNGAN	120.56	18.498	17.4	268.4	17.4	270.5	0	-2.1	0.6
34	KAO-HSIUNG	120.252	22.618	15.9	259.7	19.5	251.2	-3.6	8.5	4.5
35	CHAUAN BAY	117.292	23.609	26.3	247	16.5	265.1	9.8	-18.1	11.8
36	HONGKONG	114.207	22.249	28.9	248.7	28.6	255.5	0.3	-6.8	3.4
37	NAOZHOU DAO	110.589	20.927	39.5	275.4	35.7	281.1	3.8	-5.7	5.3
38	NORTHDANGERREEF	114.31	11.469	30	256.4	26.7	271.3	3.3	-14.9	8
39	SCARBOROUGHSHOA	117.765	15.137	30	279.4	23.9	278.3	6.1	1.1	6.1
40	LES PARACELS	111.617	16.557	23.4	260.5	25.3	270.3	-1.9	-9.8	4.6
41	PRATASREEF	116.716	20.678	16.8	250.1	26.3	260.7	-9.5	-10.6	10.3
Average SVD										7.1
RMSE								4.9	10.4	

Table A.2: Measurement and simulation results of tidal current ellipses for four primary constituents

Location	Tidal constituents			
	M_2	S_2	K_1	O_1
Tien Giang	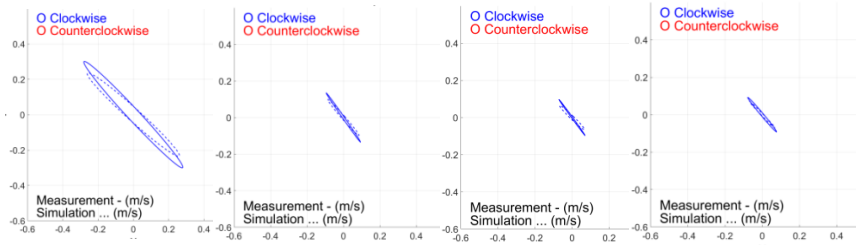			
Tra Vinh	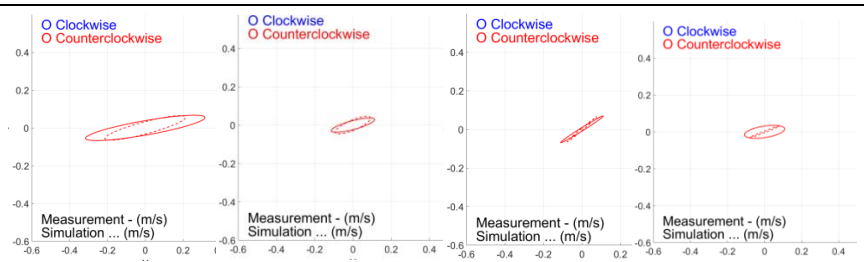			
Ca Mau Spit	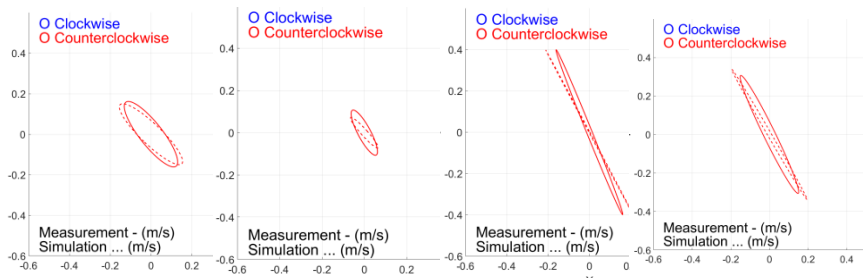			
Western Ca Mau	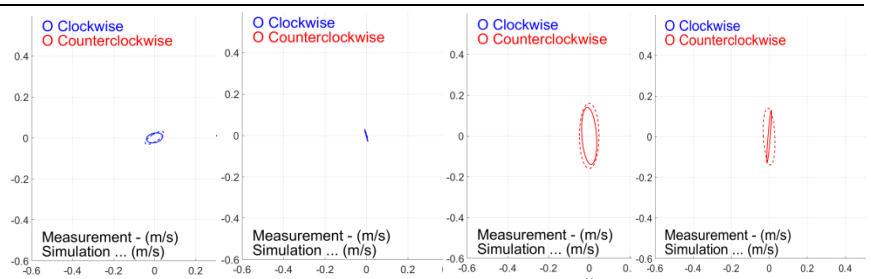			

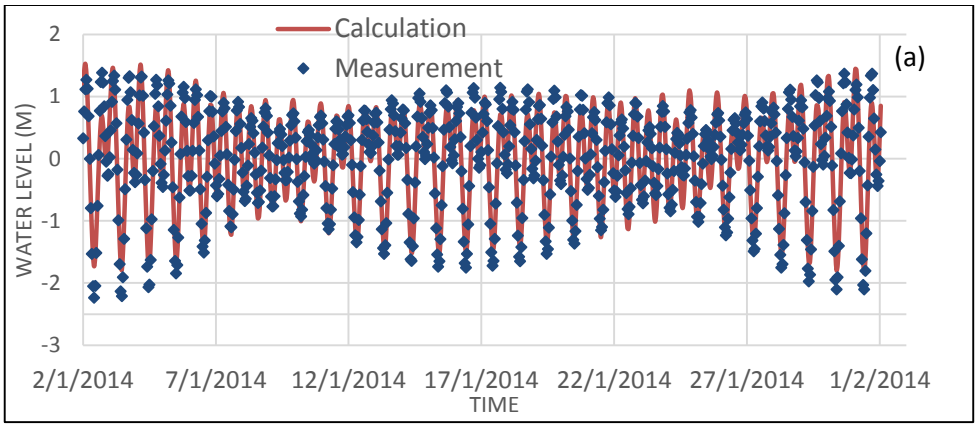

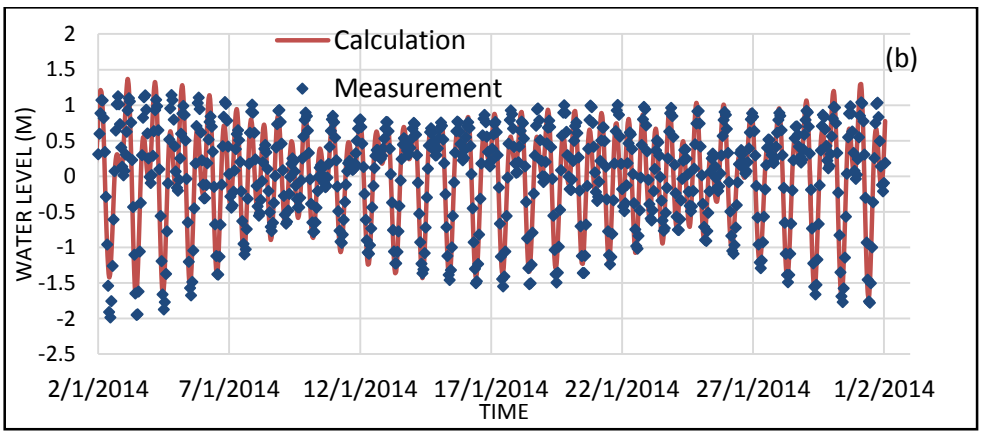

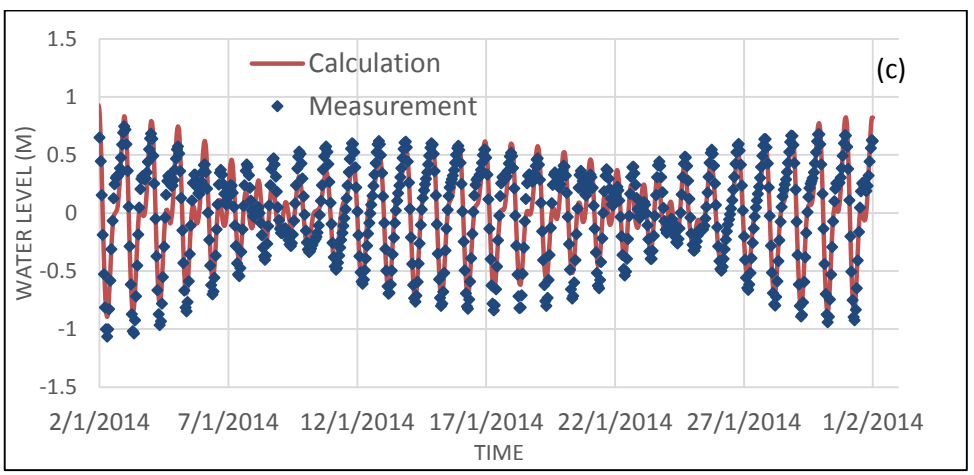

Figure A.1: Calculated and measured water level at Vungtau (a), Condao (b), Phuquy (c) stations.

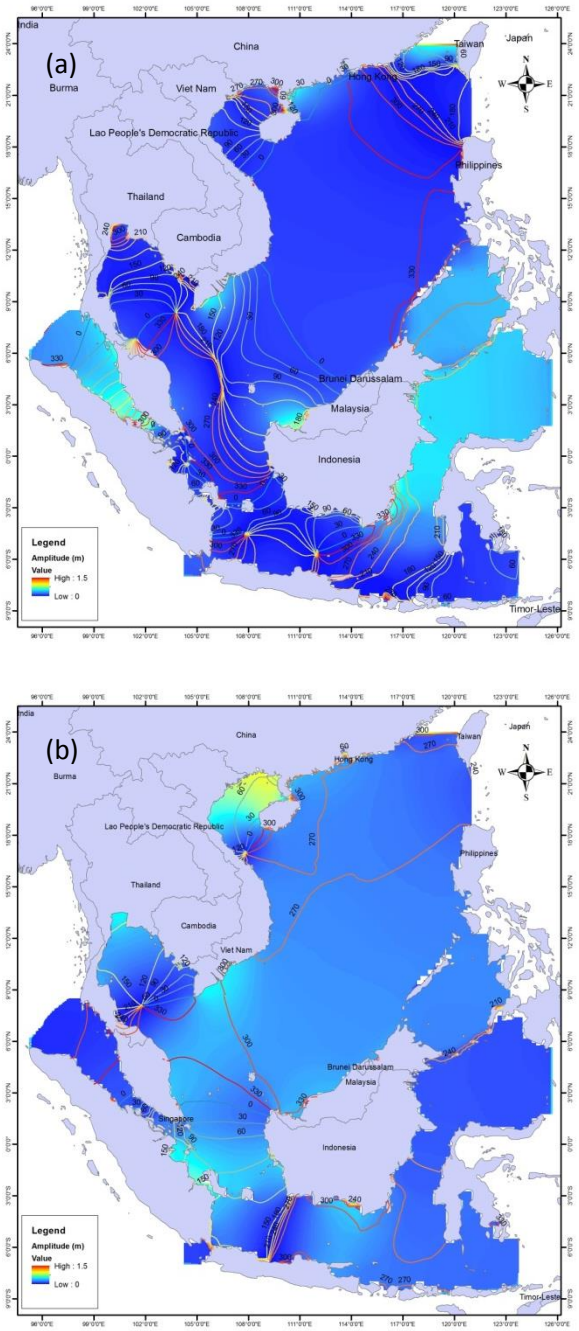

Figure A.2: Co-tidal chart of S_2 (a), O_1 (b).

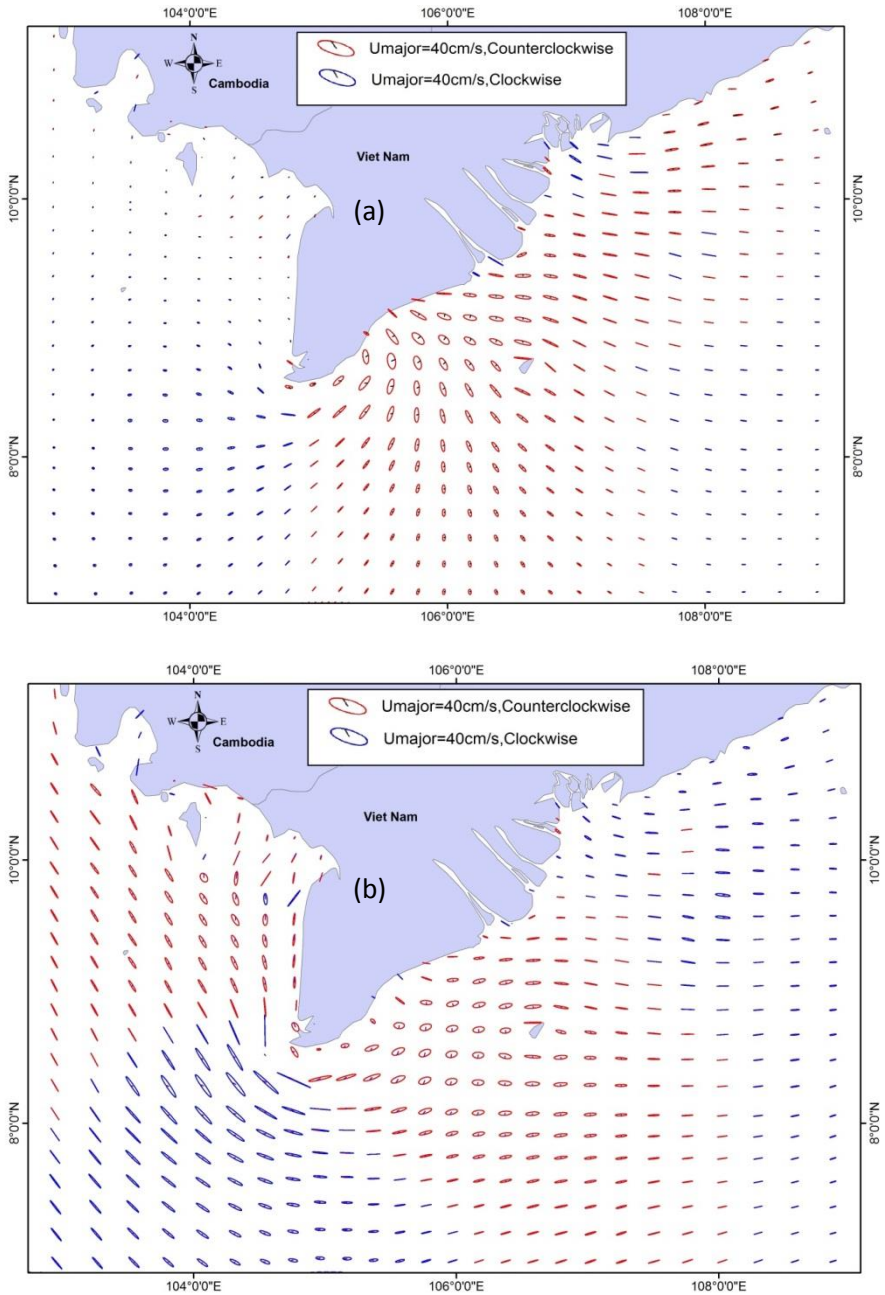

Figure A.3: Tidal current ellipses S_2 (a) and O_1 (b).

B

Residual flow velocity and residual sediment transport

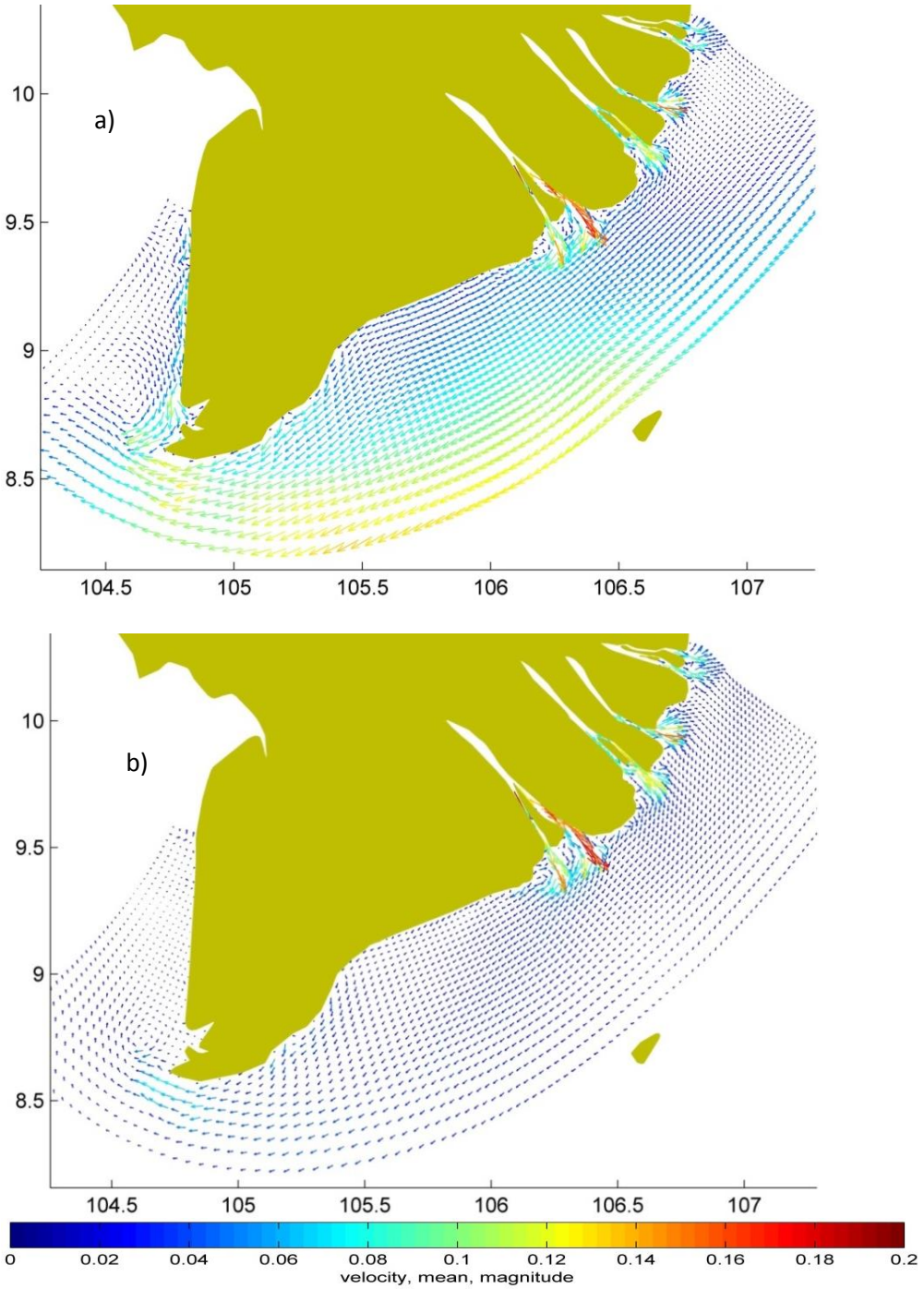

Figure B.1: Residual flow velocity (m/s) under the combined tide and wind and the combined tide and wave in the winter (a, b) and summer (c, d), respectively.

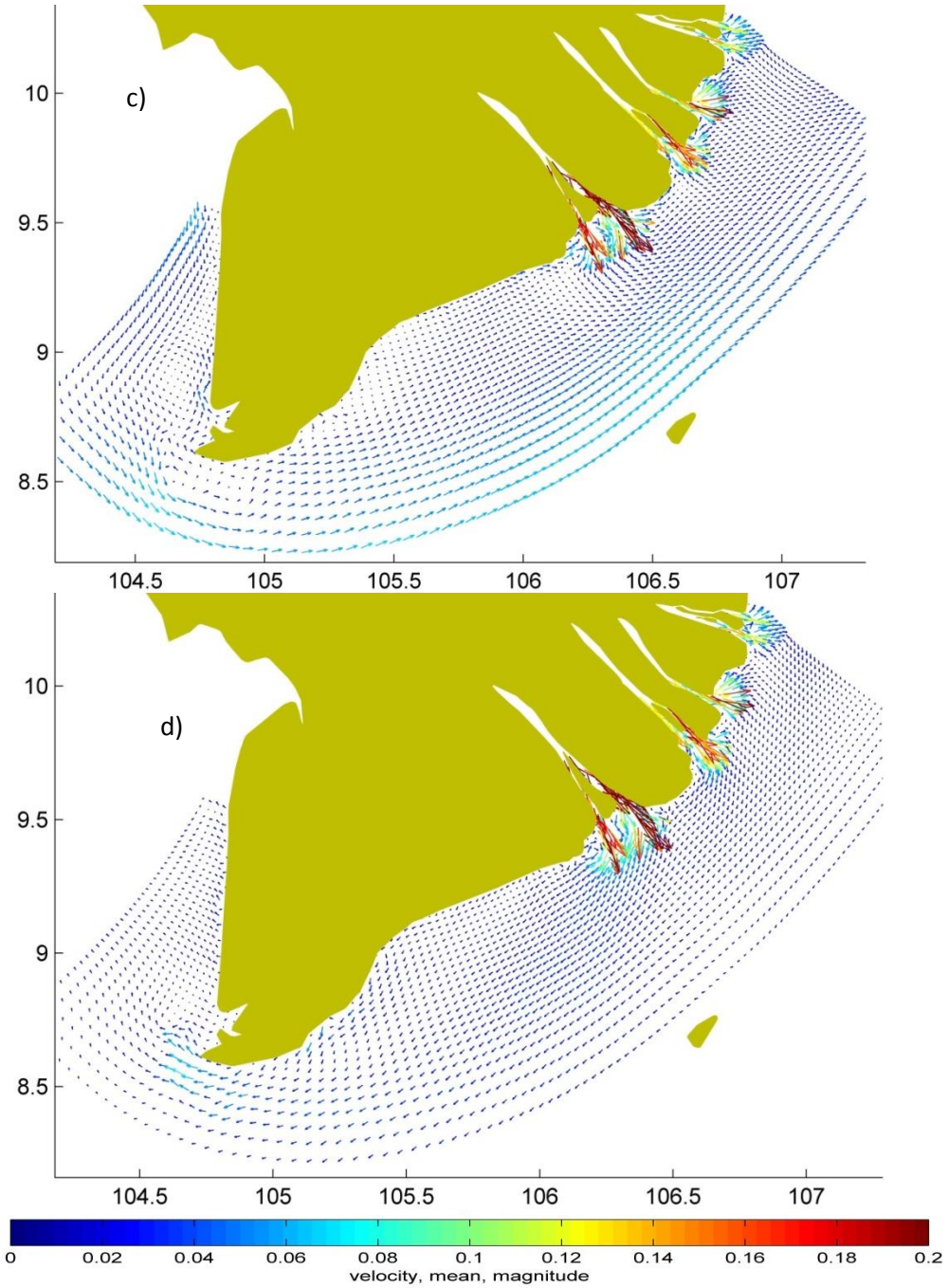

Figure B.1, continued.

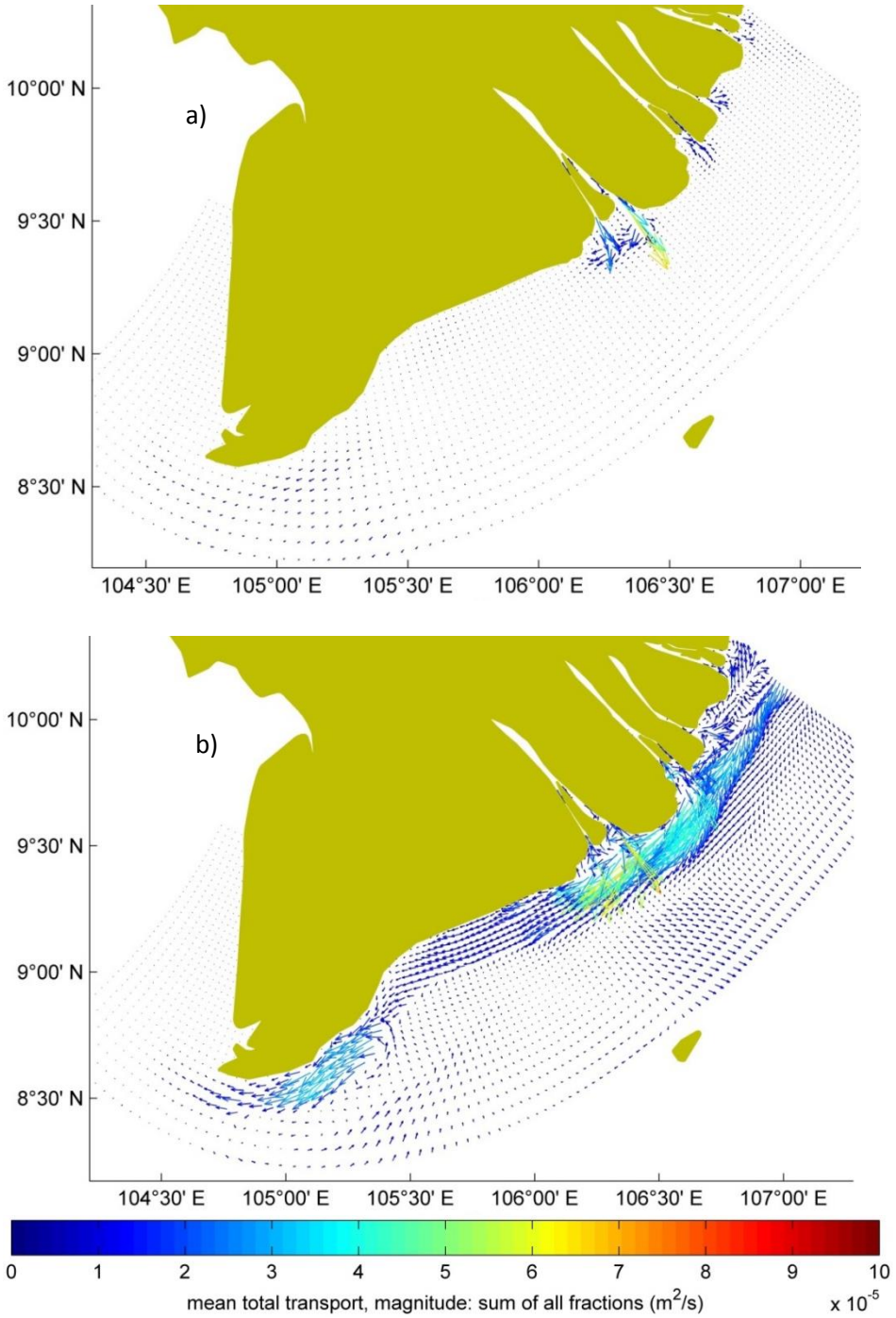

Figure B.2: Residual sediment transport ($m^3/m/s$) under the combined tide and wind and the combined tide and wave in the winter (a, b) and summer (c, d), respectively.

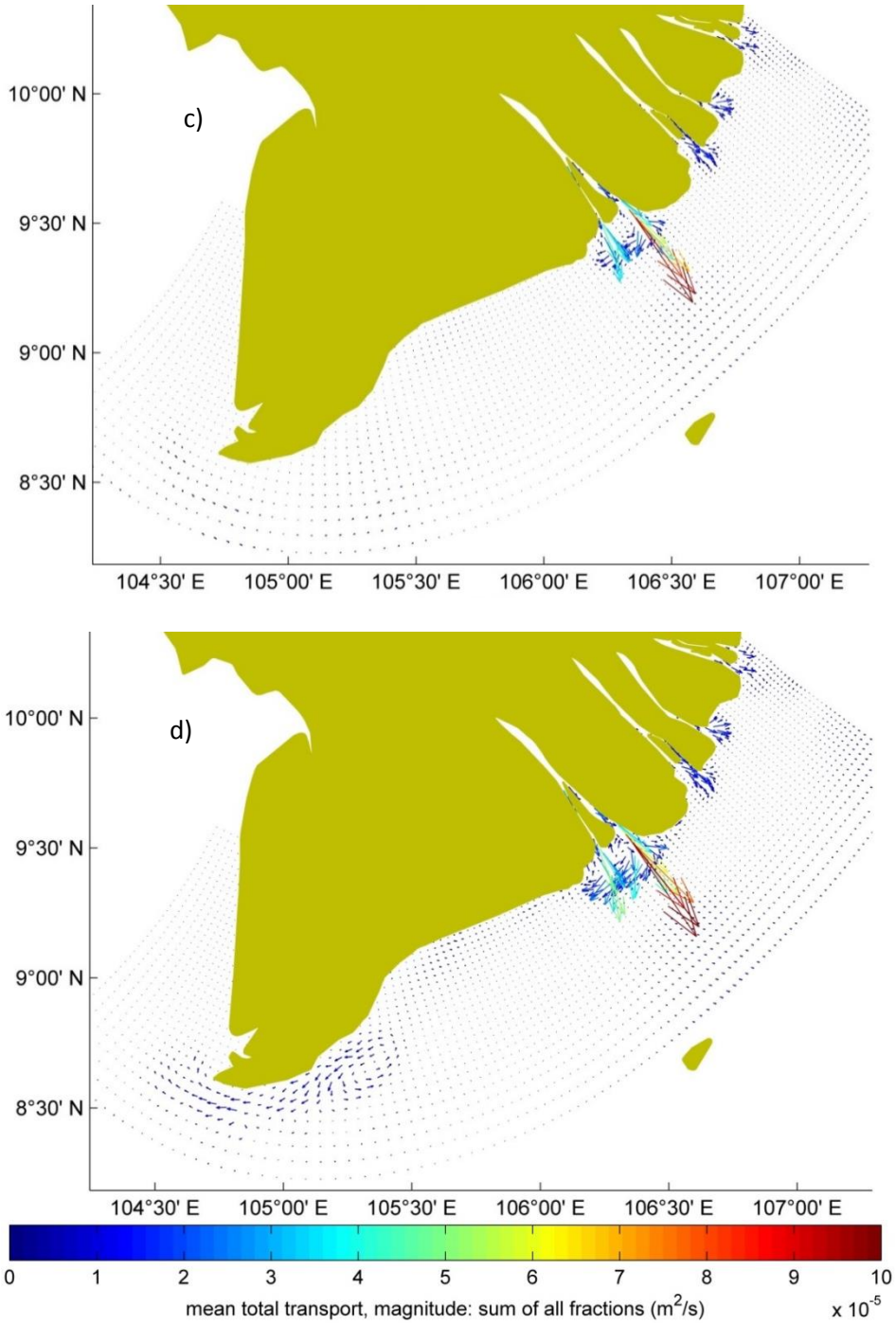

Figure B.2, continued.

Acknowledgements

This thesis is the result of a long journey which brought me not just professional, but also personal development. I was not alone during this journey and it would not be possible to complete without the support and guidance from many people.

First of all, I would like to express deep and sincere gratitude to my promotor, Professor Marcel Stive. It is a great honor to be a PhD student of Professor Marcel Stive. I have learned a lot about not only professional knowledge of coastal research but also so kind characteristic from you. You gave me incredible freedom to pursue new ideas, unconditional support, and active supervision during all stages of my research. You are an example to be followed with sharp eyes for science and warm heart for behavior in life. Truly, you are like the second father in my life, Professor Marcel.

I am also special thankful to my promotor, Professor Ad Reniers for your expert guidance and constructive suggestions that encourage me to think independently, thoughtfully and critically. The experience I gained under your guidance will be undoubtable helpful for my further scientific career. In addition, I really enjoyed the moment when we played football together, Professor Ad.

I would also like to address my special thanks to my supervisor, Dr. Qinghua Ye for your technical support of Delft3D. I learned a lot your experience on hydrodynamic and morphodynamic modelling in the deltaic coast as well.

Next, I gratefully acknowledge Professor Tang Duc Thang from Vietnam Academy for Water Resources. You have inspired me many scientific issues of Vietnam as well as Mekong delta.

I would like to thank Mariette van Tilburg for useful checking the English writing of journal papers and thesis. Besides, I also thank Veronique for partly funding to my study here. Also, I thank my mentor Sierd with your support during my doing PhD in TUDelft.

My sincere thanks also go to my great Vietnamese, Dutch and foreign colleagues at TU Delft for creating such nice, warm and friendly atmosphere in our department.

Special thanks are given to my football, tennis, ping-pong, party and life sharing teams in Delft. All you make me feel relax and leave me with so many enjoyable memories in Delft. From that, I also got best Vietnamese friends here.

I left at the end the most important persons in my life: my parents, my brother, my wife and our children. Thank you so much for your unconditional support, limitless love and patience and for being my wonderful family. My heartfelt thanks for the years spent together and for those still to come.

Finally, I acknowledge for the financial support from “The Vietnamse Scholarship” and “Het Lamminga Fonds”.

“Especially, this research is so extremely useful and meaningful for me and people in the Mekong delta”. **Thank you all so much.**

Phan Manh Hung
Delft, March 2020

About The Author

Hung Manh Phan was born in Nha Trang city, Vietnam on 9th July 1982. He received the B.Sc. degree in Water Resources Engineering in 2005 from Thuy loi University. After graduation, he worked as a researcher in Vietnam Academy for Water Resources. Thereafter, he obtained M.Sc. in Hydroinformatics from IHE-Delft Institute for Water Education in 2011 with a fund of Vietnam government and Asia Development Bank (ADB). Then, he back to Vietnam Academy for Water Resources to work as researcher. In December 2014, he was granted a scholarship from Vietnam government to pursue his Ph.D. degree in coastal engineering section, Delft University of Technology under supervision of Prof. Dr. Marcel J. F. Stive, Prof. Dr. Ad J. H. M. Reniers and Dr. Qinghua Ye.

List of Publications

1. **H. M. Phan**, H.V. Hoang, T.P.T. Nguyen, 2013. Some first results on hydro-morphodynamics processes in the coastal southern Vietnam. *Proceedings of the 14th Asian Congress of Fluid Mechanics*. ISBN: 978-604-913-145-5.
2. **H. M. Phan** and M. J. F. Stive, 2017. Dynamics of mangrove in lower Mekong Delta. *4TU Centre for Research Data*. https://doi.org/10.4121/uuid:da314d82-83f6-46d9-bdf6-a37f48d24326
3. **H. M. Phan** and M. J. F. Stive, 2017. Shoreline change of the Mekong deltaic coast. *4TU Centre for Research Data.* https://doi.org/10.4121/uuid:2d1a8002-53a8-4b60-93cc-0b2dac94af05
4. **H. M. Phan**, Q. Ye, A. J. H. M. Reniers, M. J. F. Stive, 2017. Response in the mekong deltaic coast to its changing sediment sources and sinks. *Proceedings of Coastal Dynamics 311-322*.
5. **H. M. Phan**, Q. Ye, A. J. H. M. Reniers, M. J. F. Stive, 2018. Tidal wave in the flat basin under wind monsoon climate. *Proceedings of the 6th International Conference on Estuaries and Coasts*.
6. **H. M. Phan**, Q. Ye, A. J. H. M. Reniers, M. J. F. Stive, 2019. Tidal wave propagation along The Mekong deltaic coast. *Estuarine, Coastal and Shelf Science*. 220, 73–98. https://doi.org/10.1016/j.ecss.2019.01.026.
7. **H. M. Phan** and M. J. F. Stive, 2019. Mangroves and coastal land cover in the Mekong Delta. *Ocean and Coastal Management*. [Under review].
8. **H. M. Phan**, Q. Ye, A. J. H. M. Reniers, M. J. F. Stive, 2020. Seasonal nearshore wave climate and longshore sediment transport for the Mekong Deltaic Coast. *Coastal Engineering.* [Submitted].
9. **H. M. Phan**, Q. Ye, A. J. H. M. Reniers, M. J. F. Stive, 2020. Seasonal morphodynamics along the Mekong Deltaic Coast. *Estuarine, Coastal and Shelf Science.* [Submitted].
10. **H. M. Phan**, T. V. Le, T. T. K. Nguyen, 2019. Numerical study on tidal characteristic in the flat shelf. Case study: Mekong deltaic shelf. *International conference of water science and technology in Hanoi*.
11. M.J.F. Stive, L.K.Phan, S.T.Truong, **H.M.Phan**, H.T.Dao, 2019. Innovative Vietnamese research on the Mekong Deltaic coastal processes. *Proceedings of the 10th International Conference on Asian and Pacific Coasts.*